

# **Towards a Better Understanding of the Precordial Leads: An Engineering Point of View**



**By: Hossein Moeinzadeh**

**Supervisor: A/Prof. Gaetano D. Gargiulo**

**Co-supervisor:**

**Prof. Jonathan C. Tapson**

**MD. Dr. Aiden J. C. O'Loughlin**

*A thesis submitted in fulfilment of the requirements for the degree of Doctor of Philosophy*

Biomedical Engineering and Neuromorphic Systems (BENS)  
The MARCS Institute for Brain, Behaviour and Development  
Western Sydney University

2021

## **Statement of Authentication**

The work presented in this thesis is, to the best of my knowledge and belief, original except as acknowledged in the text. I hereby declare that I have not submitted this material, either in full or in part, for a degree at this or any other institution.

(Hossein Moeinzadeh)

**Dedicated to Imam Hossein (a.s), who  
gave his life for liberty and humanity.**

## **Acknowledgements**

I have been extremely lucky for the opportunity to study under the supervision of Dr. Gaetano Gargiulo who cared so much about my work. I am highly indebted to Gaetano for his knowledge, input, kindness, patience, guidance, tireless supports, encouragements, valuable suggestions, and constructive criticisms during this journey. I have always admired his great personality. I would like to sincerely thank my co-supervisors Dr. Aiden O'Loughlin and Jonathan Tapson for their kindness, extensive supports, streams of ideas and encouragements to pursue my research goals.

My appreciation extends to and Dr. Ibrahim Shugman, who helped to record data at Campbelltown hospital. My sincere gratitude goes to Dr. Joseph Assad for sharing his knowledge and being a great help in clinical analysis of data.

I wish to express my gratitude to Professor Kate Stevens and Dr. Paul Breen for their supports and encouragements. It has been an honour to be a member of ICNS and study at the MARCS institute. I also would like to thank the members of ICNS group.

Words cannot express how grateful I am to every member of my family. My deepest gratitude to beloved my parents, Mahdi and Farahnaz, and my siblings, Hojat and Elham for their endless love, prayers and continuous support. I am incredibly grateful to my father and mother in law, Bakhtiar and Tahereh, and my sister and brother in law, Kosar and Yasin for their never-ending love, encouragements and prayers. Finally, my sincere gratitude to my loving wife, Elham, who always believed in me and supported me with her unwavering love, kindness, wisdom and encouragements throughout my study. Thanks for always being there for me.



## **Abstract**

Surface electrocardiography (ECG) is the most common non-invasive tool to diagnose cardiac diseases. It is solidly in the clinical practice from more than 80 years. The history of ECG is associated with evolution of many theories to find the best configuration for number of electrodes and their placement. The widest accepted theory originated the so called 12-lead electrocardiography, which was finalized in 1942 and it requires ten electrodes of which six are placed on the chest (precordium) and the remaining four at the extremities. The 12 lead ECG has been widely used all around the world since then. However, many hypothesis and assumptions which shape the 12-lead electrocardiography were found incorrect either during its development or after finalizing this framework. One important hypothesis is to subtract all the six chest electrodes' potential from the “zero” assumed potential reference point, named after its inventor Wilson Central Terminal (WCT). Although this hypothesis was built upon an oversimplification of human body and many suggested to use different reference points, this hypothesis eventually was accepted and widely used. The WCT was known to have a high potential, which consequently could impair diagnosis by removing important features from the precordial leads. This associated error has been neglected as there was no routine approach available to measure the influence of WCT on the precordial leads.

This thesis provides comprehensive literature review of the electrocardiography evolution to highlight the important theories behind the development of the electrocardiography device. More importantly, it discusses different electrode placement on the chest, and their clinical advantages. This work presents a technical detail of a new ECG device which was developed at MARCS institute and can record the WCT components in addition to the standard 12-lead ECG. This ECG device was used to record from 147 patients at Campbelltown hospital over three years. The first two years of recording contain 92 patients which was published in the Physionet platform under the name of Wilson Central Terminal ECG database

(WCTECGdb). This novel dataset was used to demonstrate the WCT signal characterisation and investigate how WCT impacts the precordial leads. Furthermore, the clinical influence of the WCT on precordial leads in patients diagnosed with non-ST segment elevation myocardial infarction (NSTEMI) is discussed. The work presented in this research is intended to revisit some of the ECG theories and investigate the validity of them using the recorded data. Furthermore, the influence of the left leg potential on recording the precordial leads is presented, which lead to investigate whether the WCT and augmented vector foot (aVF) are proportional. Finally, a machine learning approach is proposed to minimise the Wilson Central Terminal.

# Table of Contents

Table of Contents .....	vi
List of Figures .....	ix
List of Tables .....	xv
List of Abbreviations .....	xvii
Chapter 1 Introduction.....	1
1.1 Electrocardiography in history .....	2
1.1.1 Einthoven limb leads.....	2
1.1.2 Precordial leads.....	4
1.1.3 Augmented leads.....	16
1.2 Wilson’s Central Terminal .....	16
1.2.1 The WCT Location .....	17
1.2.2 The WCT Measurement.....	19
1.3 Research Motivation .....	21
1.4 True Unipolar ECG recording device .....	24
1.5 List of Publications.....	29
1.6 Thesis Organization.....	31
Chapter 2 Wilson Central Terminal ECG database (WCTECGdb) .....	32
2.1 Abstract .....	33
2.2 Background .....	33
2.3 Evaluation metrics.....	37
2.4 WCT characteristics .....	37
2.4.1 The WCT shape .....	38
2.4.2 The WCT Amplitude .....	38
2.4.3 The WCT Error measurement.....	44
2.5 Conclusion.....	46
Chapter 3 Einthoven Limb Potential .....	48
3.1 Abstract .....	49

3.2	Einthoven limb hypothesis .....	49
3.3	Evaluation metrics.....	50
3.4	Wilson limb potential amplitudes .....	51
3.5	The WCT and aVF resemblance .....	53
3.6	Conclusion.....	58
Chapter 4	Clinical investigation of Wilson Central Terminal .....	59
4.1	Abstract .....	60
4.2	Introduction .....	60
4.3	Clinical case reports .....	62
4.4	Conclusion.....	82
Chapter 5	The minimisation of the Wilson’s Central Terminal voltage potential via a genetic algorithm .....	83
5.1	Abstract .....	84
5.2	Background .....	84
5.3	WCT minimisation method.....	85
5.3.1	Fitness function.....	86
5.3.2	Population .....	87
5.3.3	Crossover .....	88
5.3.4	Mutation.....	88
5.4	Results and Discussion.....	88
5.5	Conclusions .....	96
Chapter 6	Discussion and Future Directions .....	97
6.1	Summary of Contributions .....	98
6.2	Future Directions.....	101
References	.....	102
Appendix A	Graphical User Interfaces and User Guidelines .....	A-1
A.1	User Guide for the ECG Visualization.....	A-1
A.2	ECG Visualization Graphical User Interface .....	A-5
Appendix B	Publications .....	B-1

# List of Figures

Figure 1. 1 Illustration of the three Einthoven limb leads constructing a closed loop. ....4

Figure 1. 2 The electrode placement of precordial leads suggested by Wilson’s group. Image taken from [35]. ..... 7

Figure 1. 3 The average potential of limbs yields Wilson Central Terminal. Image taken from [2]...... 17

Figure 1. 4 Einthoven assumed the potential of each limb only depends on the angle between  $p$  and  $R$  vectors. .... 18

Figure 1. 5 Ideal measurement of lead I vs real measurement of lead I. Left panel shows idealized measurement of lead I using voltage; right panel refers to real measurements of lead I in which includes contact impedances ( $Z_{c1}$  and  $Z_{c2}$ ) and variable impedance of torso ( $Z_t$ ). .....23

Figure 1. 6 In our approach, the limb potential and unipolar chest lead are measured in respect to the right leg. ....24

Figure 1. 7 ECG amplifier using right leg driver (lead I) .....25

Figure 1. 8 Simplified schematic limited to limbs’ connections and one of the precordial leads. ....27

Figure 1. 9 Active band-pass filter gain cell, see Table 1-2 for components’ values. ....27

Figure 2. 1 Top panel: the WCT with positive deflection (patient ID 44); middle panel: the WCT with negative deflection (patient ID 50); bottom panel: the WCT with neutral deflection (patient ID 67). ....39

Figure 2. 2 The WCT potential amplitude for 147 patients. ....39

Figure 2. 3 The influence of the WCT error in recording precordial leads. The unipolar chest leads and precordial leads are different in terms of shape and amplitude. The precordial leads are shifted by 0.5 mv from the original place for better visualization. (a) The WCT has a 0.21 mV peak-to-peak amplitude; (b)  $C_{S\&G}$  between  $V_1$  and  $UV_1$  is 0.47; (c)  $C_{S\&G}$  between  $V_2$  and  $UV_2$  is 0.42; (d)  $C_{S\&G}$  between  $V_3$  and  $UV_3$  is 0.75; (e)  $C_{S\&G}$  between  $V_4$  and  $UV_4$  is 0.33; (f)  $C_{S\&G}$  between  $V_5$  and  $UV_5$  is 0.54; (g)  $C_{S\&G}$  between  $V_6$  and  $UV_6$  is 0.66. Recorded from 75 years old female (Patient ID 100). ....41

Figure 2. 4 The influence of the WCT error in recording precordial leads. The unipolar chest leads and precordial leads are identical. The precordial leads are shifted by 0.5 mv from the original place for better visualization. (a) The WCT has a 0.19 mV peak-to-peak amplitude;

(b)  $C_{S\&G}$  between  $V_1$  and  $UV_1$  is 0.15; (c)  $C_{S\&G}$  between  $V_2$  and  $UV_2$  is 0.07; (d)  $C_{S\&G}$  between  $V_3$  and  $UV_3$  is 0.08; (e)  $C_{S\&G}$  between  $V_4$  and  $UV_4$  is 0.10; (f)  $C_{S\&G}$  between  $V_5$  and  $UV_5$  is 0.12; (g)  $C_{S\&G}$  between  $V_6$  and  $UV_6$  is 0.16. Recorded from 67 years old male (Patient ID 143). .....42

Figure 2. 5 The influence of the WCT error in recording precordial leads. The T and P waves have significant impact on the precordial leads. The precordial leads are shifted by 0.5 mv from the original place for better visualization. (a) The WCT has a 0.4 mV peak-to-peak amplitude; (b)  $C_{S\&G}$  between  $V_1$  and  $UV_1$  is 0.34; (c)  $C_{S\&G}$  between  $V_2$  and  $UV_2$  is 0.11; (d)  $C_{S\&G}$  between  $V_3$  and  $UV_3$  is 0.30; (e)  $C_{S\&G}$  between  $V_4$  and  $UV_4$  is 0.64; (f)  $C_{S\&G}$  between  $V_5$  and  $UV_5$  is 0.64; (g)  $C_{S\&G}$  between  $V_6$  and  $UV_6$  is 0.55. Recorded from 58 years old female (Patient ID 136). .....43

Figure 2. 6 The distribution of the patients having different WCT error. ....44

Figure 2. 7 Average correlation between unipolar chest leads and precordial leads within each error class. ....46

Figure 3. 1 Patient with the RA potential higher than the LA potential (47 in total) with 0.1 mV threshold. The average of three peak to peak amplitude of the RA and the LA measured for each patient. ....52

Figure 3. 2 The comparison of Einthoven limbs' potential. The LA, RA, and LL amplitudes are 0.124, 0.464 and 0.038 mV. The LA and RA are shifted 0.2 mV from the original place for better visualization. Recorded from 40 years old male (Patient ID 142). .....52

Figure 3. 3 The relative limb potential of each patient. ....53

Figure 3. 4 The relative average amplitudes of limbs potential: (a) patients having relatively small LL amplitude (minimum: 0.01, maximum: 0.09, average: 0.06); (b) patients having relative high LL amplitude (minimum: 0.10, maximum: 0.28, average: 0.15). ....54

Figure 3. 5 The influence of the LL potential on leads II, III, and WCT. To have a better visualization leads II, III, WCT are shifted 0.5 mV from the original place: (a) the average peak to peak potential of the LL among three beats is 0.09 mV which shape 4 percent of the WCT signal; (b) the correlation between lead III and -LA is 0.99 (RMS error: 0.02); (c) the correlation between lead II and -RA is 1 (RMS error: 0.02); (d) the correlation between -2/3aVF and the WCT is 0.99 (RMS error: 0.11); Recorded from 59 years old male (Patient ID 27). .....56

Figure 3. 6 The influence of the LL potential on leads II, III, and WCT. To have a better visualization leads II, III, WCT are shifted 0.5 mV from the original place: (a) the average peak to peak potential of the LL among three beats is 0.47 mV which shape 18 percent of the WCT signal; (b) the correlation between lead III and -LA is 0.94 (RMS error: 0.09); (c) the correlation between lead II and -RA is 0.91 (RMS error: 0.09); (d) the correlation between -2/3aVF and the WCT is 0.82 (RMS error: 0.22). Recorded from 72 years old male (Patient ID 141). .....57

Figure 3. 7 The influence of the LL potential on leads II, III, and WCT. To have a better visualization leads II and III are shifted 0.2 mV, and the WCT is shifted 0.05 from the original place: (a) the average peak to peak potential of the LL among three beats is 0.09 mV which shape 17 percent of the WCT signal; (b) the correlation between lead III and -LA is

0.96 (RMS error: 0.06); (c) the correlation between lead II and -RA is 0.98 (RMS error: 0.06); (d) the correlation between  $-2/3aVF$  and the WCT is 0.08 (RMS error: 0.6). Recorded from 84 years old female (Patient ID 40). .....58

Figure 4. 1 ECG abnormalities in NSTEMI patient, adopted from [108] .....62

Figure 4. 2 Comparison between the standard precordial leads ( $V_1: V_6$ ) (top panel), unipolar chest leads ( $UV_1: UV_6$ ) (middle panel), and reconstructed unipolar chest leads ( $UV_1(R): UV_6(R)$ ) (bottom panel). Recorded from a 52 years old male (PID 97). .....64

Figure 4. 3 Comparison of the WCT and  $-2/3aVF$ . Recorded from a 52 years old male (PID 97). .....65

Figure 4. 4 Comparison of left arm (LA), right arm (RA) and left leg (LL) potential. Recorded from a 52 years old male (PID 97). .....65

Figure 4. 5 Comparison of the WCT and  $-2/3aVF$ . Recorded from a 72 years old male (PID 75). .....66

Figure 4. 6 Comparison of left arm (LA), right arm (RA) and left leg (LL) potential. Recorded from a 72 years old male (PID 75). .....66

Figure 4. 7 Comparison between the standard precordial leads ( $V_1: V_6$ ) (top panel), unipolar chest leads ( $UV_1: UV_6$ ) (middle panel), and reconstructed unipolar chest leads ( $UV_1(R): UV_6(R)$ ) (bottom panel). Recorded from a 72 years old male (PID 75). .....67

Figure 4. 8 Comparison of left arm (LA), right arm (RA) and left leg (LL) potential. Recorded from a 51 years old male (PID 94). .....68

Figure 4. 9 Comparison of the WCT and  $-2/3aVF$ . Recorded from a 51 years old male (PID 94). .....68

Figure 4. 10 Comparison between the standard precordial leads ( $V_1: V_6$ ) (top panel), unipolar chest leads ( $UV_1: UV_6$ ) (middle panel), and reconstructed unipolar chest leads ( $UV_1(R): UV_6(R)$ ) (bottom panel). Recorded from a 51 years old male (PID 94). .....69

Figure 4. 11 Comparison of the WCT and  $-2/3aVF$ . Recorded from a 54 years old male (PID 85). .....70

Figure 4. 12 Comparison of left arm (LA), right arm (RA) and left leg (LL) potential. Recorded from a 54 years old male (PID 85). .....70

Figure 4. 13 Comparison between the standard precordial leads ( $V_1: V_6$ ) (top panel), unipolar chest leads ( $UV_1: UV_6$ ) (middle panel), and reconstructed unipolar chest leads ( $UV_1(R): UV_6(R)$ ) (bottom panel). Recorded from a 54 years old male (PID 85). .....71

Figure 4. 14 Comparison of left arm (LA), right arm (RA) and left leg (LL) potential. Recorded from a 52 years old male (PID 56). .....72

Figure 4. 15 Comparison of the WCT and  $-2/3aVF$ . Recorded from a 52 years old male (PID 56). .....72

Figure 4. 16 Comparison between the standard precordial leads ( $V_1: V_6$ ) (top panel), unipolar chest leads ( $UV_1: UV_6$ ) (middle panel), and the reconstructed unipolar chest leads ( $UV_1(R): UV_6(R)$ ) (bottom panel). Recorded from a 52 years old male (PID 56). .....73

Figure 4. 17 Comparison of left arm (LA), right arm (RA) and left leg (LL) potentials. Recorded from a 75 years old female (PID 94).	74
Figure 4. 18 Comparison of the WCT and -2/3aVF. Recorded from a 75 years old female (PID 94).	74
Figure 4. 19 Comparison between the standard precordial leads ( $V_1: V_6$ ) (top panel), unipolar chest leads ( $UV_1: UV_6$ ) (middle panel), and reconstructed unipolar chest leads ( $UV_1(R): UV_6(R)$ ) (bottom panel). Recorded from a 75 years old female (PID 94).	75
Figure 4. 20 Comparison of left arm (LA), right arm (RA) and left leg (LL) potential. Recorded from a 67 years old female (PID 58).	76
Figure 4. 21 Comparison of the WCT and -2/3aVF. Recorded from a 67 years old female (PID 58).	76
Figure 4. 22 Comparison of the standard precordial leads ( $V_1: V_6$ ) (top panel), unipolar chest leads ( $UV_1: UV_6$ ) (middle panel), and the reconstructed unipolar chest leads ( $UV_1(R): UV_6(R)$ ) (bottom panel). Recorded from a 67 years old female (PID 58).	77
Figure 4. 23 Comparison of the WCT and -2/3aVF. Recorded from a 55 years old male (PID 93).	78
Figure 4. 24 Comparison of left arm (LA), right arm (RA) and left leg (LL) potential. Recorded from a 55 years old male (PID 93).	78
Figure 4. 25 Comparison between the standard precordial leads ( $V_1: V_6$ ) (top panel), unipolar chest leads ( $UV_1: UV_6$ ) (middle panel), and reconstructed unipolar chest leads ( $UV_1(R): UV_6(R)$ ) (bottom panel). Recorded from a 55 years old male (PID 93).	79
Figure 4. 26 Comparison of left arm (LA), right arm (RA) and left leg (LL) potential. Recorded from a 75 years old female (PID 100).	80
Figure 4. 27 Comparison of the WCT and -2/3aVF. Recorded from a 75 years old female (PID 100).	80
Figure 4. 28 Comparison between the standard precordial leads ( $V_1: V_6$ ) (top panel), unipolar chest leads ( $UV_1: UV_6$ ) (middle panel), and the reconstructed unipolar chest leads ( $UV_1(R): UV_6(R)$ ) (bottom panel). Recorded from a 75 years old female (PID 100).	81
Figure 5. 1 Hardware (shaded square) and software (red circle) principle diagram, adapted from.....	86
Figure 5. 2 Nonlinear fitness function is used to encourage individuals to have smaller M-WCT.....	87
Figure 5. 3 Example of positive deflection WCT. M-WCT is 11.04% of lead II amplitude, while WCT is 118.82% of lead II amplitude (average); the recording is from a 73-year-old male patient admitted at the hospital (Patient ID: P050).	95
Figure 5. 4 Example of neutral deflection WCT. WCT is 45.27% of lead II amplitude, while M-WCT is 3.59% of lead II amplitude (average); the recording is from a 52-year-old male patient admitted with chest pain (Patient ID: P025). WCT for this patient presents marked P-wave and T-wave.	95



Figure 5. 5 Example of negative deflection WCT. WCT is 59.21% of lead II amplitude, while M-WCT is 2.79% of lead II amplitude (average); the recording is from a 59-year-old male patient admitted with chest pain (Patient ID: P046). .....96

Figure A. 1 ECG visualization GUI opened. ....A-1

Figure A. 2 Select a segment using segment menu .....A-2

Figure A. 3 The slide bar enables to move forward or backward in each segment. ....A-3

Figure A. 4 Choose different leads to display.....A-4

## List of Tables

Table 1. 1 The summary of researches on the precordial electrode placement .....	13
Table 1. 2 Summary of components' values for the gain cells. ....	28
Table 2. 1 The signal names and the detail of the recording presented for each segment. ....	35
Table 2. 2 List of patients with reconstructed precordial leads .....	36
Table 2. 3 Patient diagnosis list .....	36
Table 2. 4 The correlation and Sprague and Geer's error in patients having the WCT with <i>zero</i> impacts on recording precordial leads .....	45
Table 2. 5. The correlation and Sprague and Geer's error in patients having the WCT with <i>negligible</i> impacts on recording precordial leads. ....	45
Table 2. 6. The correlation and Sprague and Geer's error in patients having the WCT with <i>significant</i> impacts on recording precordial leads. ....	45
Table 3. 1 The average, standard deviation, maximum and minimum of each limb potential and Wilson centre terminal among 147 patients. All results presented in mV. ....	51
Table 3. 2 The correlation and root mean square error for 35 patients with relatively high LL potential. ....	54
Table 3. 3 The correlation and root mean square error for 112 patients with relatively small LL potential. ....	54
Table 5. 1 Average of three achieved parameters (alpha, beta, and gamma), and the number of GA iteration for each patient. ....	89
Table 5. 2 Comparison of the WCT and M-WCT amplitudes in relation to lead II. ....	92

# List of Abbreviations

aVF: Augmented vector foot

aVL: Augmented vector left

aVR: Augmented vector right

CABG: Coronary Artery Bypass Grafting

CCF: Congestive cardiac failure

CHF: Congestive cardiac failure

DRL: Driven right leg

ECG: Electrocardiography

GA: Genetic algorithm

GTN: Glyceryl trinitrate

LA: Left arm

LAD: Left anterior descending artery

LCx: left circumflex artery

LL: Left leg

LPF: Left pectoral-left leg

LPR: Left pectoral-right arm

NSTEMI: Non-ST segment elevation myocardial infarction

OCT: Optical coherent tomography

OM1: First obtuse marginal artery

RA: Right arm

RL: Right leg

RMS: Root means square

RPF: Right pectoral-left leg

RPR: Right pectoral-right arm

STEMI: ST segment elevation myocardial infarction

SVT: Supraventricular tachycardia

VF: Vector foot

VL: Vector left

VR: Vector right

VT: Ventricular tachycardia

WCT: Wilson Central Terminal

WCTECGdb: Wilson Central Terminal ECG database.

# Chapter 1 Introduction

This chapter introduces the research presented in this thesis. First, it provides detailed background information about the electrodes' placement on the body for surface electrocardiography (ECG) recording. It then discusses the validity of Wilson Central Terminal (WCT) hypothesis, and a history of attempts to measure the actual potential of the WCT to highlight the motivation behind this research. Then, it describes a new ECG device, which provides the foundation upon which the research in this thesis is built introduced along with an overview of the undertaken research, a summary of thesis contributions, and a list of publications resulting from this research presented in this thesis. Finally, the overall layout of the thesis is presented.

*Some of the work presented in this chapter has been published in:*

1. *H. Moeinzadeh, J. Assad, P. Bifulco, M. Cesarelli, A. L. McEwan, A. O'Loughlin, M. I. Shugman, J. C. Tapson, A. Thiagalingam and G. D. Gargiulo. "Unipolar Cardiac Leads Between History and Science" in Biomedical Signal Processing, (pp. 203–224).*

## 1.1 Electrocardiography in history

This section reviews the milestones in the electrocardiography history, which have led to the current understanding of the ECG, its physiological model and clinical practice. Since this thesis also proposes a new setup for recording the potential of the chest electrodes, this review is focused on the changes in electrode placement on the body. The review presented here also covers the evolution of the Einthoven limb leads, precordial leads, and augmented leads.

### 1.1.1 Einthoven limb leads

The first electrical signal variation fluctuation associated with the human heart was recorded in 1887 by Waller [1], who applied four electrodes on limbs and one electrode on the mouth. He found the detected changes in an electrometer reading synced to the heartbeat [1], [2], and named the changes *Cardiograph* [1], [3]. Einthoven then improved the electrometer, such that the electrical heart activity could present five deflections. He called these deflections 'P', 'Q', 'R', 'S', and 'T', and introduced the term *electrocardiography* to present these recordings in 1893 [4], [5]. Later, he made a major breakthrough in electrocardiography by using the string galvanometer in 1901 to record the heart activity [2]. Many believed Ader initially developed the string galvanometer in 1881 for a different application [3], [6], and Einthoven only improved its sensitivity to use it in recording the heart activity. Namely, the string galvanometer was more sensitive and convenient than the electrometer [3]. It contained a silver-coated quartz filament (or string) in a strong magnetic field to measure the strength and direction of the *current* impressed by the heart to the body surface [7]. The string was moved in the magnetic field when the current of the heart moved through it [7]. Einthoven only used three electrodes on two arms and left leg, as he believed the electrodes on the right leg and mouth were redundant [8].

Einthoven's device was very bulky and far from the hospital. Hence, he used the telephone wire to receive the patients' heart impulses from the hospital [9], [10]. He published the first clinical usage of a string galvanometer in 1906 and identified different arrhythmia patterns, including heart block, bigeminy, P mitrale, and left/right ventricular hypertrophy [3], [9]. He

then published different arrhythmia patterns from patients and showed the diagnostic possibilities for them in 1908 [11], [12]. Later, Thomas Lewis made a significant influence on electrocardiography clinical advancement. He characterised the atrial fabrication using the electrocardiogram in 1909 [11]. Lewis continued developing the clinical electrocardiogram until the late 1920s, which made him a great icon in cardiology [12].

In 1912, Einthoven introduced three leads (I, II, and III) and their mathematical relations, which is known as the *Einthoven Triangle* hypothesis [8], [13], [14]. The vertices of the Einthoven Triangle are electrodes placed on the right arm (RA), left arm (LA), and left leg (LL) [2], [14]. In this theory, the human body is characterised as a two dimensional, homogeneous conductor, and a part of infinity with the heart considered as a single dipole and located in the centroid of the triangle [2], [8], [15], [16].

$$\begin{aligned} I &= LA - RA \\ II &= LL - RA \\ III &= LL - LA \end{aligned} \tag{1-1}$$

As the three limb leads construct a closed-loop (Figure 1-1), Kirchhoff's voltage law can show the relationship between the limb leads (Eq. 1-2) [15].

$$I + III = II \tag{1-2}$$

Although some researchers suggested a different system to record the heart activity [1], [15], [17], only the Einthoven limbs' leads theory was clinically used for three decades [7], [15], [18]. While the three limb leads system was found satisfactory to determine arrhythmias, it was unsuccessful in characterizing many heart diseases, including myocardial infarction [7].

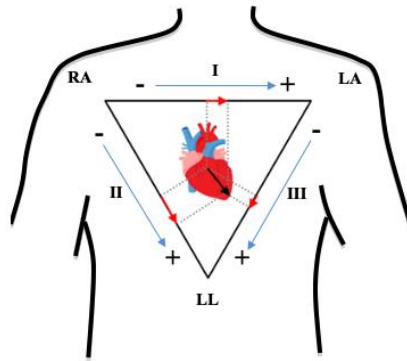


Figure 1. 1 Illustration of the three Einthoven limb leads constructing a closed loop.

### 1.1.2 Precordial leads

The origin of precordial leads goes back to 1887 when the first recording from the human heart occurred [1]. Waller applied one electrode on precordium and another on a variety of positions, including four limbs and the back [1]. In 1900, Einthoven and Lint tried different electrodes configurations to reach maximum possible deflection, and he found the right arm and the apex the best locations to fulfill this requirement [19], [20]. However, precordial leads were neglected for several years after the introduction of the Einthoven limb leads [20] and were used only for a few clinical studies.

In 1909, Lewis proposed modifying lead I and putting the right arm and left arm electrodes on the second and fourth right intercostal space [11]. He claimed this modification could improve recognition of P-wave in patients with auricular fibrillation [11], [21]. In 1914, Lewis et al. applied two electrodes directly to the ventricular surface, and showed that the recorded signal was impossible to be interpreted as it had variable shapes [22], [23].

In 1920, Wilson and Herrmann put five electrodes naming them with the letters A, B, C, D, and E, at different distances on an imaginary line drawn from fourth costal cartilage to below Poupart's ligament on the left leg [24]. They paired these electrodes and recorded four leads (AB, BC, CD, and DE) and showed that the QRS deflection decreases with distance from the heart. Furthermore, they found out in the case that the referenced electrode was located in a considerable distance from the principal electrode, the shape and size of ventricular



deflection were almost the same and independent from the referenced electrode placement [16], [24]. This hypothesis was completed ten years later by Wilson, in which he described the influence of the distance of electrodes from the heart on recorded signals [25]. He showed that the potential of electrodes placed close to the heart is much larger than the potential of those electrodes placed on the precordium region. Similarly, both are five to ten times greater than the potential variation on the extremities [25]. Therefore, he concluded that although the second electrode placement has an impact on the precordial leads, its influence is negligible [25].

In 1931, Wilson et al. further described this theory and introduced two new terms; “exploring electrode” and “indifferent electrode”. The anterior (exploring) electrode was designated as the principal electrode, while the posterior (indifferent) electrode had a minimum effect on recorded leads [26]. Therefore, the exploring electrode could be placed at every point of the human body, while the second electrode should be placed on only where it is considered far from the heart [26]. Wilson et al. also mathematically calculated the potential of the right arm (RA), left arm (LA), and left leg (LL) using three limb leads [26] (Eq.1-3). In 1932, Wilson et al. chose the left leg as an indifferent electrode and put four (or five in some cases) electrodes on precordium to record from patients having a bundle-branch block [27].

$$LL = \frac{II + III}{3}$$

$$LA = \frac{I - III}{3} \quad (1-3)$$

$$RA = -\frac{I + II}{3}$$

It is important to note that the importance of precordial leads in the diagnosis of cardiac diseases was first highlighted by Wolferth and Wood in 1932. They showed the limitation of three Einthoven leads to identify many cardiac diseases, and introduced two new precordial leads; named lead IV, and V. The lead IV was initially recorded by placing the exploring electrode near the cardiac apex and the indifferent electrode in the left paravertebral space [28]. They recorded lead IV from two patients with myocardial infarction and found "striking

deviations in the S-T interval", while three Einthoven leads were quite normal [29], [30]. Since the Lead IV required putting an electrode on the patient's back, it caused discomfort for patients. Therefore, Wolferth and Wood introduced lead V, which was recorded by placing the exploring electrode near the apex, and the indifferent electrode on the left leg [28]. They concluded that IV and V leads were identical, as both leads showed similar results. Therefore, it got customary to put the positive electrode on the left leg and refer it as lead IV [31]. These findings raised interest among researchers to employ precordial leads in the clinical practice [31] and assessed the lead IV clinical advantages [32]. It also initiated the wave of interest to apply principal and secondary electrodes on various places on the human body to find the chest lead, which yields the most information.

Arthur Master recorded a chest lead from 104 healthy volunteers and reported the characteristics of the P-wave, T-wave, and QRS deflections in 1934 [33]. He attached the exploring electrode on near the lower level of the sternum about the level of the apex and placed the indifference electrode on the back over the vertebral column for most of the volunteers, and on the left leg for thirty patients [33]. Although he did not differentiate the results of the two groups and presented all the results together, he confirmed the Wilson hypothesis and reported no critical difference in changing the reference electrodes from back to the left leg [33]. Later in the same year, Wilson et al. published an important paper which shapes the fundamental of today's precordial leads [34]. They suggested placing six electrodes on six points on the chest including the fifth rib at the right sternal edge, the fifth rib at the left sternal edge, the fifth intercostal space midway between the left sternal edge and the left midclavicular line, the fifth intercostal space in the left midclavicular line, the sixth rib in the left anterior axillary line, and the tip of the ensiform process. These six leads are designated by the symbols V<sub>1</sub>, V<sub>2</sub>, V<sub>3</sub>, V<sub>4</sub>, V<sub>5</sub>, and V<sub>E</sub>.

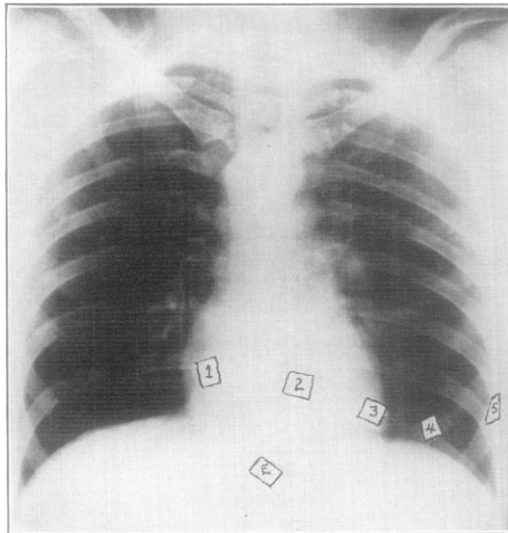


Figure 1. 2 The electrode placement of precordial leads suggested by Wilson's group. Image taken from [35].

Wilson et al. also undermined the indifference reference theory and claimed that the reference electrode has a considerable influence on some of the details of the recorded signals [34]. Therefore, they presented a new theory, which is the fundamental of today's precordial leads. They assumed the heart is a single dipole located in the centroid of the Einthoven equilateral triangle, and the average potential of three electrodes placed on right arm (RA), left arm (LA), and left leg (LL) would yield the potential of the heart, which is independent of the heart activity, and equivalent to zero (Eq. 1-4) [34].

$$WCT = \frac{1}{3}(RA + LA + LL) \quad (1.4)$$

Therefore, the potential of the dipole (heart) could be used as a reference point to record the potential of every point in the human body. Wilson et al. suggested to connect the indifference electrode to this reference point and place the exploring electrodes on any part of the body to record *unipolar leads* [34]. This reference point was called the Wilson Central Terminal (WCT) and was measured by connecting three large resistors to three limbs' electrode [34]. The introduction of WCT was associated with two hypotheses; first, the WCT was assumed null as it represents the potential of the dipole (heart), second, the sum of the potential differences between three limbs' electrode and the nodal point connected to these

electrodes through the equal resistances is zero (Kirchhoff's first law) [16], [34]. These hypotheses had absorbed researchers' attention to measure the real amplitude of the WCT and investigate the validity of the WCT zero potential. A complete survey of these attempts is listed in the next section.

Kossmann et al., who were members of Wilson's laboratory, published a complementary paper in 1935 to present more details of Wilson's leads. They used six electrodes on the chest paired with Wilson Central Terminal and characterised all the deflections on each precordial lead [35]. A year later, Kossmann compared lead IV and V with Wilson's lead by placing the reference electrode on the Wilson Central Terminal, the back, and the left leg to record a single electrode potential on the chest [36]. He only recorded from nine patients and concluded that although the influence of each reference points was small on precordial leads, each impacted differently on every patient. Since these differences were not medically important, he reported the reference point would not have a medical impact on the chest leads [36]. But they also reported the potential variation of leads coupled with the WCT is usually greater than the other two leads [36].

In 1935, Roth suggested fixing the exploring electrode on the left and right pectoral and placing the indifferent electrode on the right arm and left leg, which resulted in four new leads including left pectoral-right arm (LPR), left pectoral-left leg (LPF), right pectoral-right arm (RPR) and right pectoral-left leg (RPF) [20]. He showed that despite the indifference reference point hypothesis, the placement of the secondary electrode influenced the recorded leads. Roth characterised a reference point as ideal if the chest leads present auricular and ventricular components of the cardiac cycle, maximum deflection in all principal components, and symmetry with the standard leads. Therefore, he concluded that the right arm was a better reference point than the left leg, as it fulfills these requirements [20]. Furthermore, he also placed the exploring electrode on the apex and reported it as the least reliable chest lead [20].

Later in 1937, Larsen investigated the best placement of exploring and indifferent electrodes [37]. He recorded from one healthy subject and put two exploring electrodes on the lower left corner of the sternum and 4cm lateral to the apex [37]. He compared different reference points, including the right arm, left arm, left leg, Wilson Central Terminal, and the angle of

the right scapula to find the optimum place [37]. He claimed that the right arm is a most expedient reference point as the precordial leads' deflections, in this case, are greater than those when using any other reference points [37]. Sorsky and Wood showed the similarities and differences in leads obtained by placing the exploring electrodes on the apex, left and right pectoral which are coupled with the right arm, and left leg [38]. They found out shifting the exploring electrode to the right of the apex resulted in relatively small positive deflection and less inverted T-wave [38]. They only characterised the chest leads' deflections by recording from 150 healthy individuals, without suggesting a preferred reference electrode setup [38].

There was no common opinion among researchers regarding the number of electrodes and their locations on the chest. Thus, the American Heart Association and the Cardiac Society of Great Britain & Ireland each appointed a committee to reach an agreement over the number and position of the electrodes in 1938 [39]. Wilson was a member of the standardisation committee; therefore, the committee was aware of his research group's findings, including Wilson Central Terminal, unipolar lead concept, and the use of six electrodes on the chest. However, all the members except Wilson did not recognize the importance of these findings [18], [40]. Therefore, the standardisation committee only had a mutual agreement on using lead IV with reference to an arbitrary choice among the right arm, left arm, left leg, Wilson Central terminal, and left interscapular region [39]. A month later, the American Heart Association conducted a supplementary statement, which was more aligned with Wilson's group achievements. In this report, six electrodes were suggested to be used on the chest naming ( $V_1$ :  $V_6$ ), but still, there was no unanimous agreement on the second electrode placement [41]. Therefore, the right arm, left arm, and Wilson Central Terminal were reported as three feasible choices for the second electrode placement [41]. Additionally, this report claimed no significant difference in recording precordial leads using either the left leg or Wilson Central Terminal as the reference point [41].

In 1938, Edwards and Vander Veer used standard six electrodes on the chest associating with the right arm, left arm, and left leg [42]. They recorded from ten healthy and fifty patient volunteers with an abnormal cardiac condition. They reported that the recordings coupled with the left leg did not present any superiority, while the leads which were referenced with

the right arm showed maximum deflections in almost all cases [42]. There were only three cases in the recordings with the left arm as the reference that presented greater deflections in the QRS and T waves [42].

Groedel conducted two comprehensive studies to find the least variant reference points in 1939 [43]. In the first paper, he applied the reference electrode on the left leg, left arm, right arm, forehead, and back. He placed two exploring electrodes on the left border of the lower end of the sternum and the left axilla line at the height of the apex [43]. Groedel recorded from thirty-two subjects, including individuals with heart arrhythmia and healthy heart [43]. As in leads coupled with the right arm, the Q and S deflections were usually shown better and the T-wave was almost the highest, Groedel nominated the right arm as a better reference point [43]. In the second paper, Groedel added the WCT in the same experimental setting and recorded it from ten patients. He concluded that the LL and LA could cause having abnormality in the chest leads, while the recorded signals coupled with the RA were quite normal [44]. Furthermore, he showed that the maximum potential in each extremity presented at a very different time [44]. Consequently, the WCT amplitudes vary in different volunteers as the limbs' potential can be completely or partially summed up, or they could neutralize each other more or less [44].

In 1939, Geiger compared the IV leads referenced to the right arm, and left leg and found out that the IV R usually had more visible P, QRS, and T waves than the IV F. He recorded 400 electrocardiograms from 349 patients and reported in more than eighty percent of recordings, the IV R and IV L were mainly the same. However, in fifty-five of the instances, the arrhythmia was either better shown or it was only presented in the IV F lead. Therefore, he suggested that the left leg was a superior reference point than the right arm [45]. In the same year, Wood and Selzer applied the exploring electrodes on the apex, right and left pectoral referenced respectively to the right arm, and left leg. They recorded six precordial leads from 314 patients to clinically investigate the influence of the reference electrode's position on the recorded signals. They came to the conclusion that choosing the right arm as the reference point leads to having more convenient and informative recordings compared to when the left leg is used as the reference point [46].

In 1942, Hecht investigated the influence of using four different reference points, including right arm, left arm, left leg, and Wilson Central Terminal on precordial leads' shape and amplitudes [47]. He only used  $V_1$ ,  $V_3$ , and  $V_6$  chest electrodes and recorded from twenty healthy volunteers. He concluded that the position of reference electrode has a notable influence on the size and shape of recorded precordial leads [47]. Furthermore, all the reference points were found to distort the recorded leads, but their influence varied in different volunteers. Therefore, he could not find the most desirable reference point for all patients. Nevertheless, he reported that while the distortion caused by the right arm was not smaller than the left arm or left leg, it is more uniform in the amplitude and duration. Moreover, he found that the WCT caused minimum distortion in the precordial leads [47].

This uncertainty on choosing the WCT as the reference point continued, and it was clearly stated by Wolferth and Livezey in 1944 [48]. They suggested putting the reference electrode on the spine of the right scapula and compared the results with three precordial signals recorded with WCT as their reference point [48]. Wolferth and Livezey claimed that the Wilson Central Terminal has more interference with the potential variation of the chest electrodes; therefore, the spine of the right scapula is better for recording the unipolar leads [48]. In addition to the serious doubt in choosing the WCT as the reference point, using six electrodes on the chest was not widely accepted as most cardiologists used a single precordial lead even six years after chest electrodes standardisation [49]. Therefore, Wilson published two papers to establish the theoretical concept of using six chest electrodes and Wilson Central Terminal in 1944 and 1946 [16], [50]. In his papers, he confirmed the validity of previous experiments by measuring the actual potential of the WCT, which showed the WCT does not have a null amplitude, and it varies during the cardiac cycle. However, he still considered the WCT potential variations negligible compared to the potential of the exploring electrodes [50].

However, there was still doubt in the validity of Wilson's hypothesis, and its claimed theoretical advantages [51]. Therefore, practically every hypothesis was believed to be the only feasible approach to understand the advantages of each reference point [52]. In 1946, Wallace and Grossman compared the WCT and the left leg by recording three leads ( $V_2$ ,  $V_4$ , and  $V_5$ ) from 91 volunteers. Their results showed that the WCT did not have any advantage

over the left leg, and both are equally acceptable [51]. Hoyos and Tomayo in 1947 [53] and Dolgin et al. in 1949 [54] compared four of the most commonly known reference points, including the right arm, left arm, left leg, and the WCT. Their experiment was similar to Hecht's work in 1942 [47], except that they recorded from patients having different cardiac diseases [53], [54]. Hoyos and Tomayo recorded from ten healthy volunteers and a hundred cases diagnosed with different cardiac problems. They reported the left leg was the only reference that caused having more distortion on the precordial leads, and they did not find any particular differences in recordings obtained from healthy subjects using different reference points [53]. Furthermore, they found the chest leads coupled with right arm and WCT without having significant differences; therefore, as the right arm was easier to use, it was nominated as a better reference point [53]. Dolgin et al. used seven electrodes on precordium and confirmed the influence of different reference points on the shape and amplitude of the recorded leads [54]. They only found different interpretations in the recordings obtained using the left leg for five percent of the patients, while the recordings using other reference points showed the same interpretation [54]. Therefore, they could not find the ideal location for the reference point [54]. In 1948, Hull et al. recorded  $V_1$ :  $V_6$  using both the left leg and WCT for four healthy volunteers. They found false T-wave inversions in the recordings using the left leg as the reference point [55].

In 1949, the British Cardiac Society recommended to couple the reference electrode by the WCT and to discontinue using the right arm, and left leg [56]. However, this recommendation was not widely accepted, and the idea of finding the best reference point for the chest leads was still trending. Leatham compared the right arm, left leg, and Wilson Central Terminal by connecting them to seven electrodes on the chest in 1950 [57]. He put six electrodes on the standard positions and one on the posterior axillary line [57]. He did not clinically analyse the recorded signals and only reported the statistical factors such as mean and standard deviation of R, S, and T waves of the recorded signals. He concluded that the chest leads coupled with the left leg were too variable compared to the other references, while the WCT and right arm did not have any advantage over each other [57]. In the same year, Herrmann et al. compared the WCT, right arm, left arm, and left leg as reference points for the six standard precordial electrodes ( $V_1$ :  $V_6$ ) [52]. They recorded from 200 healthy subjects and cardiac patients. They concluded that the left leg and left arm caused the most variations



on the recorded chest signals, which demonstrated false abnormalities depending on the electrical position of the heart [52]. They concluded that the Wilson Central Terminal was the superior reference, as the false abnormalities were neither obtained nor were significant [52].

Finally, the American heart association published the second report of standardisation in 1954 and chose the Wilson Central Terminal as the reference point of precordial leads [58]. They suggested obtaining eight leads from the chest, designated as V<sub>1</sub>: V<sub>8</sub> [58]. The chest electrodes' location was standardised for each lead as described below [58]:

- V<sub>1</sub>: the right sternal margin at the fourth intercostal space.
- V<sub>2</sub>: the left sternal margin at the fourth intercostal space.
- V<sub>4</sub>: the fifth intercostal space where it is crossed by the midclavicular line.
- V<sub>3</sub>: a point midway between points 2 and 4.
- V<sub>5</sub>: the junction of the left anterior axillary line with the horizontal level of electrode on position 4.
- V<sub>6</sub>: the left midaxillary line.
- V<sub>7</sub>: the left posterior axillary line.
- V<sub>8</sub>: the left midscapular line.

Table 1-1 shows a summary of the existing studies on the development of the precordial leads. Standardisation of the precordial leads did not stop the investigation of the validity of the Wilson Central Terminal, and the effort for measuring the actual potential of WCT continued in the following years.

Table 1. 1 The summary of researches on the precordial electrode placement

<b>Year</b>	<b>Study</b>	<b>Exploring Electrode</b>	<b>Reference Electrode</b>	<b>Clinical advice</b>	<b>Chosen reference</b>
1878	Waller [1]	one electrode on precordium	four limbs, and the back	no clinical findings	No findings
1900	Einthoven and Lint [19]	one electrode on the apex	right arm	maximum deflection	Right arm
1909	Lewis [11].	one electrode on second intercostal space	one electrode on fourth intercostal space	recognition of P-wave in patients with auricular fibrillation	NA
1914, 1915	Lewis et. al. [22], [23]	one electrode on ventricular	one electrode on ventricular	impossible interpretation	NA

		surface	surface		
1920	Wilson and Herrman [16]	five electrodes from fourth costal cartilage to below Poupart's ligament on the left leg	every two adjacent exploring electrodes were paired	distance electrode did not influence on shape and size of ventricular deflections	any distance point from the heart
1930 1931	Wilson [7], Wilson et. al [26]	precordium	any distance point from the heart	no clinical difference by using any distance reference point	any distance point from the heart
1932	Wilson et. al.[27]	four (five) electrodes on precordium	left leg	diagnosis bundle-branch block	NA
1932	Wolferth and Wood [29]	IV and V: apex	IV: back V: left leg	found striking deviations in the S-T interval in patients with myocardial infarction. No difference found between two reference points, the left leg was chosen as it was more convenient	Left leg
1934	Master [33]	lower level of sternum about the level of the apex	the back the left leg	characteristics of the P-wave, T-wave, and QRS deflections. No difference found between two reference points	back and left leg were equally acceptable
1934	Wilson et. al. [34]	six electrodes on precordium	WCT	Not investigated	NA
1935	Roth [20]	Left and right pectoral	right arm and left leg	Maximum Q, S, and T deflections in recordings coupled with right arm	Right arm
1936	Kossmann [36]	apex	WCT, back, and left leg	No clinical advantages were found	WCT
1937	Larsen [37]	two electrodes on lower left corner of sternum and 4cm lateral to the apex	right arm, left arm, left leg, Wilson Central Terminal, and angle of right scapula	maximum deflections in leads obtained using the right arm	Right arm
1937	Sorsky and Wood [38]	apex, left and right pectoral	right arm, left leg	Relatively small positive deflection and less inverted T-wave by moving exploring electrode to the right of apex	NA
1938	Edwards and Vander Veer [42]	V1:V6	right arm, left arm, and left leg	Maximum deflections in recordings coupled with right arm	Right arm
1939	Groedel [43]	two electrodes on the left border of the lower end of sternum and left	left leg, left arm, right arm, forehead, and back	Maximum Q, S, and T deflections	Right arm

		axilla line at the height of the apex			
1939	Groedel [44]	two electrodes on the left border of the lower end of sternum and left axilla line at the height of the apex	left leg, left arm, right arm, forehead, and back, WCT	The WCT amplitude varies in different patient. The LL and LA cause abnormality in the chest lead. The RA causing maximum deflections in ECG recordings	Right arm
1939	Geiger [45]	one electrode on the apex	right arm, left leg	the arrhythmia was either better or only presented in the IV F lead	Left leg
1939	Wood and Selzer [46]	three electrodes on the apex, right and left pectoral	right arm, left leg	significant deflection in P and T waves in recordings coupled with right arm	Right arm
1942	Hecht [47]	three electrodes on V1, V3, and V6 locations	right arm, left arm, left leg and WCT	every reference cause different distortion on precordial leads. The WCT make a minimum distortion.	WCT
1944	Wolferth and Livezey [48]	first electrode on position of V1 with 1.5- and 3-inches distance with the other two electrodes in direction of right shoulder	spine of right scapula, and WCT	WCT has more interference with potential variation of the chest electrodes	Spine of right scapula
1946	Wallace and Grossman [51]	three electrodes on V2, V4, and V5 positions	left leg and WCT	no advantages found	WCT and left leg were equally acceptable
1947	Hoyos and Tomayo [53]	V1:V6	right arm, left arm, left leg, and the WCT	left leg causes more distortion. Right arm and WCT are equally acceptable.	Right arm
1949	Dolgin et. al. [54]	V1:V7	right arm, left arm, left leg, and the WCT	all recorded leads have the same interpretation, except for five percent of the leads, which coupled with the left leg	No findings
1948	Hull et. al. [55]	V1:V6	left leg and WCT	false T-wave inversion in recordings using the left leg as reference point	WCT
1950	Leatham [57]	V1:V7	right arm, left leg, WCT	left leg causes more distortion, while the right arm and WCT are equally acceptable	Right arm or WCT
1950	Herrmann et. al. [52]	V1:V6	WCT, right arm, left arm, and left leg	WCT shows neither false abnormalities or missed abnormalities	WCT

### 1.1.3 Augmented leads

In 1934, Wilson proposed to use three unipolar limb leads including vector right (VR), vector left (VL), and vector foot (VF), which were measured by the difference potential of limbs' electrode and the WCT reference point [34].

$$\begin{aligned}VL &= LA - \Phi_{WCT} \\VR &= RA - \Phi_{WCT} \\VF &= LL - \Phi_{WCT}\end{aligned}\tag{1-5}$$

Since the three unipolar limb leads had a small amplitude, Goldberger modified the WCT to increase the amplitude of these leads by 50% [59]. The new leads are measured as the potential difference between each limb potential and the average potential of the other two limbs. These leads are known as augmented leads and named as augmented vector right (aVR), augmented vector left (aVL), and augmented vector foot (aVF) [59].

$$\begin{aligned}aVL &= LA - \frac{1}{2}(RA + LL) \\aVR &= RA - \frac{1}{2}(LA + LL) \\aVF &= LL - \frac{1}{2}(RA + LA)\end{aligned}\tag{1-6}$$

The augmented leads were suggested in 1942 and finalized the development of the ECG lead system. In 1949, the committee of the British cardiac society suggested using three unipolar limb leads (VL, VR, and VF) [56], but seven years later, the American heart association recommended using three augmented leads [58].

## 1.2 Wilson's Central Terminal

Wilson hypothesized that a neutral reference point of the human body could be measured by averaging the limb potentials. This reference point was introduced as having a null amplitude,

being steady, and locating in the centre of the Einthoven triangle [34]. The potential in the infinite medium has a null amplitude, which could be considered as the ideal reference point. In physics, we can only measure the potential difference between two points. However, we can have the potential of one point in case the second point is located in the far distance (infinity) from the first [60]. Thus, Wilson used three large resistors through which a negligible current would pass (based on Ohm's law), and consequently, he was able to measure the limbs' potential (Figure 1-3) [34].

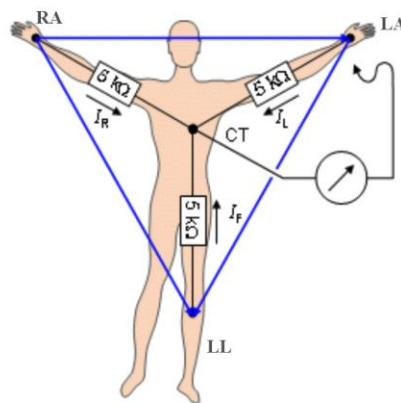


Figure 1. 3 The average potential of limbs yields Wilson Central Terminal. Image taken from [2].

### 1.2.1 The WCT Location

In theory, the WCT is located in the centroid of the Einthoven triangle. However, a research conducted in 2005 shows that many cardiologists do not have a clear understanding of unipolar leads and the WCT concept [61]. As mentioned earlier, although there was an initial wave of interest working on the fault in the WCT assumption after Wilson hypothesized this concept, the associated error has been widely accepted, and the topic received scant research attention. Furthermore, there is no consensus understanding of the Einthoven triangle, as its edges have been considered differently in the literature. Hence, a clear view of the Einthoven triangle hypothesis may lead to a more precise answer to the question, *where is Wilson Central Terminal?*

Einthoven assumed the human body is a two-dimensional conducting homogeneous medium with the shape of a triangle. The heart is regarded as a single dipole in the centre of the triangle. The dipole changes its magnitude and direction in every moment, which causes it to change its electrical field. Considering these assumptions, the potential of every point in the body is measured by Eq. 1-7 [15], in which  $\Phi$  is the potential of a single current dipole  $\vec{p}$  (with the strength of  $p$ ) in infinite homogenous medium with a conductivity of  $\sigma$ :

$$\Phi = \frac{1}{4\pi\sigma} \frac{p \cos\theta}{R^2} + c \quad (1-7)$$

$R$  is the length of the vector  $\vec{R}$  directed from dipole source location to the target point and  $\theta$  is the angle between vectors  $\vec{p}$  and  $\vec{R}$ .

As it is shown in Figure 1-4, the distance between each limb electrode and the dipole is equivalent. Therefore, the difference between the limb potential amplitudes is only dependent on the angles  $\theta_1$ ,  $\theta_2$  ( $\theta_1 + 120$ ) and  $\theta_3$  ( $\theta_1 + 240$ ). It could be easily shown that for every direction of the heart vector, the sum of the limb potential is equal to zero [62].

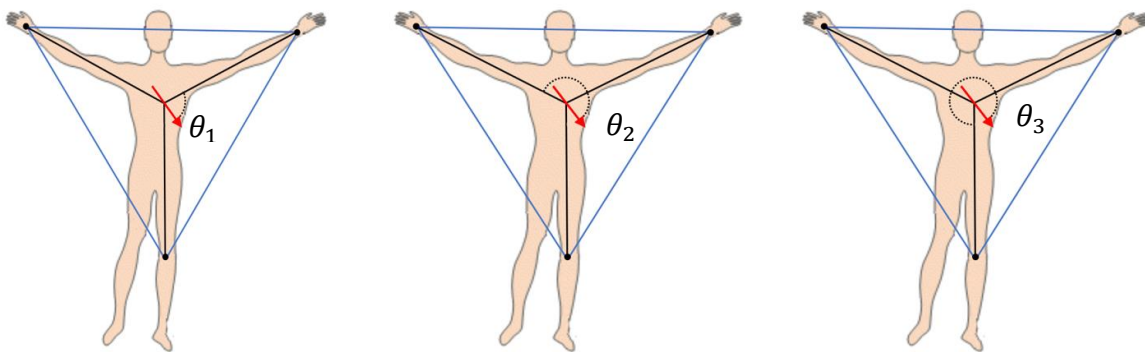


Figure 1. 4 Einthoven assumed the potential of each limb only depends on the angle between  $\vec{p}$  and  $\vec{R}$  vectors.

The geometrical position of the limb electrodes shaped the Einthoven triangle [62]–[64]. Wilson assumed the symmetrical orientation of the heart vector with respect to the electrodes on the limbs [65]. He hypothesized that the potential of the heart dipole is equal to zero and calculated by the average of the Einthoven limb potentials. Although the Einthoven hypothesis is regarded as a major breakthrough in electrocardiography, its assumptions are

known to be tainted by oversimplification of the human body, and the electrical heart activity. The same argument can be made for the Wilson hypothesis.

*The WCT located in the centroid of the Einthoven triangle, represents the potential of the single dipole, and its potential is equal to zero in the case, in which the three limb electrodes are placed in the same distance from the heart, and all Einthoven assumptions are correct.*

However, as it can be referred from Eq. 1-7, in case that the imaginary line between limb electrodes do not build up the equilateral triangle, the limb potentials depend on the  $R$  amplitude and the angle  $\theta$ . Consequently, the centroid of the triangle cannot represent the dipole anymore. Furthermore, other assumptions (the electrical activity of the heart is a single dipole located in the centre of the body, and the human body is a homogeneous conductor) are ill-posed models of the human body [62].

In some literature, there is also a misunderstanding between geometrical space and electrical space. As an example, in the standard surface ECG representation, it is possible to see that limb leads are the edges of the Einthoven triangle; this can be easily shown to be incorrect. The Einthoven law (Eq. 1-2) contradicts with the fact that equilateral triangle edges are in the same length, and more importantly, three limb leads could only construct a triangle (not equilateral) for less than 50% of the cardiac cycle [66].

### **1.2.2 The WCT Measurement**

Wilson assumed the WCT has a zero potential, which was found incorrect and attracted immediate interests among researchers to measure this systematic error in electrocardiography. The WCT measurement methods can be categorized into two different perspectives.

In the first approach, the human body is immersed in a large homogeneous conductor to measure the potential difference between the WCT and the assumed zero potential (the water itself). In 1938, Eckey and Frohlich immersed a human body into a full bathtub and determined the WCT amplitude to be in a range of 0.2-0.3 mV [67]. A year later, Burger and Wuhmann conducted the same experiment and immersed five men into a bathtub filled by water and reported an amplitude of 0.26 mV for WCT [68]. In 1946, Wilson submerged a

human in the Lake Michigan and found that the average absolute amplitude of the WCT could be as large as 0.15 mV [16]. Dolgin et al. repeated the same experiment with different adjustments in 1949. They confirmed that the WCT is not zero, and its amplitude varies in different subjects [69]. In 1954, Bayley et al. and Bayley and Kinard encased the body of volunteers inside a metal structure and immersed it in water for the duration of the recording [65], [70]. They found out that the WCT is not steady, and its amplitude could be as large as 0.4 of Einthoven's leads during the cardiac cycle [65], [70], [71]. Thus, they used three rheostats, adjusting the weights of the three WCT components, which led to minimising the WCT amplitude [65]. The legitimacy of the first approach was undermined by a variety of factors, including the effect of water pressure on ECG recording and the degree of the conductivity of surrounding water [72]. Additionally, the zero potential of surrounding water [16], [48] and the widespread use of this method [73] have been questioned.

In the second approach, the *zero potential* of the human body was measured using either numerical methods [15], [74]–[76] or surface potential mapping [77]–[79]. In these methods, the zero potential is not exactly aligned with the WCT definition. However, they referred to it as Wilson Central Terminal. The numerical methods are developed based on the theory that the summation of the electrical potential at the body surface should be zero [15]. Miyamoto et al. used 128 electrodes placed on the thorax and averaged their potentials to estimate the amplitude of the human reference point. They reported the average value of the WCT as -0.169 mV in 10 normal volunteers and -0.051 mV in all 60 subjects, including the controls and patients [72], [77], [78].

In a third approach, the potential of the right arm, left arm and left leg were directly measured using the right leg as a reference point [80]. A new electrocardiography device was recently developed, which uses the right leg as a new reference point to measure the actual potential of three limbs' electrodes and six chest electrodes. The new ECG device can simultaneously measure new nine unipolar leads in addition to the three limb leads and six precordial leads [80]–[84].

The full development of the new ECG device is not a part of this project. Therefore, the hardware description is shortly discussed in the following section.



### 1.3 Research Motivation

The presented literature review discussed the evolution of electrodes' placement in electrocardiography. There were different opinions on choosing the optimal location for both the exploring and the reference electrodes to record the chest leads. Wilson had a great influence to the development of precordial leads. He published different hypotheses, which proved to be partially incorrect over time. However, these hypotheses were (and still are) at the foundation of precordial leads standardisation.

Wilson's first hypothesis pertaining the best placement of the reference electrodes was known as the 'indifferent electrode' theory. He believed that the reference electrode could be placed anywhere on the body, as long as it was far from the exploring electrode. Later, he found that although the reference electrode was placed far from the heart, it caused distortion on the recorded chest leads. Therefore, he published his second theory in the reference electrode's placement. He introduced the Wilson Central Terminal as a new reference point, which he believed its potential amplitude to be zero. This theory was also proved to be wrong during the time in two different ways:

- Comparison of different reference electrodes: some researchers compared the WCT reference point with other possible reference points. Eleven studies in the period of [1936-1950] made this comparison. The WCT was found as an ideal reference point only in four of the studies. Three studies found the WCT and other compared reference points equally desirable; three studies found the right arm as the best reference, and one study chose the Spine of right scapula the most ideal reference point.
- Measuring the WCT amplitude: there are only a few studies in measuring the WCT amplitude in the period of [1938-1954]. They found the WCT was not constant during the cardiac cycle, and the WCT has a minimum amplitude of 0.15 mV and a maximum amplitude of 0.4 percent of lead II.

A summary table including the reviewed different configurations of electrodes placement with their clinical features is presented in Table 1-1.

Furthermore, the heart was theorized to act as a current source, and the electrocardiography model measured bio-currents using a very sensitive galvanometer (string galvanometer). Einthoven did not include the right leg in the cardiac conduction model, as the right leg is the most distant limb from the heart. Furthermore, there is no evident current pathway that includes the heart when the instrument is connected between the two legs. In other words, ECG recordings were intended as a measure of the net current impressed by the heart circulating into an external circuit closed by the measurement instrument. Therefore, Wilson could complete the transformation from the equilateral triangle (Einthoven's triangle) to the equivalent star circuit (originating the augmented leads) when he faced the problem of finding a reference for precordial leads. In theory, if each of the Einthoven leads measures the net current impressed by the heart between the two limbs, averaging all the electrodes together should give the best approximation of the point of origin, the neutral point of the cardiac electrical activity.

Impractical use of current measurement devices and the link between current and voltage resulted in the replacement of all ECG current measurements with voltage. However, this replacement neglected that measuring voltage instead of current requires dealing with the different impedances of body sections. In fact, each lead is interpreted as the voltage drop across a composed resistance (impedance, as a matter of fact) due to the net current impressed by the heart to the points of measurement based on Ohm's law ( $\text{Voltage} = \text{Resistance} * \text{Current}$ ). For example, lead I in Figure 1-5 can be interpreted as the drop of voltage across the sum of the contact impedance at both electrodes that includes the impedance of the two arms and the impedance of the chest across the shoulders that changes with respiration.

The current and voltage measurements are perfectly interchangeable if the body is simply considered as a homogeneous volume conductor (constant resistance) with the limb electrodes placed at equal distance with no or negligible contact impedance. However, in real life, recording the contact impedance imbalance between the ECG electrodes is often not verified. Additionally, the limb leads are measured across different sections of the chest, which are different in shape, and their resistance changes with respiration and body posture, resulting in adding a frequency-dependent delay and a phase difference between the voltage

and current. The modified phase relationship between the voltage and current may also affect the limbs' potential, and consequently, the WCT. Moreover, as the voltage potential difference between the reference point (right leg) and the other limb electrodes are used to measure the RA, LA and LL potentials, different body and contact impedances may impose different delays upon the limb potentials, resulting an unpredictable alteration of WCT [81], [84].

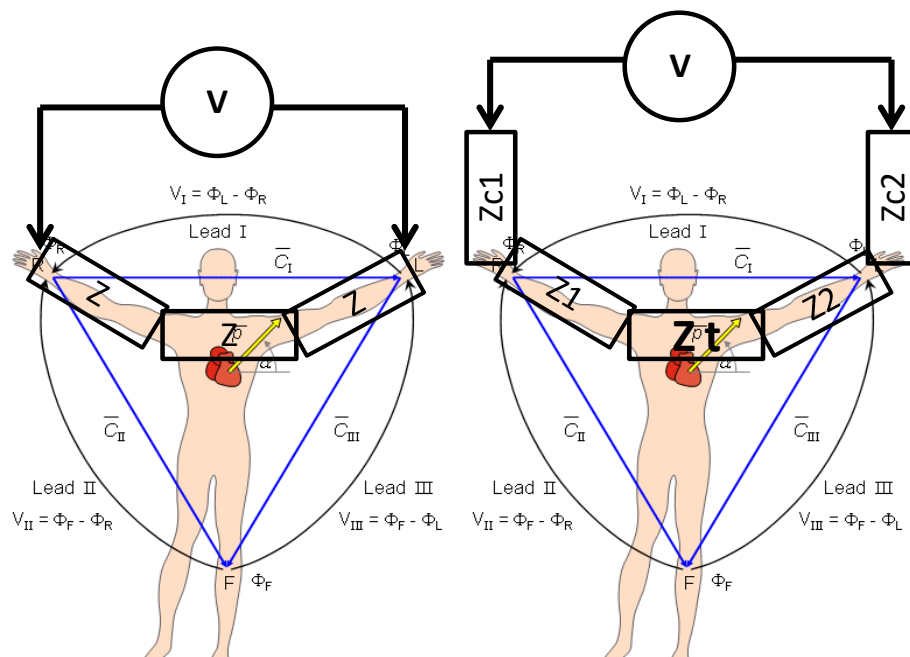


Figure 1. 5 Ideal measurement of lead I vs real measurement of lead I. Left panel shows idealized measurement of lead I using voltage; right panel refers to real measurements of lead I in which includes contact impedances ( $Z_{c1}$  and  $Z_{c2}$ ) and variable impedance of torso ( $Z_t$ ).

Based on the Einthoven theory, if the limb electrodes are placed on the same distance from the heart, the WCT presents the potential of the dipole. However, it is not the case in practice. The WCT amplitude is highly dependent on where the limb electrodes are placed (Eq. 1-7). Hence, it is evident that the amplitude of average limb potentials would not be negligible. On the other hand, the location of the limb electrodes influences the shape and amplitude of precordial leads [85]. As our device uses the right leg as the reference point to measure the potential of the electrodes on the chest, the WCT variation does not affect the true unipolar leads. On the other hand, the true unipolar leads are robust and independent from the limb electrodes' displacement.

## 1.4 True Unipolar ECG recording device

The new ECG device was designed to record traditional ECG signals in addition to the nine true unipolar leads, including three limb potentials and six unipolar chest leads. The true unipolar leads are the raw biopotential measured from the exploring electrodes directly referred to the right leg (RL) (Figure 1-6). Although the right leg was not included in the original ECG montage, it was added as a necessary return grounding for voltage amplifier as well as a way to reduce the interference from external electric fields [86]. Reduction of interference from external electrical fields is usually achieved with a technique known as a driven right leg or right leg driver, which typically implies an injection of a small current into the body (via the right leg electrode) and measuring amplifier circuits (via their reference terminal). In some specific biopotentials applications, the right leg driver is avoided using a technique known as voltage reference bootstrap, which might result in reducing the common noise capture. [2], [15], [86].

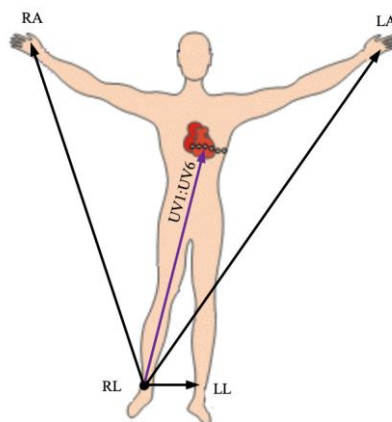


Figure 1. 6 In our approach, the limb potential and unipolar chest lead are measured in respect to the right leg.

Driven right leg circuitries (DRLs) are widely used for the majority of the designs. Using the DRL increases patient safety because the human body is not directly grounded [2], [86], [87]. Figure 1-7 shows an example of the DRL application. As can be seen, the human body is driven by a measure of the common mode signal at the measuring electrodes while the amplifier is directly grounded. The technical documentation of the INA118 can be found in [88].

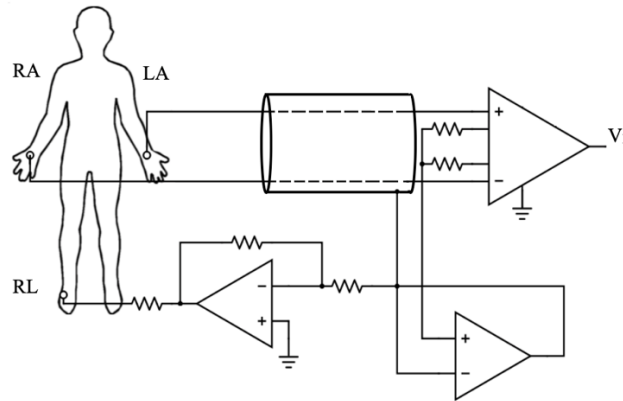


Figure 1. 7 ECG amplifier using right leg driver (lead I)

We designed our hardware around the instrumentation amplifier INA116 [89], manufactured by Texas Instruments, Dallas, Texas USA (Burr-Brown series). According to the part specifications, its bias current (i.e. the load to the physiological signal source) is typically only 5 fA. This extraordinarily small value is achieved by the combination of an extremely high input impedance with a relatively small parasitic capacitance and an embedded active guard ring buffer (see technical documentation [89] for precise details). In order to preserve the mentioned characteristics, the printed circuit board is designed to take advantage of the embedded active guard ring amplifier on a Teflon substrate. Although the guard ring amplifier's primary job is to reduce the noise pick-up at cable and board connections, as this offers a replica of the input signal, we also use it to measure the raw voltage of the WCT components [81], [83], [84], [90].

To ensure high conductivity of connections between pins and exposed pads on the board, the latter are silver-plated by immersion during manufacturing. To avoid mearing of solder under the chip body and between pins during soldering, the chip body is sealed in position prior to soldering, using a suitable printed circuit board with a non-conductive epoxy resin. As an additional precaution, the conductivity between electrode connections and chip pins is verified before soldering, using a multimeter. Each pin of the INA116 is then manually soldered to the pad using lead-free silver-based paste with a 0.2 mm diameter hot iron tip. To further minimise parasitic capacitance at the board level, the guard ring pattern is repeated on each layer of the board, and aside from the chips' necessary connections, no other traces are routed in the area under each INA116. As a last precaution, as recommended in the existing literature, wire connections to the chip are directly soldered to the board on the top layer (no

thru-hole connections) [91]–[93]. Finally, the assembled board is coated with conformal coating to protect it from moisture that could contaminate the board due to its use in the hospital environment (frequent cleaning and wiping of the enclosure/cables with disinfectant).

The simplified schematic of the hardware, limited to the four limbs and one of the precordial leads, is depicted in Figure 1-9. Protection from electrostatic discharges is achieved by interconnection of a single high-precision low-noise Panasonic surface mount ECG series 100 k $\Omega$  resistor. Protection against defibrillation discharges and simultaneous high-impedance biasing of the INA116 electrodes' connections is achieved by parallel connection of low-voltage activation gas discharge tubes with an arc voltage as low as 15 V [94]. Such connections protect the sensitive chip inputs even for voltages that are lower than the embedded overvoltage protection [94]. Discharge tubes also offer the perfect biasing pathway for INA116 due to their nominal resistance  $>10$  G $\Omega$  and a negligible parasitic capacitance. The gas discharge tubes are not represented in Figure 1-8 to avoid cluttering.

As mentioned, and as it is possible to infer from the schematic, the guard buffer of the left-leg, left-arm, and right-arm electrodes are also used to measure the WCT components' voltages directly. The gain set for the INA116 chips is 1 V/V, achieved by leaving pins 1 and 8 floating (not noted in Figure 1-8). Necessary gain and band pass filtering is achieved by two AC coupled active non-inverting low-pass filters gaining 10 V/V and 100 V/V respectively. Each gain cell is designed around the amplifier chip OPA140 [89]. Aside from its very low-noise figure, the OPA140 has been selected because of its high slew rate, immunity from phase inversion, and very low current-bias. Owing to these characteristics, we have designed a high-gain non-inverting band-pass filtering gain cell that does not require additional biasing and copes well with the frequent swings between saturation voltages due to ECG artefacts. Aside from the value of some passive components to achieve different gains, the gain cells are identical. The simplified schematic of the gain cell is depicted in Figure 1-9.

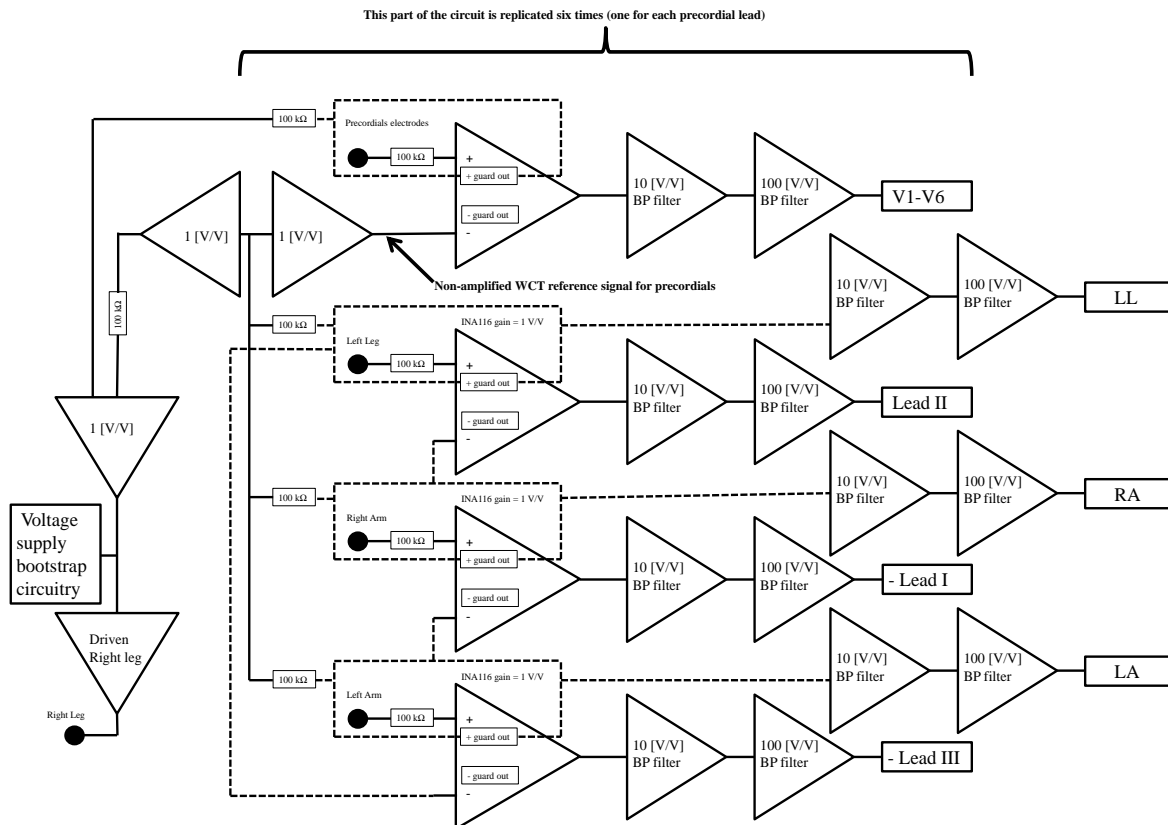


Figure 1. 8 Simplified schematic limited to limbs' connections and one of the precordial leads.

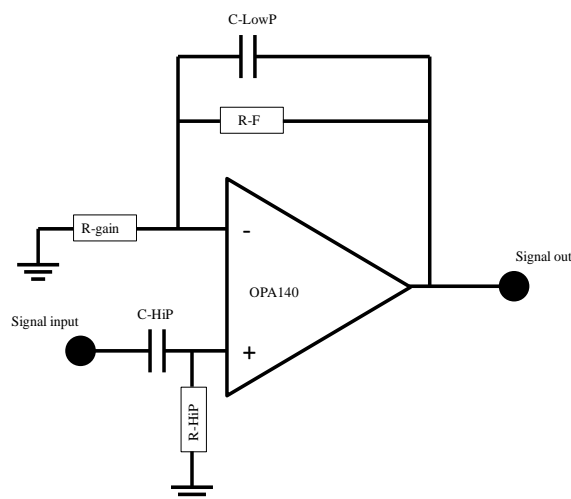


Figure 1. 9 Active band-pass filter gain cell, see Table 1-2 for components' values.

In order to achieve a diagnostic quality ECG, both the high-pass and low-pass corner frequencies of the gain cell are set with capacitors, whose value has been selected to be larger

than the theoretical values. In this way, even in the worst-case scenario of a  $-10\%$  value due to the capacitor tolerances, the required bandwidth is assured. Frequency content normalization to the diagnostic bandwidth is operated via software after the signal acquisition. Components' values are reported in Table 1-2 for both gain cells. Differences between values of components are highlighted in bold. As an additional precaution, high-precision Murata ceramic capacitors have been used.

Table 1. 2 Summary of components' values for the gain cells.

<b>Component</b>	<b>10 V/V Gain Version</b>	<b>100 V/V Gain Version</b>
C-HiP	47 $\mu$ F	47 $\mu$ F
R-HiP	100 k $\Omega$	100 k $\Omega$
C-LowP	15 nF	1.5 nF
R-F	100 k $\Omega$	1 M $\Omega$
R-gain	10 k $\Omega$	10 k $\Omega$

As noted in Figure 1-9, the circuit includes a modified voltage bootstrap circuitry [81], [82], [87], [90], [95] that directly drives the reference voltage of the circuit with a damped version of the average of all the electrodes. This solution proved successful in all of our past circuit implementations [81], [90], [96], particularly when the right-leg connection is included in the average. However, for this implementation, we introduced a driven-right-leg circuitry designed and dimensioned to contain the current drive to 20  $\mu$ A [86], [97], [98]. The input signal for the driven-right-leg circuitry is the non-amplified average of the measurement electrodes (see Figure 1-9).

The entire circuit is powered by a dual 9 V power supply formed by two 9 V batteries in series that proved sufficient for a day of recordings in the hospital. Digital conversion and data logging is operated at a 16-bit depth over the range of  $\pm 5$  V and with a sample rate of 800 Hz by the BIOADC [98], powered directly by the USB connection to a host laptop computer (battery-powered). Necessary anti-aliasing low-pass filtering at the Nyquist frequency is embedded in the BIOADC. The entire system is hosted on a standard hospital instrumentation trolley that allows easy transportation of the device around rooms, wards and ambulatories for the recording.



## 1.5 List of Publications

The work presented in this thesis has resulted in seven peer reviewed works as leading author, one published ECG dataset, and three peer reviewed journal papers as a co-author. The full text of publications is provided in the appendix B.

The ECG recorded dataset was published on Physionet platform as:

- **H. Moeinzadeh**, G. Gargiulo, “*Wilson Central Terminal ECG Database*”. PhysioNet 2019. Available at: <https://doi.org/10.13026/f73z-an96>

I was a co-author of three peer-reviewed journal papers, which are listed below:

1. G. D. Gargiulo, P. Bifulco, M. Cesarelli, A. L. McEwan, **H. Moeinzadeh**, A. O’Loughlin, M. I. Shugman, J. C Tapson, and A. Thiagalingam, “*On the ‘Zero of Potential of the Electric Field Produced by the Heart Beat’. A Machine Capable of Estimating this Underlying Persistent Error in Electrocardiography*” *Machines*, vol. 4, p. 18, Oct. 2016
2. G. D. Gargiulo, P. Bifulco, M. Cesarelli, A. L. McEwan, **H. Moeinzadeh**, A. O’Loughlin, M. I. Shugman, J. C Tapson, and A. Thiagalingam, “*On the Einthoven Triangle: A Critical Analysis of the Single Rotating Dipole Hypothesis*” *Sensors*, vol. 18, p. 2353, Jul. 2018
3. K. Rajesh N. V. P. S., R. Dhuli, P. Pławiak, G. R. Naik, **H.Moeinzadeh**, G. D. Gargiulo, and S. Gunnam. “*Towards Real-Time Heartbeat Classification: Evaluation of Nonlinear Morphological Features and Voting Method,*” *Sensors*, vol. 19, p. 5079, Nov. 2019

I was a lead author of seven published papers including two journal papers, one peer reviewed book chapter and four conference papers.

1. **H. Moeinzadeh**, G. D. Gargiulo, P. Bifulco, M. Cesarelli, A. L. McEwan, A. O’Loughlin, M. I. Shugman, J. C Tapson, and A. Thiagalingam, “*Computing a new central terminal for ECG recording using combined genetic algorithm and linear regression from real patient data*”. In: *Proceedings of the Genetic and Evolutionary Computation Conference Companion (GECCO17)*. 2017. p. 293–4.

2. **H. Moeinzadeh**, G. D. Gargiulo, P. Bifulco, M. Cesarelli, A. L. McEwan, A. O'Loughlin, M. I. Shugman, J. C Tapson, and A. Thiagalingam, “*Minimize Wilson Central Terminal Using Genetic Algorithm*”. *Hear Lung Circ.* 2018 Jan 1;27:S330.
3. **H. Moeinzadeh**, P. Bifulco, M. Cesarelli, A. L. McEwan, A. O'Loughlin, M. I. Shugman, J. C Tapson, A. Thiagalingam, and G. D. Gargiulo, “*Minimization of the Wilson’s Central Terminal voltage potential via a genetic algorithm*”. *BMC Res Notes.* 2018 Dec 20;11(1):915.
4. **H. Moeinzadeh**, G. Gargiulo, P. Bifulco, M. Cesarelli, A. O’Loughlin, M. I. Shugman, and A. Thiagalingam, “*A Modern Wilson’s Central Terminal Electrocardiography Database*” *Hear. Lung Circ.*, vol. 27, pp. S293–S294, 2018
5. **H. Moeinzadeh**, J. Assad, P. Bifulco, M. Cesarelli, A. L. McEwan, A. O’Loughlin, M. I. Shugman, J. C. Tapson, A. Thiagalingam and G. D. Gargiulo. “*Einthoven Unipolar Leads: Towards a better understanding of Wilson Central Terminal*”. In: 2019 International Conference on Electrical Engineering Research & Practice (ICEERP). IEEE, 2019:1–4. (Awarded best paper)
6. **H. Moeinzadeh**, J. Assad, P. Bifulco, M. Cesarelli, A. L. McEwan, A. O’Loughlin, M. I. Shugman, J. C. Tapson, A. Thiagalingam and G. D. Gargiulo. “*Unipolar Cardiac Leads Between History and Science*” in *Biomedical Signal Processing*, (pp. 203–224), 2019.
7. **H. Moeinzadeh**, J. Assad, P. Bifulco, M. Cesarelli, A. O’Loughlin, M. I. Shugman, and A. Thiagalingam, G. Gargiulo, “*WCTECGdb: A 12-Lead Electrocardiography Dataset Recorded Simultaneously with Raw Exploring Electrodes’ Potential Directly Referred to the Right Leg*”. *Sensors* 2020; 20:3275.

In addition, the following papers are currently under consideration for publication (at the time of submission):

1. **H. Moeinzadeh**, J. Assad, P. Bifulco, M. Cesarelli, A. L. McEwan, A. O'Loughlin, M. I. Shugman, J. C Tapson, and A. Thiagalingam, and G. D. Gargiulo, “*On the resemblance between Wilson Central Terminal (WCT) and -2/3 of augmented Foot lead (aVF)*”, **Submitted** to *Applied Science* journal, 2020.

2. **H. Moeinzadeh**, J. Assad, P. Bifulco, M. Cesarelli, A. L. McEwan, A. O'Loughlin, M. I. Shugman, J. C Tapson, A. Thiagalingam, and G. D. Gargiulo “*ECG abnormalities detected in Non-ST-segment Elevation Myocardial Infarction patients with a novel ECG device*”, **Submitted** to JACC case report, 2020

## 1.6 Thesis Organization

*Chapter 1* of the presented thesis provides a comprehensive literature review of the evolution in electrocardiogram leads. This chapter is partially published as a book chapter in the Biomedical Signal Processing book.

*Chapter 2* introduces the Wilson Central Terminal ECG database, which is published on the physionet platform. This chapter present the WCT signal features. Chapter 2 is a combination of one peer-reviewed conference paper, and a journal paper.

*Chapter 3* presents characterization of the limb’s potential, and whether the WCT and -2/3aVF are equivalent. A reformatted version of this chapter is also combination of submitted peer-reviewed journal paper and published an IEEE conference paper.

*Chapter 4* presents clinical cases to discuss the influence of the WCT on recording precordial leads. This chapter is partially submitted as a case report to the JACC-case report journal paper.

*Chapter 5* presents an expert approach to minimise the WCT using the genetic algorithm. This chapter is combination of one peer-reviewed journal paper and two conference papers.

*Chapter 6* concludes the thesis by discussing future directions and the overall contribution of the research.

*Appendix A* provides MATLAB scripts of the graphic user interfaces developed for ECG recordings visualization with its corresponding user guidelines.

*Appendix B* presents the full text of published conference and journal papers.

## Chapter 2 Wilson Central Terminal ECG database (WCTECGdb)

This chapter introduces the WCTECGdb dataset, which was published on the Physionet platform. First, a brief background, discusses the differences between precordial leads and unipolar chest leads. It then describes the WCTECGdb features. Finally, the WCT signal characteristics is fully described in this chapter.

*Some of the work presented in this chapter has been published in:*

- *H. Moeinzadeh, G. Gargiulo, “Wilson Central Terminal ECG Database”. PhysioNet 2019. Available at: <https://doi.org/10.13026/f73z-an96>*
- *H. Moeinzadeh, J. Assad, P. Bifulco, M. Cesarelli, A. O’Loughlin, M. I. Shugman, and A. Thiagalingam, G. Gargiulo, “WCTECGdb: A 12-Lead Electrocardiography Dataset Recorded Simultaneously with Raw Exploring Electrodes’ Potential Directly Referred to the Right Leg”. Sensors 2020;20:3275.*
- *H. Moeinzadeh, G. Gargiulo, P. Bifulco, M. Cesarelli, A. O’Loughlin, M. I. Shugman, and A. Thiagalingam, “A Modern Wilson’s Central Terminal Electrocardiography Database” Hear. Lung Circ., vol. 27, pp. S293–S294, 2018.*

## 2.1 Abstract

In this chapter, a unique dataset of surface electrocardiography is presented, which aside the standard 12-lead signals include the raw electrode biopotential for each of the nine exploring electrodes composing the 12-lead ECG system directly referred to the right leg as well as the Wilson's Central Terminal voltage potential (average of left arm, left leg and right arm potentials). This dataset comprises recording from 147 patients at Campbelltown Hospital, NSW Australia. With the unique 15-lead ECG device, I have been able to overcome the difficulties of recording the Wilson's Central Terminal in a clinical setting and measure the potential of the chest electrodes independent from the WCT. I present an approach to measure the influence of the WCT on recording the precordial leads, which is referred as "*the WCT error measurement*" in this chapter. The recorded data confirmed that the WCT does not have negligible impacts on recording the precordial leads for 72 percent of patients. the WCT has standard ECG characteristics such as a P-wave and a T-wave with a high variability during the cardiac cycle.

## 2.2 Background

The 15-lead ECG device can record three limb leads (I, II, and III), six precordial leads ( $V_1: V_6$ ), and the nine unipolar leads including the potential of three Einthoven limbs' electrodes (LA, RA, and LL) and six chest electrodes ( $UV_1: UV_6$ ) [80], [84], [90]. The average potential of three Einthoven limbs' potential yields Wilson Central Terminal (WCT). Furthermore, the precordial leads can be obtained using the difference potential of unipolar chest leads and Wilson Central Terminal.

$$WCT = \frac{1}{3}(LA + RA + LL) \quad (2-1)$$

$$V_1:V_6 = UV_1:UV_6 - WCT \quad (2-2)$$

Three Einthoven limbs' potential have all the ECG segments, including P-wave, QRS, and T-wave. The left leg has the lowest potential among three limbs as it has the most distance from the heart. Furthermore, the left arm has the highest potential among Einthoven limbs in

only 47 percent of the patients (67 out of 147). As it is the first time to record three Einthoven limbs' potential, they are fully discussed in chapter three.

The WCT has been known as the zero-reference point to record precordial leads, while it was found having high amplitude [16], [67]–[71]. Therefore, it is fair to consider the WCT as a systematic error, which could remove important information from the actual potential of the chest electrodes (Eq. 2-2). As the real potential of chest electrodes ( $UV_1$ :  $UV_6$ ) and the precordial leads were recorded simultaneously, it would be possible to investigate the influence of the WCT signal on the precordial leads' shape and amplitude. In other words, the WCT error measurement could be possible by calculating the difference between the precordial leads and unipolar chest leads. The WCT error is embedded in every precordial lead either recorded from patients with cardiac abnormalities or healthy individuals. In this chapter, the statistical analysis of the WCT error for 147 patients is presented, and the clinical influence of WCT for NSTEMI patients is discussed in chapter four. Database characteristics

The 15-lead ECG device can record signals using two different systems simultaneously [80]–[84]. The ECG signals were recorded from patients at the Campbelltown hospital (New South Wales, Australia) over three years (2016-2019). All the patients volunteered for this study and gave written consent. This study was approved by the Ethics Committee of the South West Sydney Health District on 23rd September 2015 with the protocol number HREC/15/LPOOL/302.

I published our recordings during the first two years in the Physionet platform. The dataset was published under the name of Wilson Central Terminal ECG database (WCTECGdb) [99], [100]. Each recording was segmented to ten seconds sections. Consequently, as the duration of the recording is different, each patient has a different number of segments, ranging between one to thirty-one. The WCTECGdb contains 540 ten seconds segments recorded from 92 patients (27 were female) [99], [101], [102].

During the past year (2018-2019), 55 additional patients were recorded. Therefore, both published and recent records were included for the analysis performed in this thesis. Hence, the dataset comprises 147 patients (48 were female) with average age of 65.20 (with a standard deviation of 13.56). The majority of the patients had a history of cardiac disease and

had been admitted to the hospital from the emergency department because of difficulties in breathing and/or persistent chest pain.

This dataset comprises raw and noise removed signals for the three limb leads, six precordial leads, nine unipolar leads including three WCT components, and six chest electrodes' potential. As the WCT is the average of the limb potential, only the cleaned WCT signal was added into the dataset. The bandpass filter (0.05 Hz-149 Hz) and a 50 Hz with harmonics notch IIR filter were used to clean the signals. Both filters are 50<sup>th</sup> order and applied with a zero-phase lag [102].

Supplementary information was included for each recorded segment, such as the patient's 'age', 'gender', 'patient diagnosis', and the 'reconstructed precordial' (if there is any). Each file in the dataset contains the signals and supplementary information listed in Table 2.1. Cleaned and raw signals are included in the dataset. The raw signals are specified by '-raw' in the dataset (e.g., V<sub>2</sub>-raw) and refer to originally recorded signals prior to the noise filtering process. The WCT signal is only presented in a clean format [102].

Table 2. 1 The signal names and the detail of the recording presented for each segment.

<b>Signals</b>	I-raw	I	limb lead I
	II-raw	II	limb lead II
	III-raw	III	limb lead III
	V <sub>1</sub> -raw: V <sub>6</sub> -raw	V <sub>1</sub> :V <sub>6</sub>	precordial leads
	LA-raw, RA-raw, LL-raw	LA, RA, LL	three WCT components
	UV <sub>1</sub> -raw: UV <sub>6</sub> -raw	UV <sub>1</sub> : UV <sub>6</sub>	unipolar chest leads
		WCT	the WCT signal
<b>Detail</b>	Age Gender Patient diagnosis Reconstructed precordials*		

\* Only included for 8 segments that needed to be synthesized for some of precordial leads.

Synthesized precordial leads were included instead of directly measured signals for a total of eight segments (from 5 patients), due to poor signal to noise ratio and/or the final stage amplifier saturation. The signal saturation usually is seen when large contact impedances and electrode polarization generate large DC drifts at the unipolar potential that once amplified by the gain stages result in saturation of the output amplifier. As the potential of chest electrodes (UV<sub>1</sub>: UV<sub>6</sub>) and the WCT signal were recorded, the missing precordial leads could be reconstructed using Eq. 2-2. It should be noted that both cleaned and raw data are

reconstructed for these signals. These signals were flagged in the header file as “reconstructed precordial”, and present the list of patients and signals in Table 2.2 [102].

Table 2. 2 List of patients with reconstructed precordial leads

Patient ID	Segment ID	Reconstructed precordial leads
Patient7	Seg1	V <sub>2</sub> , V <sub>2</sub> -raw
	Seg2	V <sub>2</sub> , V <sub>2</sub> -raw
	Seg3	V <sub>1</sub> , V <sub>1</sub> -raw
Patient8	Seg1	V <sub>1</sub> , V <sub>2</sub> , V <sub>1</sub> -raw, V <sub>2</sub> -raw
	Seg2	V <sub>1</sub> , V <sub>2</sub> , V <sub>1</sub> -raw, V <sub>2</sub> -raw
Patient10	Seg1	V <sub>2</sub> , V <sub>2</sub> -raw
Patient14	Seg1	V <sub>2</sub> , V <sub>2</sub> -raw
Patient31	Seg1	V <sub>2</sub> , V <sub>2</sub> -raw

The diagnosis quantity in the dataset is presented in Table 2.3. Unfortunately, the hospital could not provide us the diagnosis for ten patients, so the patient diagnosis labelled as “not reported” in the header files for those patients.

Table 2. 3 Patient diagnosis list

Patient diagnosis	Count	Patient diagnosis	Count
Angina	1	Non-ST segment elevation myocardial infarction (NSTEMI)	23
Atrial fibrillation	9	Pulmonary embolism-Atrial fibrillation	1
Atrial flutter	1	Pulmonary embolism	1
Atypical chest pain	5	Rapid atrial fibrillation with new cardiomyopathy	1
Cardiomyopathy	1	Rapid atrial fibrillation-pericarditis	1
Chest pain	1	Severe Mitral Stenosis	1
Complete Heart block	1	Sinus bradycardia	2
Congestive cardiac failure (CHF) exacerbation	1	Slow atrial fibrillation	1
Congestive cardiac failure (CCF)	1	ST segment elevation myocardial infarction (STEMI)	4
Coronary artery disease	3	Stable angina	7
Epigastric pain	1	Supraventricular tachycardia (SVT)	2
Fall secondary to alcohol intoxication	1	Syncope	3
Gastritis (non-cardiac chest pain)	1	Unstable angina	1
Hypertrophic obstructive cardiomyopathy	1	Urosepsis	1
Inferior ST segment elevation myocardial infarction (STEMI)	1	Ventricular tachycardia (VT)	3
Myocardial infarction-Type 2	1	Not reported	10



## 2.3 Evaluation metrics

Three consecutive beats were selected from each patient to analysis the recorded signals. The average peak-to-peak amplitude from these three beats for the WCT is measured, which was referred to the *amplitude* of the WCT. Two quantitative measurements are used to show the similarities between two signals (naming  $p$  and  $m$ ):

- Cross-Correlation: It is used to calculate the resemblance between two signals, where  $N$ ,  $\mu$  and  $\sigma$  are number of samples, the mean and the standard deviation of a signal, respectively.

$$Corr = \frac{\sum_{i=1}^N (p_i - \mu_p)(m_i - \mu_m)}{\sigma_p \sigma_m} \quad (2-3)$$

- Sprague and Geer's error [103], [104]: the agreement between two signals ( $m$  and  $p$ ), which both have a length of  $N$ , could be measured using magnitude error ( $M_{S\&G}$ ), phase error ( $P_{S\&G}$ ) and combined error ( $C_{S\&G}$ ).

$$M_{S\&G} = \sqrt{\sum_{i=1}^N p_i^2 / \sum_{i=1}^N m_i^2} - 1 \quad (2-4)$$

$$P_{S\&G} = \frac{1}{\pi} \cos^{-1} \frac{\sum_{i=1}^N p_i m_i}{\sqrt{\sum_{i=1}^N m_i^2 \sum_{i=1}^N p_i^2}} \quad (2-5)$$

$$C_{S\&G} = \sqrt{M_{S\&G}^2 + P_{S\&G}^2} \quad (2-6)$$

## 2.4 WCT characteristics

The WCT initially assumed to be a steady signal with a negligible amplitude. However, in early attempts to record the WCT signal, the WCT was characterised as a high variant signal with a large amplitude [16], [65], [67]–[71]. Although these attempts were a significant breakthrough to show the incorrect assumption associated with the electrocardiography, the legitimacy and widespread usage of these attempts were undermined [16], [48], [72], [73].

The recorded signals from patients using the 15-lead ECG device gives the opportunity to obtain and analysis the WCT characteristics. Given the WCT as a systematic noise that could remove information from the potential of the chest electrodes, analysis of the WCT shape and amplitude could present the amount of this error. In other words, the WCT influences on recording the precordial leads could be measured by finding the dissimilarity between the precordial leads ( $V_1$ :  $V_6$ ) and unipolar chest leads ( $UV_1$ :  $UV_6$ ). In this chapter, the statically analysis of the WCT error on recording precordial leads is discussed. The clinical analysis of the WCT impact on the precordial leads requires conducting a well-powered study [105]. Since the WCTECGdb does not have enough recordings for each cardiac disease yet, the clinical analysis of the WCT on recording the precordial leads is shorty discussed in the chapter four.

### **2.4.1 The WCT shape**

The WCT is constructed by three limbs' potential, which all shows the ECG characteristics such as the P-wave and the T-wave. Therefore, the WCT signal presents with all ECG features. The distribution of the WCT polarity mostly has positive deflection, with some negative deflections and a handful of neutral polarities. The 'neutral polarities' is shown in those signals whose QRS is a bipolar and has an approximately equal positive and negative deflection [96]. Figure 2.1 demonstrates an example of positive, negatives, and neutral deflection of the WCT.

### **2.4.2 The WCT Amplitude**

The WCT peak-to-peak amplitude for three consecutive beats is averaged, which presents the WCT amplitude for each patient. Figure 2.2 shows the WCT amplitude across the whole dataset. The WCT amplitude is in the range of [0.03 1.51] mV with the average and standard deviation of 0.27 mV and 0.19, respectively.

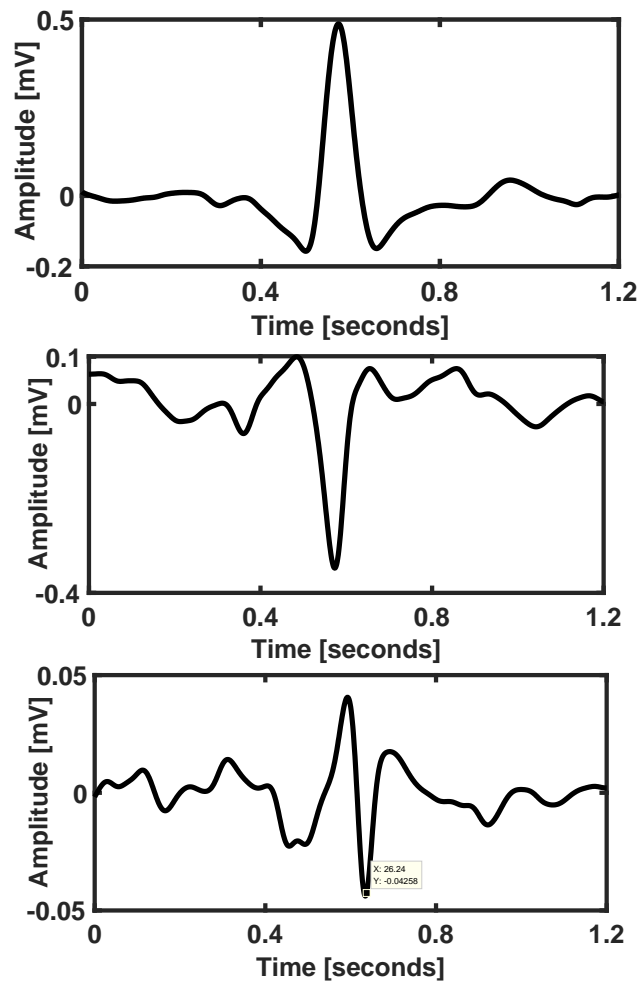


Figure 2. 1 Top panel: the WCT with positive deflection (patient ID 44); middle panel: the WCT with negative deflection (patient ID 50); bottom panel: the WCT with neutral deflection (patient ID 67).

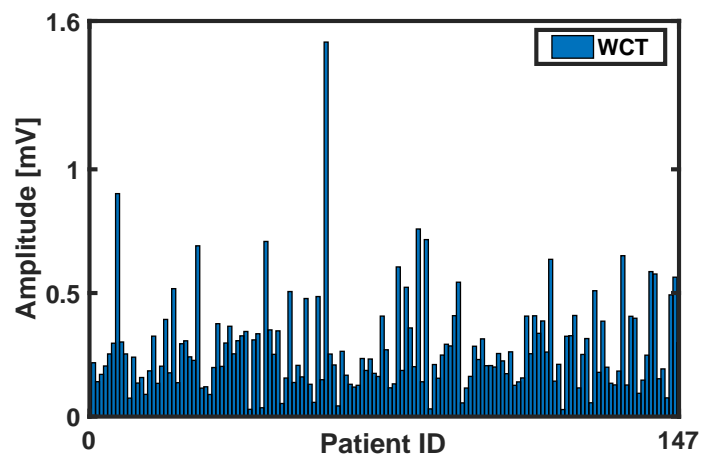


Figure 2. 2 The WCT potential amplitude for 147 patients.

As it can be seen in Figure 2.2, contradictory to the WCT initial assumptions, the WCT has a high amplitude for many patients. However, the WCT amplitude is not a proper metric to show its impact on the shape or amplitude of the precordial leads for two reasons:

- a) The WCT relative amplitude: the WCT amplitude in relation to the precordial leads should be measured to show its real impact on precordial leads. It is a possible scenario that the WCT has high peak-to-peak amplitude, while it has a relatively small amplitude in regard to the precordial leads. Figures 2.3 and 2.4 present two patients with almost the same WCT amplitude, while the WCT has different impacts on each patient's precordial leads. Figure 2.3 shows a patient with 0.21 mV peak-to-peak WCT amplitude, which causes considerable differences between the unipolar chest leads ( $UV_1$ :  $UV_6$ ) and the precordial leads ( $V_1$ :  $V_6$ ). Noted, these changes may/may not be clinically important, and I do not intend to compare these two set of signals clinically in this chapter. Figure 2.4 is an example of a patient with 0.19 mV peak-to-peak WCT amplitude. The precordial leads and unipolar chest leads are almost identical, which shows that the WCT signal has a negligible effect on recording the precordial leads. The combined Sprague and Geers' error ( $C_{S\&G}$ ) is used to show the agreement between the precordial and unipolar chest leads.
- b) P and T waves' amplitudes: The QRS section of the WCT signal is not the only important part of the WCT signal, which influences the precordial leads. The P and T waves in the WCT signal could also remove information from the chest electrodes' potential. Figure 2.5 shows the patient with high peak-to-peak amplitude (0.4 mV) and relatively large P and T waves. Therefore, the WCT has considerable impacts on the P, QRS, and T sections of precordial leads.

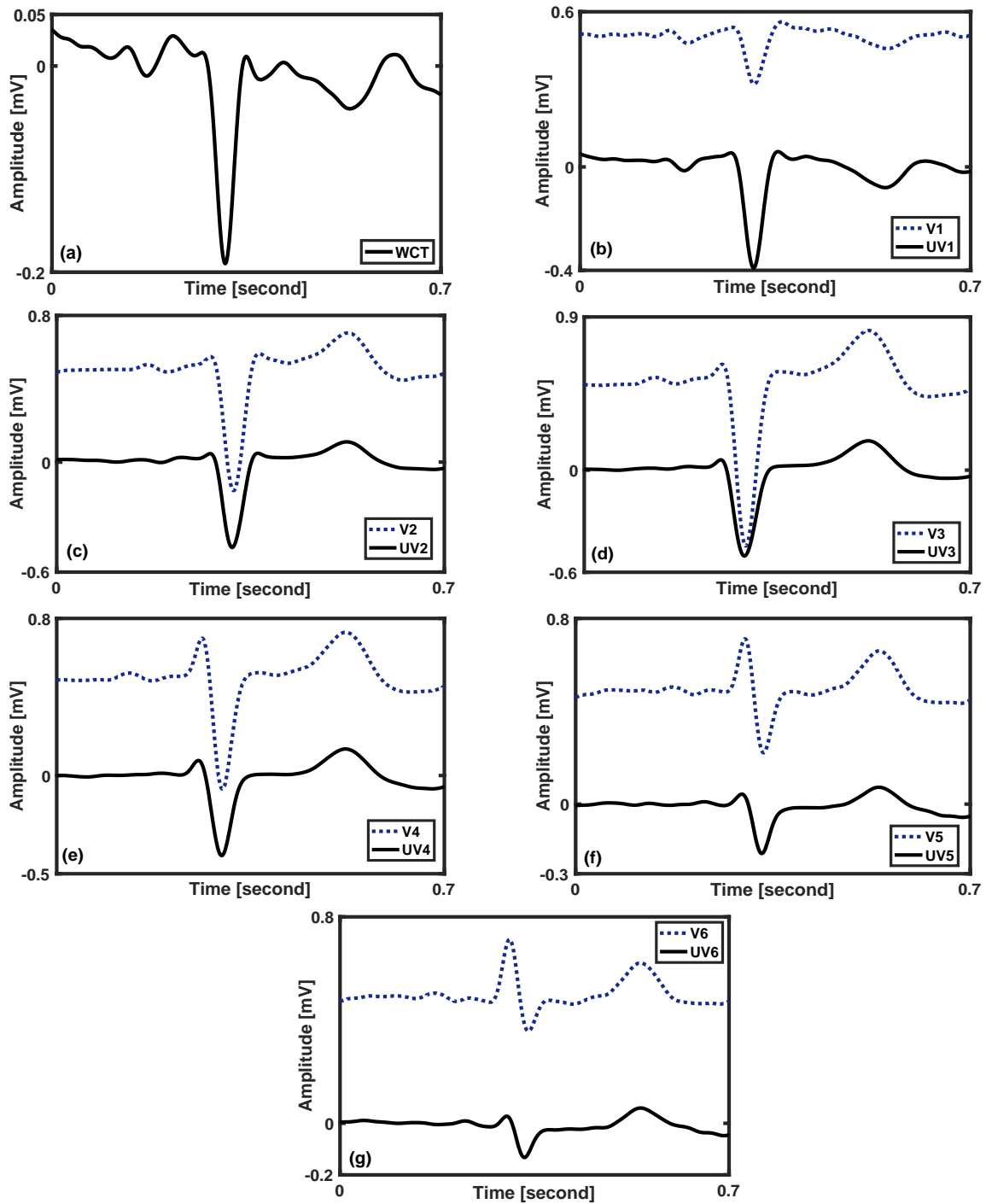


Figure 2. 3 The influence of the WCT error in recording precordial leads. The unipolar chest leads and precordial leads are different in terms of shape and amplitude. The precordial leads are shifted by 0.5 mv from the original place for better visualization. (a) The WCT has a 0.21 mV peak-to-peak amplitude; (b)  $C_{S\&G}$  between  $V_1$  and  $UV_1$  is 0.47; (c)  $C_{S\&G}$  between  $V_2$  and  $UV_2$  is 0.42; (d)  $C_{S\&G}$  between  $V_3$  and  $UV_3$  is 0.75; (e)  $C_{S\&G}$  between  $V_4$  and  $UV_4$  is 0.33; (f)  $C_{S\&G}$  between  $V_5$  and  $UV_5$  is 0.54; (g)  $C_{S\&G}$  between  $V_6$  and  $UV_6$  is 0.66. Recorded from 75 years old female (Patient ID 100).

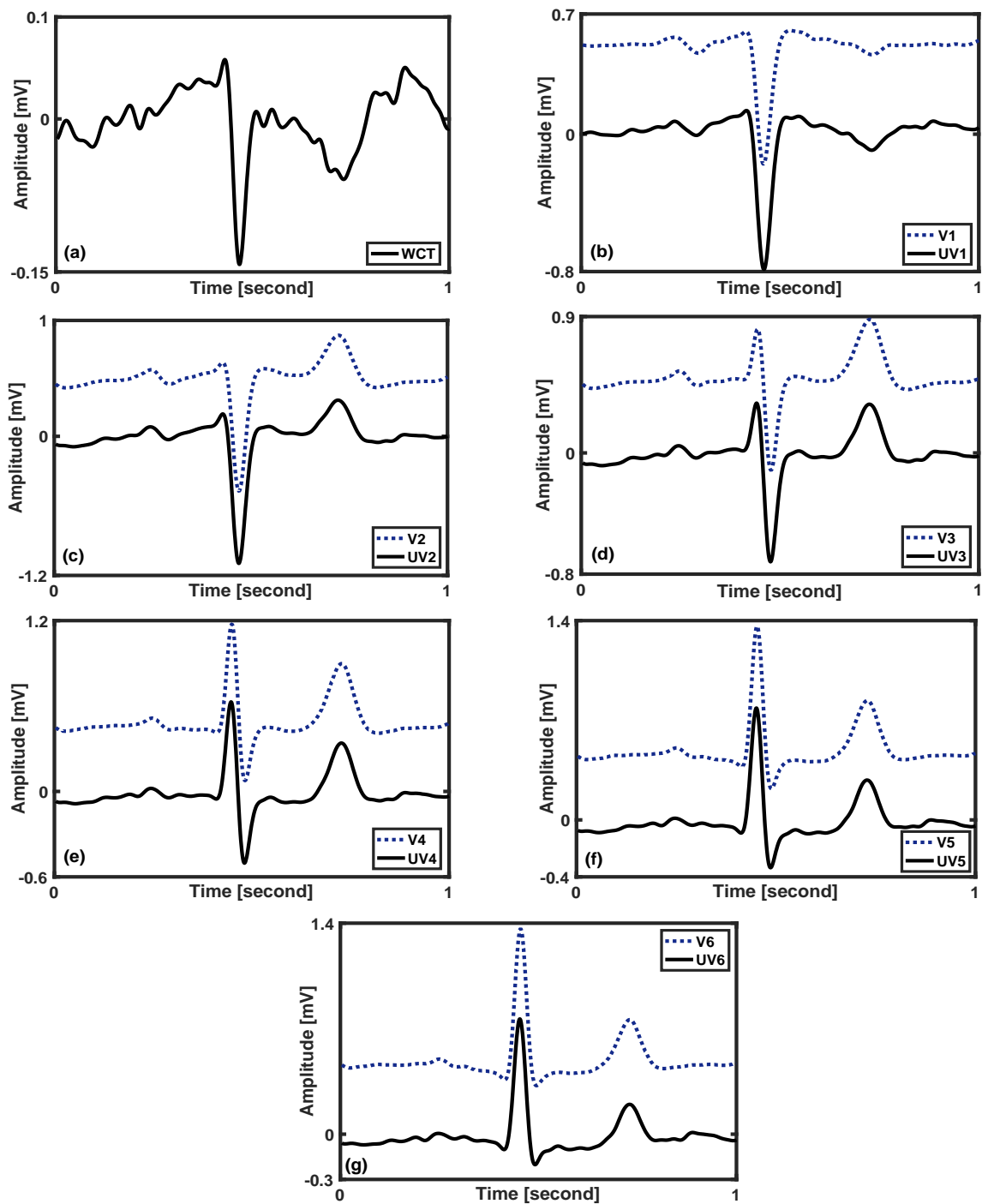


Figure 2. 4 The influence of the WCT error in recording precordial leads. The unipolar chest leads and precordial leads are identical. The precordial leads are shifted by 0.5 mv from the original place for better visualization. (a) The WCT has a 0.19 mV peak-to-peak amplitude; (b)  $C_{S\&G}$  between  $V_1$  and  $UV_1$  is 0.15; (c)  $C_{S\&G}$  between  $V_2$  and  $UV_2$  is 0.07; (d)  $C_{S\&G}$  between  $V_3$  and  $UV_3$  is 0.08; (e)  $C_{S\&G}$  between  $V_4$  and  $UV_4$  is 0.10; (f)  $C_{S\&G}$  between  $V_5$  and  $UV_5$  is 0.12; (g)  $C_{S\&G}$  between  $V_6$  and  $UV_6$  is 0.16. Recorded from 67 years old male (Patient ID 143).

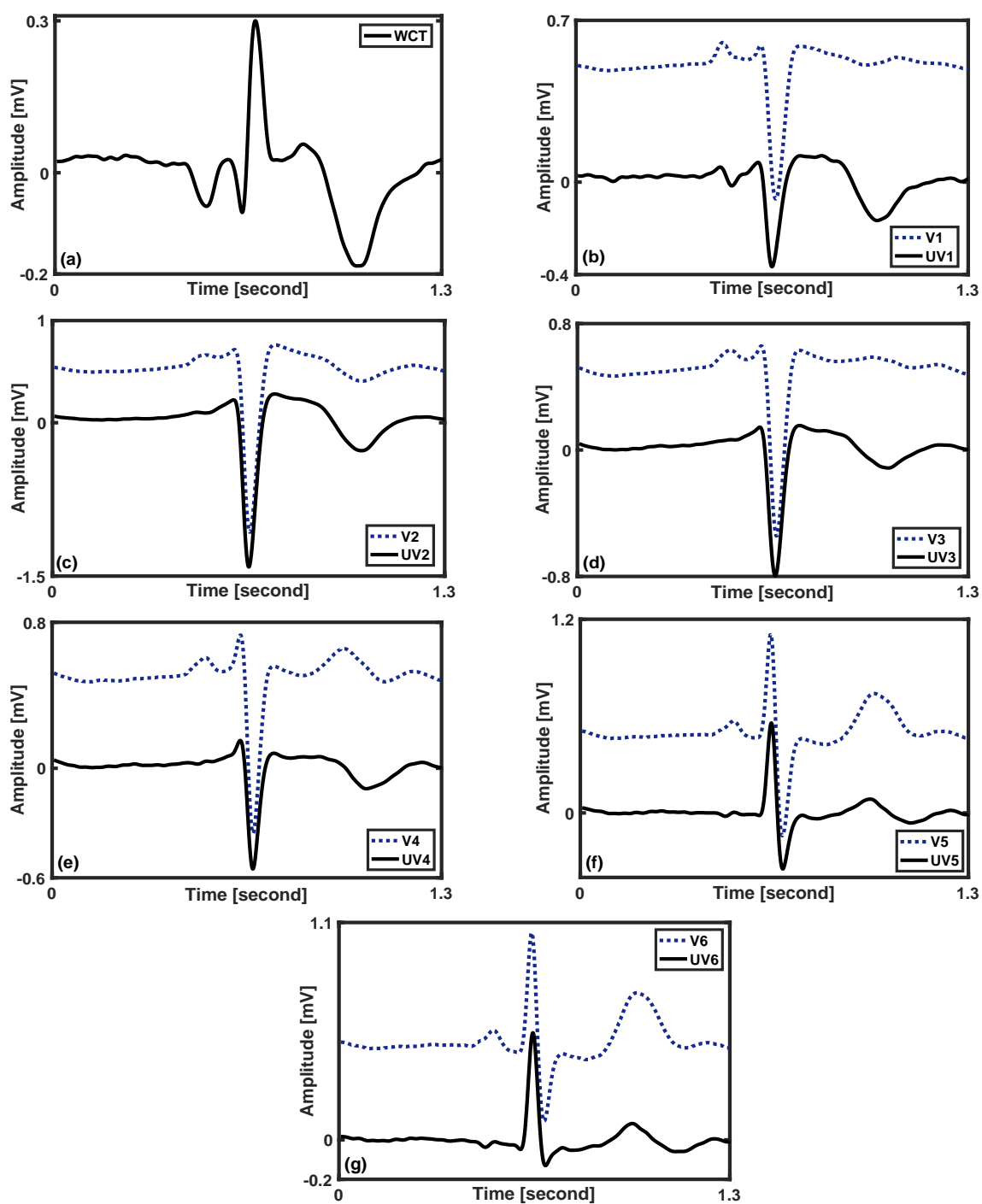


Figure 2. 5 The influence of the WCT error in recording precordial leads. The T and P waves have significant impact on the precordial leads. The precordial leads are shifted by 0.5 mv from the original place for better visualization. (a) The WCT has a 0.4 mV peak-to-peak amplitude; (b)  $C_{S\&G}$  between  $V_1$  and  $UV_1$  is 0.34; (c)  $C_{S\&G}$  between  $V_2$  and  $UV_2$  is 0.11; (d)  $C_{S\&G}$  between  $V_3$  and  $UV_3$  is 0.30; (e)  $C_{S\&G}$  between  $V_4$  and  $UV_4$  is 0.64; (f)  $C_{S\&G}$  between  $V_5$  and  $UV_5$  is 0.64; (g)  $C_{S\&G}$  between  $V_6$  and  $UV_6$  is 0.55. Recorded from 58 years old female (Patient ID 136).

### 2.4.3 The WCT Error measurement

The WCT peak-to-peak amplitude should be considered high or low in relation to the precordial leads' amplitude, and all the WCT sections (P, QRS, and T waves) can have a considerable impact on recording precordial leads. Consequently, the Sprague and Geer's error is used to measure the agreement between the precordial and unipolar chest leads. Since the Sprague and Geer metric calculates the combined phase and magnitude difference between two signals, it would reflect the precise impact of the WCT on recording the precordial leads. We defined ten error classes and plotted the number of patients within each (see Figure 2.6) to illustrate the error distribution among patients. Since there are a few patients having the WCT error greater than 0.9, they are grouped in one class with maximum error threshold of ten. The combined Sprague and Geer error ( $C_{S\&G}$ ) is measured for every pair of precordial and unipolar chest leads (such as  $V_1$  and  $UV_1$ ). If the  $C_{S\&G}$  error of the patients is less than the nominated threshold for all the six precordial leads, a patient is assigned to that error group.

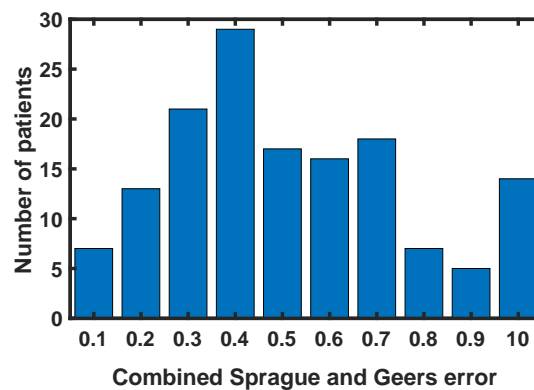


Figure 2. 6 The distribution of the patients having different WCT error.

The Sprague and Geer error presents the similarity between the unipolar chest leads and precordial leads. While an error of 0.1 presents the similarity of the signals, the error value of 10 shows a significant difference between two recorded signals. Therefore, the impact of WCT on precordial leads is expected to be negligible in patients having small  $C_{S\&G}$  error. However, only visual comparison of the precordial and unipolar chest leads within each group can determine if the impact of WCT on precordial leads is negligible. Therefore, this visual comparison is used and divides patients into three groups based on the WCT influences on precordial leads recordings:



- a) The WCT with a *zero impact*: patients having  $C_{S\&G}$  error less than 0.2 show to have identical precordial and unipolar chest leads (see Figure 2.4). About 14 percent of patients (20 out of 147) are categorized in this group (see Table 2.4).
- b) The WCT with a *negligible impact*: patients with  $C_{S\&G}$  error less than 0.3, have the WCT with insignificant impact on recording precordial leads. Therefore, the precordial leads have some minor differences from unipolar chest leads, but still they could be considered the same signals. About 14 percent of patients (20 out of 147) have the WCT with this characteristic (see Table 2.5).
- c) The WCT with a *significant impact*: the WCT has a considerable influence on recording precordial leads. For these patients, the clinical difference between precordial leads and unipolar chest leads should be investigated (see Figures 2.3 and 2.7). About 72 percent of patients (107 out of 147) have the WCT with this characteristic (see Table 2.6).

Table 2.4, 2.5 and 2.6 show the correlation and Sprague and Geer's error for each pair leads of precordial and unipolar chest leads for patients having the WCT with *zero*, *negligible* and *significant* impacts on the precordial leads recording, respectively. Noted, since the Sprague and Geer phase error ( $P_{S\&G}$ ) could be negative, the absolute average is measured for each pair of leads.

Table 2. 4 The correlation and Sprague and Geer's error in patients having the WCT with *zero* impacts on recording precordial leads

	(V <sub>1</sub> , UV <sub>1</sub> )	(V <sub>2</sub> , UV <sub>2</sub> )	(V <sub>3</sub> , UV <sub>3</sub> )	(V <sub>4</sub> , UV <sub>4</sub> )	(V <sub>5</sub> , UV <sub>5</sub> )	(V <sub>6</sub> , UV <sub>6</sub> )
<b>P<sub>S&amp;G</sub></b>	0.06	0.05	0.06	0.07	0.07	0.09
<b>M<sub>S&amp;G</sub></b>	0.08	0.05	0.05	0.05	0.06	0.07
<b>C<sub>S&amp;G</sub></b>	0.11	0.07	0.09	0.09	0.10	0.12
<b>Corr</b>	0.96	0.98	0.98	0.98	0.98	0.97

Table 2. 5. The correlation and Sprague and Geer's error in patients having the WCT with *negligible* impacts on recording precordial leads.

	(V <sub>1</sub> , UV <sub>1</sub> )	(V <sub>2</sub> , UV <sub>2</sub> )	(V <sub>3</sub> , UV <sub>3</sub> )	(V <sub>4</sub> , UV <sub>4</sub> )	(V <sub>5</sub> , UV <sub>5</sub> )	(V <sub>6</sub> , UV <sub>6</sub> )
<b>P<sub>S&amp;G</sub></b>	0.14	0.11	0.13	0.12	0.13	0.14
<b>M<sub>S&amp;G</sub></b>	0.09	0.07	0.09	0.09	0.09	0.09
<b>C<sub>S&amp;G</sub></b>	0.18	0.14	0.17	0.16	0.16	0.18
<b>Corr</b>	0.95	0.97	0.95	0.95	0.96	0.95

Table 2. 6. The correlation and Sprague and Geer's error in patients having the WCT with *significant* impacts on recording precordial leads.

	(V <sub>1</sub> , UV <sub>1</sub> )	(V <sub>2</sub> , UV <sub>2</sub> )	(V <sub>3</sub> , UV <sub>3</sub> )	(V <sub>4</sub> , UV <sub>4</sub> )	(V <sub>5</sub> , UV <sub>5</sub> )	(V <sub>6</sub> , UV <sub>6</sub> )
<b>P<sub>S&amp;G</sub></b>	0.31	0.22	0.28	0.29	0.40	0.45

<b>Ms&amp;G</b>	0.18	0.13	0.15	0.17	0.18	0.20
<b>Cs&amp;G</b>	0.37	0.27	0.34	0.36	0.48	0.52
<b>Corr</b>	0.32	0.80	0.88	0.85	0.82	0.80

Figure 2.7 depicts the correlation drop by increasing the  $C_{S\&G}$  error intervals. The patients with small  $C_{S\&G}$  error (less than 0.3) have a high correlation (greater than 0.95) between unipolar chest leads and precordial leads.

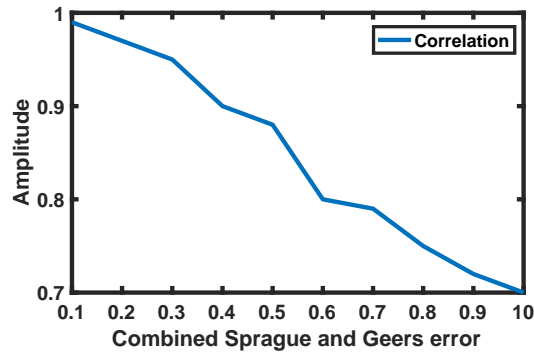


Figure 2. 7 Average correlation between unipolar chest leads and precordial leads within each error class.

As the WCTECGdb was recorded from cardiac patients at hospital, it has some limitations. These limitations include (1) lack of data recordings from healthy subjects; (2) unequal distribution of age and gender in the collected; (3) unequal distribution of data for different cardiac abnormalities. Although the later limitation could be considered as bias in the WCT error analysis, the WCT error is present in every measurement regardless of the disease.

## 2.5 Conclusion

In this chapter, the WCTECGdb dataset is presented, which contains the WCT signal, six unipolar chest leads associated with three Einthoven limb leads and six precordial leads. The data is recorded from 147 patients at Campbelltown Hospital (Campbelltown, Australia). These recordings were partially published on the Physionet platform (92 patients). This chapter also characterised the WCT signal as a systematic error, which has a different influence on recording the precordial leads in every individual. Therefore, the dataset was divided into three groups of patients having *zero*, *negligible*, and *significant* WCT error. The results show that only 14 percent of patients have the WCT with *zero* impacts on the

precordial leads; therefore, unipolar chest leads and precordial leads are identical in patients within this group. The patients with a *negligible* WCT error are shaped 14 percent of the dataset, which they have similar unipolar and precordial chest leads with minor differences. The rest of the patients are categorized as having *significant* WCT error. These records are required a clinical investigation to measure the *real* impact of this error on precordial leads and thus the diagnosis of cardiac diseases.

## Chapter 3 Einthoven Limb Potential

This chapter investigates the veracity of the Einthoven limbs' potential assumption. Then, discuss whether the WCT and aVF are proportional.

*Some of the work presented in this chapter has been published or submitted in:*

- *H. Moeinzadeh, J. Assad, P. Bifulco, M. Cesarelli, A. L. McEwan, A. O'Loughlin, M. I. Shugman, J. C. Tapson, A. Thiagalingam and G. D. Gargiulo. Einthoven Unipolar Leads: Towards a better understanding of Wilson Central Terminal. In: 2019 International Conference on Electrical Engineering Research & Practice (ICEERP). IEEE, 2019:1–4.*
- *Hossein Moeinzadeh, Gaetano D Gargiulo, Paolo Bifulco, Mario Cesarelli, Alistair L McEwan, Aiden O'Loughlin, Ibrahim M Shugman, Jonathan C Tapson, Aravinda Thiagalingam, "On the resemblance between Wilson Central Terminal (WCT) and - 2/3 of augmented Foot lead (aVF)", **Submitted**, Applied Science, 2020.*

### 3.1 Abstract

The Wilson central terminal (WCT) is at the foundation of modern electrocardiography (ECG); it is constructed as an average of the right arm, left arm, and left leg electrodes and is taught as not measurable directly. In addition, it is commonly accepted that the average of the three electrodes is dominated by the left arm (the highest potential) and that the left leg has a negligible amplitude that can be assumed as near zero. The latter assumption yields that the WCT resembles the  $-2/3$  of the augmented Vector Foot (aVF) (also known as augmented foot lead). Since the current ECG device cannot record the WCT components, the validation of these hypotheses was impossible. Using the data was recorded from 92 patients included in the published dataset WCTECGdb (available for download at Physionet) and further 55 recent recordings, all taken with the 15-lead ECG device capable of recording the WCT components together with standard 12-Lead ECG, the validity of these hypotheses was investigated. The results show that the left arm dominates the WCT for only 47% of our patients, while the left leg potential has a considerable amplitude for 25% of our recordings. These findings contradict the broadly accepted Wilson/Einthoven hypotheses and affect the shape of the WCT resulting with a low correlation between the recorded WCT and the  $-2/3aVF$ .

### 3.2 Einthoven limb hypothesis

Einthoven assumed the body is a homogenous conductor, and the heart is a single dipole located in the centroid of the equilateral triangle [14], [15]. The electrical field varies in every moment by changing the dipole magnitude and direction. Therefore, the potential of every point with a distance  $R$  from the heart is measured by Eq. 3.1 which  $\Phi$  is the potential of a dipole ( $\vec{p}$ ) in infinite homogenous medium with a conductivity of ( $\sigma$ ), and  $\theta$  is the angle between  $\vec{p}$  and  $\vec{R}$  [15], [62]:

$$\Phi = \frac{1}{4\pi\sigma} \frac{p \cos\theta}{R^2} \quad (3.1)$$

Hence, the potential decreases as  $1/R^2$  by moving away from the dipole (heart) [15]. Furthermore, the left arm is considered to have a higher potential than the right arm as the

heart is located on the left side of the chest. The left leg has a negligible amplitude due to have a longest distance from the heart.

Although this assumption is one of the results of the Einthoven hypothesis and has not directly affected the recording of 12 lead ECG, it was used to justify other assumptions and development in the field of electrocardiography [106]. Provided the left leg potential is approximately zero:

$$II = LL - RA \xrightarrow{LL \cong 0} II = -RA \quad (3.2)$$

$$III = LL - LA \xrightarrow{LL \cong 0} III = -LA \quad (3.3)$$

$$WCT = \frac{1}{3}(LA + RA + LL) \xrightarrow{LL \cong 0} WCT = -\frac{2}{3}aVF \quad (3.4)$$

Since the current electrocardiography device cannot record the WCT amplitude, the authentication of relationship between the WCT and aVF is an alternative way to estimate the WCT signal. Given that the WCT is a systematic error with clinically relevant amplitude in recording the precordial leads [65], [70], [71], [78], this approach could be regarded as a solution for removing the WCT from the precordial leads, and it would obtain the “*true unipolar leads*” from the chest electrodes. The recorded WCT and aVF signals are used to evaluate this hypothesis.

### 3.3 Evaluation metrics

Three consecutive beats are selected from each patient to evaluate this hypothesis. The average of peak-to-peak amplitude from these three beats are measured for the LA, RA, and WCT. Therefore, the averages represent the potential of each limb’s electrodes and the WCT for each patient. We used two quantitative measures to show the similarities between two signals (naming  $p$  and  $m$ ):

- **Cross-Correlation:** It is used to calculate the resemblance between two signals, where  $N$ ,  $\mu$  and  $\sigma$  are number of samples, the mean and the standard deviation of a signal, respectively.

$$Corr = \frac{\sum_{i=1}^N (p_i - \mu_p)(m_i - \mu_m)}{\sigma_p \sigma_m} \quad (3.5)$$

- Root means square (RMS): It is used to present the agreement between two signals.

$$RMS = \sqrt{\frac{1}{N} \sum_{i=1}^N (p_i - m_i)^2} \quad (3.6)$$

Statistics results are measured from the WCTECGdb and the additional 55 recently recorded data and reported as a mean ( $\mu$ ) and standard deviation ( $\sigma$ ).

### 3.4 Wilson limb potential amplitudes

The statistical analysis of three limbs' potential and Wilson central terminal among all patients is demonstrated in Table 3.1. The average and standard deviation of the WCT are not negligible, which contradicts with the Wilson hypothesis. Therefore, the WCT amplitude is clinically relevant, which may cause removing important clinical information from the precordial leads. The statistical comparison of the limbs' potential amplitudes aligns with the initial assumption in limbs' potential. The LL has the smallest average and standard deviation, while the LA has the greatest potential among three limbs. However, this summary does not present the different characteristics of limbs potential; therefore, different approaches are used to have a comprehensive view.

Table 3. 1 The average, standard deviation, maximum and minimum of each limb potential and Wilson centre terminal among 147 patients. All results presented in mV.

	LA	RA	LL	WCT
Average	0.56	0.47	0.09	0.27
Standard deviation	0.33	0.23	0.08	0.17
Maximum	1.56	1.35	0.64	0.90
Minimum	0.08	0.10	0.02	0.03

The minimum changes in the ECG signal amplitude to be considered clinically relevant is 0.1 mV. This value is the current visualization scale in clinical ECG recording and is equivalent to 10 mm in the standard ECG graph paper. In other words, the uncertainty of the ECG amplitude measurement on the medical scale is 0.1 mV. Therefore, we chose 0.1 mV as a threshold to highlight the difference between limb potential. In other words, the peak-to-

peak difference amplitude of two signals should be at least 0.1 mV to consider them having different amplitudes. Our results show that the left leg has the smallest amplitude among Einthoven limbs potential for all patients. Furthermore, the RA potential is higher than the LA potential for 47 patients (see Figure 3.1). The RA and LA have negligible different amplitudes for 31 patients due to having a less than 0.1 mV potential difference ( $|RA-LA| < 0.1$  mV). Finally, the LA has a higher amplitude than the RA for 69 patients. Figure 3.2 is an example of a patient having the RA potential near four times greater than the LA potential.

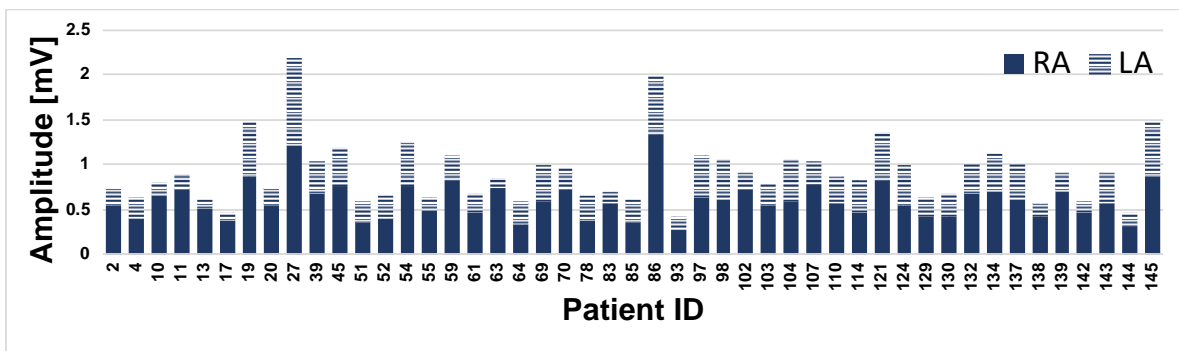


Figure 3. 1 Patient with the RA potential higher than the LA potential (47 in total) with 0.1 mV threshold. The average of three peak to peak amplitude of the RA and the LA measured for each patient.

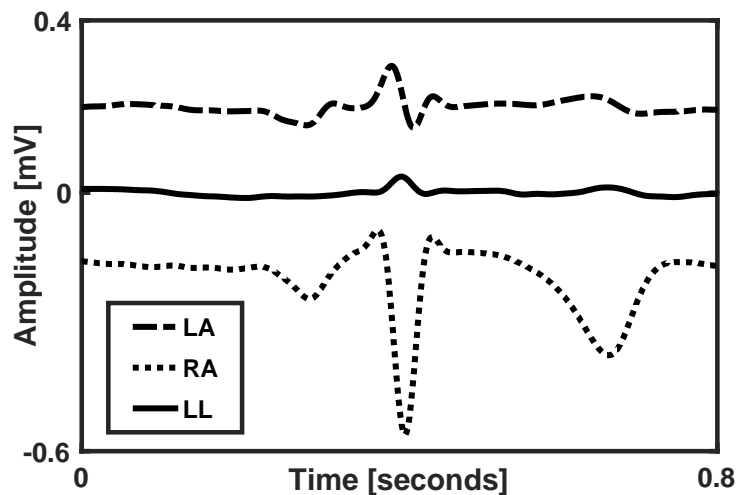


Figure 3. 2 The comparison of Einthoven limbs' potential. The LA, RA, and LL amplitudes are 0.124, 0.464 and 0.038 mV. The LA and RA are shifted 0.2 mV from the original place for better visualization. Recorded from 40 years old male (Patient ID 142).



As it was presented in Table 3.1, the LL has an average amplitude of 0.09 mV among all patients. Although the LL has the smallest potential amplitude among three limbs, it still required investigation to see whether its amplitude is negligible. Furthermore, we cannot rely on each limb potential, as all three limbs potential can be relatively high or low in different patients. Consequently, we measured the relative LA (rLA), relative RA (rRA) and relative LL (rLL) by dividing the RA, LA, and LL by their sum for each patient (Eq. 3.7).

$$\begin{aligned}
 rLA &= LA / (LA + RA + LL) \\
 rRA &= RA / (LA + RA + LL) \\
 rLL &= LL / (LA + RA + LL)
 \end{aligned}
 \tag{3.7}$$

Figure 3.3 presents the relative amplitudes of three limb potential for all patients.

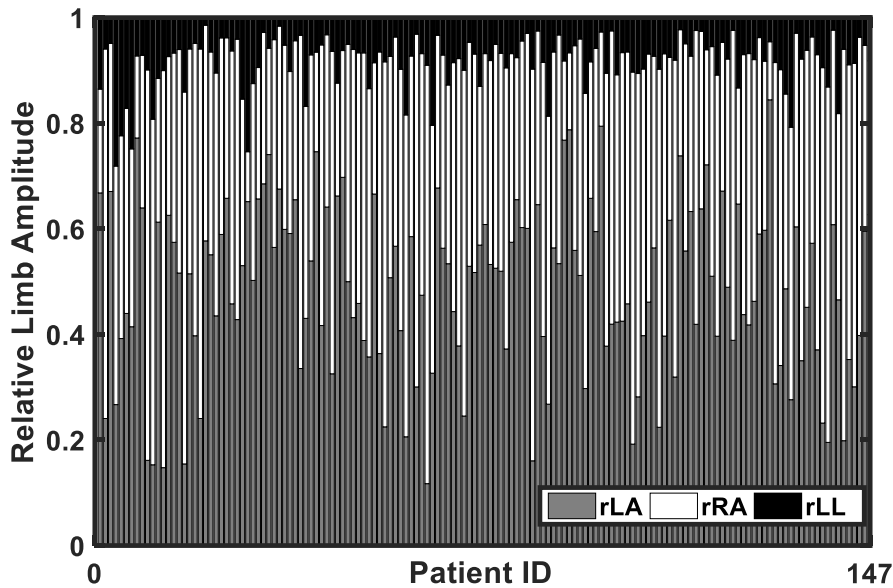


Figure 3. 3 The relative limb potential of each patient.

### 3.5 The WCT and aVF resemblance

It could be inferred from Figure 3.3 that the LL has a relatively small amplitude for most of the patients, which results to have a less impact on the shape and amplitudes of the WCT, II, and III. Nevertheless, the LL still has a relatively high amplitude for some patients. These two groups of the patients required independent analysis to reach a more precise conclusion.

Therefore, we divided our data into two groups using the threshold value of 0.1 for the relative LL amplitude. In other words, patients were grouped, which their LL amplitude shape at least 10 percent of the WCT. This threshold was chosen heuristically to maximize the correlation and minimise the root mean square error (RMSE) within each group. The class of patients with relatively small LL amplitude ( $< 0.1$ ) contains 112 patients, while only 35 patients belonged in a class with relatively high LL potential. Figure 3.4 shows the relative average amplitudes of limbs' potential for each group.

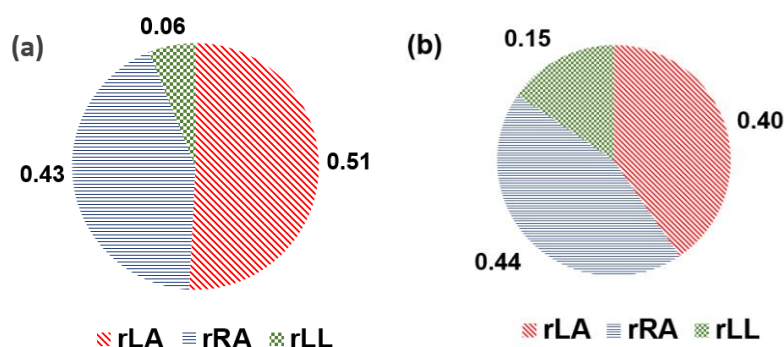


Figure 3. 4 The relative average amplitudes of limbs potential: (a) patients having relatively small LL amplitude (minimum: 0.01, maximum: 0.09, average: 0.06); (b) patients having relative high LL amplitude (minimum: 0.10, maximum: 0.28, average: 0.15).

These two groups were analysed independently using the cross-correlation (Corr) and root mean square error (RMSE). Since the left leg is the reference point to measure leads II and III, and it is also used in WCT measurement, I intend to investigate the influence of the LL potential in measuring these three signals. Therefore, three sets of signals were compared together refer to Eq. 3.2, 3.3 and 3.4: (WCT,  $-2/3aVF$ ), (III, -LA), and (II, -RA). As can be inferred from Table 3.2 and Table 3.3, the correlation is dropped considerably, and the RMS is increased in the patients with relatively high LL potential.

Table 3. 2 The correlation and root mean square error for 35 patients with relatively high LL potential

	$Corr_{\mu}$	$Corr_{\sigma}$	$RMSE_{\mu}$	$RMSE_{\sigma}$
(WCT, $-2/3aVF$ )	0.56	0.30	0.15	0.28
(II, -RA)	0.74	0.31	0.13	0.28
(III, -LA)	0.74	0.27	0.14	0.28

Table 3. 3 The correlation and root mean square error for 112

patients with relatively small LL potential

	$Corr_\mu$	$Corr_\sigma$	$RMSE_\mu$	$RMSE_\sigma$
(WCT, -2/3aVF)	0.81	0.20	0.08	0.06
(II, -RA)	0.91	0.13	0.05	0.05
(III, -LA)	0.93	0.11	0.05	0.05

Figures 3.5 and 3.6 demonstrate two patients having relatively low and high potential in the left leg. As can be seen in Figure 3.5, the potential of the LA, RA, and LL are 0.98 mV, 1.21 mV and 0.09 mV, respectively. Therefore, the LL potential amplitude in respect to two other limbs is negligible, and consequently, these three set signals are highly correlated. Figure 5 demonstrates a patient with the high LL potential (0.47 mV) while the LA and RA have the potential of 1.20 mV and 0.91 mV. Consequently, the LL has a considerable impact on the shape and amplitudes of leads II, III, and WCT.

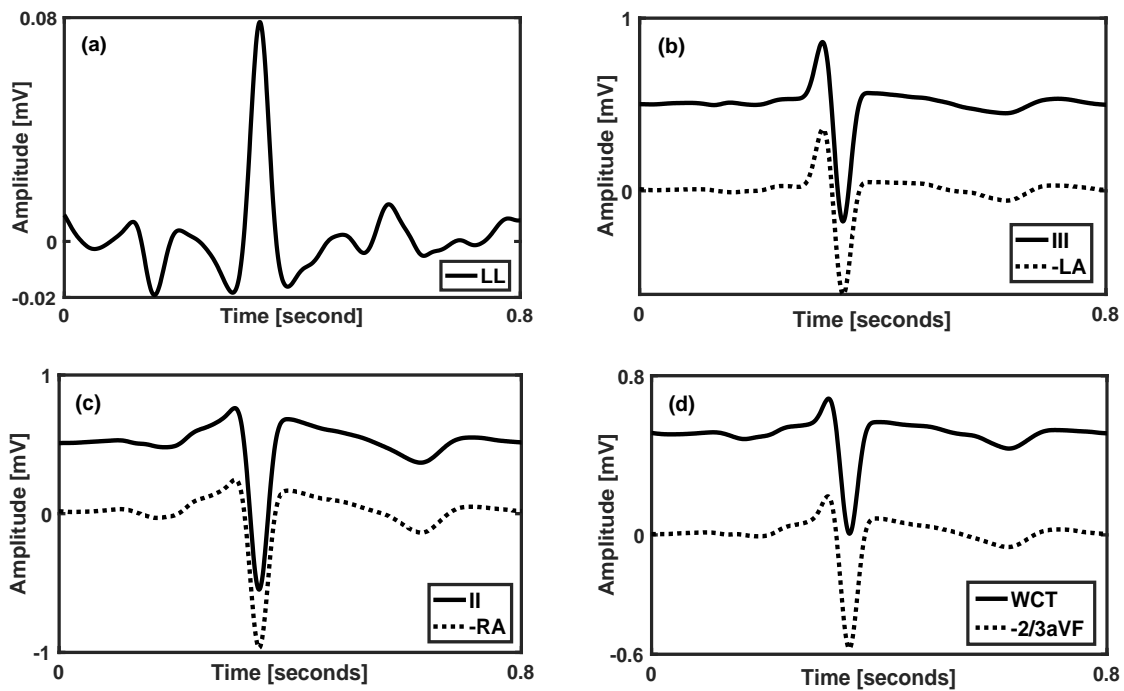


Figure 3. 5 The influence of the LL potential on leads II, III, and WCT. To have a better visualization leads II, III, WCT are shifted 0.5 mV from the original place: (a) the average peak to peak potential of the LL among three beats is 0.09 mV which shape 4 percent of the WCT signal; (b) the correlation between lead III and -LA is 0.99 (RMS error: 0.02); (c) the correlation between lead II and -RA is 1 (RMS error: 0.02); (d) the correlation between -2/3aVF and the WCT is 0.99 (RMS error: 0.11); Recorded from 59 years old male (Patient ID 27).

Although the LL potential has the smallest amplitude among three limbs, it does not necessarily mean that it has a minor impact on the WCT shape and amplitude. Figure 3.7 demonstrates a patient with the LA, RA and LL amplitudes of 0.23 mV, 21 mV, and 0.09 mV, respectively. Since the LA and RA has almost the same peak-to-peak potential with inverse deflection, the LL has a major influence on the WCT signal. Therefore, the correlation between the WCT and -2/3aVF is very small (0.08). Since the WCT has a negligible peak-to-peak amplitude, still the RMS value of the WCT and -2/3aVF is very small (0.06).

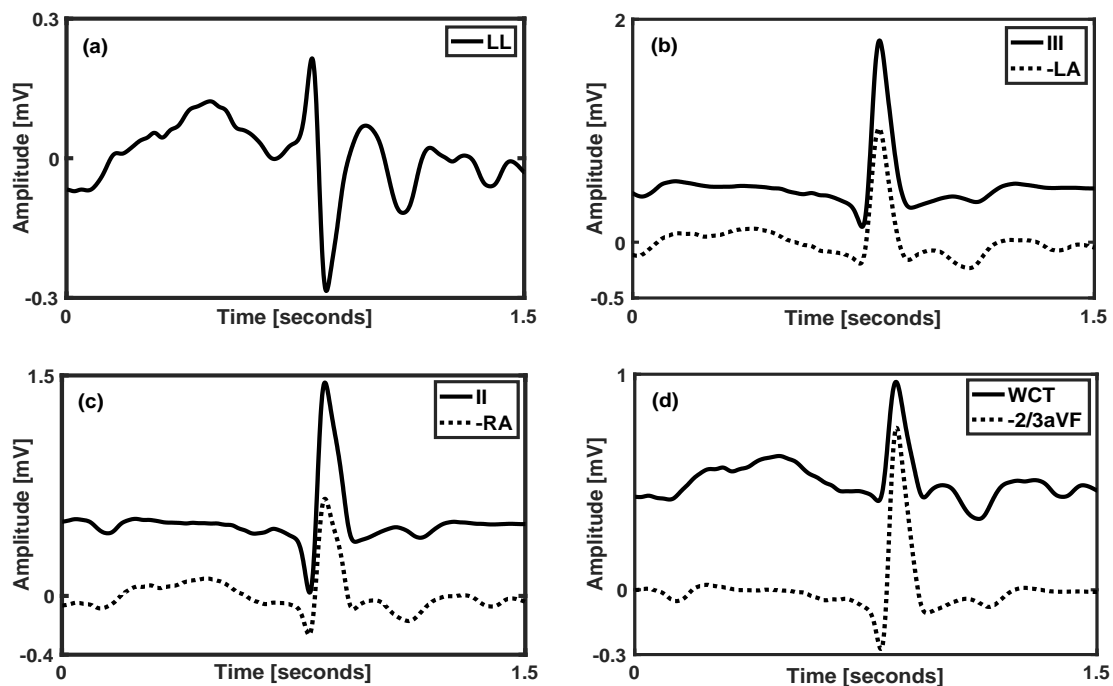
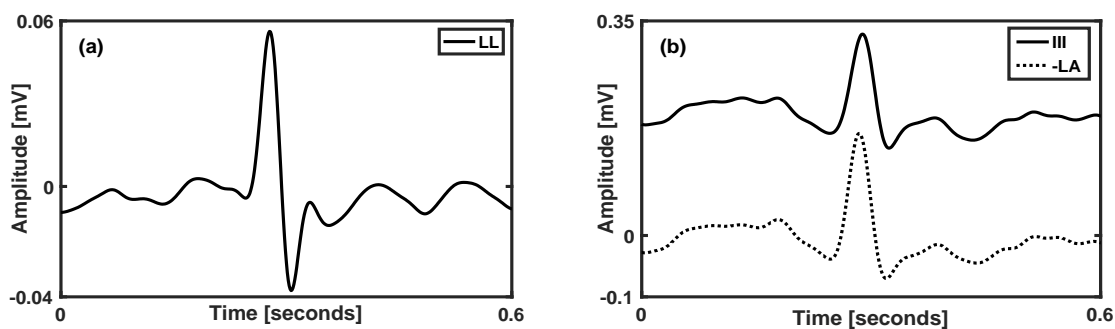


Figure 3. 6 The influence of the LL potential on leads II, III, and WCT. To have a better visualization leads II, III, WCT are shifted 0.5 mV from the original place: (a) the average peak to peak potential of the LL among three beats is 0.47 mV which shape 18 percent of the WCT signal; (b) the correlation between lead III and -LA is 0.94 (RMS error: 0.09); (c) the correlation between lead II and -RA is 0.91 (RMS error: 0.09); (d) the correlation between  $-2/3aVF$  and the WCT is 0.82 (RMS error: 0.22). Recorded from 72 years old male (Patient ID 141).

Figure 3.7 is a good example to justify the major impact of LL on the WCT signal compare to leads II and III. As it can be seen in Table 3.2 and 3.3, the correlation values between (II, -RA) and (III, -LA) are higher than that between (WCT,  $-2/3aVF$ ), while the RMS error between these three set of signals are not significantly different.

This chapter aims to statistically investigate the Einthoven limb potential hypothesis. Therefore, we did not clinically study the influence of the LL on lead II, III, and the WCT signals, which is required increasing the number of patients to have a well-powered study for each cardiac disease [105]. This research is also limited by recording from patients with cardiac diseases admitted at the hospital with the average and standard deviation age of 64.85 and 13.56, respectively. Our analysis shows that the LA has the highest potential among Einthoven limbs in only 47 percent of the patients (67 out of 147). Furthermore, the LL has the lowest amplitude among the Einthoven limb potential. Still, the LL amplitude could not be considered negligible for at least 24 percent of the patient (35 out of 147), consequently the WCT cannot be replaced by the  $-2/3aVF$  for all patient according to the derived statistical information. However, it does not necessarily mean that the difference between the WCT and  $-2/3aVF$  is clinically important, which requires more recordings for clinical investigation.



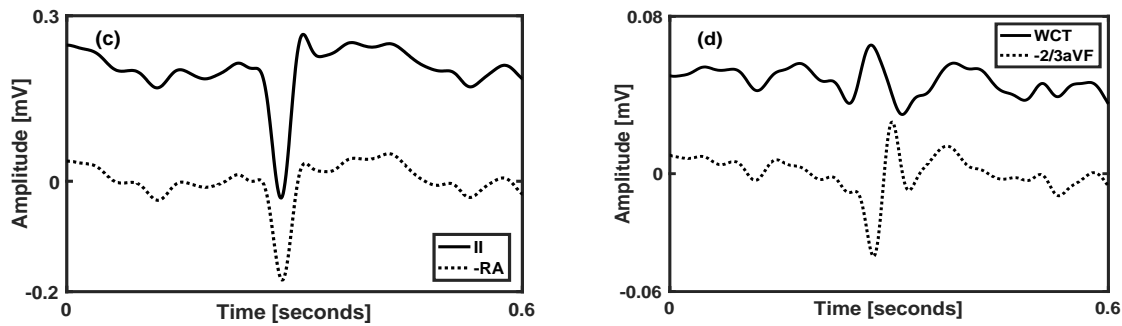


Figure 3. 7 The influence of the LL potential on leads II, III, and WCT. To have a better visualization leads II and III are shifted 0.2 mV, and the WCT is shifted 0.05 from the original place: (a) the average peak to peak potential of the LL among three beats is 0.09 mV which shape 17 percent of the WCT signal; (b) the correlation between lead III and -LA is 0.96 (RMS error: 0.06); (c) the correlation between lead II and -RA is 0.98 (RMS error: 0.06); (d) the correlation between -2/3aVF and the WCT is 0.08 (RMS error: 0.6). Recorded from 84 years old female (Patient ID 40).

### 3.6 Conclusion

In this chapter, the Einthoven limbs' potential hypothesis is evaluated to find the relation between three limbs' potential and investigate whether the WCT and aVF are proportional. The recorded data from the 15-lead ECG device is used, which include 92 records from WCTECGdb and 55 recently recorded data. The obtained results show that unlike the initial assumption, the left arm has the highest potential among the three limbs in only 47 percent of the patients and the potential of the left leg is not negligible for all patients. Furthermore, the left leg has a considerable amplitude for 25 percent of patients, which consequently influences the shape and amplitude of the WCT. Therefore, the WCT and -2/3aVF has a relatively small correlation and large RMS error in this group of patients.

## **Chapter 4    Clinical investigation of Wilson Central Terminal**

This chapter presents nine case reports, which were recorded from NSTEMI patients. The clinical analysis of unipolar chest leads and the clinical impacts of the left leg potential on the chest leads are discussed using these recordings.

*Some of the work presented in this chapter has been submitted as a journal paper:*

- Hossein Moeinzadeh, Gaetano D Gargiulo, Paolo Bifulco, Mario Cesarelli, Alistair L McEwan, Aiden O'Loughlin, Ibrahim M Shugman, Jonathan C Tapson, Aravinda Thiagalingam, “*ECG abnormalities detected in Non-ST-segment Elevation Myocardial Infarction patients with a novel ECG device*”, Submitted, JACC case reports, 2020.

## 4.1 Abstract

In patients presenting with chest pain, the electrocardiogram (ECG) and cardiac biomarkers (such as troponin) are the core tests used to diagnose non-ST-segment elevation myocardial infarction (NSTEMI). In current practice, the ECG is available in real-time whilst there is a time delay before cardiac biomarker results are available. ECG changes may include ST-segment depression and inverted or biphasic T-waves [107]. However, often patients with NSTEMI do not show any changes in their ECG. In this chapter, a series of case reports are presented to show the influence of the WCT signal on precordial leads, and to investigate whether the WCT and  $-2/3aVF$  are clinically equivalent.

## 4.2 Introduction

The precordial leads ( $V_1: V_6$ ) of current ECG devices measure the potential of the six electrodes on the chest with reference to Wilson Central Terminal (WCT). The WCT is obtained by averaging the potential of limb electrodes (Eq. 4.1) and assumed to have a zero potential. However, this assumption has been found to be incorrect by many researchers, including Wilson himself [16].

Chapter two and three discussed two assumptions in electrocardiogram. In chapter two, the legitimacy of WCT zero potential theory is investigated using the recently published dataset (WCTECGdb). This dataset contains 92 patients, which were recorded between 2016 and 2018. It is shown that the patients could be divided into three groups with *zero*, *negligible*, and *significant* WCT error. The results show that only 28% of patients have the WCT with *zero* or *negligible* impacts on the precordial leads; therefore, unipolar chest leads ( $UV_1: UV_6$ ) and precordial leads ( $V_1: V_6$ ) are expected to be identical or to have small differences in those patients. The rest of the patients are categorized as having *significant* WCT error. These recordings require a clinical investigation to measure the *real* impact of this error on precordial leads and thus the diagnosis of cardiac diseases. In the third chapter of this thesis, the influence of left leg on the WCT is discussed. The left leg is commonly assumed to have a near zero potential; therefore, the WCT and  $-2/3aVF$  are highly similar (Eq. 4.2). It is



shown that the left leg has a considerable amplitude for 25% of the patients, and consequently influences the shape and amplitude of the WCT.

$$WCT = \frac{1}{3}(LA + RA + LL) \quad (4.1)$$

$$aVF = LL - \frac{1}{2}(RA + LA) \xrightarrow{LL \cong 0} WCT = -\frac{2}{3}aVF \quad (4.2)$$

In this chapter, the standard precordial leads ( $V_1: V_6$ ) are compared with unipolar chest leads ( $UV_1: UV_6$ ) to present the clinical impacts of the WCT on precordial leads. Furthermore, the similarity of the WCT and  $-2/3aVF$  is clinically analysed and showed whether the left leg signal has any important clinical influences on shaping the WCT signal. In the case that the left leg has a zero potential, the unipolar chest leads can be reconstructed by adding  $-2/3aVF$  to the standard precordial leads (Eq. 4.3). Consequently, comparison of the unipolar chest leads ( $UV_1: UV_6$ ) and the reconstructed unipolar chest leads ( $UV_1(R): UV_6(R)$ ) is provided to present the clinical influence of the left leg on the unipolar chest leads.

$$LL \cong 0 \Rightarrow UV_1(R): UV_6(R) = V_1: V_6 + \left(-\frac{2}{3}aVF\right) \quad (4.3)$$

The WCTECGdb dataset, in addition to the recent recordings (2018-2019) are used in this chapter. Only patients diagnosed with NSTEMI are used in this analysis as their precordial leads may present abnormalities such as ST-segment depression, ST-segment elevation, inverted or biphasic T-waves (see Figure 4.1) [107]. We do not investigate the clinical impacts of WCT on the ECG recordings from patients diagnosed with other cardiac diseases as only specific cardiac diseases causes abnormalities in precordial leads, and we only have enough ECG recordings from NSTEMI patients. In this chapter, nine patients are included in the clinical analysis as their ECG was recorded the day they underwent coronary angiography.

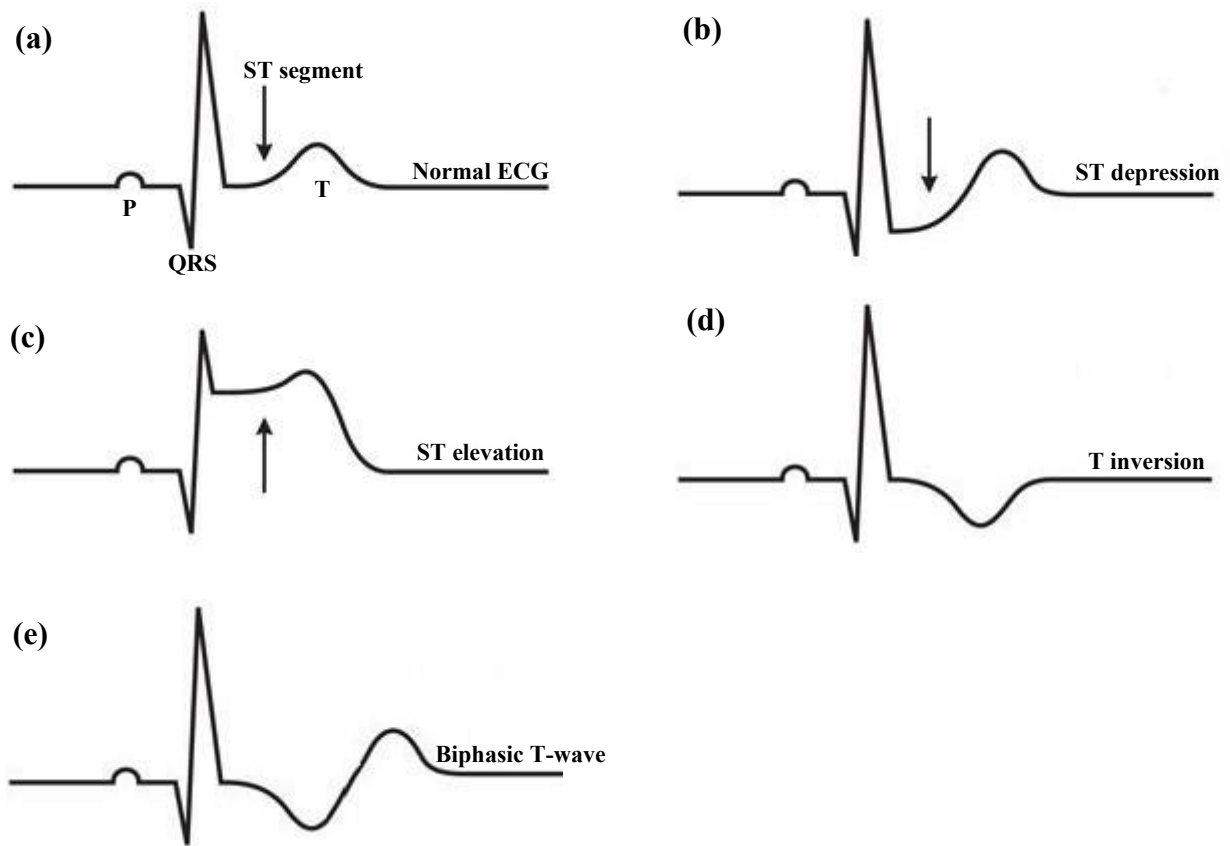


Figure 4. 1 ECG abnormalities in NSTEMI patient, adopted from [108]

### 4.3 Clinical case reports

**Case 1.** A 52 year old male presented with chest pain, on a background of hypertension and smoking. The high-sensitivity troponin-T on presentation was elevated at 34 ng/L (normal <15ng/L) and subsequently peaked at 1130 ng/L. Coronary angiography demonstrated a proximal left anterior descending lesion involving the first diagonal branch requiring percutaneous coronary intervention.

Standard 12-lead ECG demonstrated sinus rhythm with anterior T-wave inversion. Figure 4.2 (top and middle panels) shows the standard precordial leads ( $V_1$ :  $V_6$ ) and unipolar precordial leads ( $UV_1$ :  $UV_6$ ), recorded simultaneously. Whilst both ECGs have T-wave abnormalities, the unipolar leads also have ST-segment elevation. This difference is due to the incorporation

of the WCT signal in the unipolar recording. The WCT modifies the ST segment as well as T-wave in unipolar chest leads. Therefore, the WCT induces the appearance of ST-elevation in unipolar leads with a more prominent T-wave inversion in the unipolar chest leads. Figure 4.2 (bottom panel) presents the reconstructed unipolar leads ( $UV_1(R)$ :  $UV_6(R)$ ), which lost the ST-segment elevation in all six leads. This is due to the differences between the WCT and  $-2/3aVF$ .

As it can be referred from Figure 4.3, the ST is elevated near 3 mm (or mV) in the WCT signal, while the ST has near-zero amplitude in  $-2/3aVF$ . The left leg is the only difference between the WCT and  $-2/3aVF$  (Eq. 4.2); therefore, the shape and amplitude of the left leg potential add important clinical information to the unipolar chest leads (Figure 4.4). This case clearly contradicts to the common assumption about the similarity between WCT and  $-2/3aVF$  and the negligibility of the left leg potential.

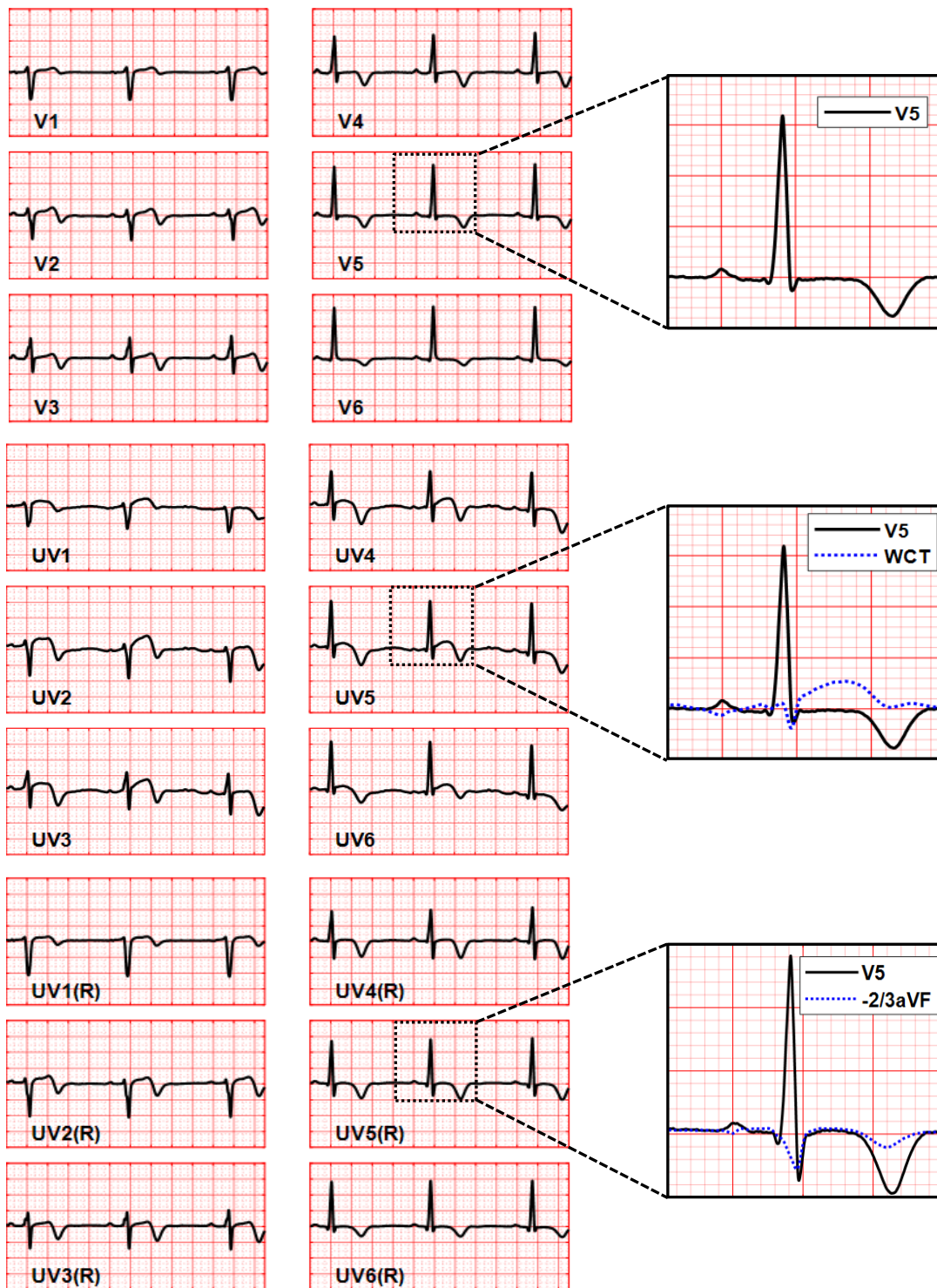


Figure 4. 2 Comparison between the standard precordial leads ( $V_1$ :  $V_6$ ) (top panel), unipolar chest leads ( $UV_1$ :  $UV_6$ ) (middle panel), and reconstructed unipolar chest leads ( $UV_1(R)$ :  $UV_6(R)$ ) (bottom panel). Recorded from a 52 years old male (PID 97).

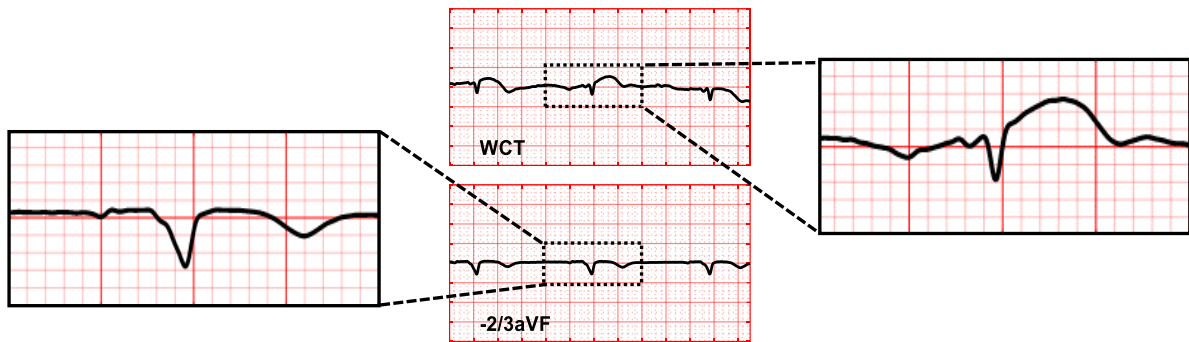


Figure 4. 3 Comparison of the WCT and -2/3aVF. Recorded from a 52 years old male (PID 97).

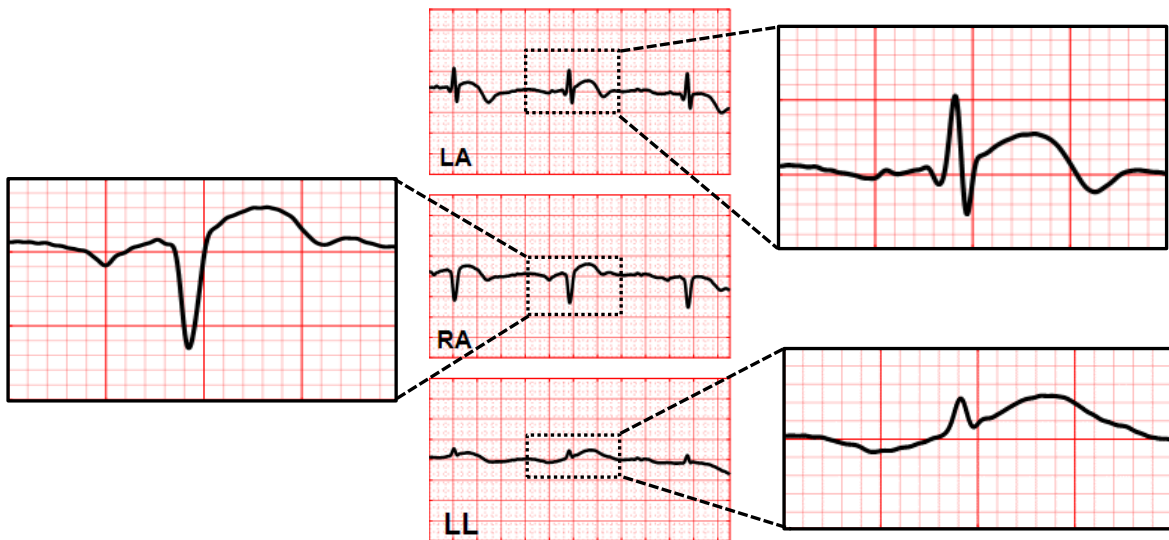


Figure 4. 4 Comparison of left arm (LA), right arm (RA) and left leg (LL) potential. Recorded from a 52 years old male (PID 97).

**Case 2.** A 70 year old male presented with one hour of chest pain. The high sensitivity troponin-T was subsequently found to be elevated with a peak of 509 ng/L. Coronary angiography showed a proximal left anterior descending artery (LAD) lesion with 90% stenosis requiring percutaneous coronary intervention.

As it can be seen from Figure 4.5, the shape and amplitude of the WCT and -2/3aVF are almost the same. It is due to the low amplitude of the left leg, which has almost zero amplitude in P, ST, and T segments (see Figure 4.6).

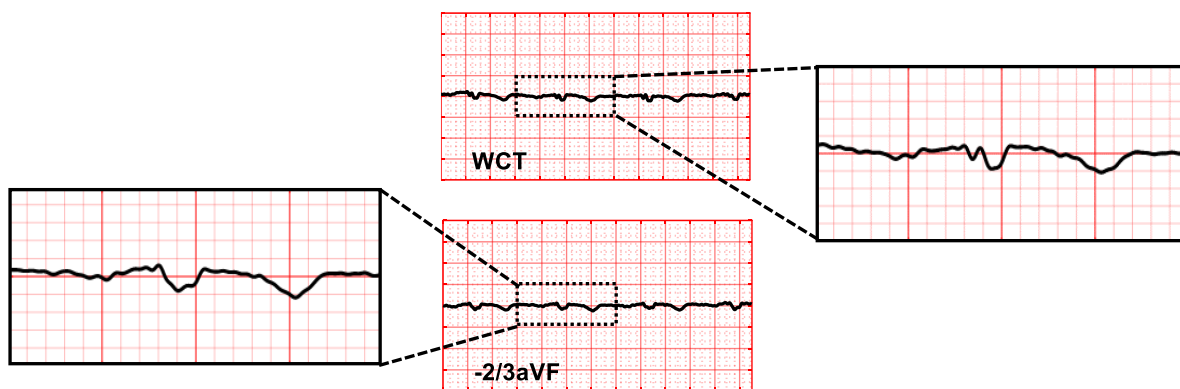


Figure 4. 5 Comparison of the WCT and -2/3aVF. Recorded from a 72 years old male (PID 75).

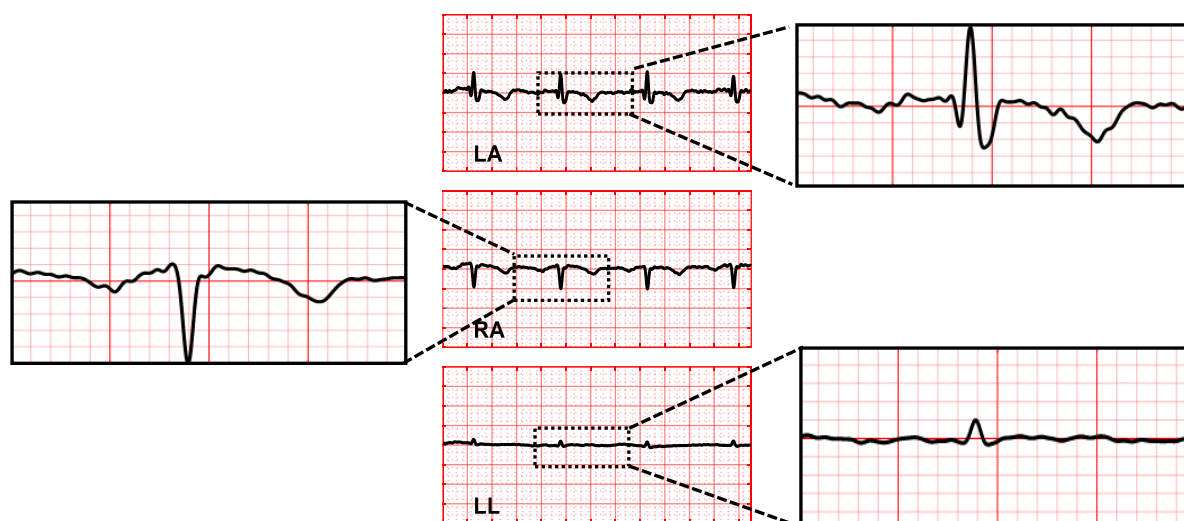


Figure 4. 6 Comparison of left arm (LA), right arm (RA) and left leg (LL) potential. Recorded from a 72 years old male (PID 75).

Figure 4.7 (top panel) shows subtle biphasic T waves in leads  $V_2$ :  $V_4$ . In the unipolar leads (Figure 4.7 middle panel) and reconstructed chest leads (Figure 4.7 bottom panel), there are much more obvious T-wave changes suggestive of Wellens' syndrome [109]. Adding WCT and -2/3aVF to the standard precordial leads results in the appearance of prominent T-wave inversion in  $UV_3$  (Figure 4.7, middle panel) and  $UV_3(R)$  (Figure 4.7, bottom panel), which demonstrates the clinical utility of our unipolar leads in the diagnosis of ischemia when compared with conventional ECG leads.

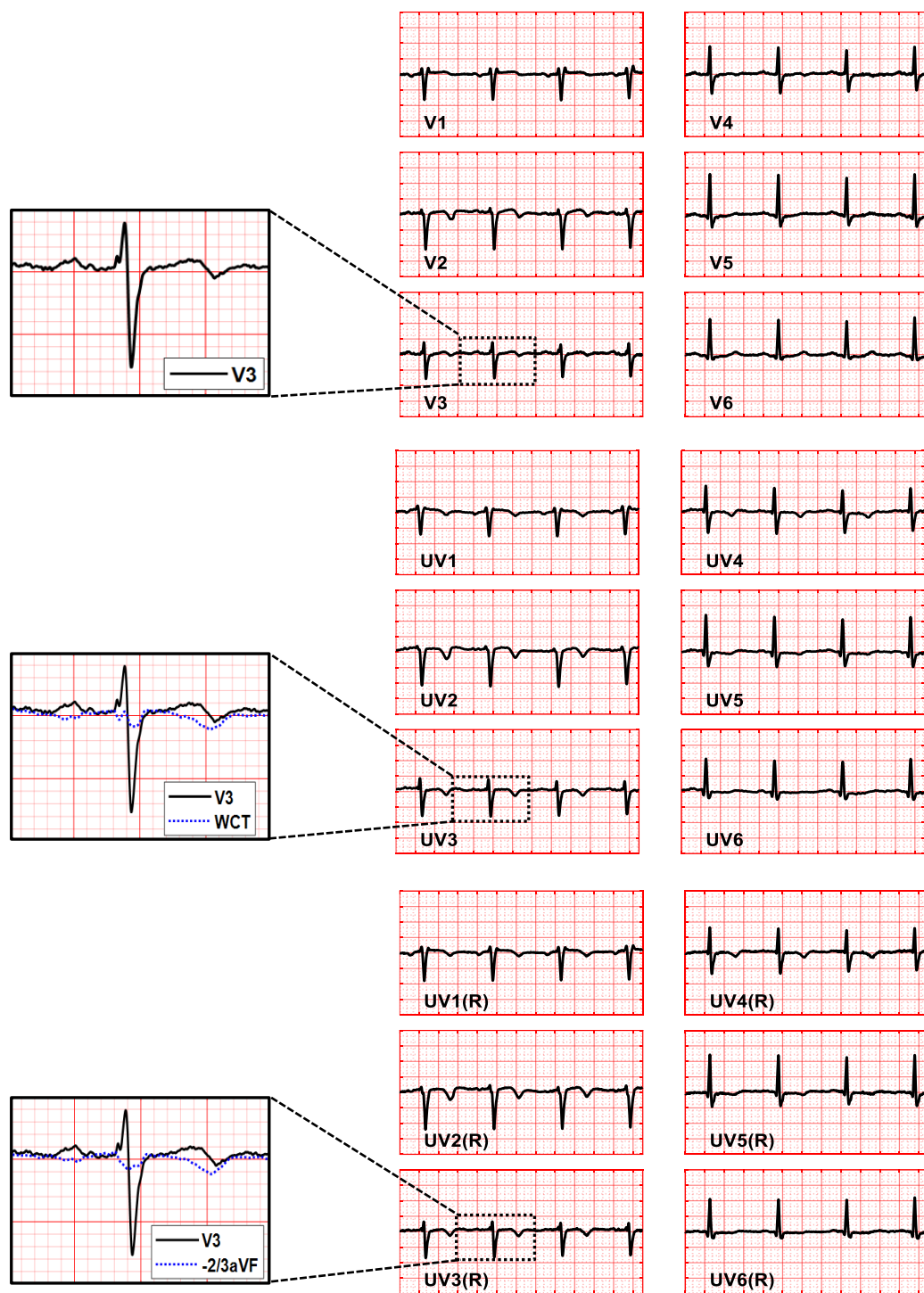


Figure 4. 7 Comparison between the standard precordial leads ( $V_1$ :  $V_6$ ) (top panel), unipolar chest leads ( $UV_1$ :  $UV_6$ ) (middle panel), and reconstructed unipolar chest leads ( $UV_1(R)$ :  $UV_6(R)$ ) (bottom panel). Recorded from a 72 years old male (PID 75).

**Case 3.** A 51 year old male presented with chest pain at the emergency department. Coronary angiography showed a proximal LAD lesion with 70% stenosis requiring percutaneous



coronary intervention. Figure 4.8 demonstrates the three limbs potential, which reconstruct the WCT signal. The LA, RA, and LL present near 1 mm (or 1 mV) positive deflection on T-wave, which cause having biphasic T-wave on the WCT signal (see Figure 4.9). Furthermore, the  $-2/3aVF$  does not show T-wave positive deflection, which confirms the influence of the left leg potential on the WCT signal and consequently on the precordial leads.

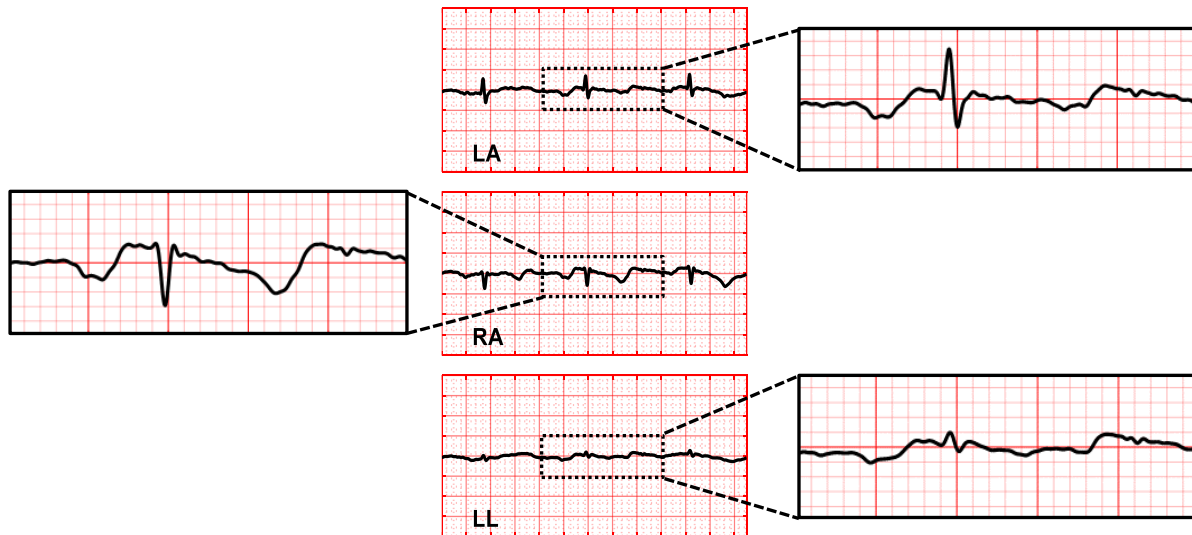


Figure 4. 8 Comparison of left arm (LA), right arm (RA) and left leg (LL) potential. Recorded from a 51 years old male (PID 94).

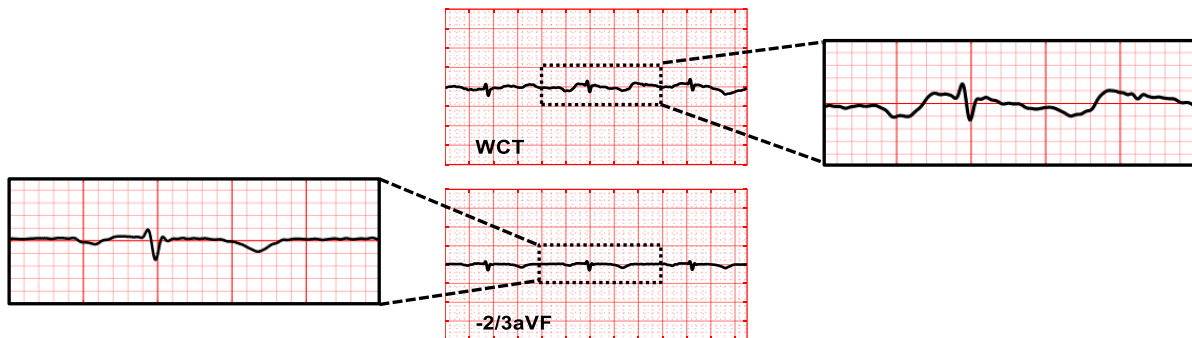


Figure 4. 9 Comparison of the WCT and  $-2/3aVF$ . Recorded from a 51 years old male (PID 94).

Figure 4.10 (middle panel) shows subtle biphasic T-waves in leads  $UV_2: UV_6$ , while standard precordial leads (top panel) and reconstructed unipolar leads (bottom panel) present normal upright T-waves. This difference is due to the incorporation of the WCT signal in the unipolar recording, as the WCT presents biphasic T-wave (see Figure 4.10).



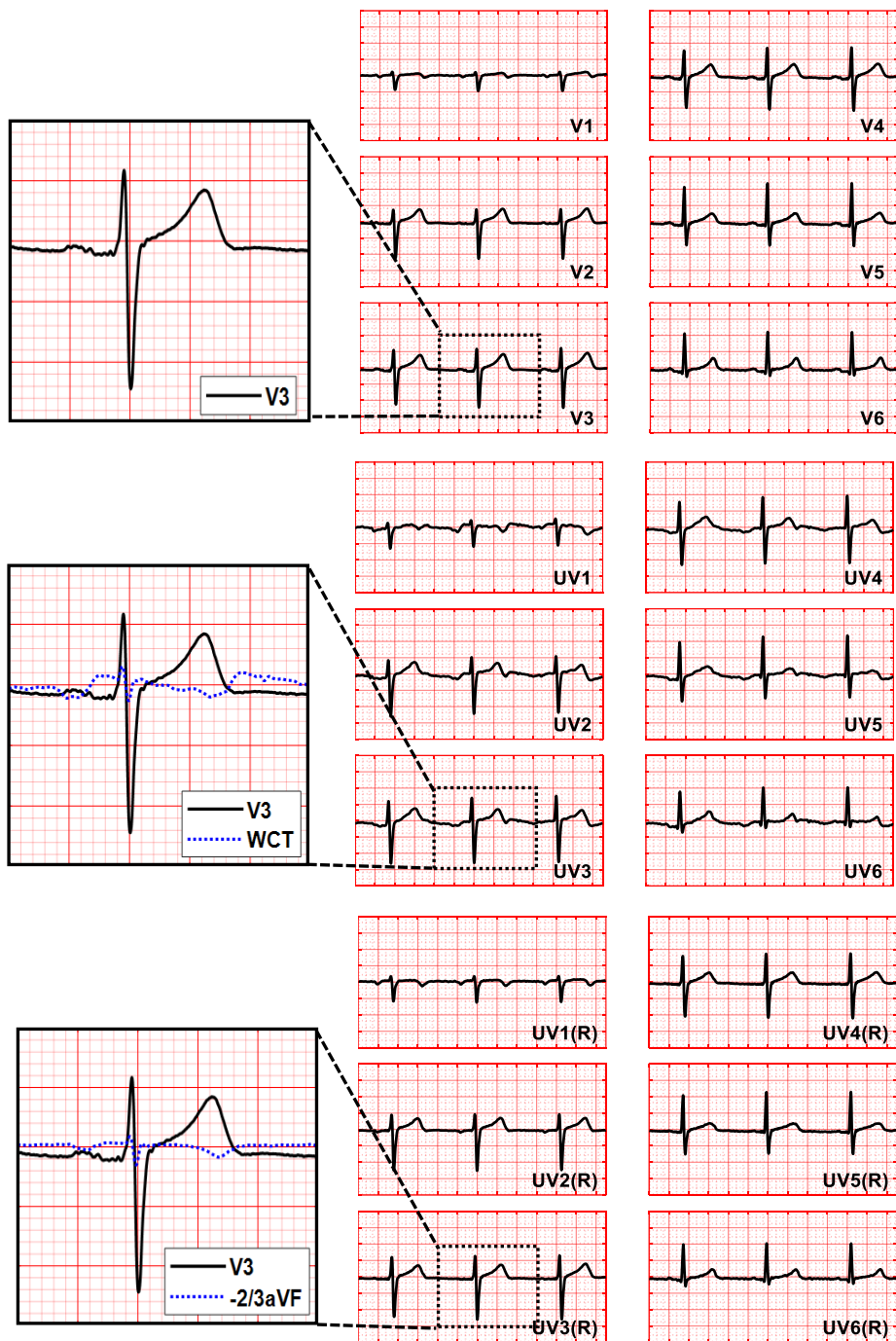


Figure 4.10 Comparison between the standard precordial leads ( $V_1$ :  $V_6$ ) (top panel), unipolar chest leads ( $UV_1$ : $UV_6$ ) (middle panel), and reconstructed unipolar chest leads ( $UV_1(R)$ :  $UV_6(R)$ ) (bottom panel). Recorded from a 51 years old male (PID 94).

**Case 4.** A 54 year old male presented with chest pain at the emergency department. His angiography showed proximal to mid LAD stenosis, which was subsequently stented (after optical coherent tomography (OCT) imaging). As seen in Figure 4.11, the WCT includes a

biphasic T-wave with an amplitude of 1 mm (or 1 mV) in both positive and negative deflections, while T-wave in  $-2/3aVF$  signal has only negative deflection with an amplitude of 0.5 mm (or 0.5 mV). This difference is clearly caused by amplitude of T-wave in the left leg potential (see Figure 4.12). The standard precordial leads and reconstructed unipolar chest leads are almost identical as the amplitude of  $-2/3aVF$  signal is negligible in T-wave section (see Figure 4.13). Nevertheless, the accumulation of WCT and standard precordial leads yields more markedly biphasic T-waves in  $UV_1: UV_3$ . The biphasic T-waves in  $UV_1: UV_3$  typically suggests proximal LAD disease which is known as Wellens Syndrome [109]. This was not apparent on the precordial leads but was predictive of the underlying culprit lesion.

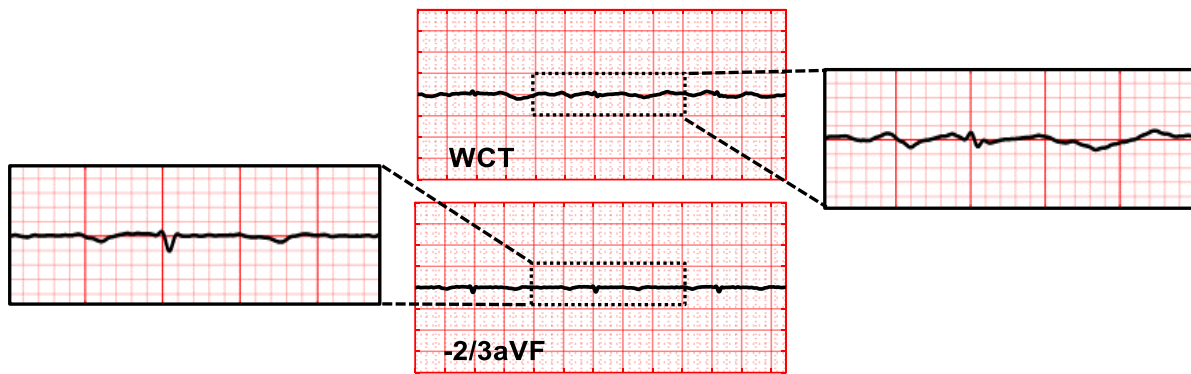


Figure 4. 11 Comparison of the WCT and  $-2/3aVF$ . Recorded from a 54 years old male (PID 85).

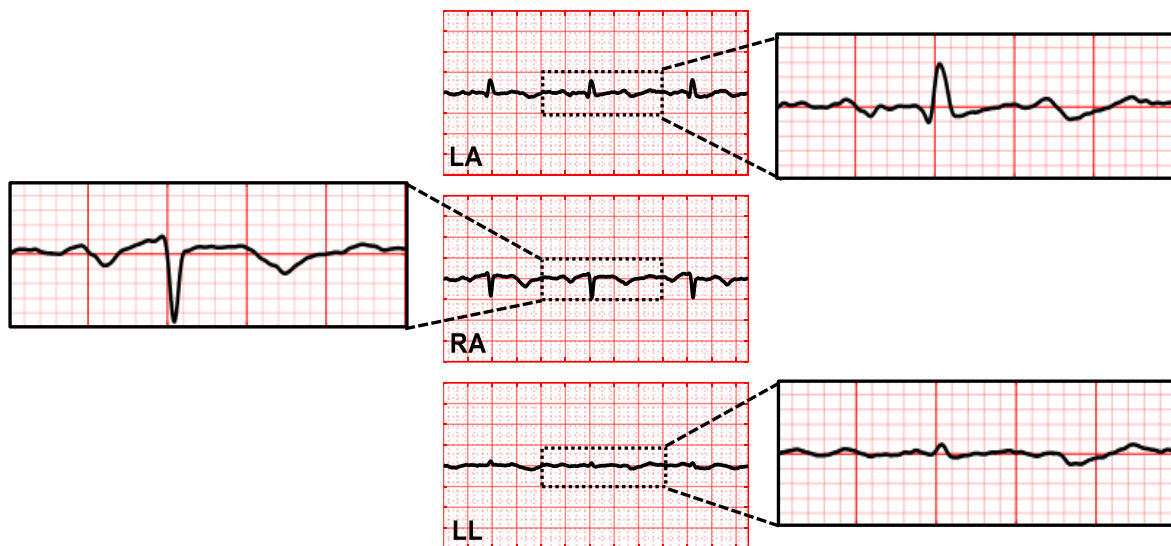


Figure 4. 12 Comparison of left arm (LA), right arm (RA) and left leg (LL) potential. Recorded from a 54 years old male (PID 85).

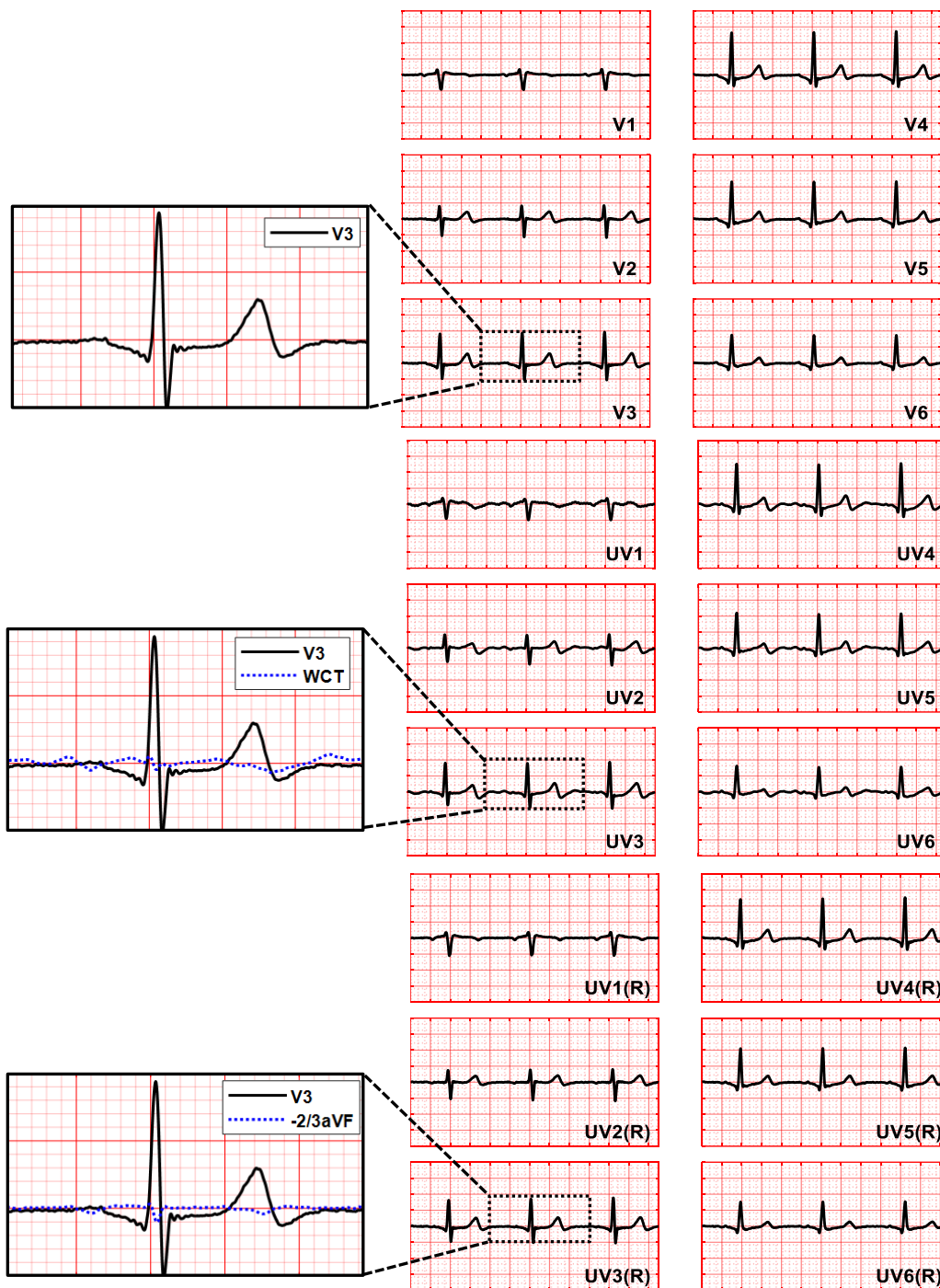


Figure 4.13 Comparison between the standard precordial leads ( $V_1$ :  $V_6$ ) (top panel), unipolar chest leads ( $UV_1$ :  $UV_6$ ) (middle panel), and reconstructed unipolar chest leads ( $UV_1(R)$ :  $UV_6(R)$ ) (bottom panel). Recorded from a 54 years old male (PID 85).

**Case 5:** A 52 year old gentleman presented to the emergency department with central chest and epigastric pain over three hours. This patient was on a background of hypertension,

central obesity and fatty liver disease. His chest pain resolved with a glyceryl trinitrate (GTN). Blood tests showed an elevated troponin (high-sensitive) of 264 ng/L with a peak troponin T (high-sensitive) of 527 ng/L. He was treated as a NSTEMI with aspirin, clopidogrel and low-molecular weight heparin infusion. A coronary angiogram was performed which demonstrated moderate left main disease (50% stenosis), an occlusion of the LAD proximally, and an ostial left circumflex artery (LCx) lesion (80% stenosis). He was referred and underwent coronary artery bypass grafting (CABG). As it can be seen in Figure 4.14, the left leg has near zero potential in P-wave and T-wave sections; therefore, the shape and amplitude of WCT and  $-2/3aVF$  are identical (see Figure 4.15).

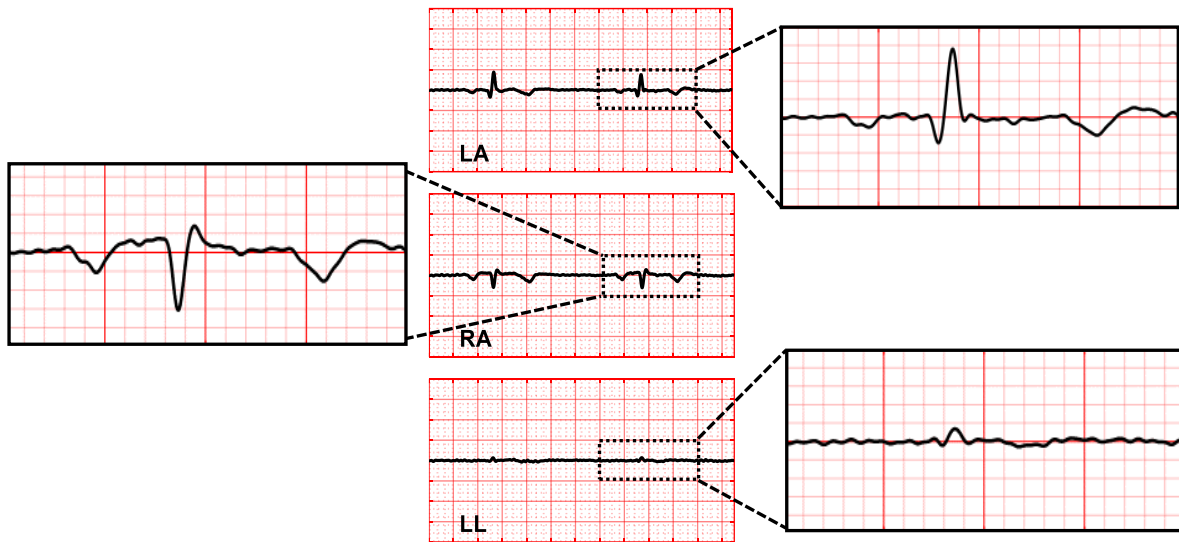


Figure 4. 14 Comparison of left arm (LA), right arm (RA) and left leg (LL) potential. Recorded from a 52 years old male (PID 56).

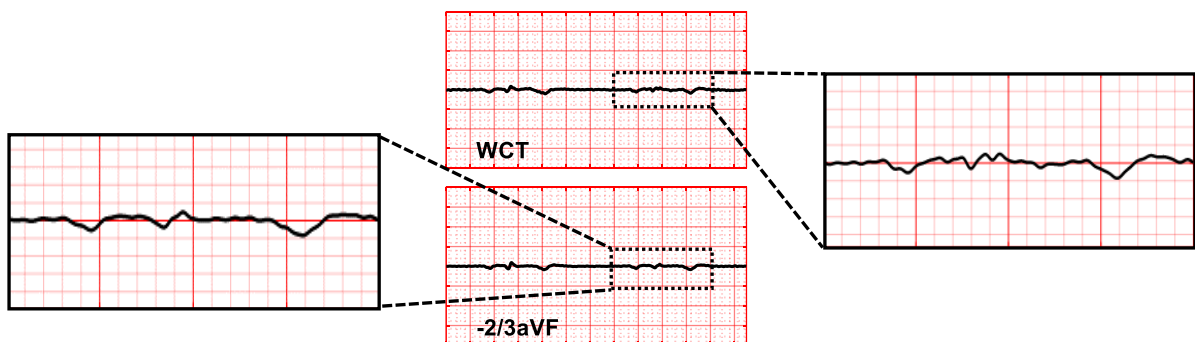


Figure 4. 15 Comparison of the WCT and  $-2/3aVF$ . Recorded from a 52 years old male (PID 56).

Furthermore, the WCT presents T-wave inversion, which modifies the T-wave on unipolar chest leads. Figure 4.16 (middle panel) presents inverted T-wave on  $UV_2:UV_3$ , and biphasic

T-wave on UV<sub>4</sub>, while standard precordial leads present less ischemic abnormalities. As seen in Figure 4.16 (top panel), V<sub>2</sub>:V<sub>3</sub> present biphasic T-wave, and V<sub>4</sub> shows upright T-wave. Therefore, the WCT clearly adds important clinical features to the precordial leads.

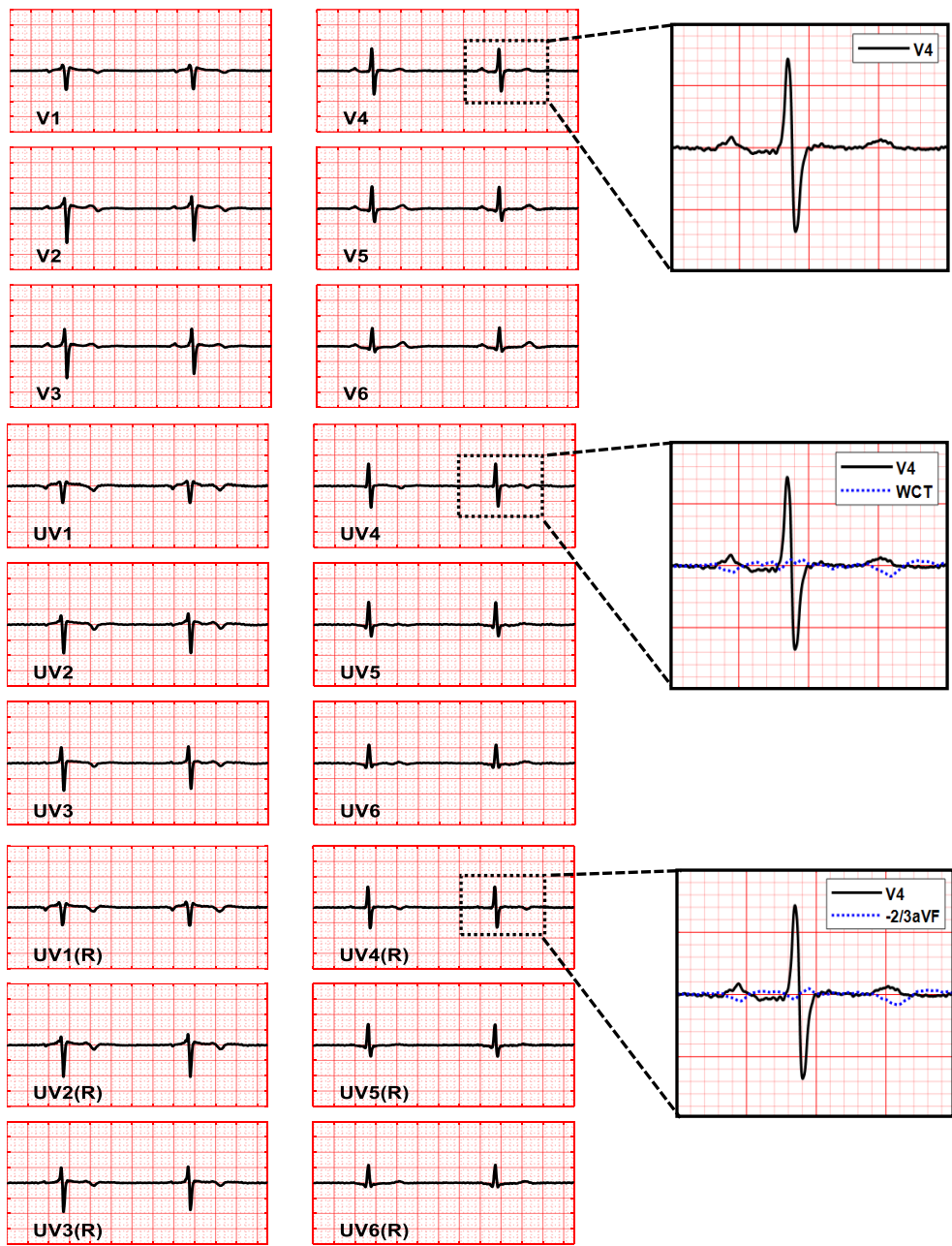


Figure 4. 16 Comparison between the standard precordial leads (V<sub>1</sub>: V<sub>6</sub>) (top panel), unipolar chest leads (UV<sub>1</sub>: UV<sub>6</sub>) (middle panel), and the reconstructed unipolar chest leads (UV<sub>1</sub>(R): UV<sub>6</sub>(R)) (bottom panel). Recorded from a 52 years old male (PID 56).



**Case 6:** A 75 year old lady presented to the emergency department with chest pain on exertion that had been occurring over the last three weeks and worsened on day of presentation. She had a background history that included cardiac risk factors of hypertension and hyperlipidaemia. Cardiac biomarkers were elevated with troponin T (high-sensitive) of 316 ng/L and peaking at 517 ng/L. She was treated for NSTEMI and underwent coronary angiography that revealed an occluded proximal D1, with moderate proximal LAD and LCx disease. As it can be referred from Figure 4.17, the left leg presents small variation on T-wave section. Therefore, the WCT and  $-2/3aVF$  are the same (see Figure 4.18).

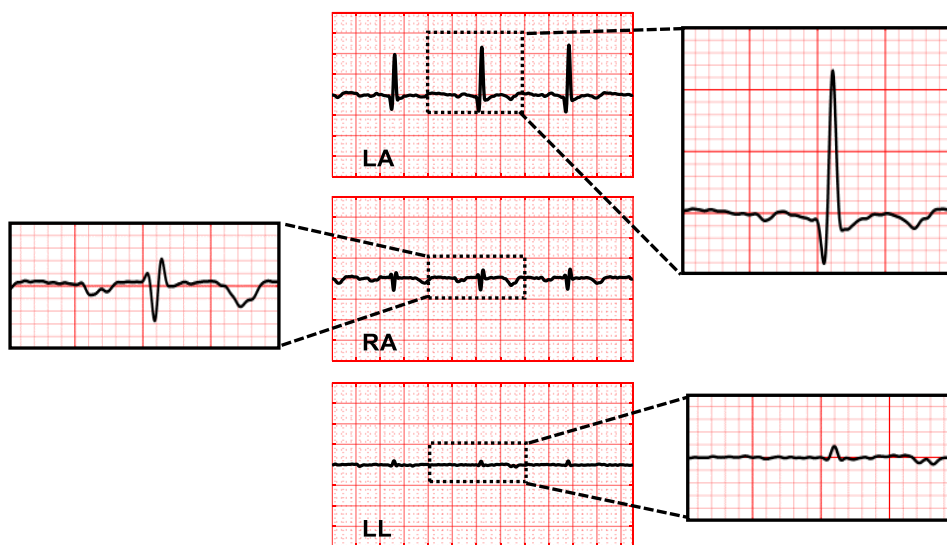


Figure 4. 17 Comparison of left arm (LA), right arm (RA) and left leg (LL) potentials. Recorded from a 75 years old female (PID 94).

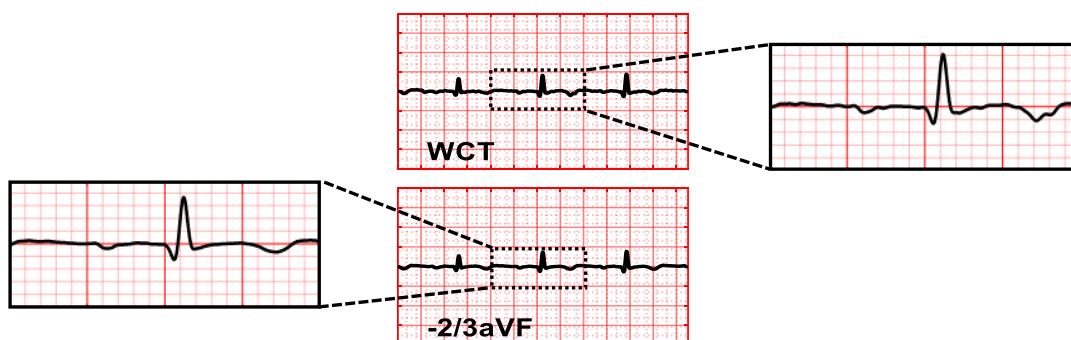


Figure 4. 18 Comparison of the WCT and  $-2/3aVF$ . Recorded from a 75 years old female (PID 94).

The standard precordial leads do not present any ischemic abnormalities, while  $UV_1$ :  $UV_2$  include T-wave inversion, and  $UV_3$  presents with biphasic T-wave. Reconstructed unipolar

leads ( $UV_1(R)$ :  $UV_6(R)$ ) and unipolar chest leads ( $UV_1$ :  $UV_6$ ) have the same clinical interpretation, as the WCT and  $-2/3aVF$  are identical.

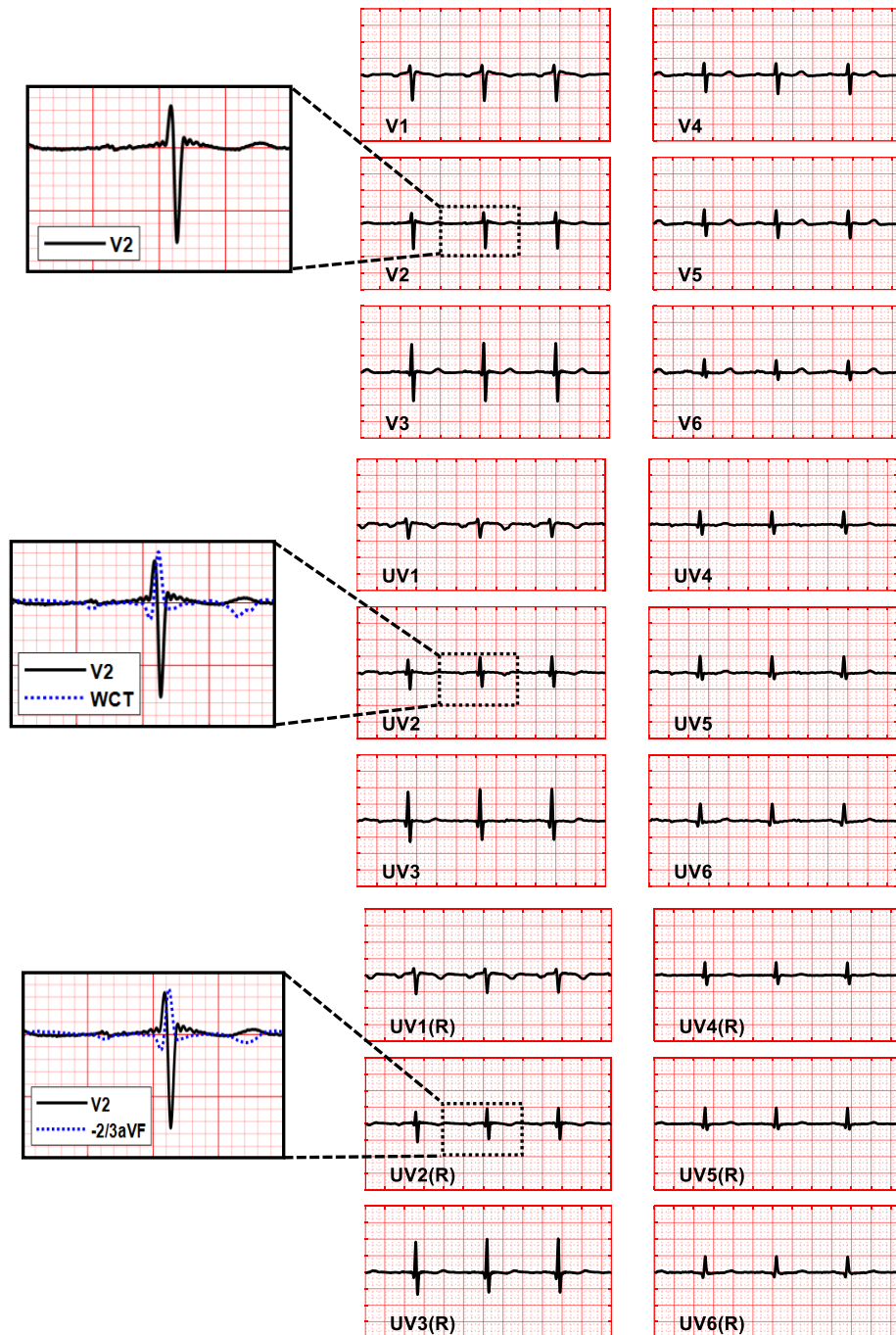


Figure 4. 19 Comparison between the standard precordial leads ( $V_1$ :  $V_6$ ) (top panel), unipolar chest leads ( $UV_1$ :  $UV_6$ ) (middle panel), and reconstructed unipolar chest leads ( $UV_1(R)$ :  $UV_6(R)$ ) (bottom panel). Recorded from a 75 years old female (PID 94).

**Case 7:** A 67 year old lady with a background of hyperlipidaemia presented to the emergency department with a two weeks history of worsening angina that became constant over the two days prior. Cardiac biomarkers were elevated at 118 ng/L and peaked at 627 ng/L. She was treated for NSTEMI and underwent coronary angiography that demonstrated a severe proximal first obtuse marginal artery (OM1) lesion (95%) for which she underwent angioplasty. The left leg presents with zero amplitude on T-wave; therefore, the WCT and  $-2/3aVF$  are clearly identical (see Figure 4.20 and Figure 4.21).

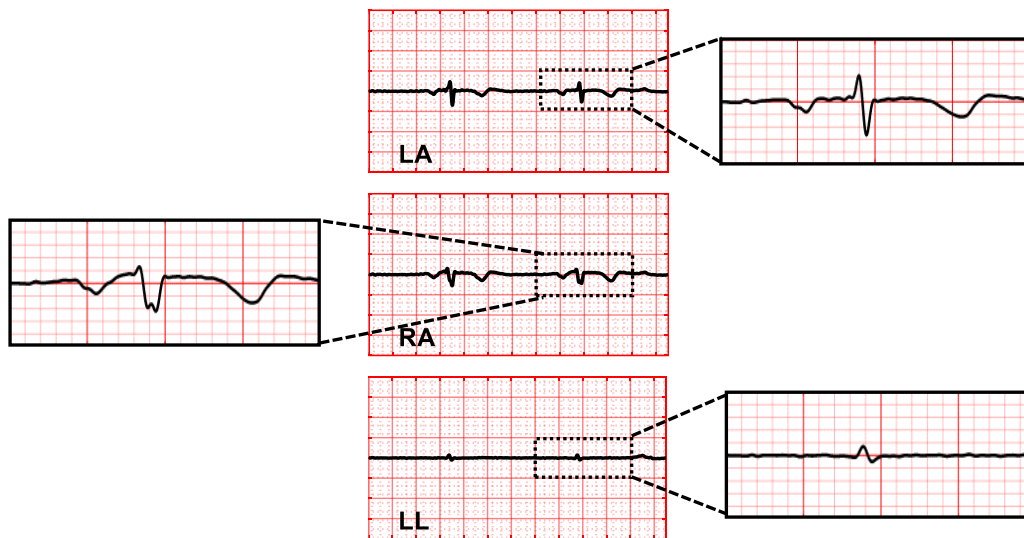


Figure 4. 20 Comparison of left arm (LA), right arm (RA) and left leg (LL) potential. Recorded from a 67 years old female (PID 58).

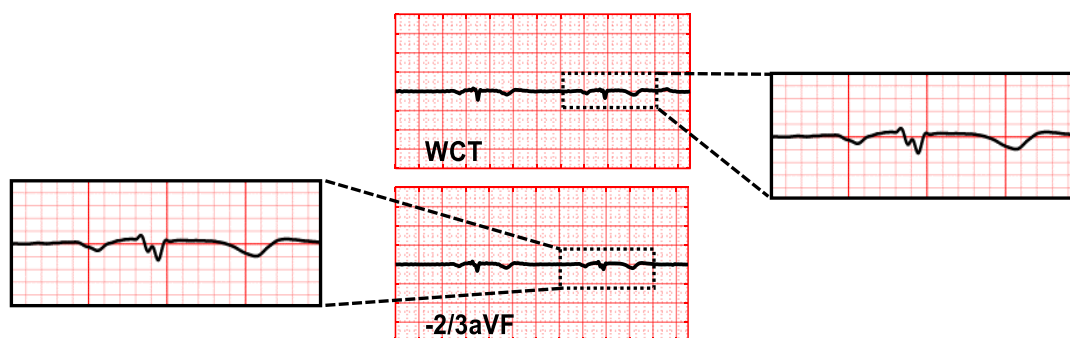


Figure 4. 21 Comparison of the WCT and  $-2/3aVF$ . Recorded from a 67 years old female (PID 58).

As it can be seen in Figure 4.22, the standard precordial leads present biphasic T-wave on  $V_1$ :  $V_5$  and upright T-wave on  $V_6$ . Since the WCT presents with T-wave inversion, the accumulation of the WCT and precordial leads only reduces the positive deflection in



unipolar chest leads. Therefore, the  $UV_1$ :  $UV_4$  show biphasic T-wave, while  $UV_5$  and  $UV_6$  present upright and flattened T-waves, respectively.

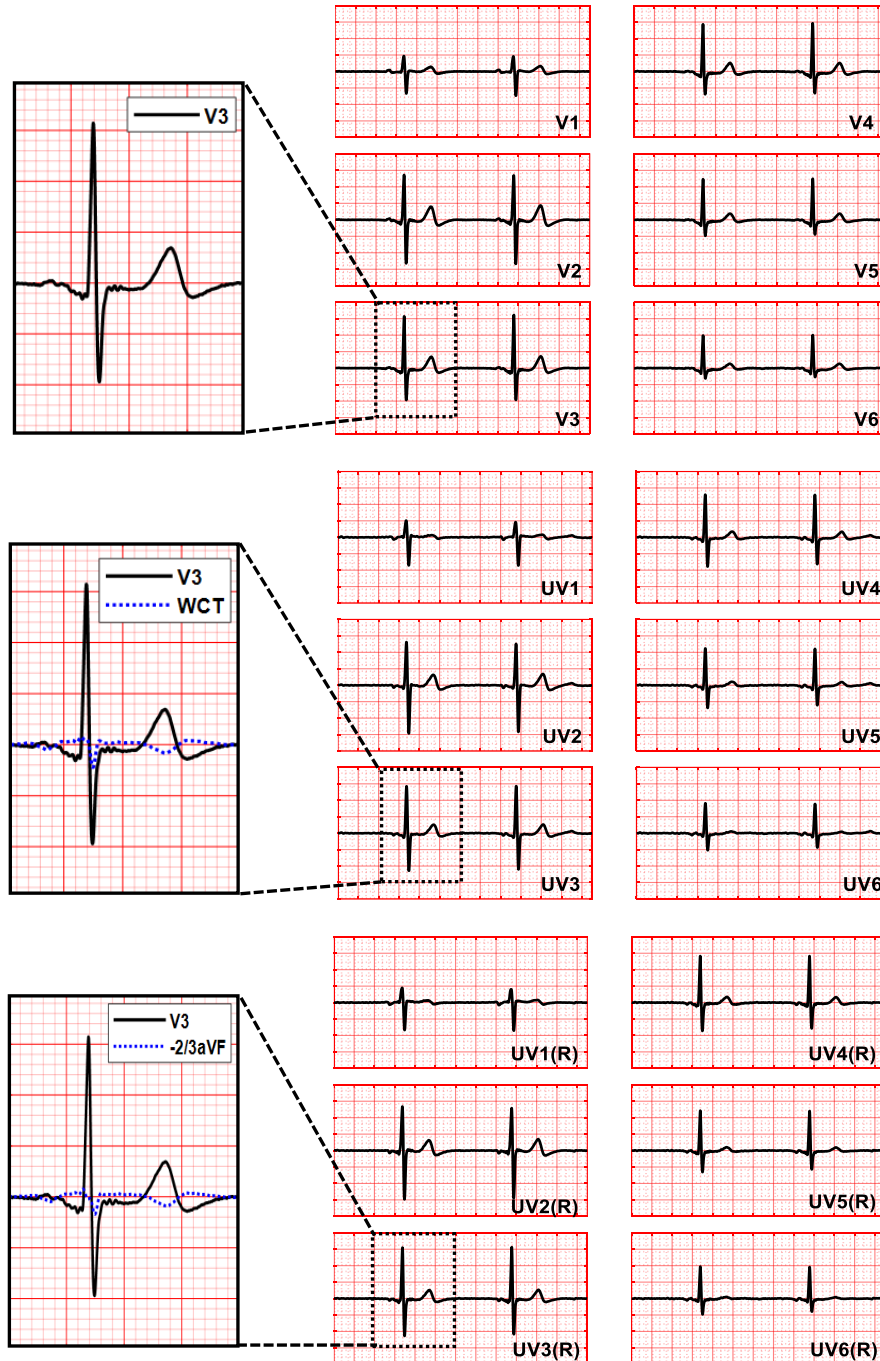


Figure 4. 22 Comparison of the standard precordial leads ( $V_1$ :  $V_6$ ) (top panel), unipolar chest leads ( $UV_1$ :  $UV_6$ ) (middle panel), and the reconstructed unipolar chest leads ( $UV_1(R)$ :  $UV_6(R)$ ) (bottom panel). Recorded from a 67 years old female (PID 58).

**Case 8:** A 55 year old male with previous history of ischemic heart disease (NSTEMI with PCI to LAD) presented with chest pain at rest, which lasted for 15 minutes. Cardiac biomarkers were elevated with troponin T (high-sensitive) 55 ng/Ln on presentation and peak Troponin T (high-sensitive) of 1079 ng/L. He was treated for NSTEMI. A coronary angiogram was performed which demonstrated a severe mid LAD lesion (95% stenosis) for which he underwent angioplasty, as well as a proximal D2 stenosis (70%) that was treated medically. As it can be referred from Figure 4.23, the WCT and -2/3 aVF present the same shape and amplitude. This is due to the negligible amplitude of the left leg potential (see Figure 4.24).

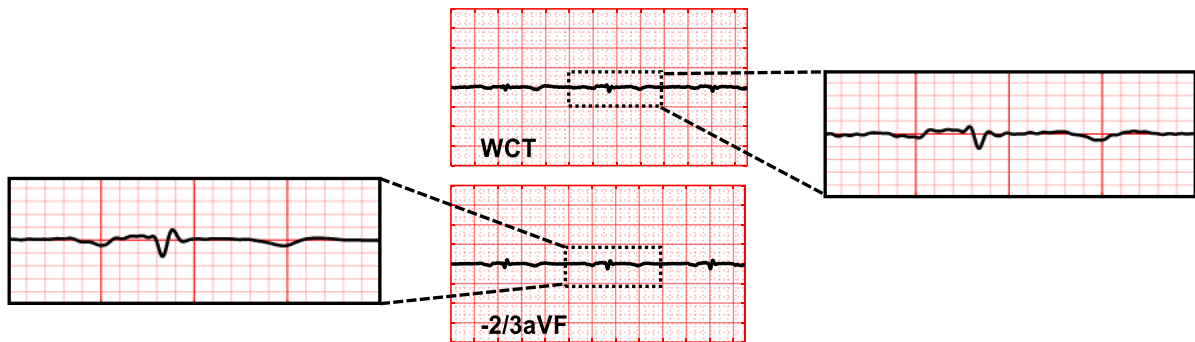


Figure 4. 23 Comparison of the WCT and -2/3aVF. Recorded from a 55 years old male (PID 93).

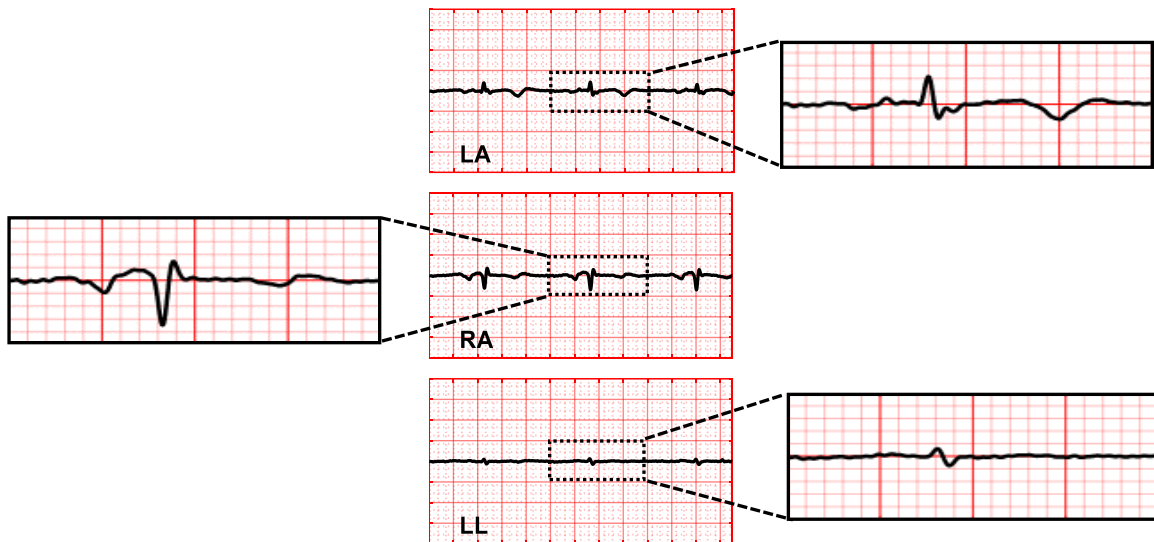


Figure 4. 24 Comparison of left arm (LA), right arm (RA) and left leg (LL) potential. Recorded from a 55 years old male (PID 93).

The standard precordial leads show T-wave inversion on V<sub>2</sub>: V<sub>6</sub>. Since the WCT has a small T-wave inversion (see Figure 4.25), the unipolar chest leads (UV<sub>1</sub>: UV<sub>6</sub>) and standard precordial leads (V<sub>1</sub>: V<sub>6</sub>) present with the same abnormalities.

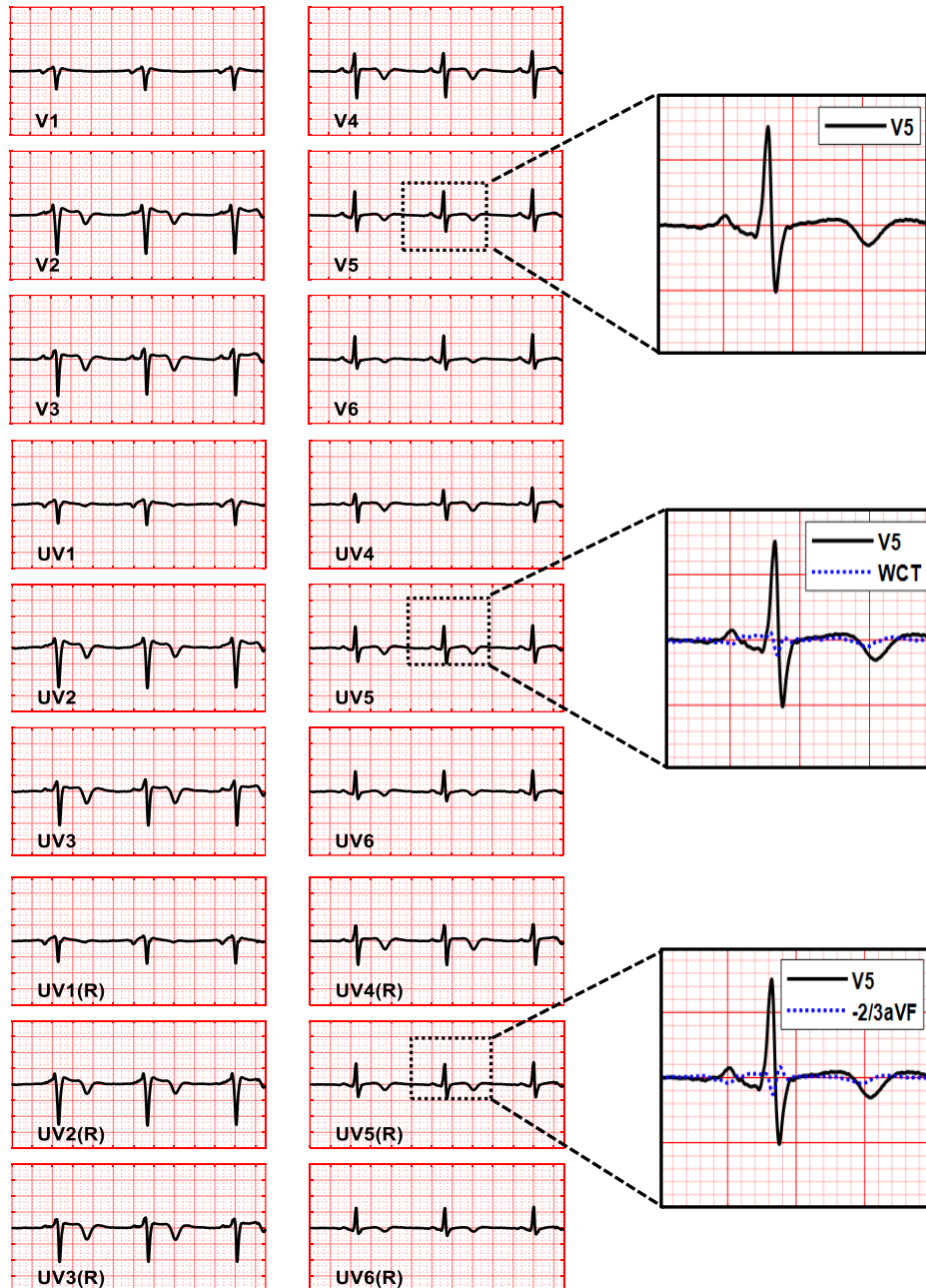


Figure 4. 25 Comparison between the standard precordial leads (V<sub>1</sub>: V<sub>6</sub>) (top panel), unipolar chest leads (UV<sub>1</sub>: UV<sub>6</sub>) (middle panel), and reconstructed unipolar chest leads (UV<sub>1</sub>(R): UV<sub>6</sub>(R)) (bottom panel). Recorded from a 55 years old male (PID 93).

**Case 9:** A 75 year old lady with a background history of small cell lung cancer for which she was receiving palliative chemotherapy was admitted with chest pain; cardiac biomarkers were elevated with troponin of 33 ng/L on presentation with a peak of 104 ng/L. She was treated for NSTEMI. A coronary angiogram was performed which demonstrated a critical proximal LAD lesion with 99% stenosis for which she underwent successful angioplasty. As can be seen in Figure 4.26, the left leg has a near-zero potential. Therefore, the WCT and  $-2/3aVF$  are almost identical (see Figure 4.27), and consequently, the unipolar chest leads ( $UV_1:UV_6$ ) and reconstructed unipolar chest leads ( $RUV_1(R):UV_6(R)$ ) have the same clinical interpretation (see Figure 4.28). The WCT signal presents with a flat T-wave; therefore, the unipolar chest leads do not show any clinical advantages.

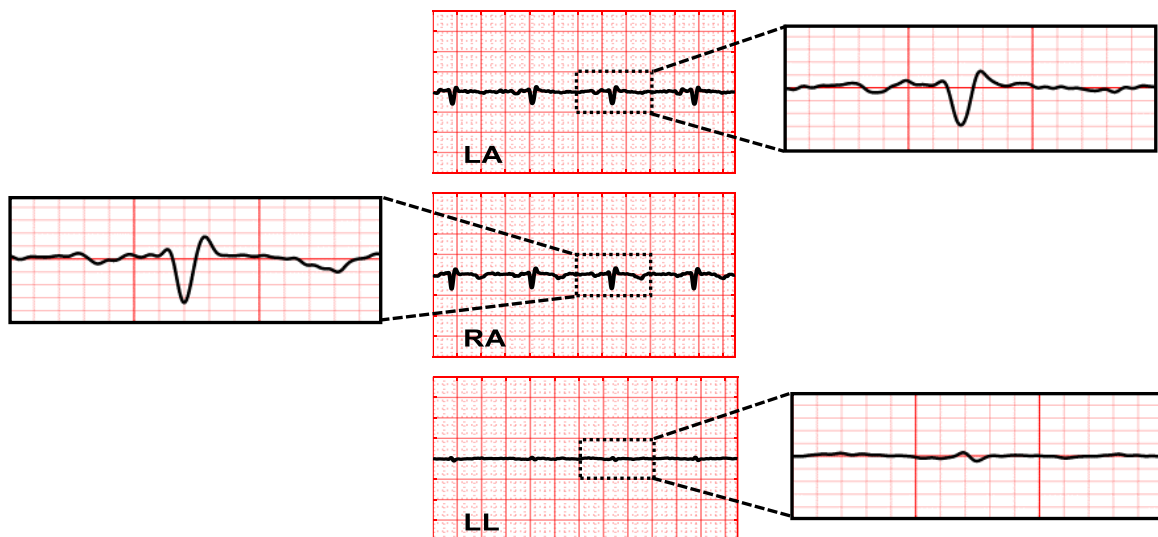


Figure 4. 26 Comparison of left arm (LA), right arm (RA) and left leg (LL) potential. Recorded from a 75 years old female (PID 100).

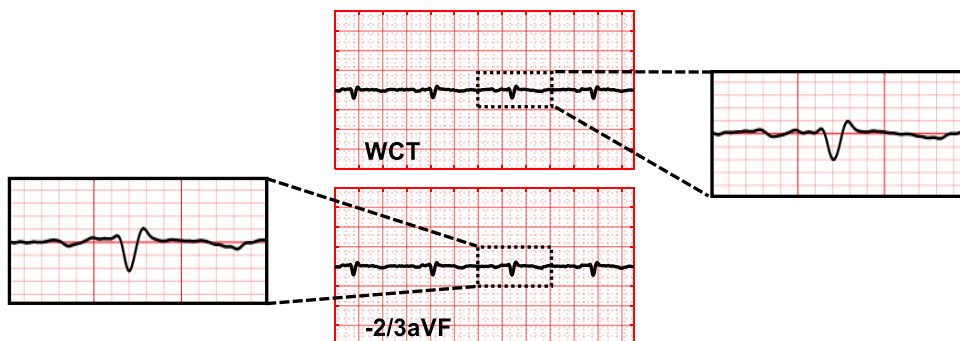


Figure 4. 27 Comparison of the WCT and  $-2/3aVF$ . Recorded from a 75 years old female (PID 100).

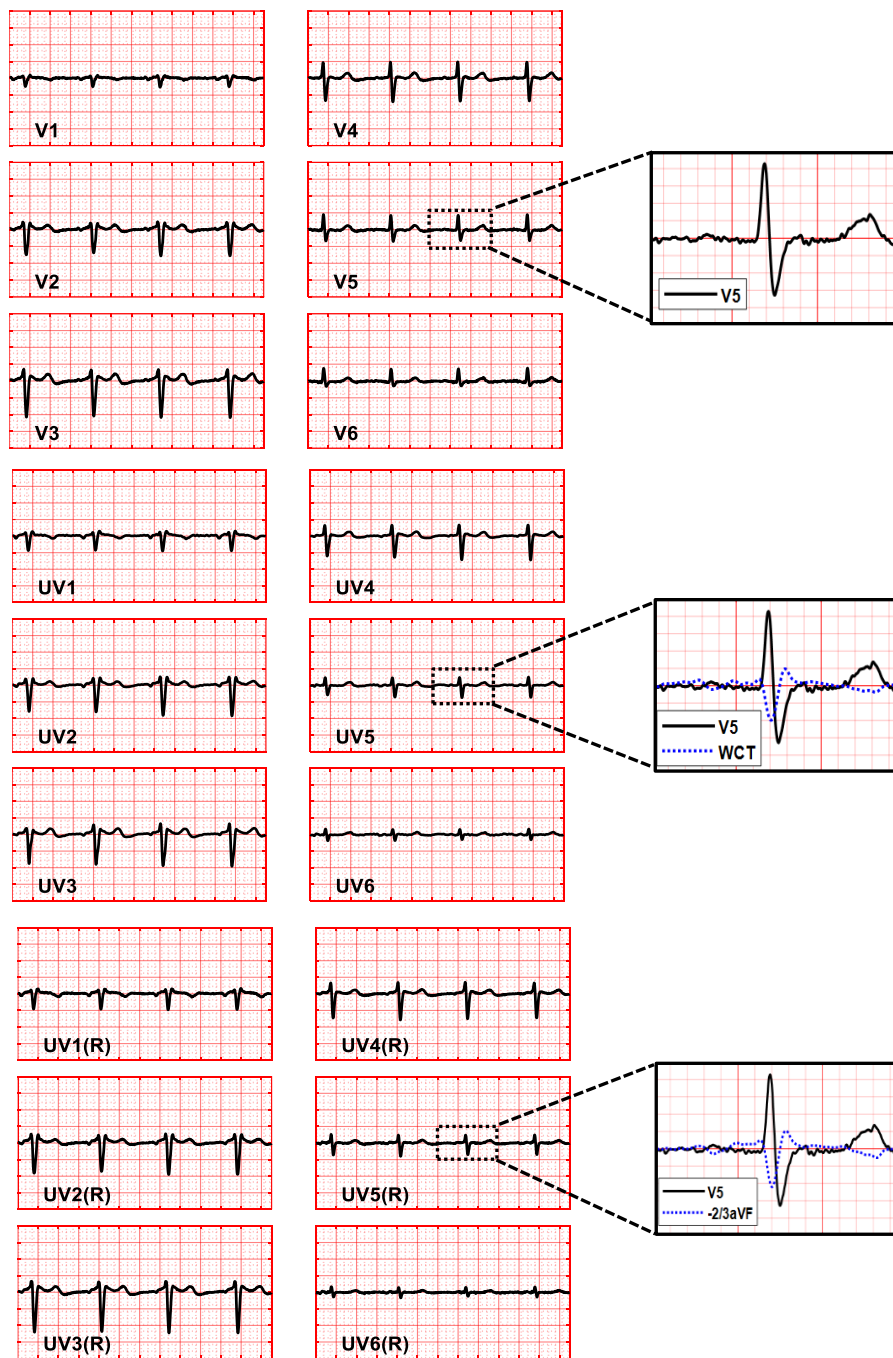


Figure 4. 28 Comparison between the standard precordial leads (V<sub>1</sub>: V<sub>6</sub>) (top panel), unipolar chest leads (UV<sub>1</sub>: UV<sub>6</sub>) (middle panel), and the reconstructed unipolar chest leads (UV<sub>1</sub>(R): UV<sub>6</sub>(R)) (bottom panel). Recorded from a 75 years old female (PID 100).

## 4.4 Conclusion

The ECG is the key real-time diagnostic test to diagnose acute coronary syndromes in patients presenting with chest pain. However, often the ECG is normal in patients with NSTEMI. This chapter presented nine NSTEMI cases, which have ECG recorded just before undergoing angiogram. The unipolar chest leads ( $UV_1$ :  $UV_6$ ), reconstructed unipolar chest leads ( $UV_1(R)$ :  $UV_6(R)$ ), and standard precordial leads ( $V_1$ :  $V_6$ ) are compared for each patient. The medical assessment shows that the unipolar chest leads are more sensitive to show abnormalities for six patients, while the standard precordial leads and unipolar chest leads present the same features for only three patients. Furthermore, it is shown that the potential of the left leg can be medically relevant, as important clinical features are lost in the reconstructed unipolar chest leads for these three patients.

The difference between the novel and standard ECG devices is in the recordings of the precordial leads, which look at the septum and anterolateral parts of the left ventricle, supplied by the left anterior descending coronary artery. Given the prognostic significance of left anterior descending coronary artery disease, improvement in ECG sensitivity as shown by this ECG device is likely clinically significant.

# Chapter 5 The minimisation of the Wilson's Central Terminal voltage potential via a genetic algorithm

This chapter introduce an expert approach to minimise the Wilson's Central Terminal using the genetic algorithm.

*Some of the work presented in this chapter has been published in:*

- *H. Moeinzadeh, G. D. Gargiulo, P. Bifulco, M. Cesarelli, A. L. McEwan, A. O'Loughlin, M. I. Shugman, J. C Tapson, and A. Thiagalingam, "Computing a new central terminal for ECG recording using combined genetic algorithm and linear regression from real patient data". In: Proceedings of the Genetic and Evolutionary Computation Conference Companion (GECCO17). 2017. p. 293–4.*
- *H. Moeinzadeh, G. D. Gargiulo, P. Bifulco, M. Cesarelli, A. L. McEwan, A. O'Loughlin, M. I. Shugman, J. C Tapson, and A. Thiagalingam, "Minimize Wilson Central Terminal Using Genetic Algorithm". Hear Lung Circ . 2018 Jan 1;27:S330.*
- *H. Moeinzadeh, P. Bifulco, M. Cesarelli, A. L. McEwan, A. O'Loughlin, M. I. Shugman, J. C Tapson, A. Thiagalingam, and G. D. Gargiulo, "Minimization of the Wilson's Central Terminal voltage potential via a genetic algorithm". BMC Res Notes. 2018 Dec 20;11(1):915.*

## 5.1 Abstract

The Wilson Central Terminal (WCT) is an artificially constructed reference for surface electrocardiography, which is assumed to be near zero and steady during the cardiac cycle; namely it is the simple average of the three recorded limbs (right arm, left arm and left leg) composing the Einthoven triangle and considered to be electrically equidistant from the electrical centre of the heart. This assumption has been challenged and disproved in 1954 with an experiment designed just to measure and minimise WCT. Minimisation was attempted varying in real time the weight resistors connected to the limbs. Unfortunately, the experiment required a very cumbersome setup and showed that WCT amplitude could not be universally minimised, in other words, the weight resistors change for each person. Taking advantage of modern computation techniques as well as of a special ECG device that aside of the standard 12-lead electrocardiogram (ECG) can measure WCT components, a software minimisation method is proposed using data recorded from 72 volunteers.

## 5.2 Background

The ‘zero’ reference for the precordial leads was introduced by F. N. Wilson in 1931 and named after him as Wilson’s Central Terminal (WCT). It is derived by averaging three limb leads and was assumed to be steady and of negligible amplitude during the cardiac cycle. However, WCT is neither steady nor of negligible amplitude [60]. To quantify the WCT, Wilson proposed immersing the body in a large homogeneous conductor and stated that 0.15 mV was its maximal value [16], [77]. Following this recommendation, Bayley and Kinard [65], [70] encased the body of volunteers inside a metal structure (called integrator electrode) that was immersed it in water for the duration of the recording. This set-up allowed them to compute what they called “zero of the potential for the human body”. With this experiment, they determined that the WCT is non-stationary during the cardiac cycle and its amplitude could be as large as 40% of Einthoven’s ECG signals [65], [70]. During the WCT measurement experiment, Bayley and Kinard also attempted a real-time minimisation of the WCT amplitude to bring it below a non-influent value [70]. During the experiment, they



made use of three rheostats instead of fixed resistors and adjusted the weights of the three WCT components continually reporting the achieved new amplitude.

This chapter describes an expert approach which similarly to the originally attempted minimisation, performs a weighted average of the WCT components. The WCT minimisation performed using the genetic algorithm (GA) [110]. The WCT minimization approach currently is a post processing method, and it is not built inside our new ECG device. The GA is a heuristic search method for finding the optimal answer for problems with high computational complexity. This approach is used for those problems, that either lacks a deterministic solution or a deterministic polynomial time complexity solution. This algorithm is called “genetic” because is based on the concept of the biological evolution of individuals within a population where “chromosomes” mutates to achieve the survival of the fittest. A “chromosome” represents a possible solution to the problem that can mutate from one population of chromosomes to the next population (generation) by using a “selection” procedure. The chromosomes that are selected to be in the next generation also could be changed or become parents of new chromosomes in the process of “mutation”, and “crossover” [110].

### **5.3 WCT minimisation method**

This work aims to make feasible the idea that the WCT amplitude can be personalized and minimised during the recording. Taking advantage of our newly developed ECG device [80], a personalized (to the patient) software minimisation of the WCT is performed. To our knowledge, this is the first attempt since Bayley and Kinard’s effort in 1954 [70]. Figure 5.1 demonstrates the schematic view of the hardware which measures the voltage of right arm (RA), left arm (LA) and left leg (LL) and the proposed approach to estimate M-WCT (whereas M stands for minimised) according to the following main criteria:

- 1) Less variation than WCT during a cardiac cycle.
- 2) Possibly be zero or near zero.
- 3) In any case (worst case scenario), M-WCT amplitude should be less than 0.1 mV, so that it can be considered clinically irrelevant.

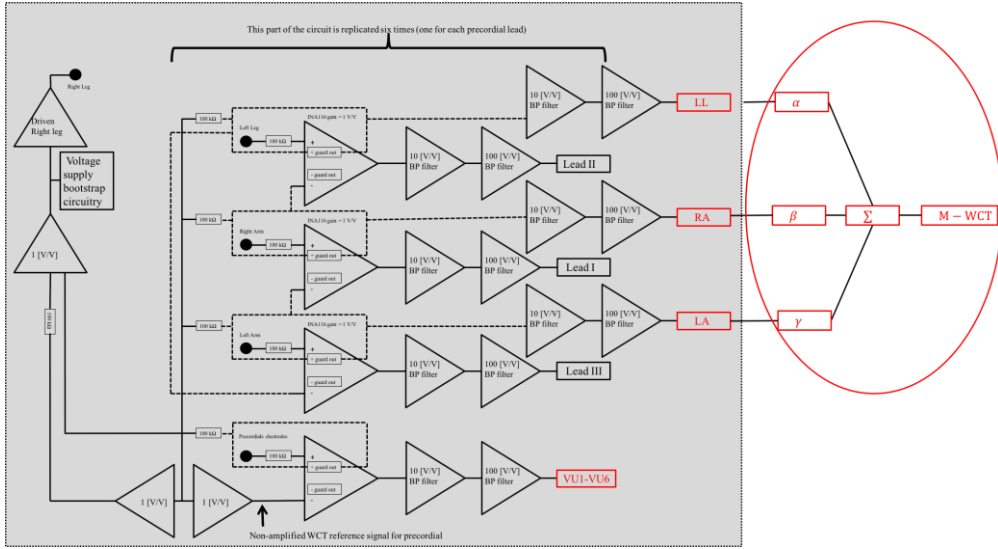


Figure 5. 1 Hardware (shaded square) and software (red circle) principle diagram, adapted from

In order to fit the M-WCT into the genetic algorithm paradigm, it is needed to formalize the problem in terms of population, mutation, crossover and fitness function. Recalling that the WCT is the average of the limbs' electrodes, the M-WCT is defined as the weighted mean of the WCT's components. In other words, weights different from 1/3 are applied to the right arm, left arm, and left leg potentials (weights are labelled as:  $\alpha$ ,  $\beta$ , and  $\gamma$ ). These weights are constrained to be positive, non-null and less than one, such that the summation of these weights is equal to one. More formally:

$$M-WCT = \alpha\phi_L + \beta\phi_F + \gamma\phi_R \quad (5.1)$$

$$0 < \alpha, \beta, \gamma < 1 \quad (5.2)$$

$$\alpha + \beta + \gamma = 1 \quad (5.3)$$

Therefore, our method will minimise (5.1) according to the three main criteria enounced above respecting the constraints (5.2) and (5.3).

### 5.3.1 Fitness function

The role of the fitness function is to measure the quality of each chromosome (possible solution), in other words, the fitness function ensures “the survival of the fittest” hence converging towards the solution. Because the goal is to find the three weighted factors that

minimise WCT, the M-WCT (Eq. 5.1) could be, in the first instance, considered as the fitness function. However, the following Eq. 5.4 works better as the fitness function. This is because its shape and its nonlinearity provide an increase in the probability of having M-WCT with smaller values; in other words, it encourages the algorithm to converge more rapidly. The plot of the fitness function is depicted in Figure 3.

$$\text{Fitness} = \log_{0.00001} |M - WCT| \quad (5.4)$$

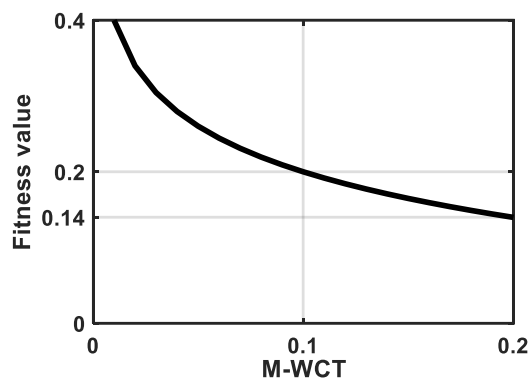


Figure 5. 2 Nonlinear fitness function is used to encourage individuals to have smaller M-WCT

As shown in Figure 5.2, the slope of fitness function is non-linearly increased for the M-WCT values less than 0.1 mV. Consequently, individuals with a medically irrelevant value ( $< 0.1$  mV) are encouraged to be produced for the next population.

### 5.3.2 Population

The population represents all possible answers (chromosomes). A new population is generated during each iteration of the GA. Each individual represents a possible answer which contains three weighted factors ( $\alpha, \beta, \gamma$ ) and 80 individuals are chosen as population size. The first population is initialized by the WCT chromosome ( $\alpha = \beta = \gamma = 1/3$ ) and the rest are generated randomly constrained only by the conditions Eq. 5.2 and Eq. 5.3.

### 5.3.3 Crossover

The role of the crossover operation is to build the next population based on selected chromosomes of the current population. The single point [111] and averaging crossover [112] methods are used randomly to populate the next generation. In single point crossover, two parents are split from the same location, and each child gets right sub-chromosome of one parent and left sub-chromosome of another parent [111]. We also use the average crossover, which in every child is the outcome of averaging two random chromosomes [112].

### 5.3.4 Mutation

The genetic algorithm exploits a mutation operator to avoid trapping into local optima while searching a diversity of possible answers. The permutation algorithm is used to change the position of three parameters in a selected chromosome.

To ensure the genetic algorithm converges to an optimal solution, the elite member of each population is moved to the next generation directly. We also constantly preserve the WCT chromosome in each population. We apply our method to every voltages sample and compute three parameters to have the M-WCT trace during the cardiac cycle.

## 5.4 Results and Discussion

For this study, 72 patients from WCTECGdb [99] are used. Each patient selected data excerpt has a normalized length of 10 seconds. As mentioned earlier, three weighted factors ( $\alpha$ ,  $\beta$ , and  $\gamma$ ), are calculated using the GA to minimise Wilson Central Terminal. In Table 5.1, the average values of the three weights ( $\alpha$ ,  $\beta$ , and  $\gamma$ ) are reported. Furthermore, the average number of iterations that the GA needs to converge for each patient is included in Table 5.1. As it can be seen in Table 5.1, the GA converges to its best with an average number of iterations of 199.39 among all patients.

Table 5. 1 Average of three achieved parameters (alpha, beta, and gamma), and the number of GA iteration for each patient.

Patient ID	Age	Gender	Alpha	Beta	Gamma	GA Iteration
P001	69	F	0.33	0.40	0.26	249.98
P002	56	M	0.30	0.33	0.35	235.43
P003	71	F	0.33	0.20	0.46	182.52
P004	78	M	0.26	0.35	0.38	246.66
P005	73	M	0.35	0.32	0.33	263.03
P006	89	M	0.27	0.37	0.36	208.37
P007	72	M	0.31	0.31	0.37	277.99
P008	80	M	0.26	0.30	0.43	258.03
P009	53	M	0.29	0.43	0.27	200.19
P010	65	M	0.27	0.33	0.39	225.71
P011	62	M	0.28	0.36	0.36	258.74
P012	52	M	0.30	0.37	0.32	256.34
P013	45	M	0.37	0.27	0.35	156.07
P014	88	F	0.21	0.26	0.52	212.91
P015	63	F	0.32	0.36	0.32	260.94
P016	70	F	0.22	0.28	0.49	187.13
P017	85	M	0.25	0.30	0.45	203.88
P018	52	F	0.31	0.39	0.29	229.00
P019	59	M	0.24	0.28	0.47	181.31
P020	68	M	0.29	0.23	0.49	133.43
P021	63	F	0.30	0.36	0.33	230.38
P022	51	F	0.31	0.35	0.34	176.66
P023	65	F	0.24	0.30	0.46	212.53
P024	71	M	0.26	0.20	0.54	142.75
P025	52	M	0.29	0.17	0.54	140.99
P026	81	F	0.21	0.31	0.47	262.09
P027	43	M	0.32	0.33	0.34	254.86
P028	68	F	0.23	0.31	0.46	142.50
P029	72	F	0.28	0.36	0.35	246.08
P030	59	M	0.13	0.13	0.74	161.74

P031	54	F	0.31	0.19	0.49	122.83
P032	67	M	0.31	0.35	0.33	204.84
P033	55	F	0.21	0.13	0.67	119.09
P034	58	M	0.26	0.20	0.54	128.99
P035	56	M	0.25	0.29	0.45	239.17
P036	70	M	0.16	0.29	0.55	143.35
P037	52	M	0.29	0.21	0.50	143.28
P038	74	F	0.28	0.27	0.45	133.95
P039	76	F	0.25	0.25	0.49	154.59
P040	53	F	0.21	0.30	0.49	207.53
P041	76	M	0.24	0.18	0.57	238.04
P042	78	M	0.18	0.29	0.52	177.94
P043	94	M	0.22	0.22	0.55	230.17
P044	82	F	0.30	0.33	0.36	225.20
P045	66	M	0.18	0.18	0.64	221.82
P046	59	M	0.29	0.16	0.55	176.14
P047	64	M	0.20	0.30	0.50	147.33
P048	75	M	0.27	0.29	0.43	253.13
P049	83	M	0.23	0.28	0.49	191.23
P050	73	M	0.28	0.35	0.36	198.35
P051	59	M	0.18	0.29	0.52	200.31
P052	57	M	0.28	0.30	0.41	202.55
P053	66	M	0.18	0.21	0.60	182.24
P054	84	F	0.29	0.31	0.40	157.48
P055	70	M	0.21	0.28	0.51	203.28
P056	58	M	0.25	0.33	0.41	140.74
P057	59	M	0.18	0.23	0.59	172.85
P058	66	F	0.21	0.26	0.52	207.90
P059	51	M	0.23	0.29	0.48	219.87
P060	61	M	0.19	0.19	0.62	217.25
P061	68	F	0.37	0.28	0.34	183.96
P062	56	F	0.30	0.32	0.37	159.35

P063	61	M	0.26	0.22	0.52	179.82
P064	84	M	0.14	0.15	0.70	206.60
P065	65	M	0.26	0.26	0.47	224.30
P066	53	F	0.20	0.15	0.65	177.41
P067	69	M	0.27	0.37	0.35	202.11
P068	47	M	0.25	0.32	0.43	204.21
P069	82	F	0.18	0.21	0.61	250.19
P070	71	F	0.20	0.26	0.54	170.94
P071	73	M	0.15	0.15	0.69	181.70
P072	77	M	0.33	0.34	0.32	255.95
Average	66.35		0.26	0.28	0.46	199.39
Total: 72 patients		35% Females				

The WCT and M-WCT amplitudes were measured for each subject and reported as a percentage of lead II. We then averaged the measured amplitudes over five consecutive beats. In Table 5.2 we report the amplitude of the M-WCT and the WCT for each patient (both reported as a relative percentage to lead II). Our results show that the M-WCT relative percentage has a mean value of 7.45% with a standard deviation value of 9.04%, while the WCT relative percentage has a mean value of 58.85% with a standard deviation of 30.84%.

Based on our measurements, the WCT recorded is highly individual, and can have standard ECG characteristics, such as a P-wave and a T-wave. Individuality was also found in the M-WCT, as we show in Figure 4 and Table 2. However, due to the negligible general amplitude of M-WCT, we conclude that the clinical impact of the M-WCT is negligible with respect to the WCT. To show the characteristics of WCT and M-WCT signals, we measured the number of irrelevant points (amplitude  $< 0.1$  mV) in both M-WCT and WCT signals and showed the decrease percentage of irrelevant points in Table 5.2. The ideal reference point has a value near zero with minimum variation during the cardiac cycle, consequently the number of points that are equal to zero (corresponding to iso-electric) also calculate for both WCT and M-WCT signals. The increase in the percentage of zero points in M-WCT is presented in Table 5.2.

Table 5. 2 Comparison of the WCT and M-WCT amplitudes in relation to lead II.

Patient ID	WCT amplitude as % of lead II	M-WCT amplitude as % of lead II	Zero points increase [%]	Medically irrelevant points decrease [%]
P001	43.32	25.22	21.35	7.67
P002	67.08	8.26	27.55	3.90
P003	34.19	2.41	50.24	5.85
P004	44.22	2.75	22.63	9.16
P005	104.37	18.73	15.77	7.37
P006	77.77	26.67	39.06	1.50
P007	22.35	0.00	9.40	6.99
P008	55.19	11.93	17.91	16.14
P009	91.05	0.00	42.68	7.86
P010	14.40	2.96	31.63	0.84
P011	34.35	11.06	17.15	10.56
P012	16.47	1.78	18.65	8.17
P013	22.25	0.00	61.35	0.31
P014	115.21	17.63	37.36	12.27
P015	35.97	8.54	16.67	2.34
P016	59.80	6.52	48.16	2.54
P017	30.40	1.08	41.01	0.64
P018	114.07	31.65	30.37	2.04
P019	134.30	28.12	49.64	2.12
P020	34.34	0.38	69.52	3.81
P021	38.80	4.95	29.10	3.07
P022	34.21	0.27	51.47	2.37
P023	41.77	5.11	36.52	3.14
P024	43.10	1.45	65.69	0.00
P025	45.27	3.59	66.44	0.00
P026	43.73	13.74	15.82	12.00
P027	21.46	8.16	18.86	6.89
P028	40.03	1.11	65.75	3.20
P029	42.85	12.20	22.47	9.59



P030	58.59	3.13	58.96	18.67
P031	25.77	0.38	73.82	2.26
P032	49.53	0.00	39.76	1.20
P033	41.64	0.34	76.63	5.76
P034	29.87	0.20	71.54	2.20
P035	78.56	10.56	25.38	14.66
P036	56.36	1.08	65.92	2.96
P037	35.47	0.94	65.39	1.39
P038	33.71	0.00	69.37	1.87
P039	42.46	0.53	60.90	5.24
P040	36.86	4.84	39.57	1.26
P041	71.01	10.81	26.52	15.32
P042	111.88	18.45	52.29	9.79
P043	91.78	13.06	29.78	6.37
P044	52.80	3.60	31.97	4.75
P045	75.27	11.70	33.45	24.50
P046	59.21	2.79	52.91	7.75
P047	56.56	5.72	65.27	4.70
P048	83.31	11.25	19.99	6.17
P049	24.86	0.00	46.37	0.00
P050	118.82	11.04	43.39	5.22
P051	123.12	25.31	42.77	3.82
P052	74.55	7.49	41.58	4.65
P053	86.42	5.11	49.64	8.22
P054	10.65	0.53	59.39	0.79
P055	68.50	3.18	40.61	6.54
P056	88.95	1.33	66.47	6.32
P057	70.29	0.21	53.51	6.86
P058	82.20	2.90	38.52	4.97
P059	68.92	8.43	33.58	6.84
P060	53.92	0.70	34.85	5.69

P061	28.19	1.59	49.59	0.17
P062	16.16	0.56	59.97	0.36
P063	34.43	1.39	51.26	2.24
P064	87.98	5.12	40.58	18.82
P065	83.79	12.31	32.48	1.05
P066	42.83	1.46	52.56	6.32
P067	143.06	47.01	41.83	3.20
P068	91.86	7.02	40.91	5.86
P069	77.69	8.60	21.42	20.97
P070	34.22	6.07	55.09	2.15
P071	60.17	1.86	50.98	11.26
P072	72.72	21.43	18.82	7.64
Average	58.85	7.45	42.58	5.96

Figure 5.3 shows an example of WCT in which a broader QRS feature with amplitude even higher than Lead II is observed. However, as one can infer comparing M-WCT and WCT (bottom panel), the relative amplitude of M-WCT has highly decreased compared to WCT relative amplitude.

An example of the WCT signal with a marked T-wave is visible in Figure 5.4. As it can be seen, a marked T-wave deflection on the WCT trace (bottom panel) is synchronized with the T-wave on lead II (top panel). The WCT trace in Figure 5.4 is also an excellent example of a highly variable WCT and an almost steady M-WCT. In one single cardiac cycle, the deflection's polarity of the WCT changes at least three times, and its amplitude reaches 45.27% of lead II (average), while the M-WCT amplitude is 3.59% of lead II.

Figure 5.5 is an example of high WCT amplitude with negative deflection. As seen, WCT has an amplitude of 59.21% of lead II, while M-WCT amplitude is only 2.79% of lead II.

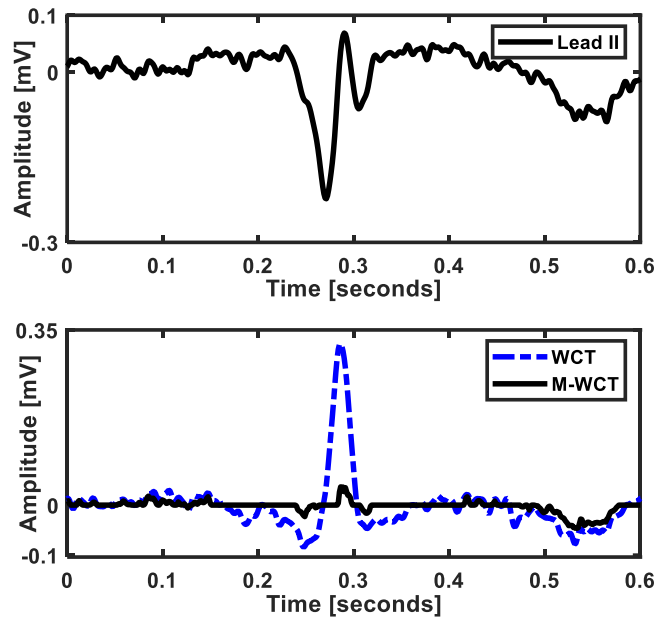


Figure 5. 3 Example of positive deflection WCT. M-WCT is 11.04% of lead II amplitude, while WCT is 118.82% of lead II amplitude (average); the recording is from a 73-year-old male patient admitted at the hospital (Patient ID: P050).

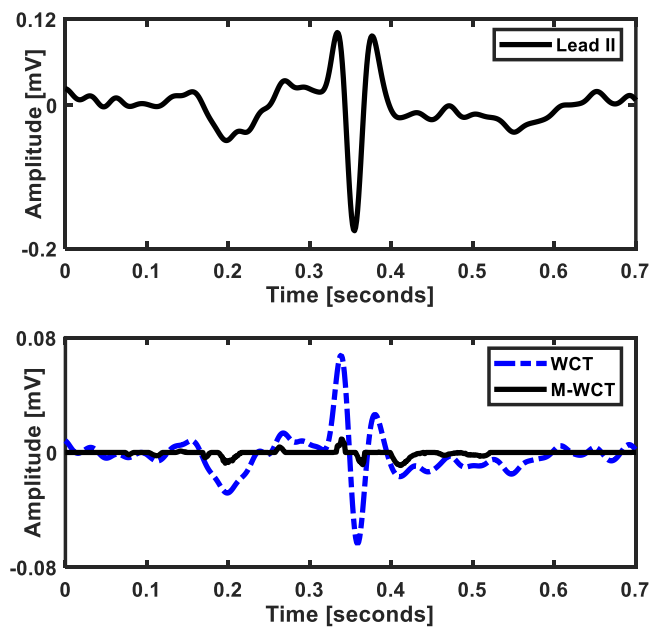


Figure 5. 4 Example of neutral deflection WCT. WCT is 45.27% of lead II amplitude, while M-WCT is 3.59% of lead II amplitude (average); the recording is from a 52-year-old male patient admitted with chest pain (Patient ID: P025). WCT for this patient presents marked P-wave and T-wave.

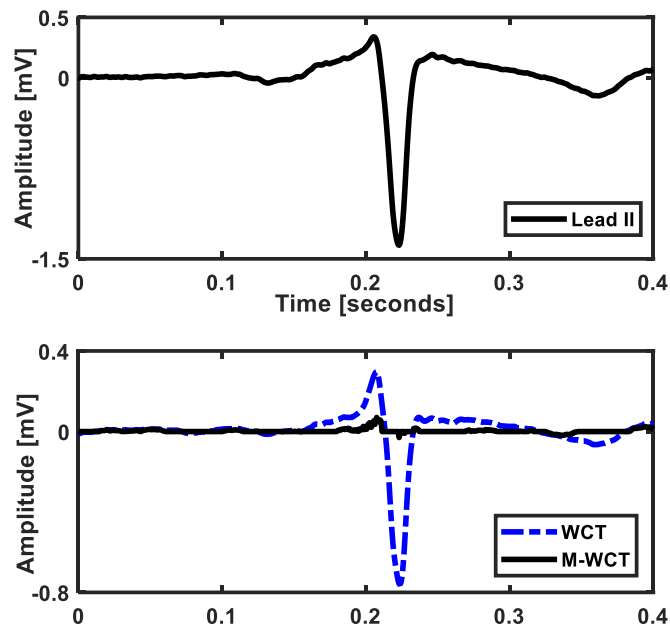


Figure 5. 5 Example of negative deflection WCT. WCT is 59.21% of lead II amplitude, while M-WCT is 2.79% of lead II amplitude (average); the recording is from a 59-year-old male patient admitted with chest pain (Patient ID: P046).

## 5.5 Conclusions

In this chapter, a software approach is proposed to minimise the reference potential for precordial ECG leads, which referred as the Minimised Wilson Central Terminal (M-WCT). Historically, minimisation and true measurement of WCT was attempted using a metal structure to encase the patient and submerged in water for the duration of the recording while operators adjusted manually reostats to vary the value of the averaging resistors. With this method, minimisation is personalized to the patient and obtained using a genetic algorithm applied to three components of the WCT. The M-WCT has near zero amplitude with small variation during the cardiac cycle. The measurements on 72 patients demonstrate that the average of the M-WCT amplitude relative to lead II is 7.45% with a standard deviation of 9.04%, while the average relative WCT amplitude is 58.85% with a standard deviation 30.84%. These results are associating with the aforementioned characteristics of M-WCT highlight the potential of the M-WCT as ideal reference point.

## **Chapter 6 Discussion and Future Directions**

This chapter provides a summary of the work presented in this thesis by briefly discussing the motivation, objectives, and achievements of the presented work. It is followed by a list of prospective future works.

## 6.1 Summary of Contributions

The surface electrocardiography (ECG) is the most widespread method to diagnose cardiac diseases. As discussed in the previous chapters, some assumptions and hypothesis at the base of electrocardiography, have been known to be incorrect even before the standardization of 12-leads electrocardiography and, thus, challenged several times during the years after standardization. Although there were some efforts to suggest different setups to record the heart rhythm, these studies were limited and consequently did not get enough attention. This research aimed to introduce a new setup to record precordial leads, which is more sensitive to show the abnormalities in patients with Non-ST segment elevation myocardial infarction (NSTEMI) and it uses the same 12-lead electrodes setup. To some extent this system can be seen as an extension of the current practice which provides the opportunity to record the Wilson's Central Terminal (WCT) and investigate the so-believed assumptions in regards with the reference point of the precordial leads preserving the well-known 12-lead system that doctors and technicians are well trained to use. The main outcomes of the presented work are listed below:

- 1- A comprehensive literature review in evolution of electrocardiography is presented in chapter one. This review highlights the studies which lead to choose Wilson's Central Terminal as the standard reference point to record precordial leads. Furthermore, the new electrocardiogram device is introduced in detail in chapter one. This ECG device uses the right leg as a new reference point to record the chest leads, and it also records the standard precordial leads simultaneously.
- 2- The Wilson Central Terminal ECG database (WCTECGdb) is introduced in chapter two. I have recorded the ECG using our new ECG device for about three years at Campbelltown hospital. The first two years (2016:2018) recordings were published on the Physionet platform. This dataset includes three limb leads, standard six precordial leads in addition to the potential of three limbs' and six chest electrodes referred to the right leg. More importantly, the WCT signal is presented for each patient in this dataset. Therefore, I was able to investigate the legitimacy of WCT assumptions. The results show that the WCT is characterised as a systematic error, which has a different influence on recording the precordial leads in every individual. Therefore, the patients

were classified into three groups, which have *zero*, *negligible*, and *significant* WCT error.

- 3- The Einthoven limbs' potential assumptions are investigated in chapter three using the data from 147 patients recorded during (2016-2019). Furthermore, the authentication of relationship between the WCT and aVF is analysed as an alternative way to estimate the WCT signal. The obtained results show that unlike the initial assumption, the left arm has the highest potential among the three limbs in only 47 percent of the patients and the potential of the left leg is not negligible for all patients. Furthermore, the left leg has a considerable amplitude for 25 percent of patients, which consequently influences the shape and amplitude of the WCT. Therefore, the WCT and  $-2/3aVF$  have a relatively small correlation and large RMS error in this group of patients.
- 4- A series of case reports are presented to show the medical implications of the WCT and  $-2/3aVF$ . Only patients diagnosed with non-ST-segment elevation myocardial infarction (NSTEMI) were selected for this study, this is because it is well-known that 12-lead ECG is not a sufficient diagnostic tool for this cardiac disease. For these patients, the WCT was found having important clinical features. Therefore, the unipolar chest leads are more sensitive to present abnormalities in these patients. Furthermore, the results show that the  $-2/3aVF$  is not medically equivalent to the WCT. Therefore, the left leg presents with important clinical features, which contradicts to previous assumption about the left leg potential. Once again, it is important to stress that the proposed system is envisioned to flank the well-known 12-lead ECG and not to replace it in the clinical practice.
- 5- Chapter five presents a novel computational approach to reduce the Wilson Central Terminal amplitude and fall back under the Wilson postulate that declared this amplitude as irrelevant with respect to the ECG leads amplitude. The problem of WCT relative large amplitude was known before the standardization of precordial leads, and prior to this attempt, there was only one attempt to reduce its amplitude optimizing (in real time) the weight resistors that compose the WCT itself. This study included a cumbersome setup and could not be performed practically for every subject. In our approach, we used genetic algorithm to find three weighted factors for

the three limbs' potential in order to minimise the WCT amplitude. This approach is highly individual, and the three weighting factors are different from one patient to another.

Overall, the work presented in thesis is a step towards the validation of new electrocardiogram device that using the same ten electrodes of the 12-lead system, could flank it and be used to validate/verify if the current patient falls under the fundamental Wilson/Einthoven hypothesis such as negligible LL amplitude and act promptly i.e. removing the WCT from precordial leads or verify its correlation with the  $-2/3$  aVF.



## 6.2 Future Directions

There are number of points, which should be considered in future extension of this thesis:

- 1- This study is very depending on the number of recordings taken using our new ECG device. Therefore, it is required to record the ECG from varieties of patients, and healthy volunteers. Since the unipolar chest leads are more sensitive to show the abnormalities for patients diagnosed with NSTEMI, it is required to record from more NSTEMI patients to establish a well-powered study. Although I recorded from more than thirty NSTEMI patients, only nine patients were recorded just before proceeding for angiogram. The recording time for all NSTEMI patients should be similar, and just before proceeding for angiogram.
- 2- In addition to point (1), since that the embedded information in the unipolar chest leads showed potential for an early diagnosis of NSTEMI. The unipolar chest leads might also contain beneficial information in regards with other cardiac diseases. Future work could include investigation of the clinical value of unipolar chest for other cardiac diseases.
- 3- Future research would examine whether the position of limb electrodes can influence the precordial leads. Many believe that the precordial leads changes by moving the limb electrodes toward the torso (proximal recordings). This assumption is based on the fact that the WCT is the average potential of the limbs 'electrodes. Since our ECG device can measure the WCT signal, the influence of different arrangement of limb electrodes on the precordial leads can be investigated performing several recordings of the same patients with progressively proximal limb electrodes placements.
- 4- Future research would synthesise the WCT for every ECG device. Since the WCT can only be recorded by our developed ECG device, the machine learning framework can be developed to reconstruct the WCT using the standard 12-lead ECG. Therefore, this framework could lead to artificially measure the WCT for every ECG device.

## References

- [1] A. D. Waller, “A Demonstration on Man of Electromotive Changes accompanying the Heart’s Beat,” *J. Physiol.*, vol. 8, no. 5, pp. 229–234, Oct. 1887, doi: 10.1113/jphysiol.1887.sp000257.
- [2] J. Malmivuo and R. Plonsey, *Bioelectromagnetism Principles and Applications of Bioelectric and Biomagnetic Fields*. Oxford University Press, 1995.
- [3] J. K. Cooper, “Electrocardiography 100 Years Ago,” *N. Engl. J. Med.*, vol. 315, no. 7, pp. 461–464, Aug. 1986, doi: 10.1056/NEJM198608143150722.
- [4] W. Einthoven, “Ueber die Form des menschlichen Electrocardiogramms,” *Pflüger, Arch. für die Gesammte Physiol. des Menschen und der Thiere*, vol. 60, no. 3–4, pp. 101–123, Mar. 1895, doi: 10.1007/BF01662582.
- [5] M. AlGhatrif and J. Lindsay, “A brief review: history to understand fundamentals of electrocardiography,” *J. Community Hosp. Intern. Med. Perspect.*, vol. 2, no. 1, p. 14383, Jan. 2012, doi: 10.3402/jchimp.v2i1.14383.
- [6] C. Cajavilca and J. Varon, “Willem Einthoven: The development of the human electrocardiogram,” *Resuscitation*, vol. 76, no. 3, pp. 325–328, Mar. 2008, doi: 10.1016/j.resuscitation.2007.10.014.
- [7] W. B. Fye, “A History of the origin, evolution, and impact of electrocardiography,” *Am. J. Cardiol.*, vol. 73, no. 13, pp. 937–949, May 1994, doi: 10.1016/0002-9149(94)90135-X.
- [8] W. Einthoven, G. Fahr, and A. de Waart, “On the direction and manifest size of the variations of potential in the human heart and on the influence of the position of the

- heart on the form of the electrocardiogram,” *Am. Heart J.*, vol. 40, no. 2, pp. 163–211, Aug. 1950, doi: 10.1016/0002-8703(50)90165-7.
- [9] W. Einthoven, “Le telecardiogramme,” *Arch Int Physiol*, vol. 4, pp. 132–164, 1906.
- [10] W. Einthoven, “The telecardiogram,” *Am. Heart J.*, vol. 53, no. 4, pp. 602–615, Apr. 1957, doi: 10.1016/0002-8703(57)90367-8.
- [11] T. Lewis, “Report cxix. Auricular fibrillation: A common clinical condition,” *Br. Med. J.*, vol. 2, no. 2552, p. 1528, Nov. 1909, doi: 10.1136/bmj.2.2552.1528.
- [12] H. B. Xiao and C. Lawrence, “Reappraisal of thomas lewis’s place in the history of electrocardiography,” *J. Electrocardiol.*, vol. 29, no. 4, pp. 347–350, Oct. 1996, doi: 10.1016/S0022-0736(96)80101-4.
- [13] W. Einthoven, “THE DIFFERENT FORMS OF THE HUMAN ELECTROCARDIOGRAM AND THEIR SIGNIFICATION.,” *Lancet*, vol. 179, no. 4622, pp. 853–861, Mar. 1912, doi: 10.1016/S0140-6736(00)50560-1.
- [14] W. Einthoven, G. Fahr, and A. de Waart, “Über die Richtung und die manifeste Grösse der Potentialschwankungen im menschlichen Herzen und über den Einfluss der Herzlage auf die Form des Elektrokardiogramms,” *Pflüger’s Arch. für die gesamte Physiol. des Menschen und der Tiere*, vol. 150, no. 6–8, pp. 275–315, Mar. 1913, doi: 10.1007/BF01697566.
- [15] P. W. Macfarlane, A. van Oosterom, and M. Janse, “Comprehensive electrocardiology,” vol. 4, 2010.
- [16] F. N. Wilson, F. D. Johnston, F. F. Rosenbaum, and P. S. Barker, “On Einthoven’s triangle, the theory of unipolar electrocardiographic leads, and the interpretation of the precordial electrocardiogram,” *Am. Heart J.*, vol. 32, no. 3, pp. 277–310, Sep. 1946, doi: 10.1016/0002-8703(46)90791-0.
- [17] “The Mechanism and Graphic Registration of the Heart Beat.,” *JAMA J. Am. Med. Assoc.*, vol. 85, no. 23, p. 1832, Dec. 1925, doi: 10.1001/jama.1925.02670230064033.

- [18] C. E. Kossmann, “Unipolar electrocardiography of Wilson: A half century later,” *Am. Heart J.*, vol. 110, no. 4, pp. 901–904, Oct. 1985, doi: 10.1016/0002-8703(85)90484-3.
- [19] W. Einthoven and K. Lint, “Ueber das normale menschliche Elektrokardiogramm und über die capillar-elektrometrische Untersuchung einiger Herzkranken,” *Pflüger, Arch. für die Gesamte Physiol. des Menschen und der Thiere*, vol. 80, no. 3–5, pp. 139–160, May 1900, doi: 10.1007/BF01663110.
- [20] I. R. Roth, “On the use of chest leads in clinical electrocardiography,” *Am. Heart J.*, vol. 10, no. 6, pp. 798–829, Aug. 1935, doi: 10.1016/S0002-8703(35)90347-7.
- [21] A. L. M. Bakker *et al.*, “The lewis lead: Making recognition of p waves easy during wide QRS complex tachycardia,” *Circulation*, vol. 119, no. 24, pp. 592–593, 2009, doi: 10.1161/CIRCULATIONAHA.109.852053.
- [22] T. Lewis, J. Meakins, and P. D. White, “The Excitatory Process in the Dog’s Heart. Part I. The Auricles,” *Philos. Trans. R. Soc. B Biol. Sci.*, vol. 205, no. 313–324, pp. 375–420, Jan. 1914, doi: 10.1098/rstb.1914.0019.
- [23] T. Lewis and M. A. Rothschild, “The Excitatory Process in the Dog’s Heart. Part II. The Ventricles,” *Philos. Trans. R. Soc. B Biol. Sci.*, vol. 206, no. 325–334, pp. 181–226, Jan. 1915, doi: 10.1098/rstb.1915.0004.
- [24] F. N. WILSON, “BUNDLE BRANCH BLOCK AND ARBORIZATION BLOCK,” *Arch. Intern. Med.*, vol. 26, no. 2, p. 153, Aug. 1920, doi: 10.1001/archinte.1920.00100020022002.
- [25] F. N. Wilson, “The distribution of the potential differences produced by the heart beat within the body and at its surface,” *Am. Heart J.*, vol. 5, no. 5, pp. 599–616, Jun. 1930, doi: 10.1016/S0002-8703(30)90254-2.
- [26] F. N. Wilson, A. G. Macleod, and P. S. Barker, “The potential variations produced by the heart beat at the apices of Einthoven’s triangle,” *Am. Heart J.*, vol. 7, no. 2, pp. 207–211, Dec. 1931, doi: 10.1016/S0002-8703(31)90411-0.
- [27] F. N. Wilson, A. G. Macleod, and P. S. Barker, “The order of ventricular excitation in

- human bundle-branch block,” *Am. Heart J.*, vol. 7, no. 3, pp. 305–330, Feb. 1932, doi: 10.1016/S0002-8703(32)90346-9.
- [28] J. B. Carter, *The fundamentals of electrocardiographic interpretation*. 1945.
- [29] C. C. WOLFERTH and F. C. WOOD, “the Electrocardiographic Diagnosis of Coronary Occlusion By the Use of Chest Leads,” *Am. J. Med. Sci.*, vol. 183, no. 1, pp. 30–34, Jan. 1932, doi: 10.1097/00000441-193201000-00003.
- [30] G. E. Burch, “History of precordial leads in electrocardiography,” *Eur. J. Cardiol.*, vol. 8, no. 2, pp. 207–236, 1978.
- [31] V. MORTENSEN, “Significance of Precordial Leads in Electrocardiography, especially in Cardiac Infarction,” *Acta Med. Scand.*, vol. 92, no. 6, pp. 603–629, Apr. 1937, doi: 10.1111/j.0954-6820.1937.tb11703.x.
- [32] R. L. Levy and H. G. Bruenn, “The precordial lead of the electrocardiogram (Lead IV) as and aid in the recognition of active carditis in rheumatic fever,” *Am. Heart J.*, vol. 10, no. 7, pp. 881–888, Oct. 1935, doi: 10.1016/S0002-8703(35)90418-5.
- [33] A. H. Master, “The precordial lead in 104 normal adults,” *Am. Heart J.*, vol. 9, no. 4, pp. 511–516, Apr. 1934, doi: 10.1016/S0002-8703(34)90099-5.
- [34] F. N. Wilson, F. D. Johnston, A. G. Macleod, and P. S. Barker, “Electrocardiograms that represent the potential variations of a single electrode,” *Am. Heart J.*, vol. 9, no. 4, pp. 447–458, Apr. 1934, doi: 10.1016/S0002-8703(34)90093-4.
- [35] C. E. Kossmann and F. D. Johnston, “The precordial electrocardiogram I. The potential variations of the precordium and of the extremities in normal subjects,” *Am. Heart J.*, vol. 10, no. 7, pp. 925–941, Oct. 1935, doi: 10.1016/S0002-8703(35)90422-7.
- [36] C. E. Kossmann, “The effect of potential variations of the distant electrode on the precordial electrocardiogram,” *Am. Heart J.*, vol. 12, no. 6, pp. 698–712, Dec. 1936, doi: 10.1016/S0002-8703(36)91005-0.

- [37] K. H. Larsen, "Some remarks on the technique in clinical electrocardiography with precordial derivation," *Am. Heart J.*, vol. 14, no. 1, pp. 1–6, Jul. 1937, doi: 10.1016/S0002-8703(37)90329-6.
- [38] E. Sorsky and P. Wood, "The use of chest leads in clinical electrocardiography: I. Normal variations," *Am. Heart J.*, vol. 13, no. 2, pp. 183–196, Feb. 1937, doi: 10.1016/S0002-8703(37)91209-2.
- [39] O. F. Precordial, O. F. T. H. E. American, T. H. E. Cardiac, S. Of, and G. Britain, "Standardization of precordial leads," *Am. Heart J.*, vol. 15, no. 1, pp. 107–108, Jan. 1938, doi: 10.1016/S0002-8703(38)90039-0.
- [40] G. E. BURCH and N. P. Depasquales, *The History of Electrocardiography*. Norman Publishing, 1964.
- [41] A. R. Barnes, H. E. B. Pardee, P. D. White, F. N. Wilson, and C. C. Wolferth, "Standardization of precordial leads: Supplementary report," *Am. Heart J.*, vol. 15, no. 2, pp. 235–239, Feb. 1938, doi: 10.1016/S0002-8703(38)90860-9.
- [42] J. C. Edwards and J. B. Vander Veer, "A study of the chest leads of the electrocardiogram with an evaluation of the positions of the precordial electrode," *Am. Heart J.*, vol. 16, no. 4, pp. 431–448, Oct. 1938, doi: 10.1016/S0002-8703(38)90780-X.
- [43] F. M. Groedel, "How Far Does the Situation of the Indifferent Electrode Influence the Electrocardiographic Unipolar Chest Leads?," *Cardiology*, vol. 3, no. 1–2, pp. 23–35, 1939, doi: 10.1159/000164631.
- [44] F. M. Groedel, "How Far Is the Unipolar Chest Electrocardiogram Influenced When Led at the Same Time to Two or Three Electrically Connected Extremities?," *Cardiology*, vol. 3, no. 1–2, pp. 36–48, 1939, doi: 10.1159/000164632.
- [45] A. J. Geiger, "A comparative study of precordial Leads IV R and IV F," *Am. Heart J.*, vol. 18, no. 6, pp. 715–728, Dec. 1939, doi: 10.1016/S0002-8703(39)90851-3.
- [46] P. Wood and A. Selzer, "CHEST LEADS IN CLINICAL

- ELECTROCARDIOGRAPHY,” *Heart*, vol. 1, no. 1, pp. 49–80, Jan. 1939, doi: 10.1136/hrt.1.1.49.
- [47] H. H. Hecht, “The influence of the indifferent electrode upon the precordial electrocardiogram,” *Am. Heart J.*, vol. 24, no. 4, pp. 529–544, Oct. 1942, doi: 10.1016/S0002-8703(42)90970-0.
- [48] C. C. Wolferth and M. M. Livezey, “A study of methods of making so-called unipolar electrocardiograms,” *Am. Heart J.*, vol. 27, no. 6, pp. 764–782, Jun. 1944, doi: 10.1016/S0002-8703(44)90311-X.
- [49] G. B. Myers, H. A. Klein, B. E. Stofer, and T. Hiratzka, “Normal variations in multiple precordial leads,” *Am. Heart J.*, vol. 34, no. 6, pp. 785–808, 1947, doi: 10.1016/0002-8703(47)90144-0.
- [50] F. N. Wilson *et al.*, “The precordial electrocardiogram,” *Am. Heart J.*, vol. 27, no. 1, pp. 19–85, Jan. 1944, doi: 10.1016/S0002-8703(44)90603-4.
- [51] L. Wallace and N. Grossman, “PRAeCORDIAL ELECTROCARDIOGRAMS: A COMPARISON OF CF AND V LEAD CONNECTIONS,” *Heart*, vol. 8, no. 2, pp. 83–86, Apr. 1946, doi: 10.1136/hrt.8.2.83.
- [52] G. R. Herrmann, M. R. Hejtmancik, and J. W. Kopecky, “The superiority of the Wilson leads and the value of unipolar limb and precordial derivations in clinical electrocardiography,” *Am. Heart J.*, vol. 40, no. 5, pp. 680–695, Nov. 1950, doi: 10.1016/0002-8703(50)90199-2.
- [53] J. M. Hoyos and G. Tomayo, “Comparative Study of Different Precordial Leads,” *Am. Heart J.*, vol. 33, no. 5, pp. 696–741, May 1947, doi: 10.1016/0002-8703(47)90087-2.
- [54] M. Dolgin, S. Grau, and L. N. Katz, “A comparison of precordial electrocardiograms obtained with CR, CL, CF, and V leads,” *Am. Heart J.*, vol. 37, no. 3, pp. 343–358, Mar. 1949, doi: 10.1016/0002-8703(49)91058-3.
- [55] E. Hull, H. de N. Tucker, and J. O. Weilbaecher, “False abnormality of precordial electrocardiograms due to the effect of changes of potential at the remote electrode,”

- Am. Heart J.*, vol. 36, no. 1, pp. 135–140, Jul. 1948, doi: 10.1016/0002-8703(48)90553-5.
- [56] T. EAST and I. G. W. HILL, “MULTIPLE UNIPOLAR LEADS REPORT OF THE COMMITTEE OF THE BRITISH CARDIAC SOCIETY,” *Heart*, vol. 11, no. 1, pp. 103–104, Jan. 1949, doi: 10.1136/hrt.11.1.103.
- [57] A. Leatham, “THE CHEST LEAD ELECTROCARDIOGRAM IN HEALTH,” *Heart*, vol. 12, no. 3, pp. 213–231, Jul. 1950, doi: 10.1136/hrt.12.3.213.
- [58] F. N. WILSON *et al.*, “Recommendations for Standardization of Electrocardiographic and Vectorcardiographic Leads,” *Circulation*, vol. 10, no. 4, pp. 564–573, Oct. 1954, doi: 10.1161/01.CIR.10.4.564.
- [59] E. Goldberger, “A simple, indifferent, electrocardiographic electrode of zero potential and a technique of obtaining augmented, unipolar, extremity leads,” *Am. Heart J.*, vol. 23, no. 4, pp. 483–492, Apr. 1942, doi: 10.1016/S0002-8703(42)90293-X.
- [60] H. C. Burger, “The zero of potential: A persistent error,” *Am. Heart J.*, vol. 49, no. 4, pp. 581–586, Apr. 1955, doi: 10.1016/0002-8703(55)90076-4.
- [61] L. Bacharova, R. H. Selvester, H. Engblom, and G. S. Wagner, “Where is the central terminal located? In search of understanding the use of the Wilson central terminal for production of 9 of the standard 12 electrocardiogram leads,” *J. Electrocardiol.*, vol. 38, no. 2, pp. 119–127, 2005, doi: 10.1016/j.jelectrocard.2005.01.002.
- [62] E. Goldberger, “The validity of the Einthoven triangle hypothesis,” *Am. Heart J.*, vol. 29, no. 3, pp. 369–377, Mar. 1945, doi: 10.1016/0002-8703(45)90338-3.
- [63] H. C. Burger, A. G. W. van Brummelen, and G. van Herpen, “Heart-vector and leads,” *Am. Heart J.*, vol. 61, no. 3, pp. 317–323, Mar. 1961, doi: 10.1016/0002-8703(61)90601-9.
- [64] W. Einthoven, “Die galvanometrische Registrirung des menschlichen Elektrokardiogramms, zugleich eine Beurtheilung der Anwendung des Capillar-Elektrometers in der Physiologie,” *Pflüger, Arch. für die Gesamte Physiol. des*



- Menschen und der Thiere*, vol. 99, no. 9–10, pp. 472–480, Nov. 1903, doi: 10.1007/BF01811855.
- [65] R. H. Bayley and C. L. Kinard, “The zero of potential of the electrical field produced by the heart beat; the problem with reference to the living human subject.,” *Circ. Res.*, vol. 2, no. 2, pp. 104–11, Mar. 1954, doi: 10.1161/01.RES.2.2.104.
- [66] G. D. G. Gargiulo *et al.*, “On the Einthoven Triangle: A Critical Analysis of the Single Rotating Dipole Hypothesis,” *Sensors*, vol. 18, no. 7, p. 2353, Jul. 2018, doi: 10.3390/s18072353.
- [67] R. Eckey, P. & Fröhlich, “Archiv für Kreislaufforschung,” pp. 349–356, 1938, doi: 10.1007/BF02127311.
- [68] R. Burger and F. Wuhrmann, “Ueber das elektrische Feld des Herzens,” *Cardiology*, vol. 3, no. 1–2, pp. 56–138, 1939, doi: 10.1159/000164634.
- [69] M. Dolgin, S. Grau, and L. N. Katz, “Experimental studies on the validity of the central terminal of Wilson as an indifferent reference point,” *Am. Heart J.*, vol. 37, no. 6, pp. 868–880, 1949.
- [70] R. H. Bayley, E. W. Reynolds, C. L. Kinard, and J. F. Head, “The zero of potential of the electric field produced by the heart beat; the problem with reference to homogenous volume conductors.,” *Circ. Res.*, vol. 2, no. 1, pp. 4–13, Jan. 1954, [Online]. Available: <http://www.ncbi.nlm.nih.gov/pubmed/13116387>.
- [71] R. H. Bayley and A. E. Schmidt, “The Problem of Adjusting the Wilson Central Terminal to a Zero of Potential in the Living Human Subject,” *Circ. Res.*, vol. 3, no. 1, pp. 94–102, Jan. 1955, doi: 10.1161/01.RES.3.1.94.
- [72] Y. Okamoto and S. Mashima, “The zero potential and Wilson’s central terminal in electrocardiography,” *Bioelectrochemistry Bioenerg.*, vol. 47, pp. 291–295, 1998, doi: 10.1016/S0302-4598(98)00201-3.
- [73] G. E. Dower, J. A. Osborne, and A. D. Moore, “Measurement of the error in Wilson’s central terminal: an accurate definition of unipolar leads.,” *Br. Heart J.*, vol. 21, pp.

- 352–60, Jul. 1959, [Online]. Available:  
<http://www.ncbi.nlm.nih.gov/pubmed/13817890>.
- [74] G. Fischer, B. Tilg, R. Modre, F. Hanser, B. Messnarz, and P. Wach, “On modeling the wilson terminal in the boundary and finite element method,” *IEEE Trans. Biomed. Eng.*, vol. 49, no. 3, pp. 217–224, 2002, doi: 10.1109/10.983455.
- [75] M. S. Lynn and W. P. Timlake, “The Use of Multiple Deflations in the Numerical Solution of Singular Systems of Equations, with Applications to Potential Theory,” *SIAM J. Numer. Anal.*, vol. 5, no. 2, pp. 303–322, Jun. 1968, doi: 10.1137/0705027.
- [76] P. Wach, B. Tilg, G. Lafer, and W. Rucker, “Magnetic source imaging in the human heart: estimating cardiac electrical sources from simulated and measured magnetocardiogram data,” *Med. Biol. Eng. Comput.*, vol. 35, no. 3, pp. 157–166, May 1997, doi: 10.1007/BF02530031.
- [77] N. Miyamoto, Y. Shimizu, G. Nishiyama, S. Mashima, and Y. Okamoto, “The absolute voltage and the lead vector of Wilson’s central terminal.,” *Jpn. Heart J.*, vol. 37, no. 2, pp. 203–14, Mar. 1996, doi: <http://dx.doi.org/10.1536/ihj.37.203>.
- [78] N. Miyamoto, Y. Shimizu, G. Nishiyama, S. Mashima, and Y. Okamoto, “On the potential of the Wilson central terminal with respect to an ideal reference for unipolar electrocardiography,” *J Electrocardiol.*, vol. 28, no. 4, pp. 336–337, Oct. 1995, doi: 10.1016/S0022-0736(05)80054-8.
- [79] R. Hoekema, G. J. . Uijen, and A. van Oosterom, “On selecting a body surface mapping procedure,” *J. Electrocardiol.*, vol. 32, no. 2, pp. 93–101, Apr. 1999, doi: 10.1016/S0022-0736(99)90088-2.
- [80] G. Gargiulo *et al.*, “On the ‘Zero of Potential of the Electric Field Produced by the Heart Beat’. A Machine Capable of Estimating this Underlying Persistent Error in Electrocardiography,” *Machines*, vol. 4, no. 4, p. 18, Oct. 2016, doi: 10.3390/machines4040018.
- [81] G. D. Gargiulo, “True Unipolar ECG Machine for Wilson Central Terminal

- Measurements,” *Biomed Res. Int.*, vol. 2015, p. 586397, 2015, doi: 10.1155/2015/586397.
- [82] G. D. Gargiulo *et al.*, “Towards true unipolar bio-potential recording: a preliminary result for ECG,” *Physiol. Meas.*, vol. 34, no. 1, pp. N1–N7, Jan. 2013, doi: 10.1088/0967-3334/34/1/N1.
- [83] G. D. Gargiulo, J. Tapson, A. van Schaik, A. McEwan, and A. Thiagalingam, “Unipolar ECG circuits: Towards more precise cardiac event identification,” in *2013 IEEE International Symposium on Circuits and Systems (ISCAS2013)*, May 2013, pp. 662–665, doi: 10.1109/ISCAS.2013.6571932.
- [84] G. D. Gargiulo, E. S. Varaki, T. J. Hamilton, P. Bifulco, M. Cesarelli, and M. Romano, “A 9-independent-leads ECG system from 10 electrodes: A practice preserving WCT-less true unipolar ECG system,” in *2015 IEEE Biomedical Circuits and Systems Conference (BioCAS)*, Oct. 2015, pp. 1–4, doi: 10.1109/BioCAS.2015.7348300.
- [85] R. M. Farrell, A. Syed, A. Syed, and D. D. Gutterman, “Effects of limb electrode placement on the 12- and 16-lead electrocardiogram,” *J. Electrocardiol.*, vol. 41, no. 6, pp. 536–545, Nov. 2008, doi: 10.1016/j.jelectrocard.2008.07.023.
- [86] J. G. Webster, *Medical Instrumentation Application and Design*. John Wiley & Sons, 2009.
- [87] B. B. Winter and J. G. Webster, “Reduction of Interference Due to Common Mode Voltage in Biopotential Amplifiers,” *Biomed. Eng. IEEE Trans.*, vol. 30, no. 1, pp. 58–62, 1983, doi: 10.1109/TBME.1983.325167.
- [88] BurrBrown, “INA 118 Precision low power Instrumentation Amplifier,” *Tech. data*, 2000, [Online]. Available: <http://www.ti.com/lit/ds/symlink/ina118.pdf>.
- [89] Texas Instruments, “OPA140, OPA2140, OPA4140 - High-Precision, Low-Noise, Rail-to-Rail Output, 11MHz JFET Op Amp,” 2010. [Online]. Available: <http://www.ti.com/lit/ds/symlink/opa4140.pdf>.
- [90] G. Gargiulo *et al.*, “True Unipolar ECG Leads Recording (Without the Use of WCT),”

- Hear. Lung Circ.*, vol. 22, p. S102, 2013, doi: 10.1016/j.hlc.2013.05.243.
- [91] G. Gargiulo *et al.*, “Giga-Ohm High-Impedance FET Input Amplifiers for Dry Electrode Biosensor Circuits and Systems,” in *Integrated Microsystems*, no. January 2016, CRC Press, 2017, pp. 165–194.
- [92] G. Gargiulo *et al.*, *Non-invasive electronic biosensor circuits and systems*, no. January. INTECH Open Access Publisher, 2010.
- [93] R. J. Prance *et al.*, “An ultra-low-noise electrical-potential probe for human-body scanning,” *Meas. Sci. Technol.*, vol. 11, no. 3, pp. 291–297, Mar. 2000, doi: 10.1088/0957-0233/11/3/318.
- [94] “CG/CG2 SN Series—Medium to High Surge GDT from Gas Discharge Tubes.” <http://www.littelfuse.com/products/gas-discharge-tubes/medium-to-high-surge-gdt/cg-cg2-sn.aspx>.
- [95] G. Gargiulo, P. Bifulco, M. Cesarelli, A. Fratini, and M. Romano, “Problems in Assessment of Novel Biopotential Front-End with Dry Electrode: A Brief Review,” *Machines*, vol. 2, no. 1, pp. 87–98, 2014, doi: 10.3390/machines2010087.
- [96] G. D. Gargiulo *et al.*, “Towards true unipolar ECG recording without the Wilson central terminal (preliminary results).,” *Physiol. Meas.*, vol. 34, no. 9, pp. 991–1012, Sep. 2013, doi: 10.1088/0967-3334/34/9/991.
- [97] In-Duk Hwang and J. G. Webster, “Direct Interference Canceling for Two-Electrode Biopotential Amplifier,” *IEEE Trans. Biomed. Eng.*, vol. 55, no. 11, pp. 2620–2627, Nov. 2008, doi: 10.1109/TBME.2008.923108.
- [98] G. Gargiulo, P. Bifulco, M. Cesarelli, A. McEwan, and A. Wabnitz, “Open platform, 32-channel, portable, data-logger with 32 PGA control lines for wearable medical device development,” *Electron. Lett.*, vol. 50, no. 16, pp. 1127–1129, Jul. 2014, doi: 10.1049/el.2014.1791.
- [99] H. Moeinzadeh and G. Gargiulo, “Wilson Central Terminal ECG Database,” *PhysioNet*, 2019, doi: 10.13026/f73z-an96.

- [100] A. L. Goldberger *et al.*, “PhysioBank, PhysioToolkit, and PhysioNet: components of a new research resource for complex physiologic signals.,” *Circulation*, vol. 101, no. 23, pp. e215–e220, Jun. 2000, doi: 10.1161/01.cir.101.23.e215.
- [101] H. Moeinzadeh *et al.*, “Unipolar Cardiac Leads Between History and Science,” in *Biomedical Signal Processing*, 2020, pp. 203–224.
- [102] H. Moeinzadeh *et al.*, “WCTECGdb: A 12-Lead Electrocardiography Dataset Recorded Simultaneously with Raw Exploring Electrodes’ Potential Directly Referred to the Right Leg,” *Sensors*, vol. 20, no. 11, p. 3275, Jun. 2020, doi: 10.3390/s20113275.
- [103] M. A. Sprague and T. L. Geers, “A spectral-element/finite-element analysis of a ship-like structure subjected to an underwater explosion,” *Comput. Methods Appl. Mech. Eng.*, vol. 195, no. 17–18, pp. 2149–2167, Mar. 2006, doi: 10.1016/j.cma.2005.03.007.
- [104] T. L. Geers, “An objective error measure for the comparison of calculated and measured transient response histories,” *Shock Vib. Bull.*, vol. 54, no. 2, pp. 99–107, 1984, [Online]. Available: <http://citeseerx.ist.psu.edu/viewdoc/summary?doi=10.1.1.208.2552>.
- [105] J. J. Z. Liao, “Sample size calculation for an agreement study,” *Pharm. Stat.*, vol. 132, no. January, p. n/a-n/a, 2009, doi: 10.1002/pst.382.
- [106] V. Krasteva, I. Jekova, and R. Schmid, “Simulating arbitrary electrode reversals in standard 12-lead ECG,” *Sensors (Switzerland)*, vol. 19, no. 13, pp. 1–19, 2019, doi: 10.3390/s19132920.
- [107] J.-L. Vincen, E. Abraham, P. Kochanek, Frederick A. Moore, and M. P. Fink, “Textbook of Critical Care E-Book,” p. 1647, 2011.
- [108] “No Title.” <https://basicmedicalkey.com/>.
- [109] B. Miner, W. S. Grigg, and E. H. Hart, “Wellens Syndrome.,” Treasure Island (FL), 2020.

- [110] M. Mitchell, *An introduction to genetic algorithms*, vol. 32, no. 6. MIT Press Ltd, 1996.
- [111] G. J. E. Rawlins, *Foundations of Genetic Algorithms 1991 (FOGA 1)*. Morgan Kaufmann; 1 edition (July 15, 1991), 1991.
- [112] T. D. Gwiazda, *Genetic Algorithms Reference*, vol. 1. Tomasz Gwiazda, 2006.

# Appendix A Graphical User Interfaces and User Guidelines

## A.1 User Guide for the ECG Visualization

- The Matlab script in section A.2 is named ECG\_Visualization.m.
- Run ECG\_Visualization.m and the GUI will open as shown in Figure A.1. Once you run the GUI, you can open the patient file by clicking on the “open” button.:

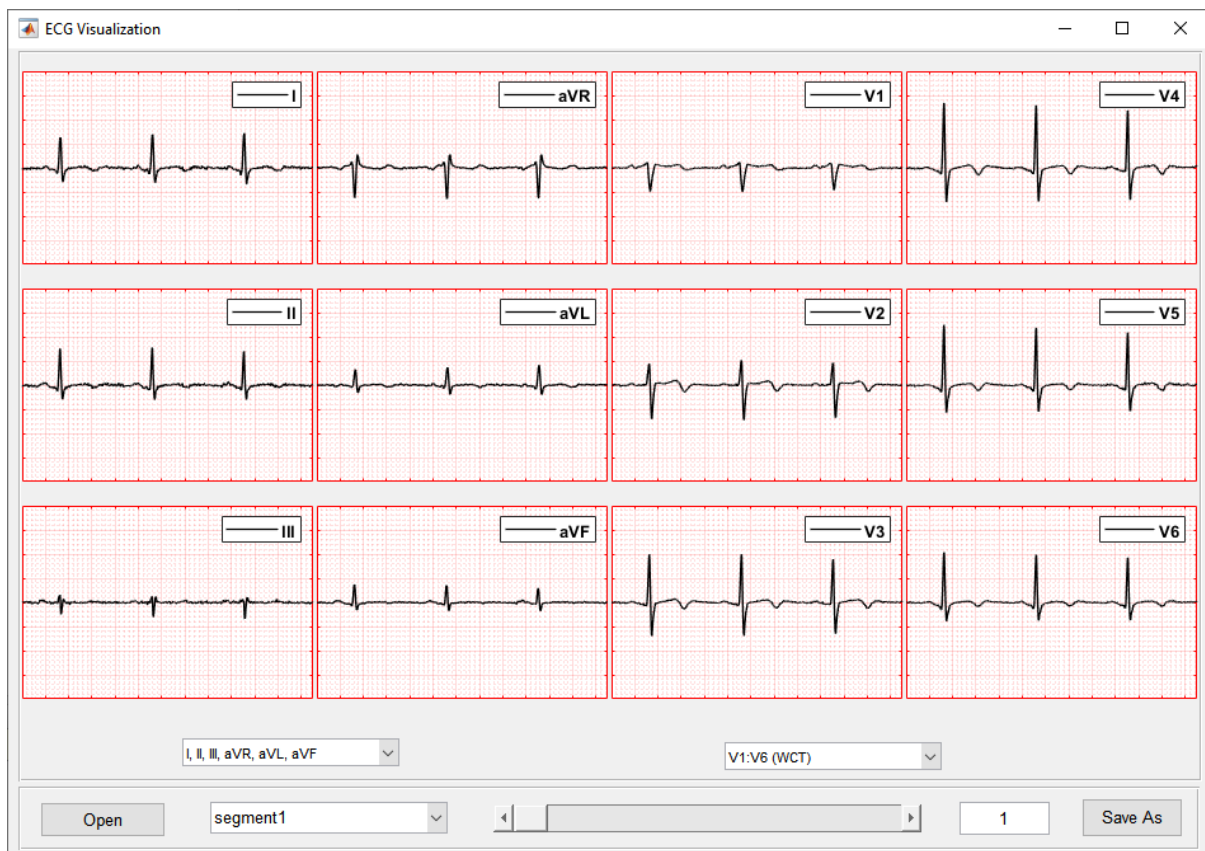


Figure A. 1 ECG visualization GUI opened.

- Each patient may have more than one segment, which has a length of ten seconds. You can choose different segment to display on GUI using segment popup menu (see Figure A.2).



Figure A. 2 Select a segment using segment menu

- By clicking on the “Save As” button, the displayed leads will be saved as a picture with *jpeg* file extension.
- In the bottom panel of the GUI, moving the sliding button enables to move forward in time in the displayed signals (see Figure A.3).



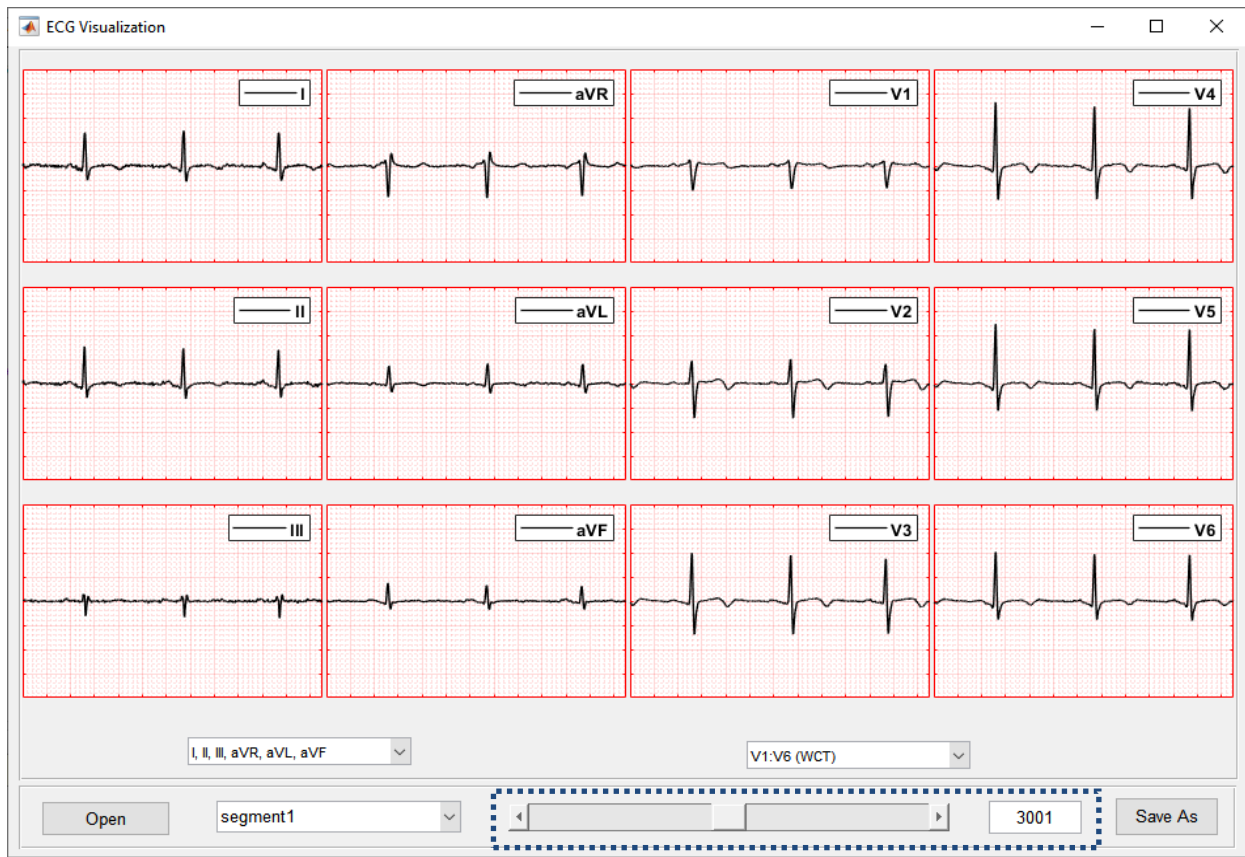


Figure A. 3 The slide bar enables to move forward or backward in each segment.

- Since the WCTECGdb enables synthesis chest leads in reference to every desired point, you can select different leads to display and compare on the GUI (see Figure A.4). The list is presented as below:
  - V<sub>1</sub>:V<sub>6</sub> (WCT): The chest leads in reference to the WCT.
  - UV<sub>1</sub>:UV<sub>6</sub> (RL): The chest leads in reference to the right leg (RL).
  - UV<sub>1</sub>:UV<sub>6</sub>(-2/3aVF): the synthesised unipolar chest leads using -2/3aVF.
  - V<sub>1</sub>:V<sub>6</sub> (LA): The chest leads in reference to the left arm (LA).
  - V<sub>1</sub>:V<sub>6</sub> (RA): The chest leads in reference to the right arm (RA).
  - V<sub>1</sub>:V<sub>6</sub> (LL): The chest leads in reference to the left leg (LL).
  - I, II, III, aVR, aVL, aVF: three limbs 'lead and augmented leads.
  - LA, RA, LL, WCT, aVF: three limb potential, Wilson Central Terminal, augmented vector foot.



Figure A. 4 Choose different leads to display

## A.2 ECG Visualization Graphical User Interface

```
function varargout = ECG_visualization(varargin)
% ECG_PRINT MATLAB code for ECG_visualization.fig
%   ECG_visualization, by itself, creates a new ECG_visualization or raises the
%   existing singleton*.
%
%   H = ECG_visualization existing returns the handle to a new ECG_PRINT or the
%   handle to the existing singleton*.
%
%   ECG_visualization ('CALLBACK',hObject,eventData,handles,...) calls the local
%   function named CALLBACK in ECG_visualization.M with the given inputargument.
%
%   ECG_PRINT('Property','Value',...) creates a new ECG_PRINT or raises the
%   existing singleton*. Starting from the left, property value pairs are
%   applied to the GUI before ECG_print_OpeningFcn gets called. An
%   unrecognized property name or invalid value makes property application
%   stop. All inputs are passed to ECG_print_OpeningFcn via varargin.
%
%   *See GUI Options on GUIDE's Tools menu. Choose "GUI allows only one
%   instance to run (singleton)".
%
% See also: GUIDE, GUIDATA, GUIHANDLES

% Edit the above text to modify the response to help ECG_print

% Last Modified by GUIDE v2.5 12-Jun-2020 15:15:15

% Begin initialization code - DO NOT EDIT

gui_Singleton = 1;
gui_State = struct('gui_Name',       mfilename, ...
                  'gui_Singleton',   gui_Singleton, ...
                  'gui_OpeningFcn', @ECG_print_OpeningFcn, ...
                  'gui_OutputFcn',  @ECG_print_OutputFcn, ...
                  'gui_LayoutFcn',  [], ...
                  'gui_Callback',    []);
if nargin && ischar(varargin{1})
    gui_State.gui_Callback = str2func(varargin{1});
end

if nargout
    [varargout{1:nargout}] = gui_mainfcn(gui_State, varargin{:});
else
    gui_mainfcn(gui_State, varargin{:});
end
% End initialization code - DO NOT EDIT

% --- Executes just before ECG_print is made visible.
```

```

function ECG_print_OpeningFcn(hObject, eventdata, handles, varargin)
% This function has no output args, see OutputFcn.
% hObject    handle to figure
% eventdata  reserved - to be defined in a future version of MATLAB
% handles    structure with handles and user data (see GUIDATA)
% varargin   command line arguments to ECG_print (see VARARGIN)
global myindex2print
myindex2print=0;
% Choose default command line output for ECG_print
handles.output = hObject;

% Update handles structure
guidata(hObject, handles);

% UIWAIT makes ECG_print wait for user response (see UIRESUME)
% uiwait(handles.figure1);

% --- Outputs from this function are returned to the command line.
function varargout = ECG_print_OutputFcn(hObject, eventdata, handles)
% varargout  cell array for returning output args (see VARARGOUT);
% hObject    handle to figure
% eventdata  reserved - to be defined in a future version of MATLAB
% handles    structure with handles and user data (see GUIDATA)

% Get default command line output from handles structure
varargout{1} = handles.output;

% --- Executes on slider movement.
function slider1_Callback(hObject, eventdata, handles)
% hObject    handle to slider1 (see GCBO)
% eventdata  reserved - to be defined in a future version of MATLAB
% handles    structure with handles and user data (see GUIDATA)

% Hints: get(hObject,'Value') returns position of slider
%         get(hObject,'Min') and get(hObject,'Max') to determine range of slider

% --- Executes during object creation, after setting all properties.
function slider1_CreateFcn(hObject, eventdata, handles)
% hObject    handle to slider1 (see GCBO)
% eventdata  reserved - to be defined in a future version of MATLAB
% handles    empty - handles not created until after all CreateFcns called

% Hint: slider controls usually have a light gray background.
if isequal(get(hObject,'BackgroundColor'),
get(0,'defaultUicontrolBackgroundColor'))
    set(hObject,'BackgroundColor',[.9 .9 .9]);
end

% --- Executes on button press in pushbutton_open.
function pushbutton_open_Callback(hObject, eventdata, handles)
% hObject    handle to pushbutton_open (see GCBO)
% eventdata  reserved - to be defined in a future version of MATLAB
% handles    structure with handles and user data (see GUIDATA)

```

```

global pstart slider_start slider_end ECG_allsection Unip_allsection index
Foldername Filename

```

```

str= mfilename( 'fullpath' );
index=1;
[file,path] = uigetfile(str,'*.mat');

```

```

if file==0
    return;
else
    address_input=[path, file];
end

```

```

load(address_input)
names=split(address_input,'/'); %Mac user
if length(names)==1
    names=split(address_input,'\'); % windows user
end

```

```

Filename=char(names(length(names)));
Filename=Filename(1:end-4);

```

```

Foldername=char(names(length(names)-1));

```

```

ECG_allsection=ECG_lead;
Unip_allsection=Unip_lead;
str_sec='{';
for i=1:length(ECG_allsection)
    str_sec=[str_sec, ''segment', num2str(i),'';'];
end
str_sec=[str_sec(1:end-1),']'];
eval(['set1=',str_sec]);
pstart=1;
set(handles.popupmenu_sections,'String',set1,'Value',1)
set(handles.edit_loc, 'String', num2str(pstart));

slider_start=1;
slider_end=size(ECG_allsection{index},1)-2000; %2000: fs*2.5
set(handles.slider2, 'value', 0);

```

```

plot_newecg(handles);

```

```

function plot_newecg(handles)
    global ECG_allsection Unip_allsection index plotID pstart
    Data=[ECG_allsection{index},Unip_allsection{index}];
    aVR=Data(:,11)-(Data(:,12)+Data(:,10))/2; % using unipolar LA, RA, LL
    aVL=Data(:,10)-(Data(:,11)+Data(:,12))/2;
    aVF=Data(:,12)-(Data(:,11)+Data(:,10))/2;
    pos1=[0.001,0.251,0.501,0.751];
    Fs=800
    f=Fs*2.5;
    start_p=1;
    leads=[Data(:,1:3),aVR,aVL,aVF,Data(:,4:9)];
    mylegends={'I','aVR','V1','V4','II','aVL','V2','V5','III','aVF','V3','V6'};
    leads=leads(:,[1,4,7,10,2,5,8,11,3,6,9,12]); %order of leads to plot (hint:
similar to legend)
    leds_clean=DC_removal(leads(start_p:start_p+f-2,:));
    set(handles.edit_loc, 'String', num2str(pstart));

```

```

for i=1:12
    h=subplot(3,4,i);

    p = get(h, 'pos');
    if rem(i,4)==0
        p(1) = pos1(4);
    else
        p(1)=pos1(rem(i,4));
    end
    p(3) = p(3)+0.09;
    p(4)= p(4)+0.05;
    set(h, 'pos', p);

    plotID(i)=plot(leds_clean(:,i),'k','LineWidth',1);
    axis([0,f,-2,2]);
    set(gca,'XTick',(0:160:f))
    set(gca,'YTick',(-2:0.5:2))
    grid on;
    grid minor;
    set(gca, 'XColor', 'r')
    set(gca, 'YColor', 'r')
    set(gca,'xticklabel',[])
    set(gca,'yticklabel',[])
    legend(mylegends{i});

end

function plt_leads(leads, legends, Fs,start_p, panel_ID)
% plot precordial signals V1:V6
f=Fs*2.5; %number of points to plot
leds_clean=DC_removal(leads(start_p:start_p+f-2,:));

set(panel_ID(1), 'YData', leds_clean(:,1));
legend(panel_ID(1),legends{1})
set(panel_ID(2), 'YData', leds_clean(:,2));
legend(panel_ID(2),legends{2})
set(panel_ID(3), 'YData', leds_clean(:,3));
legend(panel_ID(3),legends{3})
set(panel_ID(4), 'YData', leds_clean(:,4));
legend(panel_ID(4),legends{4})
set(panel_ID(5), 'YData', leds_clean(:,5));
legend(panel_ID(5),legends{5})
set(panel_ID(6), 'YData', leds_clean(:,6));
legend(panel_ID(6),legends{6})

function plot_selection(panel_Fig_index,myIndex)
% panel_Fig_index: the reference to each six plots
% myIndex: selected plot
global ECG_allsection Unip_allsection pstart
Data=[ECG_allsection{index},Unip_allsection{index}];
aVR=Data(:,11)-(Data(:,12)+Data(:,10))/2; % using unipolar LA, RA, LL
aVL=Data(:,10)-(Data(:,11)+Data(:,12))/2;
aVF=Data(:,12)-(Data(:,11)+Data(:,10))/2;
WCT=mean(Data(:,10:12),2);

Fs=800;

switch (myIndex)
    case 1 % V1:V6 using WCT as reference point

```

```

        led=Data(:,4:9);
        legends={'V1','V2','V3','V4','V5','V6'};
    case 2 %UV1:UV6 using RL as reference point
        led=Data(:,13:18);
        legends={'UV1','UV2','UV3','UV4','UV5','UV6'};
    case 3 %UV1:UV6 using -2/3aVF as reference point
        led=Data(:,4:9)-2*aVF/3;
        legends={'UV1 (aVF)','UV2 (aVF)','UV3 (aVF)','UV4 (aVF)','UV5
(aVF)','UV6 (aVF)'};
    case 4 %V1:V6 using LA as reference point
        led=Data(:,13:18)-Data(:,10);
        legends={'UV1 (LA)','UV2 (LA)','UV3 (LA)','UV4 (LA)','UV5 (LA)','UV6
(LA)'};
    case 5 %V1:V6 using RA as reference point
        led=Data(:,13:18)-Data(:,11);
        legends={'UV1 (RA)','UV2 (RA)','UV3 (RA)','UV4 (RA)','UV5 (RA)','UV6
(RA)'};
    case 6 %V1:V6 using LL as reference point
        led=Data(:,13:18)-Data(:,12);
        legends={'UV1 (LL)','UV2 (LL)','UV3 (LL)','UV4 (LL)','UV5 (LL)','UV6
(LL)'};
    case 7
        led=[Data(:,1:3),aVR,aVL,aVF];
        legends={'I','II','III','aVR','aVL','aVF'};
    case 8
        led=[Data(:,10:12),WCT,-2*aVF/3,WCT];
        legends={'LA','RA','LL','WCT','-2/3aVF','WCT'};

    case 9
        figure (2)

end

if myIndex~=9

    plt_leads(led, legends, Fs,pstart,panel_Fig_index)
end

% text for text boxes:
%txt='Speed: 25 mm/s (1 square = 5 mm) Limbs/Chest: 10 mm/mV F 50~ 0.15-150 Hz ';

% --- Executes on slider movement.
function slider2_Callback(hObject, eventdata, handles)
% hObject    handle to slider2 (see GCBO)
% eventdata  reserved - to be defined in a future version of MATLAB
% handles    structure with handles and user data (see GUIDATA)

% Hints: get(hObject,'Value') returns position of slider
%        get(hObject,'Min') and get(hObject,'Max') to determine range of slider
global pstart slider_start slider_end ECG12led ECG12led_unip

val=get(hObject,'Value');
min=get(hObject,'Min');

```

```

max=get(hObject,'Max');

progress=val/(max-min);
pstart=round(progress*(slider_end-slider_start)+slider_start);
set(handles.edit_loc, 'String', num2str(pstart));

listbox_leftPanel_Callback(hObject, eventdata, handles)
popupmenu_rightPanel_Callback(hObject, eventdata, handles)
%plot_newecg();

% --- Executes during object creation, after setting all properties.
function slider2_CreateFcn(hObject, eventdata, handles)
% hObject    handle to slider2 (see GCBO)
% eventdata  reserved - to be defined in a future version of MATLAB
% handles    empty - handles not created until after all CreateFcns called

% Hint: slider controls usually have a light gray background.
if isequal(get(hObject,'BackgroundColor'),
get(0,'defaultUicontrolBackgroundColor'))
    set(hObject,'BackgroundColor',[.9 .9 .9]);
end

% --- Executes during object creation, after setting all properties.
function popupmenu_sections_CreateFcn(hObject, eventdata, handles)
% hObject    handle to popupmenu_sections (see GCBO)
% eventdata  reserved - to be defined in a future version of MATLAB
% handles    empty - handles not created until after all CreateFcns called

% Hint: popupmenu controls usually have a white background on Windows.
%         See ISPC and COMPUTER.
if ispc && isequal(get(hObject,'BackgroundColor'),
get(0,'defaultUicontrolBackgroundColor'))
    set(hObject,'BackgroundColor','white');
end

% --- Executes on button press in pushbutton_saveas.
function pushbutton_saveas_Callback(hObject, eventdata, handles)
% hObject    handle to pushbutton_saveas (see GCBO)
% eventdata  reserved - to be defined in a future version of MATLAB
% handles    structure with handles and user data (see GUIDATA)
global first_run Filename Foldername index pstart plotID myindex2print
myindex2print=myindex2print+1;
myindex2print
temp_plotID=plotID;

filter = {'*.jpeg';'*.*'};
[file,name,path]=uiputfile(filter,'File Selection',[Filename,'.jpeg']);
if path==0 % pressed cancel button
    return;
end
mkdir([name,Foldername]);
mkdir([name,Foldername,'/',file(1:end-5)])

print_precordial=get(handles.radiobutton_pre,'value');

```



```

print_unipolar=get(handles.radiobutton_uni,'value');

set(0,'DefaultFigureVisible','off')
% print precordial
set(handles.radiobutton_pre,'value',1);
first_run=1;

figure('units','normalized','outerposition',[0 0 1 1])
plot_newecg(handles);
txt=['    Precordial leads (V1:V6)          ',newline,'Speed: 25 mm/s (1 square = 5 mm)
Limbs/Chest: 10 mm/mV  F 50~ 0.15-150 Hz '];
annotation('textbox',[0.001, 0.001, 0.1, 0.1], 'String', txt);
saveas(gcf,[name,Foldername,'/',file(1:end-
5),'/',num2str(myindex2print),'_precordial.jpeg'])
savefig(gcf,[name,Foldername,'/',file(1:end-
5),'/',num2str(myindex2print),'_precordial.fig'])

% print unipolar
set(handles.radiobutton_uni,'value',1);
first_run=1;
figure('units','normalized','outerposition',[0 0 1 1])
plot_newecg(handles);
txt=['    Unipolar leads (UV1:UV6)        ',newline,'Speed: 25 mm/s (1 square = 5 mm)
Limbs/Chest: 10 mm/mV  F 50~ 0.15-150 Hz '];
annotation('textbox',[0.001, 0.001, 0.1, 0.1], 'String', txt);
saveas(gcf,[name,Foldername,'/',file(1:end-
5),'/',num2str(myindex2print),'_unipolar.jpeg'])
savefig(gcf,[name,Foldername,'/',file(1:end-
5),'/',num2str(myindex2print),'_unipolar.fig'])

% print unipolar using aVF
set(handles.radiobutton_uniavf,'value',1);
first_run=1;
figure('units','normalized','outerposition',[0 0 1 1])
plot_newecg(handles);
txt=['    Unipolar leads using -2/3aVF (UV1:UV6)          ',newline,'Speed: 25 mm/s (1
square = 5 mm) Limbs/Chest: 10 mm/mV  F 50~ 0.15-150 Hz '];
annotation('textbox',[0.001, 0.001, 0.1, 0.1], 'String', txt);
saveas(gcf,[name,Foldername,'/',file(1:end-
5),'/',num2str(myindex2print),'_unipolar_avf.jpeg'])
savefig(gcf,[name,Foldername,'/',file(1:end-
5),'/',num2str(myindex2print),'_unipolar_avf.fig'])

% write details in text file
my_text=['Folder: ',Foldername,newline,'File:
',Filename,newline,'Segment=',num2str(index),newline,'Loc: ',num2str(pstart)];
fileID = fopen([name,Foldername,'/',file(1:end-
5),'/',num2str(myindex2print),'_info.txt'],'w');
fprintf(fileID, my_text);
fclose(fileID);
set(0,'DefaultFigureVisible','on')
if print_precordial==1
    set(handles.radiobutton_pre,'value',1);
elseif print_unipolar==1
    set(handles.radiobutton_uni,'value',1);
else
    set(handles.radiobutton_uniavf,'value',1);
end
end

```

```

plotID=temp_plotID; % as the plot ID was changed by calling the function twice

function popupmenu_sections_Callback(hObject, eventdata, handles)
% hObject      handle to popupmenu_sections (see GCBO)
% eventdata    reserved - to be defined in a future version of MATLAB
% handles      structure with handles and user data (see GUIDATA)

% Hints: contents = cellstr(get(hObject,'String')) returns popupmenu_sections
contents as cell array
%           contents{get(hObject,'Value')} returns selected item from
popupmenu_sections
global index pstart slider_start slider_end ECG_allsection
pstart=1;
slider_start=1;
slider_end=size(ECG_allsection{index},1)-2000; %2000: fs*2.5
set(handles.slider2, 'value', 0);
index=get(handles.popupmenu_sections,'value');
listbox_leftPanel_Callback(hObject, eventdata, handles)
popupmenu_rightPanel_Callback(hObject, eventdata, handles)

function edit_loc_Callback(hObject, eventdata, handles)
% hObject      handle to edit_loc (see GCBO)
% eventdata    reserved - to be defined in a future version of MATLAB
% handles      structure with handles and user data (see GUIDATA)

% Hints: get(hObject,'String') returns contents of edit_loc as text
%           str2double(get(hObject,'String')) returns contents of edit_loc as a double
global pstart ECG_allsection index
data=ECG_allsection{index};

min=1;
max=length(data(:,1));
val=str2double(get(hObject,'string'));
if val<min || val>max
    return;
end
pstart=val;
progress=val/(max-min);
set(handles.slider2, 'Value', progress);
plot_newecg(handles);

% --- Executes during object creation, after setting all properties.
function edit_loc_CreateFcn(hObject, eventdata, handles)
% hObject      handle to edit_loc (see GCBO)
% eventdata    reserved - to be defined in a future version of MATLAB
% handles      empty - handles not created until after all CreateFcns called

% Hint: edit controls usually have a white background on Windows.
%           See ISPC and COMPUTER.
if ispc && isequal(get(hObject,'BackgroundColor'),
get(0,'defaultUicontrolBackgroundColor'))
    set(hObject,'BackgroundColor','white');
end

% --- Executes when figure1 is resized.

```

```

function figure1_SizeChangedFcn(hObject, eventdata, handles)
% hObject    handle to figure1 (see GCBO)
% eventdata  reserved - to be defined in a future version of MATLAB
% handles    structure with handles and user data (see GUIDATA)

% --- Executes on selection change in listbox_leftPanel.
function listbox_leftPanel_Callback(hObject, eventdata, handles)
% hObject    handle to listbox_leftPanel (see GCBO)
% eventdata  reserved - to be defined in a future version of MATLAB
% handles    structure with handles and user data (see GUIDATA)

% Hints: contents = cellstr(get(hObject,'String')) returns listbox_leftPanel
contents as cell array
%         contents{get(hObject,'Value')} returns selected item from
listbox_leftPanel
    global plotID
    myindex=get(handles.listbox_leftPanel,'value');
    Fig_index=[1,5,9,2,6,10]; % right panel index
    Panel_Fig_index=plotID(Fig_index);
    plot_selection(Panel_Fig_index,myindex)

% --- Executes during object creation, after setting all properties.
function listbox_leftPanel_CreateFcn(hObject, eventdata, handles)
% hObject    handle to listbox_leftPanel (see GCBO)
% eventdata  reserved - to be defined in a future version of MATLAB
% handles    empty - handles not created until after all CreateFcns called

% Hint: listbox controls usually have a white background on Windows.
%         See ISPC and COMPUTER.
if ispc && isequal(get(hObject,'BackgroundColor'),
get(0,'defaultUicontrolBackgroundColor'))
    set(hObject,'BackgroundColor','white');
end

% --- Executes on selection change in popupmenu_rightPanel.
function popupmenu_rightPanel_Callback(hObject, eventdata, handles)
% hObject    handle to popupmenu_rightPanel (see GCBO)
% eventdata  reserved - to be defined in a future version of MATLAB
% handles    structure with handles and user data (see GUIDATA)

% Hints: contents = cellstr(get(hObject,'String')) returns popupmenu_rightPanel
contents as cell array
%         contents{get(hObject,'Value')} returns selected item from
popupmenu_rightPanel
    global plotID
    myindex=get(handles.popupmenu_rightPanel,'value');
    Fig_index=[3,7,11,4,8,12]; % right panel index
    Panel_Fig_index=plotID(Fig_index);
    plot_selection(Panel_Fig_index,myindex)

% --- Executes during object creation, after setting all properties.
function popupmenu_rightPanel_CreateFcn(hObject, eventdata, handles)
% hObject    handle to popupmenu_rightPanel (see GCBO)
% eventdata  reserved - to be defined in a future version of MATLAB

```

```
% handles    empty - handles not created until after all CreateFcns called

% Hint: popupmenu controls usually have a white background on Windows.
%       See ISPC and COMPUTER.
if ispc && isequal(get(hObject,'BackgroundColor'),
get(0,'defaultUicontrolBackgroundColor'))
    set(hObject,'BackgroundColor','white');
end

function[signal]=DC_removal(signal)
lamda=0.98; % remember what we said about it!!
b = [1 -1];
a = [1 -lamda];

%figure, freqz(b,a); %plot the frequency response

signal=filtfilt(b,a,signal);
```

## **Appendix B Publications**

Article

# On the “Zero of Potential of the Electric Field Produced by the Heart Beat”. A Machine Capable of Estimating this Underlying Persistent Error in Electrocardiography

Gaetano D. Gargiulo <sup>1,2,\*</sup>, Paolo Bifulco <sup>2</sup>, Mario Cesarelli <sup>2</sup>, Alistair L. McEwan <sup>3</sup>, Hossein Moeinzadeh <sup>1</sup>, Aiden O’Loughlin <sup>4</sup>, Ibrahim M. Shugman <sup>5</sup>, Jonathan C. Tapson <sup>1</sup> and Aravinda Thiagalingam <sup>6</sup>

<sup>1</sup> The MARCS Institute, Western Sydney University, Milperra NSW 2214, Australia;

h.moeinzadeh@westernsydney.edu.au (H.M.); j.tapson@westernsydney.edu.au (J.C.T.)

<sup>2</sup> Department of Electrical Engineering and Information Technology (DIETI), “Federico II”

The University of Naples, Naples 80100, Italy; pabifulc@unina.it (P.B.); cesarell@unina.it (M.C.)

<sup>3</sup> School of EIE, University of Sydney, Sydney NSW 2006, Australia; alistair.mcewan@sydney.edu.au

<sup>4</sup> School of Medicine, Western Sydney University, Campbelltown NSW 2650, Australia;

aiden.oloughlin@gmail.com

<sup>5</sup> Cardiology Department, Campbelltown Hospital, Campbelltown NSW 2650, Australia;

shugmano@hotmail.com

<sup>6</sup> School of Medicine, The University of Sydney, Sydney NSW 2006, Australia;

aravinda.thiagalingam@sydney.edu.au

\* Correspondence: g.gargiulo@westernsydney.edu.au; Tel.: +61-2-4736-0920

Academic Editor: Dan Zhang

Received: 21 July 2016; Accepted: 30 September 2016; Published: 15 October 2016

**Abstract:** Modern electrocardiography (ECG) uses a constructed reference potential for the majority of leads. This reference potential, named after its inventor as the Wilson central terminal, is assumed to have negligible value and to be stationary during the cardiac cycle. However, the problem of its variability during the cardiac cycle has been known almost since the inception of 12-lead electrocardiography. Due to the cumbersomeness of the measurement system required to fully appreciate these variations, this topic has received scant research attention during the last 60 years. Taking advantage of modern electronic amplifiers’ capability to detect small voltages, drawing only femtoamperes from physiological equivalent signal sources and of the right-leg connection availability, we developed a complete electrocardiography device that, aside from the eight independent signals of the standard 12-lead ECG, allows direct recording of the Wilson central terminal components. In this paper, we present details of the circuit together with its initial clinical evaluation. For this trial, we recorded data from 44 volunteer patients at Campbelltown Hospital (Campbelltown, Australia) and we found that the Wilson central terminal amplitude, as foreseen by Frank and others in the 1950s, is not negligible, its amplitude in relation to the lead II is, on average, 51.2%, and thus it may be clinically relevant.

**Keywords:** electrocardiography; Wilson Central Terminal; potential reference

## 1. Introduction

The majority of modern-day clinicians and researchers appear to have forgotten that at the base of modern electrocardiography (ECG) is a largely simplifying assumption, that reduces the extremely complex electrical activity of the heart to a single equivalent electrical dipole rotating in the chest around a fixed point. This simplifying assumption, formulated in the 1930s by Wilson [1], allowed

assessment of cardiac electrical activity in the whole body space rather than in its two-dimensional (2-D) projection over the limbs, as originally outlined by W. Einthoven in 1906 [1]. In other words, Wilson devised a virtual stationary fixed point (which was named after him: Wilson central terminal or simply WCT) as a current average of Einthoven's limb electrodes [1].

The assumption of a single dipole rotating around Wilson's virtual fixed point was soon recognized to be the source of potential errors for ECG. In 1954, Frank, in his famous dissertation "General Theory of Heart-Vector Projection" [2] warned clinicians about the use of this oversimplifying assumption. Empirical confirmation of Frank's hypotheses about the amplitude and variability of the WCT came almost simultaneously when measurements of WCT (requiring the human body to be encased in a metal structure totally submerged in water for the duration of the recording), showed that Wilson's central point is non-stationary during the cardiac cycle and has a large amplitude (up to 40% of Einthoven's ECG signal amplitudes). Details of these results were published by both H.C. Burger and R. Bayley et al. [3,4]. However, until now, without a valid alternative, this largely simplified hypothesis still lies at the base of modern clinical practice.

In the late 1950s, the electronic amplifier substituted the original string galvanometer, leading to the ECG gaining in popularity, reducing its cumbersomeness, and allowing simultaneous observation of more than one lead. However, electronic amplifiers required the addition of a further limb to the ECG measurement that original inventors of the system had not taken into account: the "right leg." Remembering that electronic amplifiers, by construction and design, are better equipped to measure voltages rather than currents [5–7], and also bearing in mind that an additional reference terminal may be required for common mode signal rejection reasons, particularly at power-line frequencies [7–10], it was a natural choice for engineers to connect this additional terminal to the right leg [8,9]. The right leg was traditionally excluded from the original Einthoven/Wilson ECG model because the string galvanometer measures directly the current circulating into the surrounding tissues as a consequence of the shift in the electromagnetic field impressed by the heart's activation. Therefore, the original ECG electrical model is arranged as a closed circuit (Einthoven's triangle) and each of its branches includes the heart in the current pathway. As can be inferred from the original model, there is no evident current pathway between the heart and the legs (see Figure 1) [1,11–15].

Taking advantage of the right-leg connection and of the negligible load upon equivalent physiological signal sources offered by modern voltage amplifiers (in the order of femtoamperes [10–15]), we developed a full 15-lead ECG device that, aside from the standard 12-lead signals, can record the independent voltages of the right arm, left arm and left leg. These additional independent voltages (directly referred to the right leg) can be used to:

- 1) Measure the WCT amplitude without the need to encase the patient into a metal structure submerged in water.
- 2) Correlate the amplitude of the WCT to the cardinal limb leads.

In this paper, we detail the hardware used together with the results of our clinical evaluation. For this clinical evaluation, we recorded data from 44 patients at Campbelltown Hospital (NSW) and we measured the amplitude of the WCT and correlated it with the amplitude of lead II. We found that the amplitude of the WCT could exceed the amplitude of lead II and on average across our entire population, WCT amplitude is 51.2% of lead II. All the patients volunteered for this study and gave written consent (this study was approved on 23 September 2015 with the protocol number HREC/15/LPOOL/302).

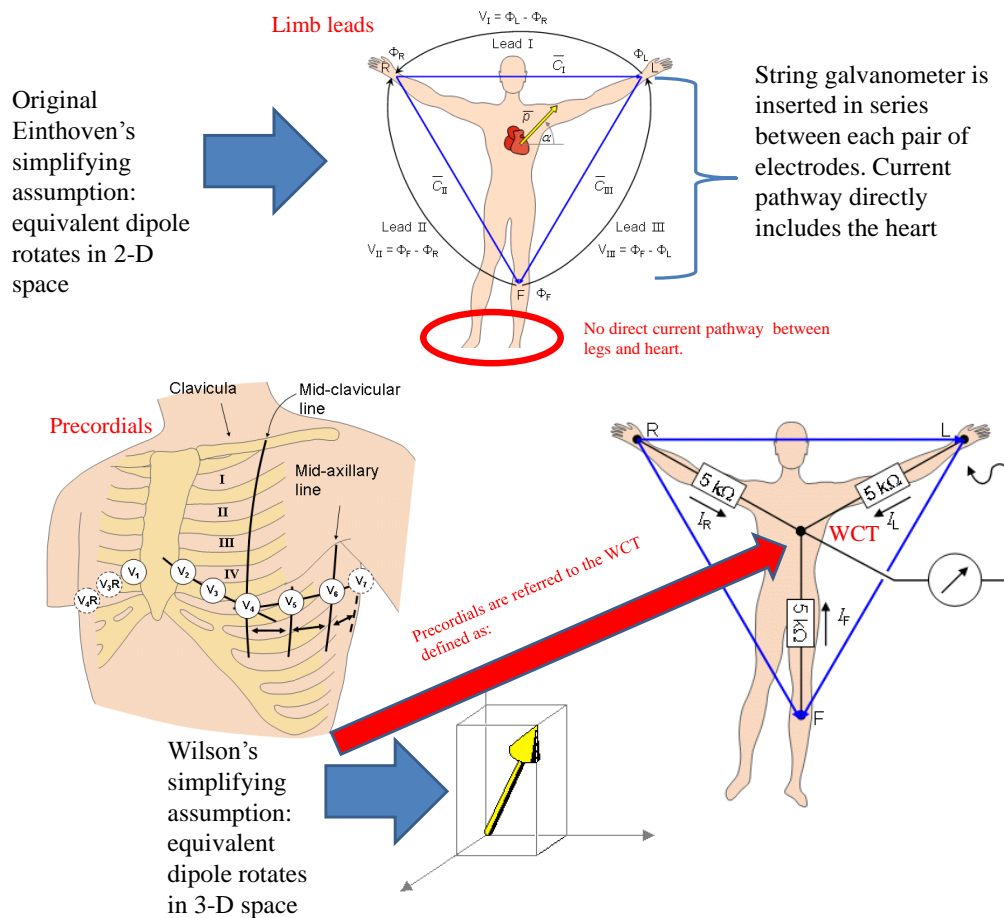


**Figure 1.** ECG conduction model evolution: Original Einthoven model (top), which included only the three limbs that form a triangular circuit around the heart, whereas the heart is included in each branch current pathway; Wilson's precordial leads (bottom) with WCT definition as current return formed as the center of Einthoven's triangle (bottom right). Modified from [1].

## 2. Methods

We designed our hardware around the instrumentation amplifier INA116 [16], manufactured by Texas Instruments, Dallas, TX, USA (Burr-Brown series). According to the chip specifications, its bias current (i.e., the load to the physiological signal source) is typically only 5 fA. This extraordinarily small value is achieved by the combination of an extremely high input impedance with a relatively small parasitic capacitance and embedded active guard ring buffer (see technical documentation [16] for precise details). In order to preserve the mentioned characteristics, the printed circuit board is designed to take advantage of the embedded active guard ring amplifier on a Teflon substrate. Although the guard ring amplifier's primary job is to reduce the noise pick-up at cable and board connections, because this offers a replica of the input signal, we also use it to measure the raw voltage of the WCT components [17–20].

To ensure high conductivity of connections between pins and exposed pads on the board, the latter are silver-plated by immersion during manufacturing. To avoid smearing of solder under the chip body and between pins during soldering, the chip body is sealed in position prior to soldering, using a suitable printed circuit board non-conductive epoxy resin. As an additional precaution, the conductivity between electrode connections and chip pins is verified prior to soldering, using a multimeter. Each pin of the INA116 is then manually soldered to the pad using lead-free silver-based paste with a 0.2 mm diameter hot iron tip. To further minimize parasitic capacitance at board level, the guard ring pattern is repeated on each layer of the board and aside from the chips' necessary



connections, no other traces are routed in the area under each INA116. As a last precaution, as recommended in the existing literature, wire connections to the chip are directly soldered to the board on the top layer (no thru-hole connections) [10,21–23]. Finally, the assembled board is coated with conformal coating to protect it from moisture that could contaminate the board due to its use in the hospital environment (frequent cleaning and wiping of the enclosure/cables with disinfectant).

The simplified schematic of the hardware, limited to the four limbs and one of the precordials, is depicted in Figure 2. Protection from electrostatic discharges is achieved by interconnection of a single high-precision low-noise Panasonic surface mount ECG series 100 k $\Omega$  resistor. Protection against defibrillation discharges and simultaneous high-impedance biasing of the INA116 electrodes' connections is achieved by parallel connection of low-voltage activation gas discharge tubes; with an arc voltage as low as 15 V [24] they protect the sensitive chip inputs even for voltages that are lower than the embedded overvoltage protection [24]. Discharge tubes also offer the perfect biasing pathway for INA116 due to their nominal resistance >10 G $\Omega$  and a negligible parasitic capacitance. To avoid cluttering Figure 2, the gas discharge tubes are not represented.

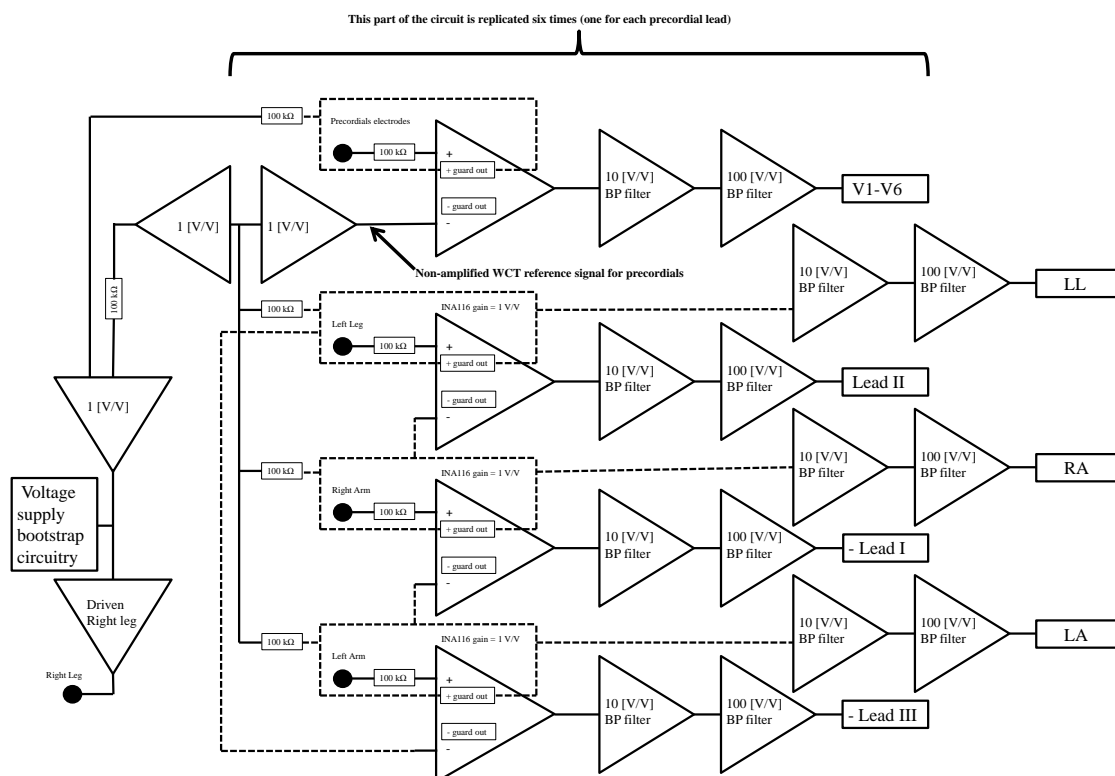


**Figure 2.** Simplified schematic limited to limbs' connections and one of the precordials.

As mentioned, and as it is possible to infer from the schematic, the guard buffer of the left-leg, left-arm and right-arm electrodes are also used to directly measure the WCT components' voltages. The gain set for the INA116 chips is 1 V/V, achieved by leaving pins 1 and 8 floating (not noted in Figure 2). Necessary gain and band pass filtering is achieved by two AC coupled active non-inverting low-pass filters gaining 10 V/V and 100 V/V, respectively. Each gain cell is designed around the amplifier chip OPA140 [25]. Aside from its very low-noise figure, the OPA140 has been selected because of its high slew rate, immunity from phase inversion and very low current-bias. Owing to these characteristics, we have designed a high-gain non-inverting band-pass filtering gain cell that does not require additional biasing and copes well with the frequent swings between saturation voltages due to ECG artefacts. Aside from the value of some passive components to achieve different gains, the gain cells are identical. The simplified schematic of the gain cell is depicted in Figure 3.

In order to achieve a diagnostic quality ECG, both the high-pass and low-pass corner frequencies of the gain cell are set with capacitors whose value has been selected to be larger than the theoretical values. In this way, even in the worst case scenario of a  $-10\%$  value due to the capacitor tolerances, the required bandwidth is assured. Frequency content normalization to the diagnostic bandwidth is operated via software after signal acquisition. Components' values are reported in Table 1 for both gain cells. Differences between values of components are highlighted in bold. As an additional precaution, high-precision Murata ceramic capacitors have been used.

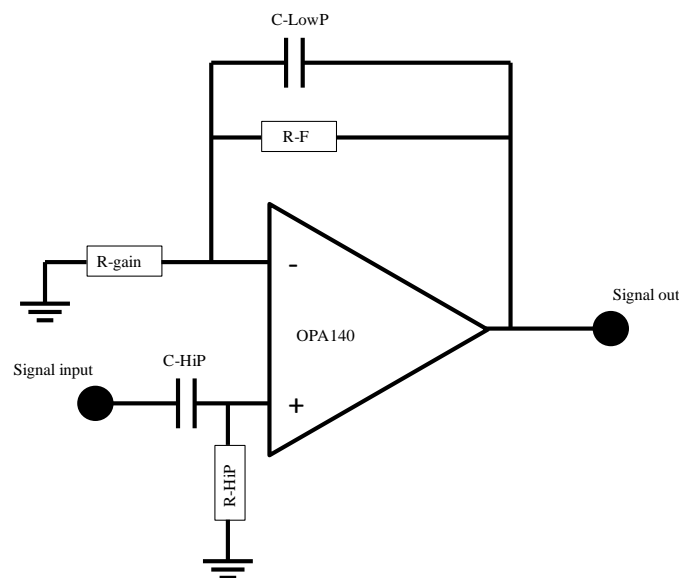


**Figure 3.** Active band-pass filter gain cell, see Table 1 for components' values.

**Table 1.** Summary of components' values for the gain cells.

Component	10 V/V Gain Version	100 V/V Gain Version
C-HiP	47 $\mu$	47 $\mu$
R-HiP	100 k $\Omega$	100 k $\Omega$
C-LowP	15 nF	1.5 nF
R-F	100 k $\Omega$	1 M $\Omega$
R-gain	10 k $\Omega$	10 k $\Omega$

As noted in Figure 2, the circuit includes a modified voltage bootstrap circuitry [18,20,26–28] that directly drives the reference voltage of the circuit with a damped version of the average of all the electrodes. This solution proved successful in all of our past circuit implementations [18,20,29], particularly when the right-leg connection is included in the average. However, for this implementation we introduced a driven-right-leg circuitry designed and dimensioned to contain current drive to 20  $\mu$ A [8,30,31]. The input signal for the driven-right-leg circuitry is the non-amplified average of the measurement electrodes (see Figure 2).

The entire circuit is powered by a dual 9 V power supply formed by two 9 V batteries in series that proved sufficient for a day of recordings in the hospital. Digital conversion and data logging is operated at a 16-bit depth over the range of  $\pm 5$  V at the sample rate of 800 Hz by the BIOADC [32], powered directly by the USB connection to a host laptop computer (battery-powered). Necessary anti-aliasing low-pass filtering at the Nyquist frequency is embedded in the BIOADC. The entire system is hosted on a standard hospital instrumentation trolley that allows easy transportation of the device around rooms and ambulatories for the recording. More details pertaining to the hardware tests are reported in Appendix A.

Recorded data have been firstly assessed for quality, comparing visually the shapes and amplitude of 12-lead ECG traces recorded by our machine with the one obtained from the resident device used for routine investigation. Data sets, whose amplitude and shapes passed the visual test, have been included in this database (100% inclusion). For this study, we measured the WCT amplitude and reported it as a percentage of lead II in 44 patients who had volunteered for the study. We also report the polarity of the WCT based upon the orientation of the QRS feature present in the signal. Similarly to previous studies [3,4], we noted that with “N” signals, polarity is not clearly positive or negative i.e., the positive deflection amplitude almost matches the negative deflection at the QRS feature. Reported amplitude measurements are averaged across at least five consecutive beats. To compare the WCT’s amplitude we selected lead II because, according to the circuit principles applied to the electrocardiography (see Figure 1), lead II is the result of the sum of lead I and lead II. Therefore, lead II should be the largest of the limb leads [1]. Furthermore, lead II is used as a calibration signal from many patient simulators used in standard engineering practice and often represented, at the bottom of the standard clinical ECG diagnostic sheets, longer traces for cardiac rhythm assessment.

### 3. Results

Bench tests of the assembled prototype show that the gain of each channel is  $1023 \pm 5\%$  V/V and the bandwidth contains the diagnostic ECG frequency [1,8]. A custom-made import script takes into account precise measured gains, normalizes the frequency content to 0.05–150 Hz via a 50th order Infinite Impulsive Response (IIR) band-pass filter; and removes power-line noise at 50 Hz and harmonics up to the Nyquist frequency, via a batch of 50th order IIR notch filters each with a quality factor of 35. All filters have been implemented as “non-causal” to avoid introducing phase delays.

As mentioned, only data sets that passed the visual inspection test (see Methods section) have been included in this data set. A total of twelve recordings have been discarded due to the necessity to abort the recording (i.e., patient required transportation to other wards for procedures) or due to the presence of large artifacts or the persistent presence of pacemaker activations on the recorded traces. Of the 44 recordings, 17 patients were female. The average age of the study’s patient population is 66.8 years (with a standard deviation of 13.4 years); the majority of the patients have a history of cardiac disease and have been admitted to the hospital from the emergency department because of difficulties in breathing and/or chest pain.

The summary of our measurement results is reported in Table 2 for each patient. Amplitude of the WCT is measured as a relative percentage of lead II. The average WCT amplitude for our data set is 51.2% of lead II with a standard deviation of 27.4%, which is slightly larger than that described in the existing literature [1,8], where relative amplitudes of up to the 40% are reported. However, those studies used a different and cumbersome setup and date back to the 1950s. Nevertheless, to our surprise, for several patients, the amplitude of the WCT is as large as lead II, with several beats in which WCT’s amplitude exceeds lead II by up to 20%; in Table 2, all of the cases where the WCT’s average amplitude was larger than 99% of lead II, were approximated with 100%. Although positive deflection of WCT seems to be the majority (see Table 2), with only a handful of neutral (noted with N) polarities, it is not possible to find characteristic or uniform shapes of WCT. Based upon our measurements, WCT is highly individual, can have standard ECG characteristics, such as a p-wave and a t-wave, and thus should be included in the ECG signal space used for diagnosing diseases.

An example of the WCT signal with a marked t-wave is visible in Figure 4. As can be seen, a marked t-wave deflection on the WCT trace (bottom panel) is synchronized with the t-wave on lead II (top panel). The WCT trace in Figure 4 is also a good example of a highly variable WCT, which in one single cardiac cycle changes the deflection’s polarity at least three times, with an amplitude that reaches 65% of lead II (average).

An example of high-amplitude WCT is depicted in Figure 5. As can be seen, the amplitude of the WCT (positive deflection) has a similar amplitude to the lead II with a broader QRS feature. In Figure 6 we present an example of multimodal WCT: for this patient, on average the WCT has

a positive deflection, and shape alteration is observable during ectopic beats, where the WCT exhibits a broader QRS. Other examples of WCT which mutate from positive deflection to almost neutral and fully negative during ectopic beats are depicted in Figures 7 and 8.

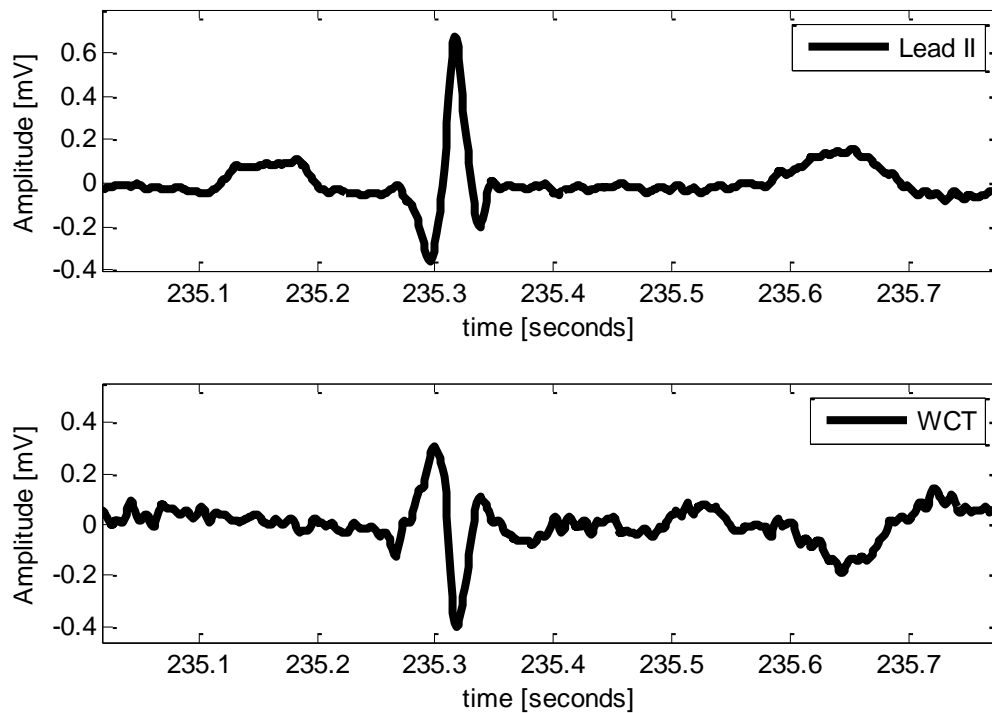


**Figure 4.** Example of negative deflection WCT. WCT is 65% of lead II amplitude (average); recording is from a 70-year-old female patient admitted with chest pain. WCT for this patient presents a marked t-wave.

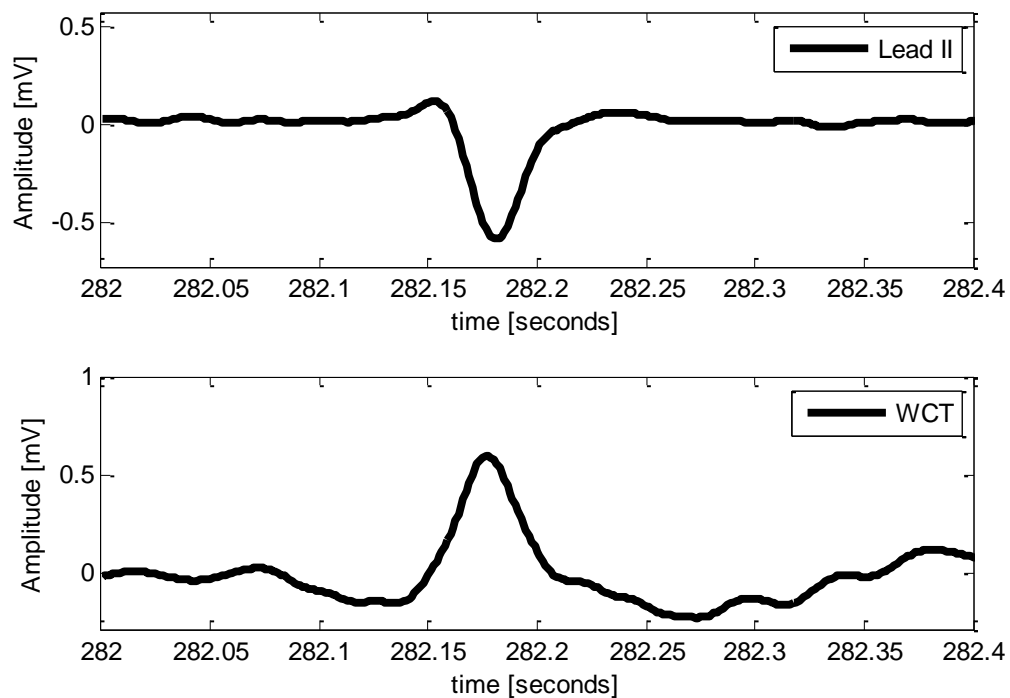


**Figure 5.** Example of positive deflection WCT. WCT is 100% of lead II amplitude (average); recording is from an 82-year-old female patient admitted from the emergency department (unconfirmed diagnosis).

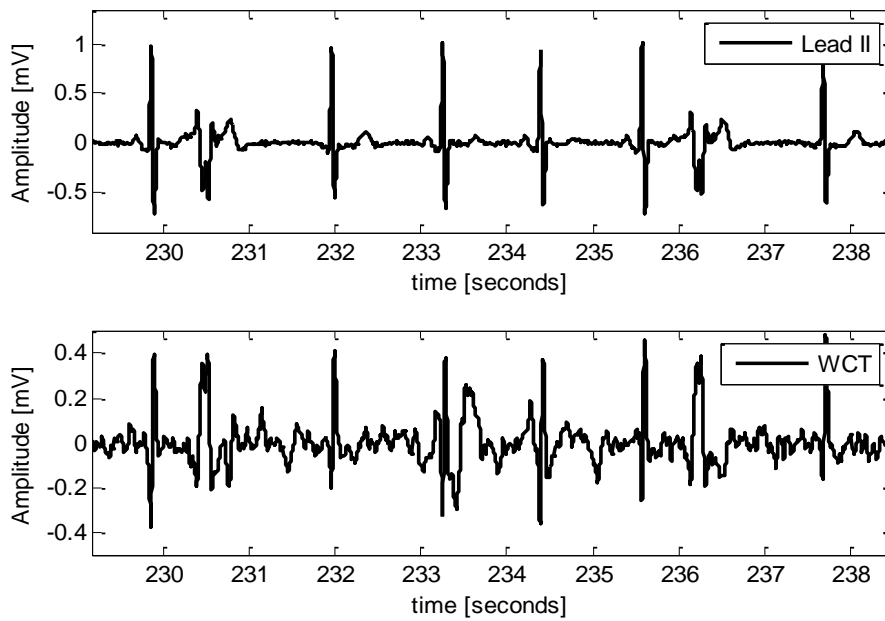


**Figure 6.** Example of multimodal WCT with severe alteration during ectopic beats (noted with a black arrow). WCT is 45% of lead II amplitude (average); recording is from a 72-year-old female patient admitted from the emergency department with severe chest pain.

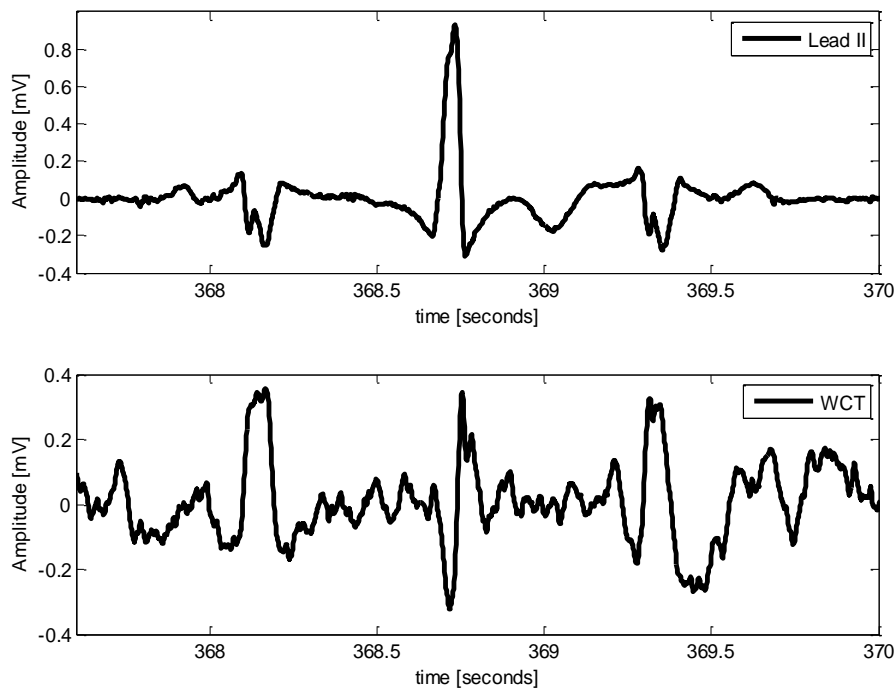


**Figure 7.** Example of positive WCT that mutates into almost neutral (almost identical value for positive and negative peak) during an ectopic beat (noted by the arrow). WCT amplitude also varies from >100% of lead II amplitude (average) to approximately 50% of lead II during the ectopic beat; recording is from an 85-year-old male patient admitted from the emergency department with severe chest pain and unconfirmed myocardial infarction.

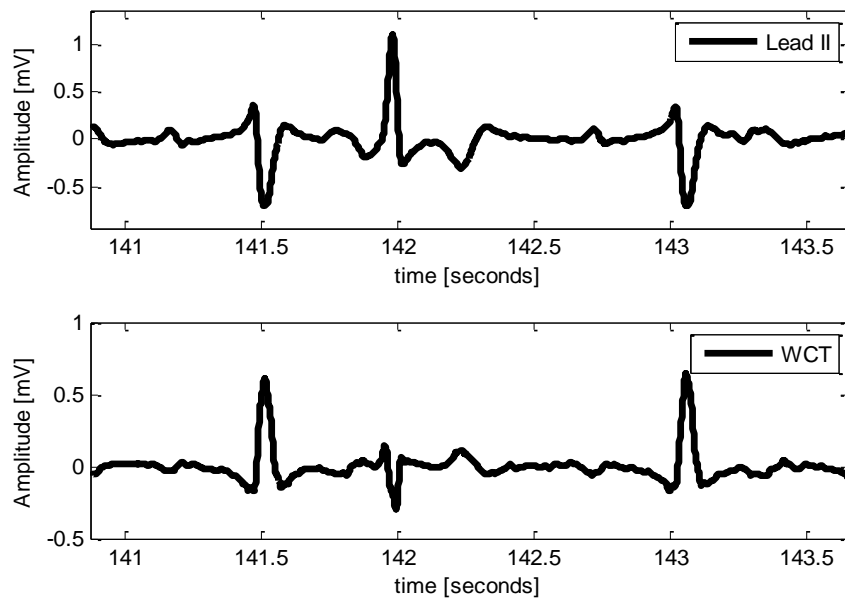


**Figure 8.** Example of positive WCT that mutates into negative during an ectopic beat (noted by the arrow). WCT amplitude also varies from 65% of lead II amplitude (average) to 33% of lead II during the ectopic beat; recording is from a 79-year-old male patient admitted due to arrhythmia.

In Figure 9, we show an example of WCT that exhibits all of the characteristics of an ECG trace. For this patient, the WCT has a marked p-wave and t-wave that, for some beats, have a larger amplitude than the multimodal QRS complex. This is another example of highly variable WCT, which in this case changes deflection polarity at least five times into a single cardiac cycle. Of note, from Table 2 it is possible to observe that the relative amplitude of the WCT, with respect to lead II, is below 15% for only one patient.

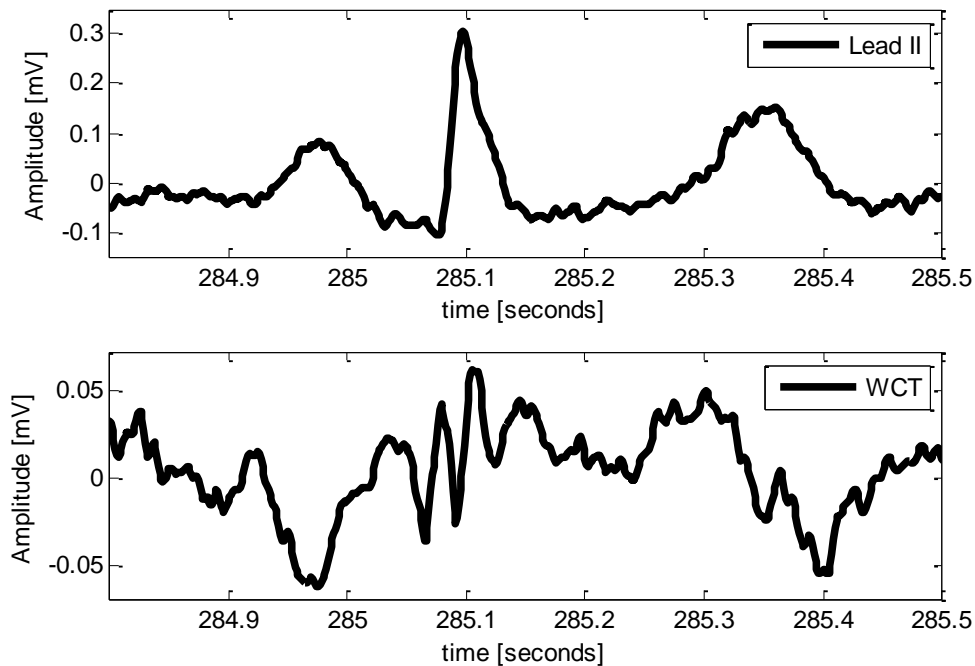


**Figure 9.** Example of multimodal WCT with evident features in correspondence with “p” and “t” waves. WCT is 23% of lead II amplitude (average); recording is from a 63-year-old female patient admitted from the emergency department with severe chest pain.

**Table 2.** Summary of measurement results. WCT relative amplitudes are approximated to the nearest integer and capped to 100% for the measurements larger than 99% (see text).

Patient ID	Age (y.o.)	Gender	WCT Amplitude As % of Lead II	WCT Polarity	Figure
P001	63	F	27	+	
P002	51	F	40	+	
P003	65	F	35	−	
P004	63	F	30	+	
P005	88	F	90	+	
P006	52	F	90	+	
P007	70	F	59	+	
P008	55	F	44	+	
P009	82	F	12	−	
P010	71	F	23	+	
P011	69	F	19	+	
P012	89	F	25	−	
P013	63	F	23	+	Figure 9
P014	70	F	41	N	
P015	72	F	45	+	Figure 6
P016	70	F	65	−	Figure 4
P017	82	F	100	+	Figure 5
P018	59	M	100	−	
P019	68	M	33	−	
P020	79	M	65	+	Figure 8
P021	55	M	50	+	
P022	71	M	40	N	
P023	52	M	60	+	
P024	45	M	20	−	
P025	79	M	50	+	
P026	85	M	22	+	
P027	52	M	30	+	
P028	62	M	41	−	
P029	64	M	31	−	
P030	25	M	50	−	
P031	76	M	46	−	
P032	56	M	51	−	
P033	78	M	57	+	
P034	73	M	100	+	
P035	85	M	100	+	Figure 7
P036	89	M	75	+	
P037	72	M	25	+	
P038	56	M	48	+	
P039	60	M	20	+	
P040	65	M	27	+	
P041	80	M	48	−	
P042	53	M	95	+	
P043	53	M	100	+	
P044	75	M	100	+	
Average	66.8		51.2		
			Polarity distribution	N: 4.5%; Negative: 29.5%	
Total:	44	38% Females			

#### 4. Conclusions

We presented a viable solution for the measurement of the WCT amplitude in a clinical setting. Our electrocardiographic device does not require the patient to be encased in a metallic structure submerged in water. Employing the latest components and printed circuit board technologies, we produced a compact design that employs standard ECG cables and electrode placement. Our ongoing clinical trial using this device has already confirmed the inadequateness of the WCT as a neutral reference for ECG signals. Our measurements performed on 44 volunteer patients confirmed that the WCT amplitude relative to lead II amplitude (average across the entire study's population), is 51.2% (standard deviation of 27.4%), with peaks of over 100%. Our measurements also confirmed, as

foreseen by Frank in the 1950s, that the WCT is another ECG lead with a high amplitude and typical characteristic waveforms, hence it should be included in the signal space used to diagnose diseases. We are currently assessing the clinical implications of our finding and continuing the data-recording campaign with the aim of collecting a larger, statistically significant sample of recordings, which will be released to researchers upon request.

**Acknowledgments:** The authors wish to thank the patients at Campbelltown Hospital (NSW) who volunteered for this study, and the nurses and the ECG technicians who helped with the data collection. The authors also gratefully acknowledge Texas Instruments who supplied chip samples for the construction of the prototype. This study is funded by the office for Research Engagement and Development with Industry (REDI) at the Western Sydney University and by the MARCS Institute (Biomedical Engineering and Neuro-Science BENS group).

**Author Contributions:** G.D.G. invented the technology, designed the hardware and conceived the study, M.C. and P.B. contributed to the design of the hardware, A.L.M., J.C.T. and H.M. contributed to the measurement analysis and data collection; I.M.S., A.O.L. and A.T. contributed to the design of the clinical study and facilitated the recording in hospital.

**Conflicts of Interest:** The authors declare no competing interests.

## Appendix A

### *Reconstruction of cardinal leads from limb components*

As mentioned in the methods section, device bandwidth and gains have been verified using a proper signal generator, capable of generating 1 mV<sub>pp</sub> sine waves (Medi Cal Instruments model 220 Biomedical Function Generator) [26]. In addition, we assessed the point to point correlation between limb leads reconstructed using the limb components and limb leads that are recorded directly. To reconstruct the limbs, we simply operated a point by point subtraction between recorded signals and assessed the correlation between signals using the embedded MATLAB correlation function [19,20].

As an example (see Figure A1) we can compute lead I from simple subtraction of the WCT's components Left Arm(LA) and Right Arm (RA) (lead I = LA – RA [1]). In all the assessed cases, correlation scored in excess of 99% and signals cannot be distinguished unless labeled and plotted on different axis. We conclude that the LA, RA and LL components that we record with our device are the actual components of the WCT.

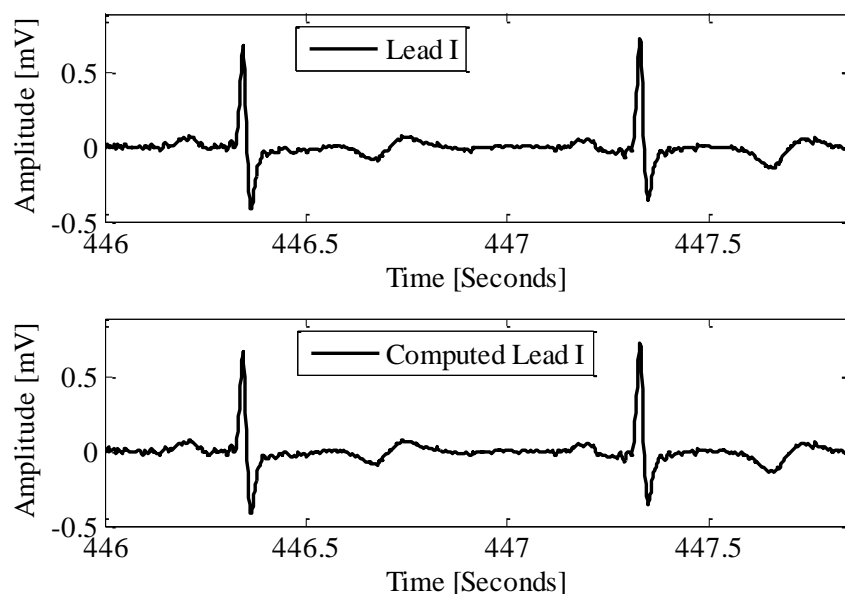


**Figure A1.** Example reconstruction of limb leads from components (P016). In this example, we reconstructed (computed) lead I from the LA and RA potentials recorded by our hardware; correlation between signals scored in excess of 99%.



## References

- Malmivuo, J.; Plonsey, R. *Bioelectromagnetism: Principles and Applications of Bioelectric and Biomagnetic Fields*; Oxford University Press: Oxford, UK, 1995.
- Frank, E. General theory of heart-vector projection. *Circ. Res.* **1954**, *2*, 258–270. [[CrossRef](#)] [[PubMed](#)]
- Bayley, R.H.; Reynolds, E.W.; Kinard, C.L.; Head, J.F. The Zero of Potential of the Electric Field Produced by the Heart Beat: The Problem with Reference to Homogeneous Volume Conductors. *Circ. Res.* **1954**, *2*, 4–13. [[CrossRef](#)] [[PubMed](#)]
- Bayley, R.H.; Kinard, C.L. The Zero of Potential of the Electric Field Produced by the Heart Beat: The Problem with Reference to living human subject. *Circ. Res.* **1954**, *2*, 104–111. [[CrossRef](#)] [[PubMed](#)]
- Horowitz, P.; Hill, W.; Robinson, I. *The Art of Electronics*; Cambridge University Press: Cambridge, UK, 1980.
- Sedra, A.S.; Smith, K.C. *Microelectronic Circuits*; Oxford University Press: Oxford, UK, 2004.
- Northrop, R.B. *Analysis and Application of Analog Electronic Circuits to Biomedical Instrumentation*; CRC Press: Boca Raton, FL, USA, 2012.
- Webster, J. *Medical Instrumentation: Application and Design*; John Wiley & Sons: Hoboken, NJ, USA, 2009.
- Enderle, J.D. *Bioinstrumentation*; Morgan & Claypool: Williston, VT, USA, 2006.
- Gargiulo, G.; Bifulco, P.; Calvo, R.A.; Cesarelli, M.; Mcewan, A.; Jin, C.; Ruffo, M.; Romano, M.; Shephard, R.; Schaik, A.V. Giga-ohm high-impedance fet input amplifiers for dry electrode biosensor circuits and systems integrated microsystems: Electronics, photonics, and biotechnology ed k iniewski. In *Integrated Microsystems: Electronics, Photonics, and Biotechnology*; CRC Press: Boca Raton, FL, USA, 2011.
- Bronzino, J.D. *Biomedical Engineering Handbook*; CRC Press: Boca Raton, FL, USA, 1999.
- Burger, H.; Van Milaan, J. Heart-vector and leads: Part III geometrical representation. *Br. Heart J.* **1948**, *10*, 229–233. [[CrossRef](#)]
- Burger, H.; Van Milaan, J. Heart-vector and leads. Part II. *Br. Heart J.* **1947**, *9*, 154–160. [[CrossRef](#)] [[PubMed](#)]
- Wilson, F.N.; Johnston, F.D.; Rosenbaum, F.F.; Barker, P.S. On einthoven's triangle, the theory of unipolar electrocardiographic leads, and the interpretation of the precordial electrocardiogram. *Am. Heart J.* **1946**, *32*, 277–310. [[CrossRef](#)]
- Burger, H.C.; Van Milaan, J. Heart-vector and leads. *Br. Heart J.* **1946**, *8*, 157–161. [[CrossRef](#)] [[PubMed](#)]
- INA116—Texas Instruments. Available online: <http://www.ti.com/lit/ds/symlink/ina116.pdf> (accessed on 1 May 2016).
- Gargiulo, G.D.; Tapson, J.; van Schaik, A.; McEwan, A.; Thiagalingam, A. Unipolar ecg circuits: Towards more precise cardiac event identification. In Proceedings of the 2013 IEEE International Symposium on Circuits and Systems (ISCAS2013), Beijing, China, 19–23 May 2013; pp. 662–665.
- Gargiulo, G.; Thiagalingam, A.; Mcewan, A.; Cesarelli, M.; Bifulco, P.; Tapson, J.; van Schaik, A. True unipolar ecg leads recording (without the use of wct). *Heart Lung Circ.* **2013**, *22*, S102. [[CrossRef](#)]
- Gargiulo, G.D.; Varaki, E.S.; Hamilton, T.J.; Bifulco, P.; Cesarelli, M.; Romano, M. A 9-independent-leads ecg system from 10 electrodes: A practice preserving wct-less true unipolar ecg system. In Proceedings of the Biomedical Circuits and Systems Conference (BioCAS), Atlanta, GA, USA, 22–24 October 2015; pp. 1–4.
- Gargiulo, G.D. True unipolar ecg machine for wilson central terminal measurements. *BioMed. Res. Int.* **2015**, *2015*, 586397. [[CrossRef](#)] [[PubMed](#)]
- Gargiulo, G.; McEwan, A.; van Schaik, A.; Jin, C.; Cesarelli, M.; Bifulco, P.; Calvo, R.A. *Non-Invasive Electronic Biosensor Circuits and Systems*; INTECH Open Access Publisher: Rijeka, Croatia, 2010.
- Prance, R.J.; Beardsmore-Rust, S.; Aydin, A.; Harland, C.J.; Prance, H. Biological and medical applications of a new electric field sensor. In Proceedings of the ESA Annual Meeting in Electrostatics, Minneapolis, MN, USA, 17–19 June 2008; pp. 1–4.
- Prance, R.J.; Debray, A.; Clark, T.D.; Prance, H.; Nock, M.; Harland, C.J.; Clippingdale, A.J. An ultra-low-noise electrical-potential probe for human-body scanning. *Meas. Sci. Technol.* **2000**, *11*, 291–297. [[CrossRef](#)]
- CG/CG2 SN Series—Medium to High Surge GDT from Gas Discharge Tubes. Available online: <http://www.littelfuse.com/products/gas-discharge-tubes/medium-to-high-surge-gdt/cg-cg2-sn.aspx> (accessed on 1 May 2016).
- OPA140 High-Precision, Low-Noise, Rail-to-Rail Output, 11-MHz JFET Op Amp. Available online: <http://www.ti.com/lit/ds/symlink/opa140.pdf> (accessed on 1 May 2016).

26. Gargiulo, G.D.; Bifulco, P.; Cesarelli, M.; Fratini, A.; Romano, M. Problems in assessment of novel biopotential front-end with dry electrode: A brief review. *Machines* **2014**, *2*, 87–98. [[CrossRef](#)]
27. Gargiulo, G.D.; McEwan, A.L.; Bifulco, P.; Cesarelli, M.; Jin, C.; Tapson, J.; Thiagalingam, A.; van Schaik, A. Towards true unipolar bio-potential recording: A preliminary result for eeg. *Physiol. Meas.* **2012**, *34*, N1. [[CrossRef](#)] [[PubMed](#)]
28. Winter, B.B.; Webster, J.G. Reduction of interference due to common mode voltage in biopotential amplifiers. *IEEE Trans. Biomed. Eng.* **1983**, *30*, 58–62. [[CrossRef](#)] [[PubMed](#)]
29. Gargiulo, G.; McEwan, A.; Bifulco, P.; Cesarelli, M.; Jin, C.; Tapson, J.; Thiagalingam, A.; Van Schaik, A. Towards true unipolar eeg recording without the wilson central terminal (preliminary results). *Physiol. Meas.* **2013**, *34*, 991–1012. [[CrossRef](#)] [[PubMed](#)]
30. Akay, M. *Wiley Encyclopedia of Biomedical Engineering*; John Wiley & Sons: Hoboken, NJ, USA, 2006.
31. Hwang, I.-D.; Webster, J.G. Direct interference canceling for two-electrode biopotential amplifier. *IEEE Trans. Biomed. Eng.* **2008**, *55*, 2620–2627. [[CrossRef](#)] [[PubMed](#)]
32. Gargiulo, G.D.; Bifulco, P.; Cesarelli, M.; McEwan, A.; Wabnitz, A. Open platform, 32-channel, portable, data-logger with 32 PGA control lines for wearable medical device development. *Electron. Lett.* **2014**, *50*, 1127–1129. [[CrossRef](#)]



© 2016 by the authors; licensee MDPI, Basel, Switzerland. This article is an open access article distributed under the terms and conditions of the Creative Commons Attribution (CC-BY) license (<http://creativecommons.org/licenses/by/4.0/>).

# Computing a New Central Terminal for ECG recording using combined Genetic Algorithm and linear regression from real patient data

Hossein Moeinzadeh<sup>1</sup>, Gaetano D. Gargiulo<sup>1,2</sup>, Paolo Bifulco<sup>2</sup>, Mario Cesarelli<sup>2</sup>, Alistair L. McEwan<sup>3</sup>, Aiden O'Loughlin<sup>4</sup>, Ibrahim M. Shugman<sup>5</sup>, Jonathan C. Tapson<sup>1</sup> and Aravinda Thiagalingam<sup>6</sup>

<sup>1</sup> The MARCS Institute, Western Sydney University, NSW Australia

<sup>2</sup> Department of Electrical Engineering and Information Technology (DIETI), "Federico II" The University of Naples, Italy

<sup>3</sup> School of EIE, University of Sydney, NSW Australia

<sup>4</sup> School of Medicine, Western Sydney University, NSW Australia

<sup>5</sup> Cardiology Department, Campbelltown Hospital, NSW, Australia

<sup>6</sup> School of Medicine, The University of Sydney, NSW Australia

{H.Moeinzadeh,G.Gargiulo,J.Tapson,A.O'Loughlin}@Westernsydney.edu.au, pabifulc@unina.it, cesarell@unina.it, shugmano@hotmail.com, aravinda.thiagalingam@sydney.edu.au

## ABSTRACT

Modern electrocardiography (ECG)<sup>1</sup> uses the Wilson Central Terminal (WCT) as a reference point for the majority of leads. WCT is assumed to be near zero and steady during the cardiac cycle. However, due to the measurement encumbrances of the real amplitude of WCT, this assumption has never been verified in clinical practice. Using our own recently developed 15-lead ECG device that can measure WCT components in addition to 12-lead ECGs in a clinical setting, we propose a framework to derive a New Central Terminal (NCT) with demonstrated less variation and near zero amplitude during the cardiac cycle. Our method is based upon application of a Genetic Algorithm (first 1000 samples), and then a linear regression to calculate the NCT for the rest of the recording.

## CCS CONCEPTS

**Computing Methodology** → **Machine learning**; Machine learning approaches • **Applied Computing** → Health informatics

## KEYWORDS

Electrocardiography, Genetic Algorithm, Linear Regression, Wilson Central Terminal

## 1 INTRODUCTION

<sup>1</sup> Permission to make digital or hard copies of part or all of this work for personal or classroom use is granted without fee provided that copies are not made or distributed for profit or commercial advantage and that copies bear this notice and the full citation on the first page. Copyrights for third-party components of this work must be honored. For all other uses, contact the owner/author(s).  
GECCO '17 Companion, July 15-19, 2017, Berlin, Germany  
© 2017 Copyright is held by the owner/author(s).  
ACM ISBN 978-1-4503-4939-0/17/07.  
<http://dx.doi.org/10.1145/3067695.3076090>

In 12-lead electrocardiogram (ECG) recordings, precordial leads are measured as the potential differences between each of the six exploring electrodes on the chest and a virtual reference point known as the Wilson Central Terminal (WCT) which was described in 1931[1]. It is defined as the voltage average of right arm ( $\phi_R$ ), left arm ( $\phi_L$ ), and left leg ( $\phi_F$ ), and assumed to be near zero and steady during the cardiac cycle (Eq. 1) with condition c1.

$$WCT = \alpha\phi_L + \beta\phi_R + \delta\phi_F \quad (1)$$

$$\alpha, \beta, \gamma = 1/3 \quad (c1)$$

However, this assumption was proved wrong and has been recognized as a source of potential error in ECG [2]. In 1954, Frank was the first researcher who raised concern about WCT amplitude and variation. He warned clinicians that WCT is not null or steady during the cardiac cycle, and how it can bias ECG measurement [3]. Later, Bayley and Kinard were able to measure the raw amplitude by putting a human being inside a metal structure and immersing it into the water during the measurement of ECG [4, 5]. Due to the difficulties of the real WCT measurement, the WCT assumptions as they have been conceived by Wilson, have been widely accepted and considered as a systematic error in ECG recording.

We recently proposed a new ECG device that could record 12-lead ECG together with the raw voltages of the WCT components (right arm, left arm, and left leg) [6, 7]. Our results confirm the previous findings in 1954 by Bayley, and show that WCT amplitude is in average as large as 51.2% of lead II [6] Whereas lead II is the voltage difference between left arm ( $\phi_L$ ), and left leg ( $\phi_F$ ).

In this paper, we address the problem of the high variability of WCT in ECG recording, and propose a new reference point for human body.

## 2 PROPOSED METHOD

Availability of raw WCT components allows us to propose a new framework to compute a New Central Terminal (NCT) using a combination of the Genetic Algorithm (GA) and the Linear Regression model (LRM) that ultimately may lead to the use of NCT in real time data acquisition.

Recalling that WCT is the average of limb electrodes, NCT is defined as weighted mean of WCT components. We use a GA to compute the three weighted factors ( $\alpha, \beta, \gamma$ ) (neglecting  $c_1$  in Eq.1) with constraints of being non-zero, positive, and less than one in module. Our ideal reference point has a small variation, near zero amplitude during the cardiac cycle; in other words, NCT amplitude should be less than 0.1 mV to be considered clinically irrelevant. Off-note, WCT optimization using weighted resistors was also attempted in real time during the original experiment performed in 1954 with little success [4]. During this remarkable experiment, researchers attempted real-time changes of the summing resistors of WCT components whilst recording. With our method, we compute (GA) the prototype of NCT for the first 1000 recorded samples (1.25 s) of WCT components. NCT is then refined and computed for the full signal using LRM (Fig.1). The population size contains 80 individuals, each of which is a vector of float in interval (0, 1). In every iteration, elite members are moved to the next generation, and if unchanged after five consecutive iterations, it was considered as the optimum answer. In this paper, we use data recorded from 29 volunteer patients (written consent), age range: 45-89 years (average 66; 38% females) (study protocol number HREC/15/LPOOL/302).

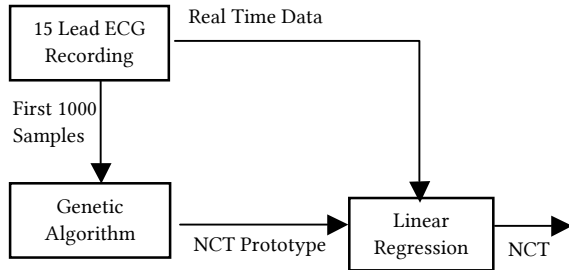


Figure 1 : The flowchart of NCT computation

### 3 Results

The average number of iterations necessary for the method to converge is quite small (16.36 in average). Since linear regression has linear time complexity, the overall performance of our proposed algorithm can be considered as time efficient.

Our assessment shows that while WCT exhibits proper ECG characteristics such as a P-wave and a T-wave, a large amplitude and variability (including random polarity), NCT is more close to the ideal reference point as it is almost steady with little variation during the cardiac cycle and has less medically relevant points. In comparison with WCT, NCT average relative percentage to lead II is 2.76% with standard deviation 3.68%, while WCT relative percentage to lead II has a mean value of 48.31% with a standard deviation 25.67%.

Table 1: Summary of measurement results. WCT and NCT relative amplitudes to lead II

Patient ID	Age	Gender	WCT amplitude as % of lead II	NCT amplitude as % of lead II	NCT medically irrelevant points decrease percentage
P001	63	F	27	1	-0.06
P002	51	F	40	2	-0.04
P003	65	F	35	5	-0.26
P005	88	F	90	12	-0.24
P006	52	F	90	3	-0.19
P007	70	F	59	3	-0.20
P010	71	F	23	0	-0.06
P012	89	F	25	1	-0.20
P013	63	F	23	1	0.00
P014	70	F	41	3	-0.08
P016	70	F	65	1	-0.15
P018	59	M	100	7	-0.05
P019	68	M	33	0	-0.11
P020	79	M	65	1	-0.18
P021	55	M	50	1	-0.30
P022	71	M	40	1	0.00
P023	52	M	60	0	-0.09
P024	45	M	20	0	-0.01
P025	79	M	50	5	-0.29
P026	85	M	22	0	-0.01
P027	52	M	30	1	-0.15
P028	62	M	41	5	-0.48
P033	78	M	57	1	-0.25
P034	73	M	100	13	-0.35
P037	72	M	25	0	-0.02
P038	56	M	48	0	0.00
P039	60	M	20	1	-0.34
P040	65	M	27	1	-0.01
P042	53	M	95	11	-0.09
Average	66.07		48.31	2.76	-0.14
			Polarity distribution		N: 6.9%; Negative: 24.1%
Total:	29		38% Females		

### REFERENCES

- [1] B. J. Malmivuo and R. Plonsey, *Principles and Applications of Bioelectric and Biomagnetic Fields*. Oxford University Press, 1995.
- [2] H. C. Burger, "The zero of potential: A persistent error," *American Heart Journal*, vol. 49, no. 4, pp. 581-586, 1955.
- [3] E. Frank, "General Theory of Heart-Vector Projection," (in English), *Circulation Research*, vol. 2, no. 3, pp. 258-270, 1954.
- [4] R. H. Bayley and C. L. Kinard, "The zero of potential of the electrical field produced by the heart beat; the problem with reference to the living human subject," *Circ Res*, vol. 2, no. 2, pp. 104-111, Mar 1954.
- [5] R. H. Bayley, E. W. Reynolds, Jr., C. L. Kinard, and J. F. Head, "The zero of potential of the electric field produced by the heart beat; the problem with reference to homogenous volume conductors AA," *Circ Res*, vol. 2, no. 1, pp. 4-13, Jan 1954.
- [6] G. Gargiulo *et al.*, "On the "Zero of Potential of the Electric Field Produced by the Heart Beat". A Machine Capable of Estimating this Underlying Persistent Error in Electrocardiography," *Machines*, vol. 4, no. 4, p. 18, 2016.
- [7] G. D. Gargiulo, "True unipolar ECG machine for Wilson Central Terminal measurements," *Biomed Res Int*, vol. 2015, p. 586397, 2015.

neous coronary intervention. He remained headache free at 2-year follow-up.

The case serves as an excellent opportunity to highlight this uncommon, but potentially life-threatening disorder. The discussion reviews available literature on the pathophysiology, incidence and prognosis, before looking at the current diagnostic criteria, as well as in whom to consider the diagnosis. Distinguishing cardiac cephalgia from migraine is important, as vasoconstrictive treatments (e.g., triptans) would be contraindicated. Clues to diagnosis include: exertional headache, no prior headache history, age > 55 years, and presence of vascular risk factors.

<http://dx.doi.org/10.1016/j.hlc.2018.06.556>

0556

### A Double-Blind Randomised Placebo Controlled 2 × 2 Factorial Trial of the Effect of Vitamin K and Colchicine on Vascular Calcification Activity in Subjects With Diabetes Mellitus: The Rationale and Design of the Vikcovac Diabetes Trial

J. Bellinge<sup>1,\*</sup>, G. Chew<sup>1,2</sup>, S. Gan<sup>1,2</sup>, R. Francis<sup>1,3</sup>, W. Macdonald<sup>1,4</sup>, C. Schultz<sup>1,2</sup>

<sup>1</sup> University of Western Australia, Perth, Australia

<sup>2</sup> Royal Perth Hospital, Perth, Australia

<sup>3</sup> Sir Charles Gairdner Hospital, Nedlands, Australia

<sup>4</sup> Fiona Stanley Hospital, Murdoch, Australia

**Introduction:** Cardiovascular disease is the leading cause of death in the Western world. Diabetes mellitus confers a doubling in risk of cardiovascular disease. Computed tomographic (CT) coronary calcium scoring (CCS) is an effective method for cardiovascular risk stratification in asymptomatic individuals. The rate of progression of coronary calcium on consecutive CT scans provides further cardiovascular disease-risk stratification capabilities. Patients with no progression of their CCS are at low risk of cardiovascular disease events [1]. There are no known therapies that prevent vascular calcification (VC). 18F-Sodium Fluoride Positron Emission Tomography is a novel molecular imaging modality that identifies regions of vascular calcification activity that subsequently develop into established macrocalcifications, allowing a unique approach for clinical trials studying potential modifiers of CCS [2].

**Interventions:** Inflammation is a key trigger for the development of VC. Colchicine is a unique anti-inflammatory agent with promising plaque-modifying capabilities [3]. In addition, a deficit in VC-specific inhibitors is thought to promote further propagation of VC. Incomplete activation of Matrix-GLA protein, a potent local inhibitor of VC that requires Vitamin-K-dependent carboxylation, may also contribute to VC. This study aims to test whether Colchicine or vitamin K could halt the progression of coronary artery calcification.

**Population and Study Design:** This double-blinded randomised 2 × 2 factorial placebo controlled trial will include 154 participants with diabetes mellitus and elevated coro-

nary calcium scores who will receive Colchicine 0.5mg and Phytomenadione 10 mg (vitamin K) and matching placebos.

**Outcomes:** A change in vascular 18F-Sodium Fluoride PET activity from baseline will be assessed after 3 months.

### References

- [1] Budoff M, et al. *J Am Coll Cardiol* 2013;61:1231–9.
- [2] Irkle A, et al. *Nature Commun* 2015;6:7495.
- [3] Vaidya K, et al. *JACC Cardiovasc Imaging* 2017; ePub.

<http://dx.doi.org/10.1016/j.hlc.2018.06.557>

0557

### A Modern Wilson's Central Terminal Electrocardiography Database



H. Moeinzadeh<sup>1,\*</sup>, G. Gargiulo<sup>1,2</sup>, P. Bifulco<sup>2</sup>, M. Cesarelli<sup>2</sup>, A. O'Loughlin<sup>3</sup>, M.I. Shugman<sup>4</sup>, A. Thiagalingam<sup>5,6,7</sup>

<sup>1</sup> Marcs Institute for Brain, Behaviour & Development, Western Sydney University, Penrith, Australia

<sup>2</sup> Department of Electrical Engineering and Information Technology (DIETI), 'Federico II' The University of Naples, Italy

<sup>3</sup> School of Medicine, Western Sydney University, Sydney, Australia

<sup>4</sup> Cardiology Department, Campbelltown Hospital, Sydney, Australia

<sup>5</sup> School of Medicine, The University of Sydney, Sydney, Australia

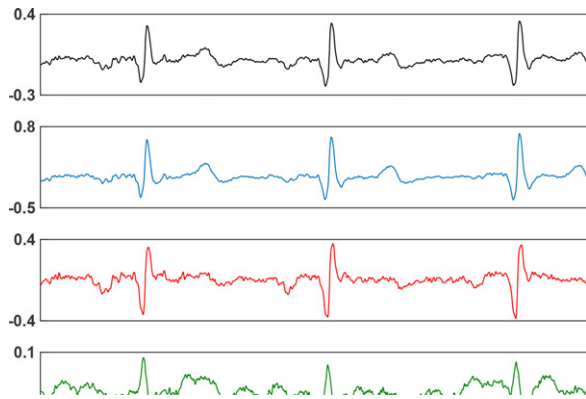
<sup>6</sup> Cardiology Department, Westmead Hospital, Sydney, Australia

<sup>7</sup> Westmead Institute for Medical Research, NSW, Sydney, Australia

Wilson's Central Terminal (WCT) is an artificially constructed virtual reference potential for surface electrocardiography (ECG). It is derived by averaging the voltage of the right arm ( $\Phi_R$ ), left arm ( $\Phi_L$ ), and left leg ( $\Phi_F$ ), and is assumed to be steady and with negligible amplitude during the cardiac cycle. In order to measure WCT, in 1954, Bayley and Kinard encased volunteers inside a metal structure that was immersed in water for the duration of the recording. Due to the impracticality in measuring WCT using this method, it is an accepted methodological error in modern ECG.

This study employed a novel '15-lead ECG device' in which the 'right leg' is used as the ground reference terminal for measuring all signals. It was able to record WCT components ( $\Phi_R$ ,  $\Phi_L$ , and  $\Phi_F$ ) and a 12-lead ECG. Data from 85 patients (35 (41%) patients were female) at Campbelltown Hospital were recorded. Patients with pacemakers were excluded from the dataset. The average age of the study population was 65.31 years (SD 11.59). The absolute average amplitudes of WCT components among all patients were ( $\Phi_R = 0.076$  mV,  $\Phi_L = 0.070$  mV, and  $\Phi_F = 0.044$  mV). Ten-second periods of recording without any artefacts was selected, and 413 10-second periods were extracted. It was found that recorded WCT is highly individual, and has standard ECG characteristics, including a P-wave, QRS complex, and T-wave.





<http://dx.doi.org/10.1016/j.hlc.2018.06.558>

0558

### A Partner in Medication Management and Safety: A Review of the Addition of a Pharmacist to Cardiology Out-Patient Clinics



L. Steel\*, J. Eglington

RBWH, Brisbane, Australia

**Background:** Cardiology patients often have high medication burden; hence, they are at high risk of medication misadventure. Worldwide studies have demonstrated that pharmacists, through a number of activities including interventions, improve medication management and patient safety.

**Method:** A pharmacist was added to the cardiology outpatient clinic at a tertiary Queensland hospital. The pharmacist recorded all interventions in the first 12 months, classified the nature and risk rated the interventions based on a validated risk scoring tool. The benefit of the pharmacist was also assessed through a survey completed by cardiology clinic staff.

**Results:** The pharmacist conducted 1072 reviews and recorded 429 interventions. Of these, 4.2% were risk rated as extreme, 23.1% high, 52.4% moderate and 20.2% low. An example of an extreme risk intervention was pharmacist identification of a patient taking twice the maximum daily dose of flecainide. The nature of interventions was also recorded with non-adherence, non-cardiac medication interventions and medication counselling making up the top three classes of interventions: 16.5%, 13.9% and 11.4% respectively. The medication counselling cohort largely included the pharmacists counselling on the importance of medication adherence post myocardial infarction. From the staff survey, all respondents agreed that the addition of the pharmacist to the clinic was valuable to both clinicians and their patients with 100% requesting that the service continue.

**Conclusion:** With a significant number of interventions recorded and positive feedback in the survey it was suggestive that the addition of a pharmacist to the cardiology clinic made a positive impact to patient medication management and safety.

<http://dx.doi.org/10.1016/j.hlc.2018.06.559>

0559

### A Rare Case of *Corynebacterium* Endocarditis



N. Iyer<sup>1,\*</sup>, I. Wilcox<sup>1,2</sup>

<sup>1</sup> Royal Prince Alfred Hospital, Camperdown, Australia

<sup>2</sup> Sydney Medical School, The University of Sydney, Sydney, Australia

A 26-year-old gentleman presented with a 1-month history of fevers, malaise and weight loss. He was born in China and had moved to Australia during his childhood. He was appropriately vaccinated. There was no history of recent dental procedures or illicit drug use. On examination, the temperature was 39 °C. Heart rate, blood pressure and oxygen saturations were normal. There was a pan-systolic murmur over the apex. There were small, non-tender, erythematous macules over both palms consistent with Janeway lesions. Neurological examination was unremarkable. Blood tests revealed raised inflammatory markers (C-reactive protein 87 mg/L). Four separate sets of blood cultures at admission isolated *Corynebacterium pseudodiphtheriticum*, sensitive to penicillin. Urgent transthoracic echocardiography revealed a large vegetation (11 × 9 mm) attached to the anterior mitral leaflet with associated moderate-severe regurgitation. Left ventricular function was preserved. The patient was commenced on empirical therapy for endocarditis, subsequently rationalised to intravenous benzylpenicillin. Embolic workup revealed multiple cerebral lesions suspicious for mycotic aneurysms and a small subacute infarction in the right frontal lobe. He underwent mechanical mitral valve replacement after 2 weeks of intravenous antibiotic therapy. Valve tissue and subsequent blood cultures were negative and the patient was discharged home following a 6-week admission.

This study reports a case of *Corynebacterium pseudodiphtheriticum* endocarditis in an immunocompetent individual without traditional risk factors. This is a nasopharyngeal commensal, which is a rare cause of native valve endocarditis, with predilection for causing metastatic infections. Surgical referral is indicated for a large vegetation with evidence of systemic embolism.

<http://dx.doi.org/10.1016/j.hlc.2018.06.560>

0560

### A Rare Case of Very Late Recurrent Multivessel Spontaneous Coronary Artery Dissection in a Postmenopausal Woman



A. Dina\*, C. Chow, L. Ponnuthurai, W. van Gaal

Northern Hospital, Epping, Australia

A 60-year-old lady with a background history of hypertension, hyperlipidaemia, and an ex-smoker presented to this hospital with a 2-day history of chest pain. She had previously been diagnosed with acute coronary syndrome in 2009 following an angiogram, which revealed severe dif-

RESEARCH NOTE

Open Access



# Minimization of the Wilson's Central Terminal voltage potential via a genetic algorithm

Hossein Moeinzadeh<sup>1\*</sup> , Paolo Bifulco<sup>2</sup>, Mario Cesarelli<sup>2</sup>, Alistair L. McEwan<sup>3</sup>, Aiden O'Loughlin<sup>4</sup>, Ibrahim M. Shugman<sup>5</sup>, Jonathan C. Tapson<sup>1</sup>, Aravinda Thiagalingam<sup>6,7,8</sup> and Gaetano D. Gargiulo<sup>1,2,9</sup>

## Abstract

**Objective:** The Wilson Central Terminal (WCT) is an artificially constructed reference for surface electrocardiography, which is assumed to be near zero and steady during the cardiac cycle; namely it is the simple average of the three recorded limbs (right arm, left arm and left leg) composing the Einthoven triangle and considered to be electrically equidistant from the electrical center of the heart. This assumption has been challenged and disproved in 1954 with an experiment designed just to measure and minimize WCT. Minimization was attempted varying in real time the weight resistors connected to the limbs. Unfortunately, the experiment required a very cumbersome setup and showed that WCT amplitude could not be universally minimized, in other words, the weight resistors change for each person. Taking advantage of modern computation techniques as well as of a special ECG device that aside of the standard 12-lead Electrocardiogram (ECG) can measure WCT components, we propose a software minimization (genetic algorithm) method using data recorded from 72 volunteers.

**Result:** We show that while the WCT presents average amplitude relative to lead II of 58.85% (standard deviation of 30.84%), our minimization method yields an amplitude as small as 7.45% of lead II (standard deviation of 9.04%).

**Keywords:** Electrocardiography, Wilson Central Terminal, Genetic algorithm, Potential reference

## Introduction

The very first surface electrocardiogram was conceived and outlined by E. Einthoven in the 1900s, and entered clinical practice in the 1940s as 12-lead-Electrocardiogram (ECG). Since then, it is still the most popular non-invasive diagnostic tool for cardiac assessment [1, 2].

The 12-lead ECG is composed of twelve signals or 'leads' measured from the limbs and six positions on the chest called precordials. The precordials (1/2 of the signals) are measured as the potential difference between each exploring electrode located on the chest, and an assumed constructed 'zero' reference. This 'zero' reference was introduced by F. N. Wilson in 1931 and named after him as Wilson's Central Terminal (WCT) [1]. By

definition, it is the simple average of the three exploring electrodes connected to the right arm (RA), left arm (LA) and left leg (LL) and it is assumed to be steady and of negligible amplitude during the cardiac cycle.

However, the WCT voltage is neither steady nor of negligible amplitude [3]. Frank [4] was the first to undermine the idea of having a constant WCT during the cardiac cycle and discussed how this variation could affect the ECG measurement [2, 4–6]. Later, Burger clarified the true meaning of zero potential and defined the WCT as the average of the three limb leads which is symmetrical with respect to the limb leads [3]. To quantify the WCT voltage, Wilson proposed immersing the body in a large homogeneous conductor and theorized that 0.15 mV was its maximal value [7, 8].

Following this recommendation, Bayley and Kinard [9, 10] encased the body of volunteers inside a metal structure (called integrator electrode) that was immersed in water for the duration of the recording. With this

\*Correspondence: h.moeinzadeh@westernsydney.edu.au

<sup>1</sup> The MARCS Institute, Western Sydney University, Sydney, NSW, Australia  
Full list of author information is available at the end of the article



experiment, they determined that the WCT is non-stationary during the cardiac cycle and its amplitude could be as large as 40% of Einthoven's ECG signals [9, 10]. During this experiment, Bayley and Kinard also attempted a real-time minimization of the WCT amplitude to bring it below a non-influent value [10]. To achieve minimization they made use of three rheostats instead of fixed resistors and adjusted the weights of the three WCT components continually reporting the achieved new amplitude. To Achieve the WCT recording for the minimization, the volunteer was encased by a metal structure that was submerged in the water for the duration of the recording [10].

Although the notion that a large WCT voltage may be affecting the clinical recordings, aside from the few notable research studies [11, 12], all recording methods currently employed use the raw WCT as a reference for precordials. Eventually, after an initial wave of interest, the WCT has received scant research attention during the past decades [2]. Recently Gargiulo et al. [2, 12] proposed a way to record unipolar ECG without using the WCT and suggested a new device and a method to measure and store the WCT components. Taking advantage of the availability of these unique recording we present a software minimization for the WCT.

Our method similarly to the originally attempted minimization performs a weighted average of the WCT components. To achieve this goal we use a genetic algorithm (GA) [13]. The GA is a heuristic search method for finding the optimal answer for problems with high computational complexity. This approach is used for those problems, like ours, that either lacks a deterministic solution or a deterministic polynomial time complexity solution. This algorithm is called "genetic" because is based on the concept of the biological evolution of individuals within a population where "chromosomes" mutates to achieve the survival of the fittest. A "chromosome" represents a possible solution to the problem that can mutate from one population of chromosomes to the next population (generation) by using a "selection" procedure. The chromosomes that are selected to be in the next generation also could be changed or become parents of new chromosomes in the process of "mutation", and "crossover" [13]. In this paper, we show results of our minimization method applied to data recorded from 72 patients (25 female, age average 66.35 year-old  $\pm$  11.46 year-old), at Campbelltown Hospital, New South Wales, Australia.

## Main text

To our knowledge, this is the first attempt to the WCT minimization employing new data since Bayley and Kinard's effort in 1954 [10]. The proposed approach to

estimate M-WCT (whereas M stands for minimized) is engineered to fulfill:

1. Possibly be zero or near zero;
2. In any case (worst case scenario), M-WCT amplitude should be less than 0.1 mV, so that it can be considered clinically irrelevant and smaller than Wilson estimation of max amplitude [14].

In order to fit the M-WCT into the genetic algorithm paradigm, we need to formalize our problem regarding population, mutation, crossover and fitness function. Recalling that the WCT is the average of the limbs' electrodes, we can define M-WCT as the weighted mean of the WCT's components (weights can be different from 1/3, positive, not null and add up to one). More formally:

$$M-WCT = \alpha\vartheta_L + \beta\vartheta_R + \gamma\vartheta_F \quad (1.1)$$

$$0 < \alpha, \beta, \gamma < 1 \quad (1.2)$$

$$\alpha + \beta + \gamma = 1 \quad (1.3)$$

whereas  $\alpha, \beta,$  and  $\gamma$  are the minimization parameters;  $\vartheta_L, \vartheta_R$  and  $\vartheta_F$  are the raw potential of the limb electrodes placed on LA, RA, and LL respectively; thus  $\alpha, \beta,$  and  $\gamma$  are related to LA, RA and LL respectively, and will replace the averaging 5 k $\Omega$  resistors in our minimization.

To summarize, our method minimizes (1.1) according to the three main criteria enounced above constrained by (1.2) and (1.3).

## Fitness function

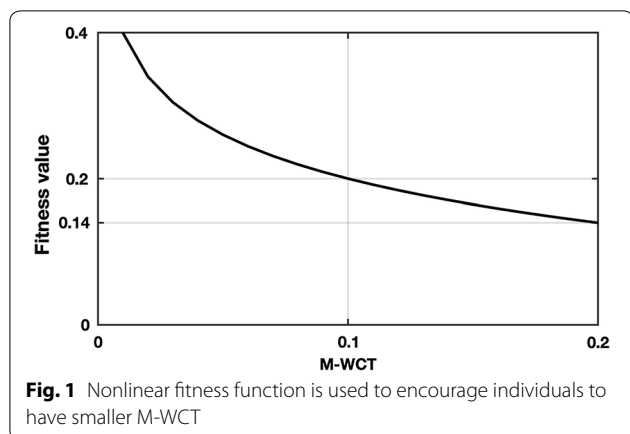
As mentioned, the role of the fitness function is to ensure "the survival of the fittest" hence converging towards the solution. Equation (1.4) is selected as the fitness function. This is because its shape and its nonlinearity provide an increase in the probability of having M-WCT with smaller values; in other words, it encourages the algorithm to converge more rapidly to amplitudes smaller than 0.1 mV. The plot of the fitness function is depicted in Fig. 1.

$$\text{Fitness} = \log_{0.00001} |M-WCT| \quad (1.4)$$

## Population

Represents all possible answers (chromosomes), a new population is generated during each iteration where each individual is a tern of weighted factors ( $\alpha, \beta, \gamma$ ). 80 individuals are chosen as population size. In the first population, only one chromosome is initialized by the WCT chromosome ( $\alpha = \beta = \gamma = 1/3$ ) and the rest are generated randomly constrained only by the conditions (1.2) and (1.3). Also, (1) the elite members of each population are moved to the next generation directly; (2) the WCT chromosomes are preserved in each population.





**Crossover**

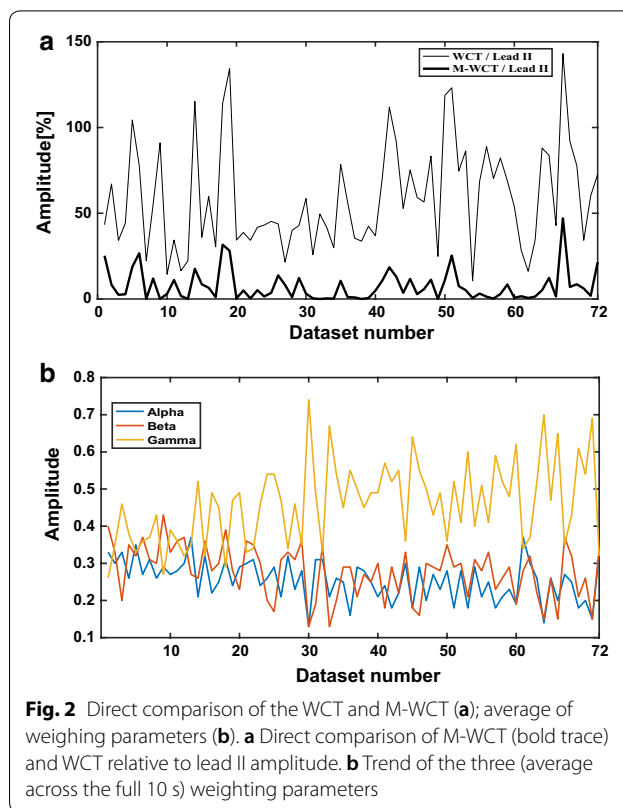
The role of the crossover operation is to build the next population based on selected chromosomes of the current population. We use single point and averaging crossover methods randomly to populate the next generation. For details see [15, 16].

**Mutation**

To avoid trapping into local optima the permutation algorithm is used to change the position of three parameters in a selected chromosome (mutation probability is equal to 0.1).

This method is applied to every voltages sample of the recording and computes three parameters to have the M-WCT trace during the cardiac cycle. For this study, we included data from 72 patients; each selected data excerpt has a normalized length of 10 s. As mentioned earlier, three weighting factors  $\alpha, \beta,$  and  $\gamma$  are calculated using the GA to minimize Wilson Central Terminal. In Additional file 1: Table S1, we report the average values of the three weights and the average number of iterations that the GA needs to converge for all patients.

Similarly to previous studies [9, 10], the WCT and M-WCT amplitudes are measured averaging five consecutive beats for each dataset and reported as a percentage of lead II. We used the orientation of the QRS complex to report the polarity of the WCT. “N” denotes signals with an unclear polarity in which the positive deflection amplitude closely matched the negative deflection at the QRS. In Fig. 2, we report the amplitude of the M-WCT and the WCT for each patient as well as the average across the full 10 s of the three weighting parameters. As it can be seen in Fig. 2b, the variation of each parameter is too high among all the patients, and three optimal parameters cannot be found



for all the patients. Summary of our findings are summarized in Additional file 1: Table S1.

Similarly, to previous studies, we found a variety of the WCT shapes and polarities (slightly in favor, see Additional file 1: Table S1, for positive polarity) hence it is possible to say that the WCT is highly individual, and can have standard ECG characteristics, such as a P-wave and a T-wave. Individuality was also found in the M-WCT, as we show in Fig. 3. However, due to the negligible general amplitude of M-WCT (see Fig. 2), we conclude that the clinical impact of the M-WCT is negligible with respect to the WCT.

Figure 3 shows an example of WCT in which a broader QRS feature with amplitude even higher than Lead II. However, as one can infer comparing M-WCT and WCT (bottom panel), the relative amplitude of M-WCT has highly decreased compared to the WCT relative amplitude.

An example of the WCT signal with a marked T-wave is visible in Additional file 2: Figure S1. As it can be observed, a marked T-wave deflection on the WCT trace (bottom panel) is synchronized with the T-wave on lead II (top panel). The WCT trace in Additional file 2: Figure S1 is also an excellent example of a highly variable WCT and an almost steady M-WCT. In one single cardiac cycle, the deflection’s polarity of the

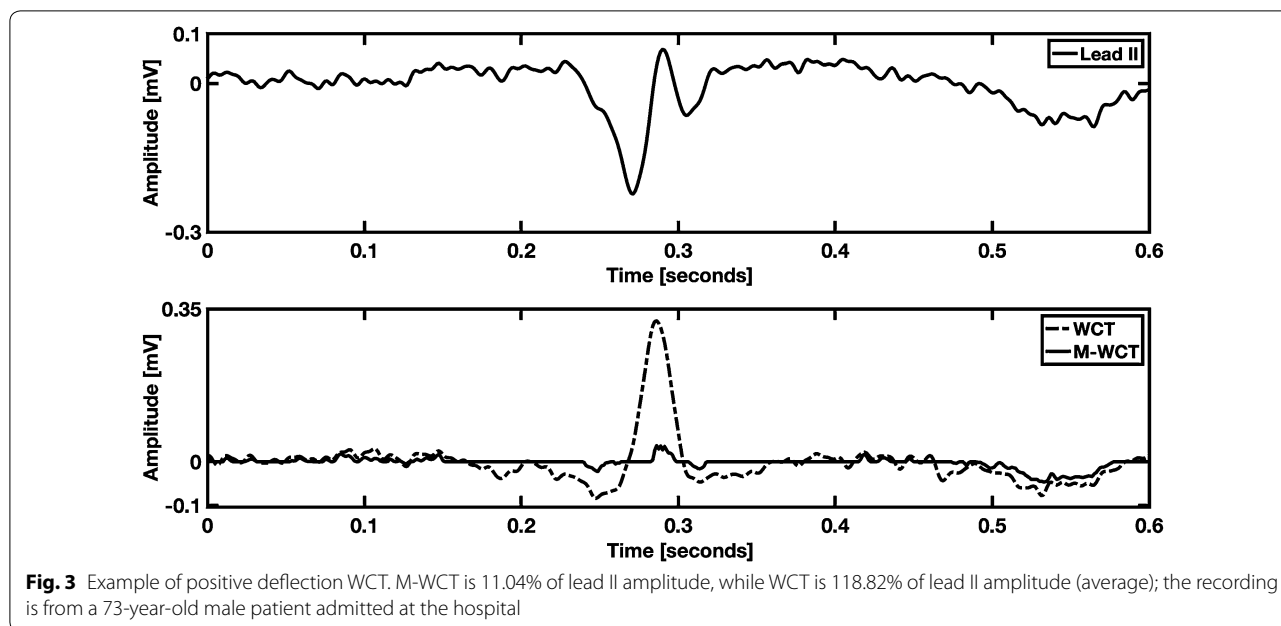


**Fig. 3** Example of positive deflection WCT. M-WCT is 11.04% of lead II amplitude, while WCT is 118.82% of lead II amplitude (average); the recording is from a 73-year-old male patient admitted at the hospital

WCT changes at least three times, and its amplitude reaches 45.27% of lead II (average), while the M-WCT amplitude is 3.59% of lead II. Additional file 3: Figure S2 is an example of high WCT amplitude with negative deflection. As seen, the WCT has an amplitude of 59.21% of lead II, while M-WCT amplitude is only 2.79% of lead II.

Recall that there was an attempt to measure and minimize the WCT in 1954 with a peculiar experiment which required a very cumbersome setup [9, 10, 17]. Minimization was attempted by varying the weight resistors connected to the limbs in real time, and it showed that the WCT amplitude could not be universally minimized (see Additional file 4: Figure S3). They found out the value of the WCT is zero for half of their subjects when the three resistors were chosen as ( $r = l = 2.6f$ ). Unfortunately, this resistors selection, for the other tested subjects) decreased the WCT amplitude to less than 50% when compared to an unweighted terminal selection ( $r = l = f$ ) [17]. Our results (see Fig. 2b) shows that to minimize WCT amplitude, different weights should be used similarly to Bayley et al. experiment [17]. Additionally, we found that  $\gamma$  (the weighting factor of  $\vartheta_F$ ) have usually larger amplitudes in comparison with  $\alpha$  and  $\beta$ . However, as the WCT component signals ( $\vartheta_L$ ,  $\vartheta_R$  and  $\vartheta_F$ ) are highly individual, the computed weighted factors are also different for each patient. In our dataset, the ratio of  $\gamma$  to  $\alpha$  is in the range of [0.78, 5.69], and the ratio of  $\gamma$  to  $\beta$  is in the range of [0.62, 5.69] (see Fig. 2).

**Limitations**

Although with this work we overcome the need to submerge the patients in water and use manual rheostats actually achieving a real minimization, probably the largest limitation is represented by the need to collect an excerpt of data that need to be used for the GA. For this work, we used a data excerpt of 10 s that at a sample rate of 800 Hz means a buffer for 8000 samples. Although this may seem like a small number, considering that to converge our GA takes  $200 \pm 41$  iterations requiring few minutes on an average computer before that the new precordials can be computed adding considerable delay to the ECG diagnosis. To improve our method, we are currently working on faster minimization techniques that could make the use of M-WCT viable in clinical practice.

**Additional files**

- Additional file 1: Table S1.** Measurements summary.
- Additional file 2: Figure S1.** Example of negative deflection WCT. WCT is 59.21% of lead II amplitude, while M-WCT is 2.79% of lead II amplitude (average); the recording is from a 59-year-old male patient admitted with chest pain.
- Additional file 3: Figure S2.** Example of negative deflection WCT. WCT is 59.21% of lead II amplitude, while M-WCT is 2.79% of lead II amplitude (average); the recording is from a 59-year-old male patient admitted with chest pain.

**Additional file 4: Figure S3.** Comparison of three resistors for right hand, left hand, and foot electrodes for 33 patients, experiment done by Bayley and Schmidt.

### Abbreviations

WCT: Wilson Central Terminal; ECG: electrocardiogram; GA: genetic algorithm; RA: right arm; LA: left arm; LL: left leg; M-WCT: Minimized Wilson Central Terminal.

### Authors' contributions

MH conceptualized this study and wrote the necessary code. GG, IS, and AOL performed data recording in hospital and data analysis. PB, MC, AM, and JT contributed to the data analysis and to the writing of the text. IS, AOL, and AT gave also clinical advice. All authors read and approved the final manuscript.

### Author details

<sup>1</sup> The MARCS Institute, Western Sydney University, Sydney, NSW, Australia. <sup>2</sup> Department of Electrical Engineering and Information Technology (DIETI), "Federico II", The University of Naples, Naples, Italy. <sup>3</sup> School of Electrical and Information Engineering, University of Sydney, Sydney, NSW, Australia. <sup>4</sup> School of Medicine, Western Sydney University, Sydney, NSW, Australia. <sup>5</sup> Cardiology Department, Campbelltown Hospital, Sydney, NSW, Australia. <sup>6</sup> School of Medicine, The University of Sydney, Sydney, NSW, Australia. <sup>7</sup> Cardiology Department, Westmead Hospital, Sydney, NSW, Australia. <sup>8</sup> Westmead Institute for Medical Research, Sydney, NSW, Australia. <sup>9</sup> School of Computing, Engineering and Mathematics, Western Sydney University, Sydney, NSW, Australia.

### Acknowledgements

The authors wish to thank the patients at Campbelltown Hospital (New South Wales, Australia) who volunteered for this study, and the hospital staff who supported and helped with the data collection, particularly the nurses of the Coronary Care Unit.

### Competing interests

The authors declare that they have no competing interests.

### Availability of data and materials

Although we are still working to the data collection and planning to release the full dataset before the end of the year, the data used for this paper are available upon request.

### Consent for publication

Not applicable.

### Ethics approval and consent to participate

All the patients volunteered for this study and gave written consent (this study was approved by the Ethics Committee of the South West Sydney Health District on 23rd September 2015 with the protocol number HREC/15/LPOOL/302).

### Funding

This study is supported by the office for Research Engagement and Development with Industry (REDI) at the Western Sydney University and by the MARCS Institute.

### Publisher's Note

Springer Nature remains neutral with regard to jurisdictional claims in published maps and institutional affiliations.



Received: 21 October 2018 Accepted: 13 December 2018  
Published online: 20 December 2018

### References

- Malmivuo J, Plonsey R. Bioelectromagnetism Principles and Applications of Bioelectric and Biomagnetic Fields. Oxford University Press; 1995. p. 1–506. <http://www.oxfordscholarship.com/view/10.1093/acprof:oso/9780195058239.001.0001/acprof-9780195058239>.
- Gargiulo GD. True unipolar ECG machine for Wilson Central Terminal measurements. *Biomed Res Int.* 2015;2015:586397.
- Burger HC. The zero of potential: a persistent error. *Am Heart J.* 1955;49(4):581–6.
- Frank E. General theory of heart-vector projection. *Circ Res.* 1954;2(3):258–70. <https://doi.org/10.1161/01.RES.2.3.258>.
- Dower GE, Osborne JA, Moore AD. Measurement of the error in Wilson's central terminal: an accurate definition of unipolar leads. *Br Heart J.* 1959;21:352–60.
- Frank E, Kay CF. The construction of mean spatial vectors from null contours. *Circulation.* 1954;9(4):555–62.
- Wilson FN, Johnston FD, Rosenbaum FF, Barker PS. On Einthoven's triangle, the theory of unipolar electrocardiographic leads, and the interpretation of the precordial electrocardiogram. *Am Heart J.* 1946;32(3):277–310. <https://doi.org/10.1111/j.1365-2818.1858.tb04542.x>.
- Miyamoto N, Shimizu Y, Nishiyama G, Mashima S, Okamoto Y. The absolute voltage and the lead vector of Wilson's central terminal. *Jpn Heart J.* 1996;37(2):203–14.
- Bayley RH, Kinard CL. The zero of potential of the electrical field produced by the heart beat; the problem with reference to the living human subject. *Circ Res.* 1954;2(2):104–11.
- Bayley RH, Reynolds EW, Kinard CL, Head JF. The zero of potential of the electric field produced by the heart beat; the problem with reference to homogenous volume conductors. *Circ Res.* 1954;2(1):4–13.
- Gargiulo G, Thiagalangam A, McEwan A, Cesarelli M, Bifulco P, Tapson J, et al. True unipolar ECG leads recording (without the use of WCT). *Hear Lung Circ.* 2013;22:S102.
- Gargiulo GD, McEwan AL, Bifulco P, Cesarelli M, Jin C, Tapson J, et al. Towards true unipolar ECG recording without the Wilson central terminal (preliminary results). *Physiol Meas.* 2013;34(9):991–1012. <http://stacks.iop.org/0967-3334/34/i=9/a=991?key=crossref.3ee57f77157cc5fa56247c2775f2317d>.
- Mitchell M. An introduction to genetic algorithms, vol. 32. In: Computers and mathematics with applications. MIT Press Ltd; 1996. [https://books.google.ca/books/about/An\\_Introduction\\_to\\_Genetic\\_Algorithms.html?id=0eznlz0TF-IC&pgis=1%5Cn](https://books.google.ca/books/about/An_Introduction_to_Genetic_Algorithms.html?id=0eznlz0TF-IC&pgis=1%5Cn), <http://www.amazon.ca/exec/obidos/redirect?tag=citeulike09-20&path=ASIN/0262631857%5Cn>, <http://linkinghub.elsevier.com/retrieve/pii/S0898122196902278>.
- Sheppard JP, Barker TA, Ranasinghe AM, Clutton-Brock TH, Frenneaux MP, Parkes MJ. Does modifying electrode placement of the 12 lead ECG matter in healthy subjects? *Int J Cardiol.* 2011;152(2):184–91.
- Rawlins GJE. Foundations of genetic algorithms 1991 (FOGA 1). Foundations of genetic algorithms (Book 1). Morgan Kaufmann; 1 edition (July 15, 1991); 1991.
- Gwiazda TD. Genetic algorithms reference, vol. 1. Tomasz Gwiazda; 2006.
- Bayley RH, Schmidt AE. The problem of adjusting the Wilson central terminal to a zero of potential in the living human subject. *Circ Res.* 1955;3(1):94–102. <https://doi.org/10.1161/01.RES.3.1.94>.

Communication

# On the Einthoven Triangle: A Critical Analysis of the Single Rotating Dipole Hypothesis

Gaetano D. Gargiulo <sup>1,2,\*</sup> , Paolo Bifulco <sup>2</sup>, Mario Cesarelli <sup>2</sup>, Alistair L. McEwan <sup>3</sup>, Hossein Moeinzadeh <sup>1</sup> , Aiden O'Loughlin <sup>4</sup>, Ibrahim M. Shugman <sup>5</sup>, Jonathan C. Tapson <sup>1</sup> and Aravinda Thiagalingam <sup>6</sup>

<sup>1</sup> The MARCS Institute, Western Sydney University, Milperra, NSW 2214, Australia;

h.moeinzadeh@westernsydney.edu.au (H.M.); j.tapson@westernsydney.edu.au (J.C.T)

<sup>2</sup> Department of Electrical Engineering and Information Technology (DIETI),

“Federico II” The University of Naples, 80100 Naples, Italy; pabifulc@unina.it (P.B.); cesarell@unina.it (M.C.)

<sup>3</sup> School of Electrical and Information Engineering, University of Sydney, Sydney, NSW 2006, Australia;

alistair.mcewan@sydney.edu.au

<sup>4</sup> School of Medicine, Western Sydney University, Campbelltown, NSW 2650, Australia;

aiden.oloughlin@gmail.com

<sup>5</sup> Cardiology Department, Campbelltown Hospital, Campbelltown, NSW 2650, Australia;

shugmano@hotmail.com

<sup>6</sup> School of Medicine, University of Sydney, Sydney, NSW 2006, Australia;

aravinda.thiagalingam@sydney.edu.au

\* Correspondence: g.gargiulo@westernsydney.edu.au

Received: 15 June 2018; Accepted: 17 July 2018; Published: 20 July 2018



**Abstract:** Since its inception, electrocardiography has been based on the simplifying hypothesis that cardinal limb leads form an equilateral triangle of which, at the center/centroid, the electrical equivalent of the cardiac activity rotates during the cardiac cycle. Therefore, it is thought that the three limbs (right arm, left arm, and left leg) which enclose the heart into a circuit, where each branch directly implies current circulation through the heart, can be averaged together to form a stationary reference (central terminal) for precordials/chest-leads. Our hypothesis is that cardinal limbs do not form a triangle for the majority of the duration of the cardiac cycle. As a corollary, the central point may not lie in the plane identified by the limb leads. Using a simple and efficient algorithm, we demonstrate that the portion of the cardiac cycle where the three limb leads form a triangle is, on average less, than 50%.

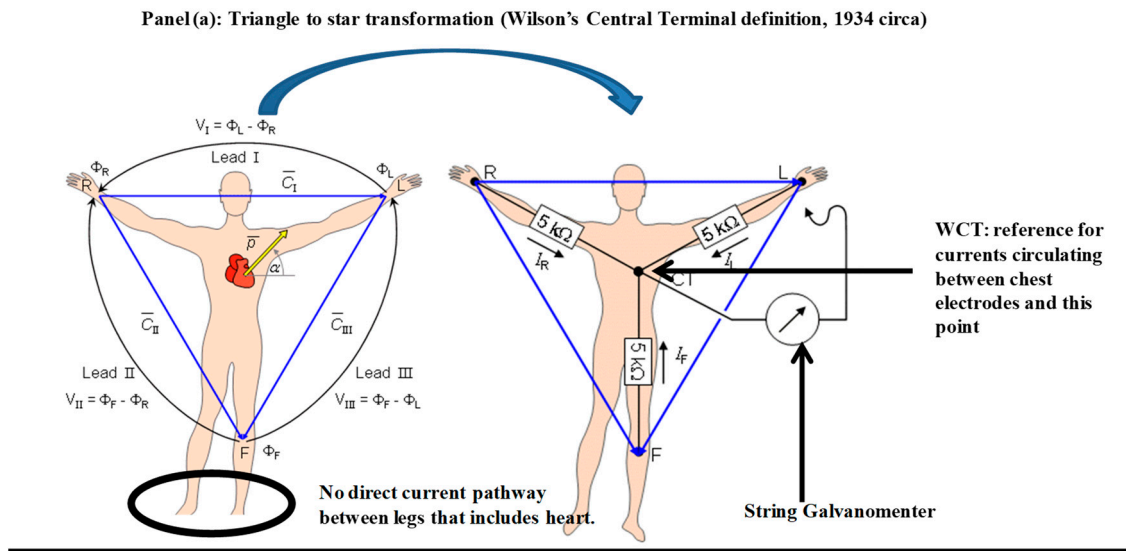
**Keywords:** basic cardiology science; ECG; Wilson Central Terminal; Einthoven triangle

## 1. Introduction

Modern electrocardiography (ECG) is still based upon the simplified assumption that the electrical activity of the heart can be reduced to that of a single electrical dipole rotating around a fixed point in the chest, the projection of which constitutes the so-called 12-lead ECG on the direction identified by pairs of electrodes [1]. This assumption was formulated in the 1930s by F.N. Wilson, who introduced the so-called precordials, or chest leads. In modern electrocardiography, precordials are voltage measurements. Having said that, at the time, precordials were measured as the current circulating into a circuit composed of one out of six pre-defined positions on the chest, and an estimation of the fixed point around which the equivalent heart dipole is supposed to rotate during the cardiac cycle [1]. Wilson himself defined this reference point as the average of the Einthoven limb electrodes: Left Arm (LA), Right Arm (RA), and Left Leg (LL), whereas the average is simply operated by connecting the three electrodes to a single common point via three identical, “high value” resistors [1].

As one may note, the Right Leg (RL) is not included in the original electrical activity of the heart model [1–3]. This is because the original instrument used to demonstrate the limbs' ECG by Einthoven was an extremely sensitive galvanometer (Ampere-meter) [1,4]. Therefore, also the limbs' ECG at the time was, by definition, a measure of the tiny current impressed from the heart to the limbs. Because there is no direct current pathway between the RL and LL that includes the heart, the circulating current is measured only between the arms, and between each arm and the LL.

In summary, it is possible to conclude that ECG recordings were originally a measure of the net current impressed by the electrical activity of the heart circulating into an external circuit closed by the measurement instrument. With this assumption, it was natural for Wilson to complete the transformation from the triangle (Einthoven's triangle) to the equivalent star circuit when he faced the problem of finding a reference for his chest leads (see Figure 1 panel (a)). In theory, if each of the Einthoven leads measures the net current impressed by the heart between two limbs, averaging all the electrodes together should give the best approximation of the point of origin: the neutral point of the cardiac electrical activity. In honor of his measurements and experiments, this reference terminal was named after him (Wilson's central terminal, or simply WCT), and the term 'unipolar' was introduced for precordial leads.



**Panel (b): Voltage WCT, currently employed in 12-Lead ECG measurements**

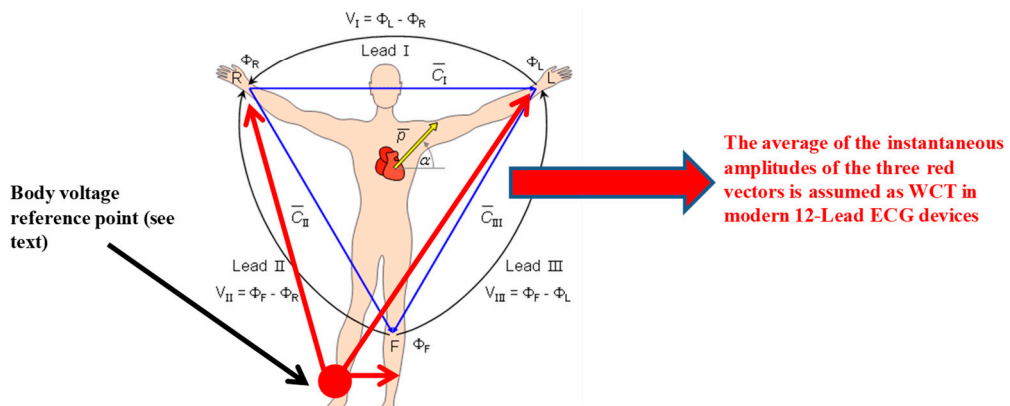


**Figure 1.** Traditional VS modern definition of WCT: Panel (a): Einthoven's triangle (left) and Wilson's transformation (right); Panel (b): modern voltage WCT.



In this framework, with this study we will demonstrate the following research hypothesis:

*Voltage measurement of limb leads, although measured in a closed circuit, does not form a triangle for the majority of the duration of a cardiac cycle; hence, a centre and centroid that constitute the WCT cannot be identified, as per Wilson's hypothesis.*

We prove this research hypothesis by analysing a total of 599 12-lead ECG recordings that include 549 recordings taken from the PTB database (freely available of Physionet [5]), and 50 recording taken the pilot study for our ECG device which is capable of recording the components of the WCT [2,6]. Using these recordings, we first assess where the limb leads form a triangle, and calculate the inner angles. Assessment of WCT amplitude is performed only for the 50 recordings where this is available.

## 2. Materials and Methods

For this paper, we employed a total of 599 ECG recordings. The first 549 were taken from the online Physionet databank [5] PTB database [7], while the remaining 50 were selected from one of our recent studies [2]. All subjects volunteered for our study and gave written consent (this study was approved on 23 September 2015 by the National Human Ethics Committee of Liverpool Hospital with the protocol number HREC/15/LPOOL/302).

This method section is divided into three parts. In the first part, we introduce the theoretical background and principles of physiological measurements of Voltage/Current for electrocardiography that form the context of our research hypothesis; in the second, we delve into the details of the equilateral triangle hypothesis which is at the base of the standard ECG theory (this is used to demonstrate the study hypothesis); in the third and the final parts of this method section we give a summary of the hardware used for the 50 recordings where WCT components are available.

During the work for this paper, we produced a very large amount of processed data and figures. As we aim to make our research entirely reproducible, the necessary processing scripts are included, together with the results of the processing for each single dataset we employed as additional material. The new data that we recorded during our clinical evaluation [2] are also available for download in Matlab format upon request.

### 2.1. Methodology Background: Principles of Voltage/Current Measurement in Electrocardiography

Before delving into the full explanation of our method, we must mention that Wilson's hypothesis and the related triangle to star transformation has been challenged at both the theoretical [8–13] and practical level [2,3,6,10,11,13–21] several times in the past 80 years, with several researchers confirming that, contrary to what Wilson's principal postulates [1,22,23], the amplitude of the WCT can be comparable to (or even larger than) the limb leads, and can exhibit variability during the cardiac cycle similar to any other ECG signal [2,8,10,16,24–28]. Still, as already mentioned, one may note that the original instrument that both Einthoven and Wilson used to formalize the triangular ECG model and the WCT was measuring the current impressed by the heart to the body surface, while modern electrocardiography uses voltage amplifiers [28]. Therefore, it is possible to evince that, contrary to the original definition of WCT, in modern ECG devices the WCT used is the instantaneous average of the voltages of the three limbs (RA, LA, and LL) relative to a reference voltage (see Figure 1 panel (b)) [3,17].

Moreover, once again we must stress the consequences of exchanging voltage measurements for current ones, as this difference is crucial for our method. Although it is clear that there is a well-known relationship of cause and effect between the voltage potential measured between two points of a circuit and the current circulating in the circuit itself, one must not forget that voltages are relative measurements performed by differential reading with respect to a reference point assumed to be neutral (or steady). Even the so-called "true differential" electronic amplifiers require a reference point to operate correctly [29–31]. In biomedical applications, particularly ECG, this reference is created virtually by the internal circuitry (i.e., voltage supply bootstrap [32]), and one may have the

impression that the amplifier works off the two points of connection in a true differential manner, i.e., this is only an impression, as the virtual reference voltage “moves” within the power supply rails according to the estimated common mode. This solution is often employed in single-lead ECG designs. In multiple-lead designs, this reference point is a true reference point on the body, and usually this additional connection is used also to re-inject a part of the measured signal inside the body to increase the signal-to-noise ratio at certain frequencies (i.e., power line frequencies). In both cases, the selected reference point on the human body is placed at the RL, and the circuitry designed to re-inject the signal inside the body is known as the Right Leg Driver (RLD), or Driven Right Leg (DRL) [32–35]; for this reason, in Figure 1, panel (b), the reference point for voltage measurements is noted on the RL [3,17].

Due to the natural link between voltage and current, and to the impractical use of sensitive current-measuring devices, cardiologists became used to referring to all measurements pertaining to ECGs in mV, neglecting the fact that measuring voltages rather than current implies having to deal with the different impedances of body sections. Taking Ohm’s law into account, which states that the voltage is the product of current and resistance (Voltage = Resistance  $\times$  Current), each lead can be interpreted as the voltage drop across a composed resistance (impedance, as a matter of fact) due to the net current impressed by the heart to the points of measurement. As an example, lead I (see Figure 2) can be interpreted as the voltage drop across the sum of the contact impedance at both electrodes, the impedance of each arm, and the variable impedance of the chest (due to respiration) across the shoulder.

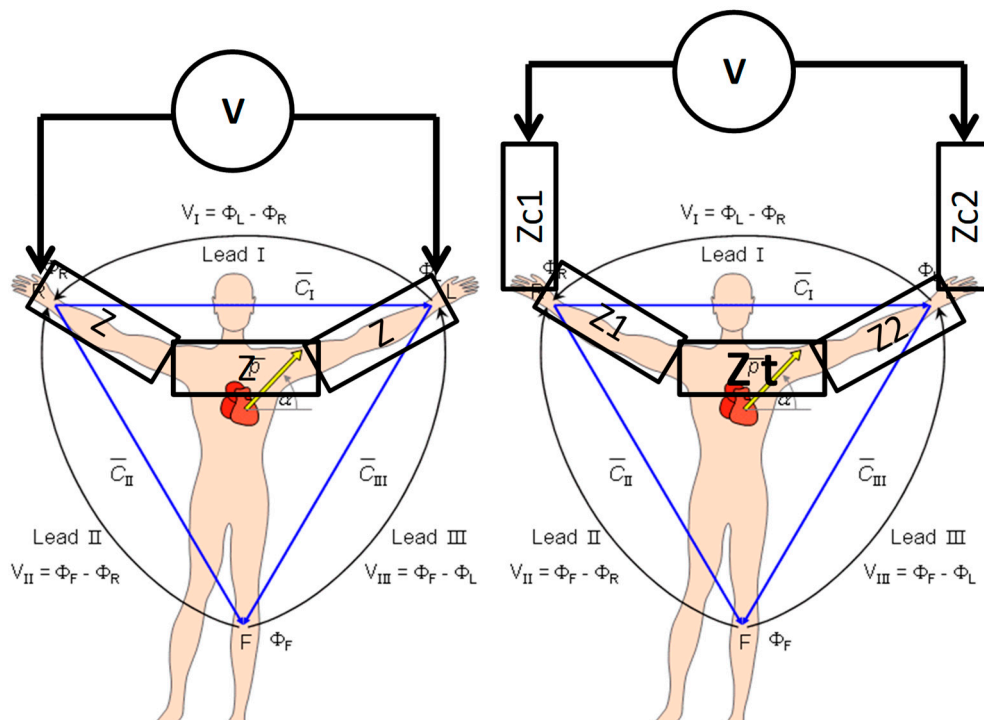


**Figure 2.** Direct comparison of idealized (left) measurement of lead I as voltage VS real measurement (right) that takes into account contact impedances ( $Z_{c1}$  and  $Z_{c2}$ ), different limbs impedance ( $Z_1$  and  $Z_2$ ) and the variable torso impedance ( $Z_t$ ) which changes rhythmically following the respiration.

Of course, evoking the simplifying hypothesis that the body is a homogeneous volume conductor, and hence, limb electrodes are all placed at an equal distance on a homogeneous conductor (constant resistance), with no (or negligible) contact impedance aside from a simple constant proportion between the values of current and voltages, these are perfectly interchangeable. However, in real life recordings, this is not always the case, and often, impedance/contact impedance imbalance between

ECG electrodes is not verified, or is fixed. Impedances which are not purely resistive or homogeneous can alter the phase relationship between voltage and current, adding a delay variable with frequency; this may affect the limb leads which are measured across different portions of the torso that change in shape with respiration and body posture. Altered phase relationships may also affect raw limbs' potential to form the WCT. Because RA, LA, and LL potentials are first measured as voltage potential difference between the reference point (RL) and the other limbs' electrodes, different body impedances and contact impedances may impose different delays upon the signals, thus affecting the final WCT shape in an unpredictable manner [3,17].

## 2.2. Study Hypothesis: On the Equilateral Triangle Hypothesis

If the three cardinal leads are indeed on a plane and form a triangle (even if not equilateral), in order to obtain a WCT which is at least at the centroid of the triangle (center coincide with centroid only in equilateral triangles), the three cardinal limbs need to satisfy the basic condition of a triangle. This is because, under the original Einthoven/Wilson assumption, the equivalent electrical activity of the heart is entirely projected into the geometrical plane identified by the limbs [1,4,36]. In other words, the ECG values need to satisfy the so-called triangular inequality which states that the sum of any two of the three lengths that are candidates for the triangle must be greater than the third. If this is satisfied, it is then possible to calculate the inner angles.

In order to prove this hypothesis with a computationally efficient method, we assumed that at every point of the cardiac cycle, the three cardinal leads form a triangle, and we calculated the area using Heron's formula:

$$\text{Area} = \sqrt{p(p-a)(p-b)(p-c)} \quad (1)$$

where  $a$ ,  $b$  and  $c$  are the three measurements of the sides and  $p$  indicates half of the perimeter:

$$p = \frac{a+b+c}{2} \quad (2)$$

Obviously, if  $a$ ,  $b$ , and  $c$  do not form a triangle, the area calculated using (1) is either null or a complex number. We proceeded to calculate the inner angles only for those terns of points constituting a triangle or, in other words, where (1) gives a positive result. To our calculation script, we passed the cardinal leads following their cardinal order (I, II and III), and received the calculated angles with the following order: 'opposed to lead I', 'opposed to lead II', and 'opposed to lead III'.

Because the ECG has some brief iso-potential segments (i.e., following the p-wave), we expected some percentage of points within each cardiac cycle where (1) is not satisfied (i.e., the same iso-potential value for all three leads), as well as some iso-potential segments between beats. While there is nothing that we can do to remove the iso-potential segment between ECG characteristic waveforms, we can remove the one between beats, limiting the calculation to one single cardiac cycle. According to the existing literature, flat iso-potential segments between characteristic waveforms can account for up to 40% of the length of a single beat [1]. Therefore, it would be normal to find (1) satisfied only in roughly 60% of the points for each cardiac cycle. Namely, we expect (1) to have a solution only during the QRS, p-wave, and T-wave. Furthermore, because noise, particularly baseline drift/wandering, could alter the ECG, we removed such noise using a zero phase lag non-causal filter with a cut-off frequency at 0.6 Hz. To minimize the effect of artifacts and power-line noise, the signals are also filtered using an array of zero phase lag non-causal notch filters at power-line and harmonics frequencies, together with a low pass filter at 149 Hz. For each of the 599 recordings, a single beat was selected manually from the cleaned signal. We attempted to select a beat with the following characteristics:

High signal-to-noise ratio: no muscles/movements artifacts

Avoid pacemaker where possible

Avoid multiple p-waves in case of atrial flutter

Avoid ectopic where possible.



Once the selected beat is isolated, Equation (1) is applied to each term of points corresponding to each of the signal samples. The percentage of points where (1) is satisfied, together with the length of each beat, is stored in a separate variable, and the inner angles are calculated only where (1) is satisfied (non-null real value).

### 2.3. A Brief Summary of the Hardware Used

Full details of the hardware we used to record the data can be found in our previous publications. In particular, the general description of the true unipolar recording channel can be found in [2]. We want to highlight that our hardware can also record true unipolar precordials (see Figure 3). In other words, similar to what we have done to record the WCT components, we record and store the voltage potential of each of the precordial electrodes as directly referred to the RL. This allows us to calculate new precordials, i.e., to subtract in the post-process a reference potential different from the WCT. Coherence between the true unipolar leads and 12-lead ECGs is ensured by the extremely high correlation between the recorded 12-lead signal and the calculated 12-lead signal. In other words, using lead I as an example, we ensured that:

$$\text{Correlation}([RA - LA], I_{12\text{lead}}) > 98\%$$

As shown in the block diagram of Figure 3, each exploring electrode is connected to the non-inverting input of one instrumentation amplifier. For our design we selected the INA116 by Texas Instruments. This peculiar amplifier includes a special buffer for each input (see the dashed rectangles around each electrode connection in Figure 3) that allows direct measurement of the electrode potential, signal duplication [2], as well as input shielding [2,30].

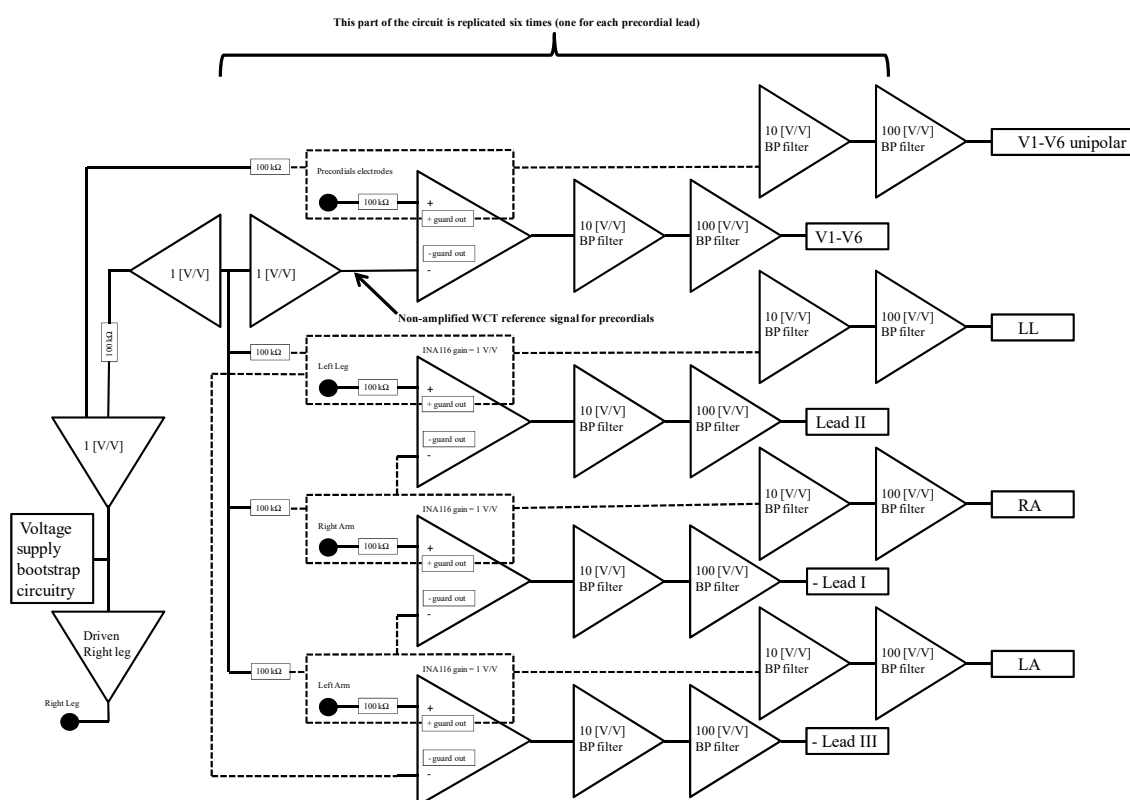


Figure 3. Block diagram of the employed hardware (adapted from [2]).

The signal supplication feature is directly employed for the limb electrodes to create direct limb leads. For instance, as it is possibly to infer from Figure 3, once duplicated by the buffer inside the INA11,6 the Left-Leg electrode signal is connected to the last instrumentation amplifier on the diagram to create Lead III. In this way, due to our design choice of connecting electrodes only to non-inverting inputs, some leads (i.e., Limb III) output negative values. The negative leads are multiplied by  $-1$  by the recording software [2]. The complete circuit uses a voltage supply bootstrap and a Driven Right-Leg circuitry (calibrated to contain leakage current below  $100 \mu\text{A}$ ) to minimize noise pick-up and increase the signal to noise ratio [2,4,32].

### 3. Results

As expected, Equation (1), when applied to a single beat for all 599 datasets, produced correct results only for a fraction of the points. In Figure 4, we present the detailed histograms of the distribution of the percentage of points within each beat that satisfy (1). For this measurement we accepted (considered satisfied) any small positive result obtained by application of (1); in other words, we compared directly with zero. In Figure 4a, we depict the general histogram for all 599 datasets; histograms for the PTB dataset alone, and for fifty recordings constituting our Dataset 2, are shown in Figure 4b,c respectively. The averages where (1) is satisfied are 49% (STD = 12) for the total, 49% (STD = 11) for the PTB database and 46% (STD = 15) for Dataset 2 (values rounded to the nearest integer, interpolations with normal distribution have been implemented using the statistical fitting tool included with Matlab<sup>®</sup>). As can be inferred from the histograms, for the majority of the datasets, the percentage of points where (1) is satisfied is below 50%, which is below what should be expected ( $\sim 60\%$ ) from the theory.

For this reason, we restricted our investigation to the QRS only, where there are no iso-electric segments. From the application of Equation (1) to the QRS only (see Figure 4 panels d to e), we found that, similar to what we observed for the full beat, Equation (1) is satisfied on average for only 48% of the points composing the QRSs with even larger standard deviations. In detail, the averages where (1) is satisfied are 48% (STD = 22) for the total, 48% (STD = 21) for the PTB database, and 47% (STD = 26) for our study.

When we looked at the inner angles, although their values (in average) are quite close to the theoretical value of 60 deg, particularly for the QRS (see Table 1), the standard deviations are very high. Full histograms of the inner angles for the full beat, and one single QRS, are depicted in Figure 5; as it is possible to infer from the histograms, the distributions of the bins are very wide, with many bins with similar height.

An example of how the points where Equation (1) is satisfied distribute in one single cardiac cycle is given in Figure 6. In Figure 6, the points within the cardiac cycle where the absolute value of the three leads do not form a triangle have been “zeroed”; as it is possible to observe from the figure, these sections also affect the QRS region. These seem to be due to a specificity of the patient, and do not vary much in different recordings of the same patient; please compare Figure 6, panel b with the panel belonging to the same PTB database patient recorded on different days. One might also observe that the inner angles of the triangle vary a lot during the cardiac cycle and the QRS (please compare bottom traces of the Figure 6 panels). This suggests that the triangle, when closed, changes shape during the cardiac cycle, and in some cases, it can become quite “open”, with one of the angles exceeding 100 deg. Once again, as it is possible to see from Table 2, there is a lot of variability around the mean for the inner angles.

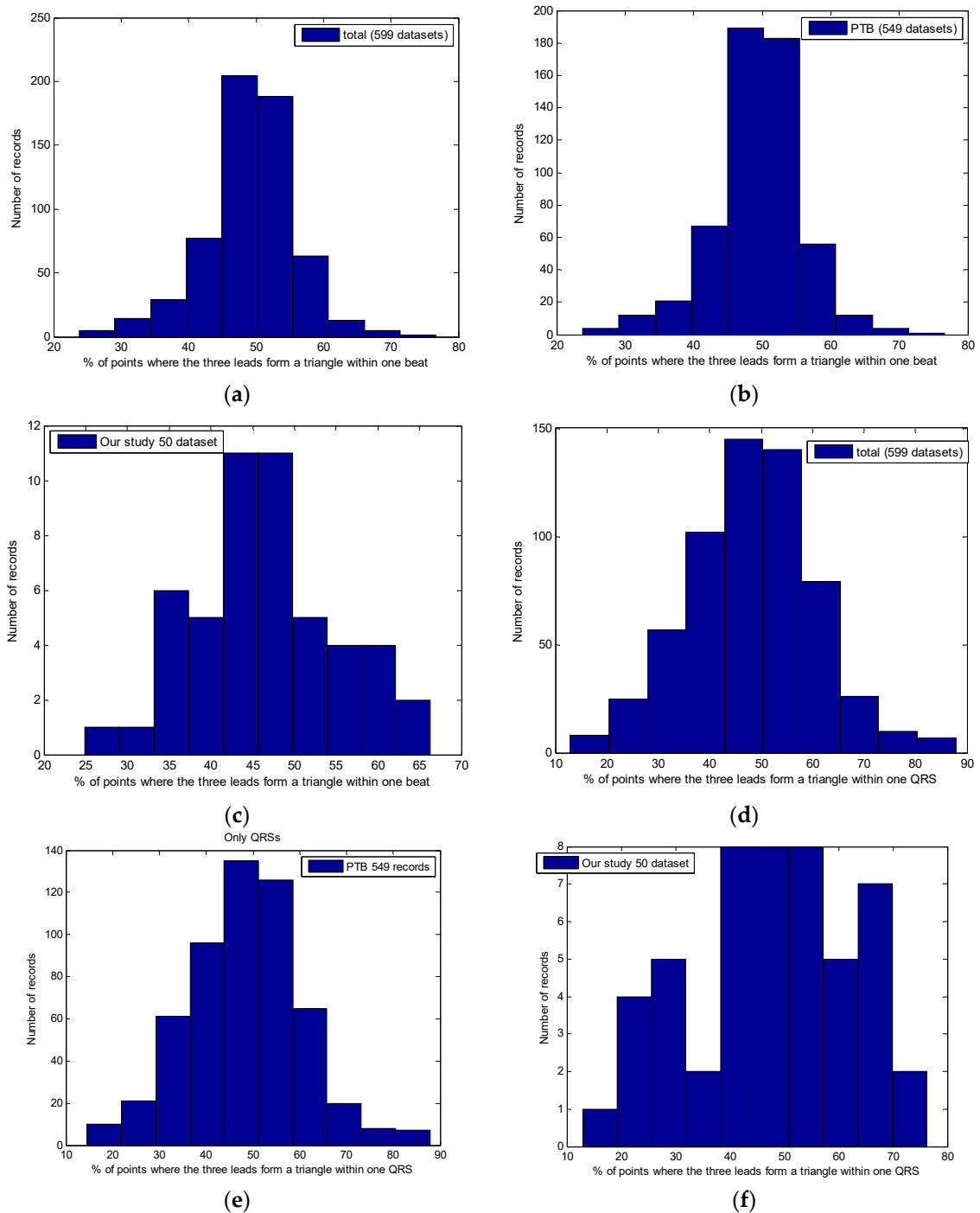


**Figure 4.** Percentage of points where Equation (1) is satisfied within one beat (panels a to c) and one QRS (panels d to e): (a) total, mean 49%; (b) PTB database, mean 49%; (c) our study only, mean 46%; (d) total, mean 48%; (e) PTB database, mean 48%; (f) our study only, mean 47%.

**Table 1.** Summary of inner angles.

Angle	Opposed to Lead I [deg]		Opposed to Lead II [deg]		Opposed to Lead III [deg]	
	Mean	STD	Mean	STD	Mean	STD
One beat	59	31	70	36	51	30
One QRS	64	40	66	41	50	37

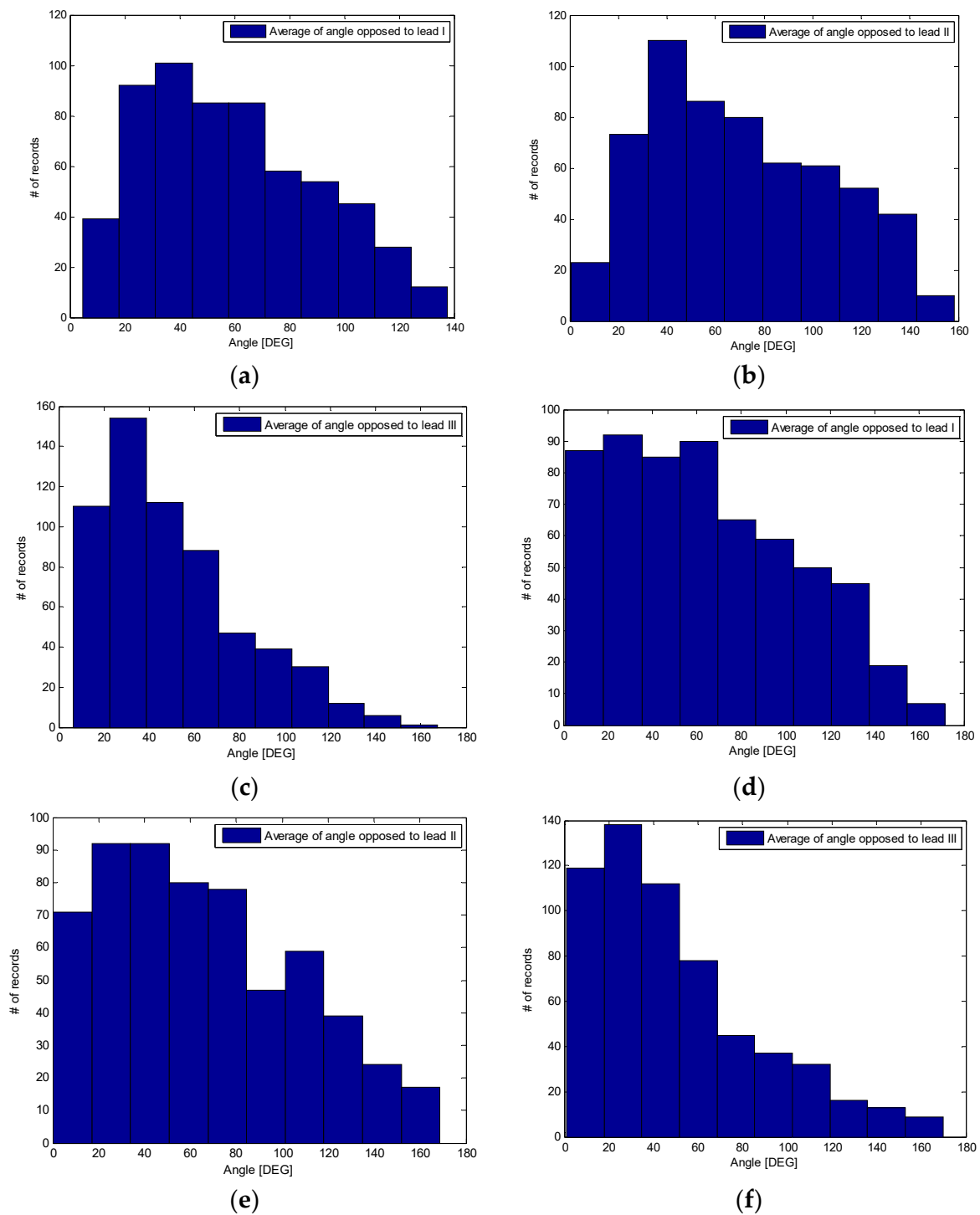
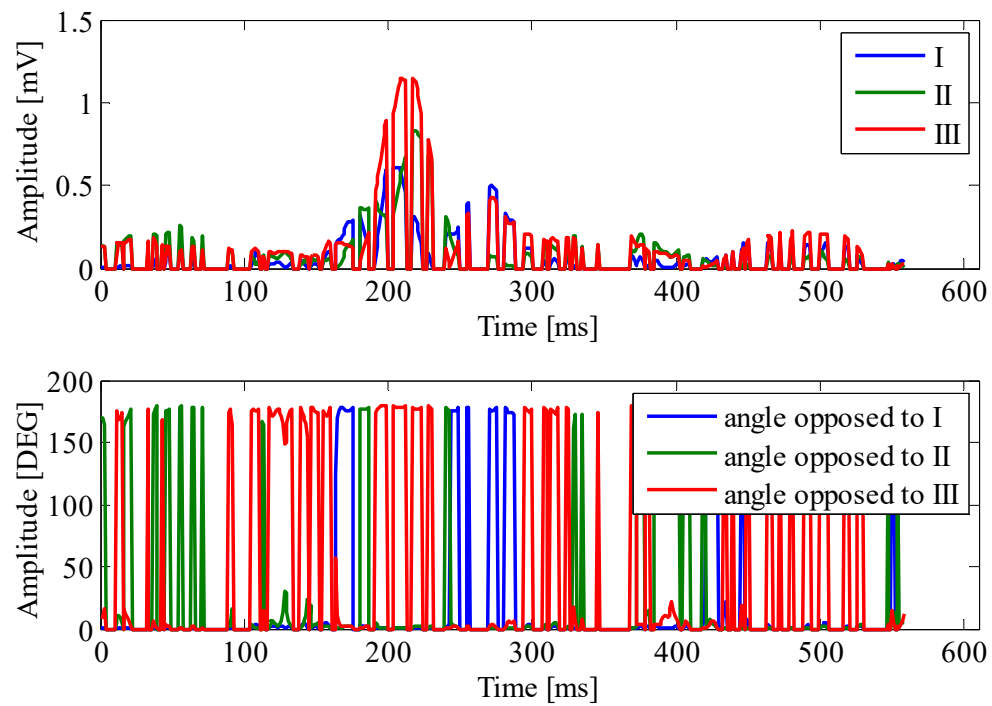
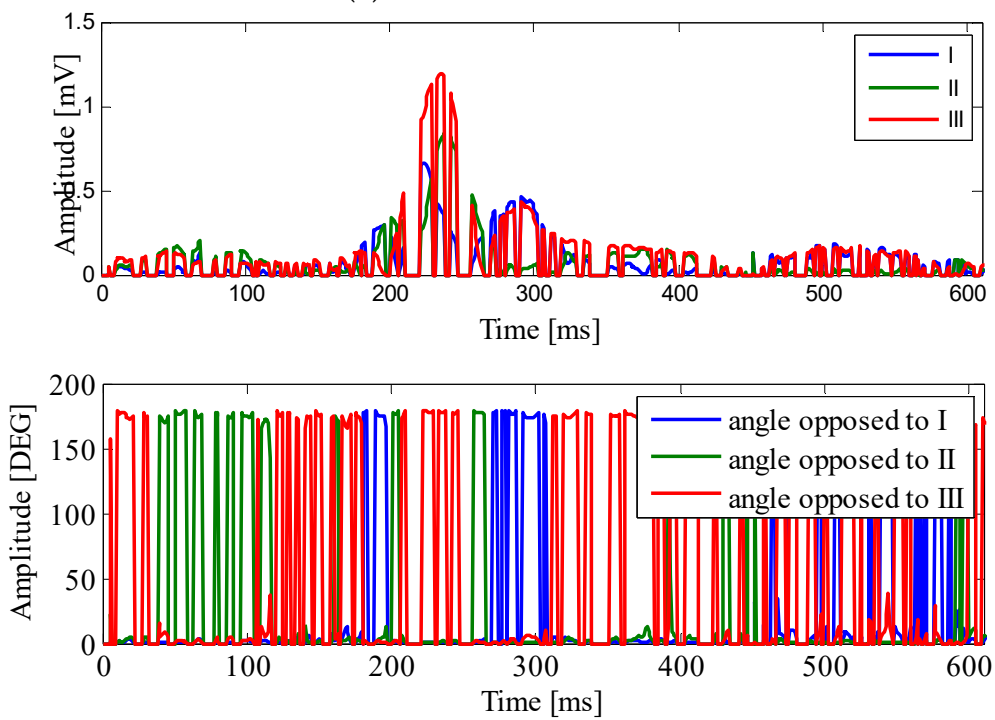


**Figure 5.** Angle opposed to cardinal leads where Equation (1) is satisfied within one beat (panels a to c) and within one QRS (panels d to f): (a) opposed to lead I, mean 59 deg; (b) opposed to lead II, mean 70 deg; (c) opposed to lead III, 51 deg; (d) opposed to lead I, mean 64 deg; (e) opposed to lead II, mean 66 deg; (f) opposed to lead III, mean 50 deg.

The amplitude of WCT relative to lead II has been measured for this study too. On average, the WCT amplitude is 78% of lead II, with a standard deviation of 42%. These results are discussed further in the following section.



(a) Patient001/s0041re



(b) Patient001/s00161re

**Figure 6.** Patient001 recordings on different days. In each panel top: ABS of leads I, II, and III only plotted at the point where Equation (1) gives a non-null real result; Bottom: inner triangle angles plotted only where Equation (1) gives a non-null real result (see text).

**Table 2.** Summary of WCT and cardinal leads measurements (see text).

Patient Record Number	Lead II Amplitude [mV]	Lead I Amplitude as % of Lead II	Lead III Amplitude as % of Lead II	WCT Amplitude as % of Lead II	Age [years]	Gender
1	1.02	118	152	117	70	F
2	0.48	333	283	95	53	M
3	1.55	87	82	77	80	M
4	0.52	240	285	174	85	M
5	1.19	126	43	45	69	F
6	0.83	105	113	52	78	M
7	0.46	199	235	120	73	M
8	0.94	160	121	57	55	F
9	0.20	202	176	114	52	F
10	0.88	158	170	60	70	F
11	1.12	57	115	82	79	M
12	0.58	217	125	56	51	F
13	0.30	123	88	45	52	M
14	1.28	71	46	59	88	F
15	0.77	176	100	30	68	F
16	0.45	222	153	101	49	M
17	0.78	180	122	60	67	M
18	0.70	246	170	206	60	F
19	0.99	105	21	24	54	F
20	0.86	104	32	29	58	M
21	1.13	78	134	63	56	M
22	0.42	136	111	53	70	M
23	1.35	107	78	42	55	F
24	1.18	134	97	38	76	F
25	0.65	81	46	37	74	F
26	0.60	331	385	151	53	M
27	0.87	126	67	26	48	M
28	0.86	177	168	74	57	M
29	0.67	300	267	88	44	M
30	1.81	41	90	56	59	M
31	0.62	144	67	21	84	F
32	0.92	76	133	70	70	M
33	0.66	287	256	79	58	M
34	0.92	141	168	91	51	M
35	0.55	98	193	110	66	F
36	0.41	108	127	117	96	M
37	0.57	170	108	82	53	M
38	0.55	130	159	80	59	M
39	1.06	55	56	50	61	M
40	0.38	136	62	64	68	F
41	0.70	193	106	58	52	F
42	0.92	115	88	49	61	M
43	0.30	115	126	144	70	M
44	1.29	65	55	52	53	F
45	0.32	194	226	173	69	M
46	0.68	299	221	73	47	M
47	0.92	62	150	107	82	F
48	0.61	107	66	33	71	F
49	1.60	24	106	60	73	M
50	0.67	137	120	147	77	M
<b>Means</b>	0.80	148	133	78	64.48	
<b>STDs</b>	0.36	75	75	42	12.19	

M = 60%

#### 4. Discussion

The small percentage of points where Heron's formula is satisfied (Equation (1)) suggests that the voltage potential of the CT can actually exceed the cardinal leads in the module, as this point may be located external to the triangle, and may even be outside the geometrical plane identified by the limb electrodes. This may explain why we found peak-to-peak amplitudes for the WCT larger than

those reported in the literature in our previous study [2,6]. For this work, in light of our findings, we re-evaluated the peak-to-peak amplitude of the WCT (we also added several patients to our database). However, this time, we measured the amplitude of the WCT at its largest feature and in one beat only, i.e., the one used for the triangle evaluation. The full summary of our measurements is reported in Table 2, and as can be inferred from the table, for a few patients the WCT amplitude is almost double that of lead II.

Since the introduction of the 12-lead ECG into medical practice, practitioners have learned how to interpret the signals and make diagnoses based on the results of WCT. For this reason, it is extremely difficult to formulate study hypotheses that, while backed up by a suitable statistical body of evidence, can unveil the extent of the implications that the use of a signal this large (and laying on a different geometrical plane) as a reference for precordials has on the practice. However, as it is possible to observe in Figure 7, the WCT influences the precordials. For instance, in this case, while the QRS complex results are slightly larger in the lead V2 (see peak to peak amplitude of dashed bold black trace versus thin black trace) when WCT is subtracted from the v2 electrode, one can easily see that the P-wave is greatly affected (almost erased from the lead V2). Suppression of waveforms, as well as waveform alteration, can have severe implications for the diagnosis of cardiac diseases. For instance, as it is possible to observe from Figure 7, the ST segment is also affected by the WCT, which superimpose a ST depression to V2. ST segment alterations are normally linked to cardiac ischemia or other myocardium illnesses [36]. For this reason, we are still collecting data with our device in a hospital setting, in order to carefully assess the relationship between WCT and cardiac diseases.

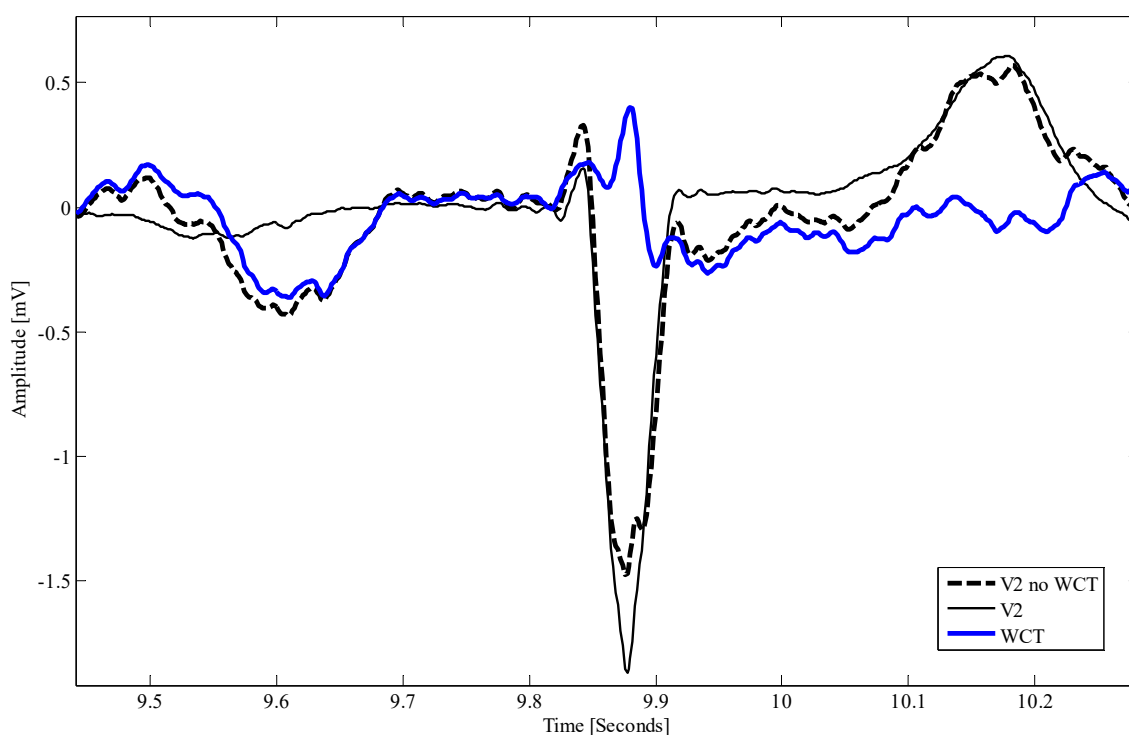


**Figure 7.** Direct comparison among lead V2 (12-lead ECG), V2 recorded without WCT (bold dashed trace) and WCT (blue bold trace).

## 5. Conclusions

We presented a critical study of the triangular model of the ECG. Although we now have to carefully assess the clinical relevance of our findings, we particularly need to build a solid database of recordings where diagnoses are evaluated by comparing standard 12-lead ECG precordials and precordials obtained using the new personalized CT. We conclude that the WCT introduced for current

recordings, due to its large amplitude (sometimes larger than cardinal leads), should not be used as a reference for precordials. Furthermore, our study assessment, based upon a simple method to evaluate when three lengths form a triangle, shows that voltage measurements of cardinal leads fail to form a triangle for the largest part of the duration of a single cardiac cycle, even when calculation is restricted to the QRS complex only, suggesting that the so called ‘Central Terminal’ may actually be outside the geometrical plane identified by the cardinal leads.

**Author Contributions:** Author G.G. conceptualized this study and invented the “true unipolar” device described in this study and in some of the referred works. Authors H.M., I.S. and A.O.L. performed data recording in hospital. All the authors contributed to the data analysis and to the writing of the text. Authors I.S., A.O.L. and A.T. gave also clinical advice.

**Funding:** This study is supported by the office for Research Engagement and Development with Industry (REDI) at the Western Sydney University and by the MARCS Institute (Biomedical Engineering and Neuro-Science BENS group).

**Acknowledgments:** The authors wish to thank the patients at Campbelltown Hospital (Campbelltown, NSW, Australia) who volunteered for this study, and the hospital staff who supported and helped with the data collection, particularly the nurses of the Coronary Care Unit. The authors also gratefully acknowledge Texas Instruments, who supplied chip samples for the construction of the prototype.

**Conflicts of Interest:** Authors declare that they have no conflict of interests.

## References

- Malmivuo, J.; Plonsey, R. *Bioelectromagnetism—Principles and Applications of Bioelectric and Biomagnetic Fields*; Oxford University Press: Oxford, UK, 1995.
- Gargiulo, G.D.; Bifulco, P.; Cesarelli, M.; McEwan, A.L.; Moenizadeh, H.; O’Loughlin, A.; Shugman, I.M.; Tapson, J.C.; Thiagalingam, A. On the “Zero of potential of the electric field produced by the heart beat”. A machine capable of estimating this underlying persistent error in electrocardiography. *Machines* **2016**, *4*, 18. [[CrossRef](#)]
- Gargiulo, G.D.; Varaki, E.S.; Hamilton, T.J.; Bifulco, P.; Cesarelli, M.; Romano, M. A 9-independent-leads ECG system from 10 electrodes: A practice preserving WCT-less true unipolar ECG system. In Proceedings of the Biomedical Circuits and Systems Conference (BioCAS), Atlanta, GA, USA, 22–24 October 2015.
- Webster, J.G. (Ed.) *Medical Instrumentation Application and Design*; John Wiley: Hoboken, NJ, USA, 2009.
- Goldberger, A.L.; Amaral, L.A.; Glass, L.; Hausdorff, J.M.; Ivanov, P.C.; Mark, R.G.; Mietus, J.E.; Moody, G.B.; Peng, C.K.; Stanley, H.E. PhysioBank, PhysioToolkit, and PhysioNet: Components of a new research resource for complex physiologic signals. *Circulation* **2000**, *101*, e215–e220. [[CrossRef](#)] [[PubMed](#)]
- Gargiulo, G.; Bifulco, P.; Cesarelli, M.; McEwan, A.; O’Loughlin, A.J.; Tapson, J.C.; Thiagalingam, A. The Wilson’s Central Terminal (WCT): A Systematic error in ECG recordings. *Heart Lung Circ.* **2016**, *25*, S263. [[CrossRef](#)]
- Bousseljot, R.; Kreiseler, D.; Schnabel, A. Nutzung der EKG-Signaldatenbank CARDIODAT der PTB über das internet. *Biomed. Tech.* **1995**, *40*, S319. [[CrossRef](#)]
- Frank, E. General theory of heart-vector projection. *Circ. Res.* **1954**, *2*, 258–270. [[CrossRef](#)] [[PubMed](#)]
- Frank, E.; Kay, C.F. The construction of mean spatial vectors from null contours. *Circulation* **1954**, *9*, 555–562. [[CrossRef](#)] [[PubMed](#)]
- Dower, G.E.; Osborne, J.A.; Moore, A. Measurement of the error in Wilson’s central terminal: An accurate definition of unipolar leads. *Br. Heart J.* **1959**, *21*, 352–360. [[CrossRef](#)] [[PubMed](#)]
- Miyamoto, N.; Shimizu, Y.; Nishiyama, G.; Mashima, S.; Okamoto, Y. The absolute voltage and the lead vector of Wilson’s central terminal. *Jpn. Heart J.* **1996**, *37*, 203–214. [[CrossRef](#)] [[PubMed](#)]
- Bacharova, L.; Selvester, R.H.; Engblom, H.; Wganer, H.S. Where is the central terminal located? In search of understanding the use of the Wilson central terminal for production of 9 of the standard 12 electrocardiogram leads. *J. Electrocardiol.* **2005**, *38*, 119–127. [[CrossRef](#)] [[PubMed](#)]
- Madias, J.E. On recording the unipolar ECG limb leads via the Wilson’s vs. the Goldberger’s terminals: AVR, aVL, and aVF Revisited. *Indian Pacing Electrophysiol. J.* **2008**, *8*, 292–297. [[PubMed](#)]



14. Miyamoto, N.; Shimizu, Y.; Nishiyama, G.; Mashima, S.; Okamoto, Y. On the potential of the Wilson central terminal with respect to an ideal reference for unipolar electrocardiography. *J. Electrocardiol.* **1995**, *28*, 336–337. [[CrossRef](#)]
15. Bayley, R.H.; Schmidt, A.E. The problem of adjusting the Wilson central terminal to a zero of potential in the living human subject. *Circ. Res.* **1955**, *3*, 94–102. [[CrossRef](#)] [[PubMed](#)]
16. Burger, H.C. The zero of potential: A persistent error. *Am. Heart J.* **1955**, *49*, 581–586. [[CrossRef](#)]
17. Gargiulo, G.D. True unipolar ECG machine for Wilson central terminal measurements. *BioMed Res. Int.* **2015**, *2015*, 7. [[CrossRef](#)] [[PubMed](#)]
18. Gargiulo, G.D.; Tapson, J.; van Schaik, A.; McEwan, A.; Thiagalingam, A. Unipolar ECG circuits: Towards more precise cardiac event identification. In Proceedings of the 2013 IEEE International Symposium on Circuits and Systems (ISCAS2013), Beijing, China, 19–23 May 2013; pp. 662–665.
19. Gargiulo, G.D.; McEwan, A.; Bifulco, P.; Cesarelli, M.; Jin, C.; Tapson, J.; Thiagalingam, A.; van Schaik, A. Towards true unipolar bio-potential recording: A preliminary result for ECG. *Physiol. Meas.* **2013**, *34*. [[CrossRef](#)] [[PubMed](#)]
20. Gargiulo, G.; Thiagalingam, A.; McEwan, A.; Cesarelli, M.; Bifulco, P.; Tapson, J.; van Schaik, A. True unipolar ECG leads recording (without the use of WCT). *Heart Lung Circ.* **2013**, *22*, s102. [[CrossRef](#)]
21. Gargiulo, G.D.; McEwan, A.L.; Bifulco, P.; Cesarelli, M.; Jin, C.; Tapson, J.; Thiagalingam, A.; van Schaik, A. Towards true unipolar ECG recording without the Wilson central terminal (Preliminary results). *Physiol. Meas.* **2013**, *34*, 991–1012. [[CrossRef](#)] [[PubMed](#)]
22. Wilson, F.N.; Johnston, F.D.; Rosenbaum, F.F.; Barker, P.S. On Einthoven's triangle, the theory of unipolar electrocardiographic leads and the interpretation of the precordial electrocardiogram. *Am. Heart J.* **1946**, *32*, 277–310. [[CrossRef](#)]
23. De Medina MD, E.O.R.; Peteers MD, H.A.P.; Wittkampf, F.H.M. F.N. Wilson: The unipolar electrocardiogram. *ACC Curr. J. Rev.* **2000**, *9*, 4.
24. Burger, H.C.; van Milaan, J.B. Heart-vector and leads. *Br. Heart J.* **1946**, *8*, 157–161. [[CrossRef](#)] [[PubMed](#)]
25. Burger, H.C.; van Milaan, J.B. Heart-vector and leads Part II. *Br. Heart J.* **1947**, *9*, 154–160. [[CrossRef](#)] [[PubMed](#)]
26. Burger, H.C.; van Milaan, J.B. Heart-vector and leads Part III Geometrical representation. *Br. Heart J.* **1948**, *10*, 229–233. [[CrossRef](#)] [[PubMed](#)]
27. Bayley, R.H.; Kinard, C.L. The zero of potential of the electric field produced by the heart beat: The problem with reference to living human subject. *Circ. Res.* **1954**, *2*, 104–111. [[CrossRef](#)] [[PubMed](#)]
28. Bayley, R.H.; Reynolds, E.W.; Kinard, C.L.; Head, J.F. The zero of potential of the electric field produced by the heart beat: The problem with reference to homogeneous volume conductors. *Circ. Res.* **1954**, *2*, 4–13. [[CrossRef](#)] [[PubMed](#)]
29. Tyner, F.S.; Knott, J.R.; Mayer, W.B. *Fundamentals of EEG Technology*; Lippincott Williams & Wilkins: Philadelphia, PA, USA, 1983.
30. Horowitz, P.; Hill, W. *The Art of Electronics*; PediaPress: Cambridge, UK, 2002.
31. Byes, W. (Ed.) *Instrumentation Reference Book*; CRC Press: Boca Raton, FL, USA, 2002.
32. Winter, B.B.; Webster, J.G. Reduction of interference due to common mode voltage in biopotential amplifiers. *IEEE Trans. Biomed. Eng.* **1983**, *BME-30*, 58–62. [[CrossRef](#)]
33. Hwang, I.-D.; Webster, J.G. Direct interference canceling for two-electrode biopotential amplifier. *IEEE Trans. Biomed. Eng.* **2008**, *55*, 2620–2627. [[CrossRef](#)] [[PubMed](#)]
34. Gargiulo, G.; Calvo, R.; Jin, C. Giga-ohm high-impedance FET input amplifiers for dry electrode biosensor circuits and systems. In *Integrated Microsystems Electronics; Photonics, and Biotechnology*; Iniewski, K., Ed.; CRC Press: Boca Raton, FL, USA, 2011.
35. Gargiulo, G.D.; Bifulco, P.; Cesarelli, M.; Fratini, A.; Romano, M. Problems in assessment of novel biopotential front-end with dry electrode: A brief review. *Machines* **2014**, *2*, 87–98. [[CrossRef](#)]
36. Lilly, L.S.; Braunwald, E. *Braunwald's Heart Disease: A Textbook of Cardiovascular Medicine*; Elsevier: New York, NY, USA, 2012; p. 2048.



0638

### Minimize Wilson Central Terminal Using Genetic Algorithm



H. Moeinzadeh<sup>1,\*</sup>, G. Gargiulo<sup>1,2</sup>, P. Bifulco<sup>2</sup>, M. Cesarelli<sup>2</sup>, A. O'Loughlin<sup>3</sup>, M.I. Shugman<sup>4</sup>, A. Thiagalingam<sup>5,6,7</sup>

<sup>1</sup> *Marcus Institute for Brain, Behaviour & Development, Western Sydney University, Penrith, Australia*

<sup>2</sup> *Department of Electrical Engineering and Information Technology (DIETI), 'Federico II' The University of Naples, Italy*

<sup>3</sup> *School of Medicine, Western Sydney University, Sydney, Australia*

<sup>4</sup> *Cardiology Department, Campbelltown Hospital, Sydney, Australia*

<sup>5</sup> *School of Medicine, The University of Sydney, Sydney, Australia*

<sup>6</sup> *Cardiology Department, Westmead Hospital, Sydney, Australia*

<sup>7</sup> *Westmead Institute for Medical Research, NSW, Sydney, Australia*

We recently developed 15-lead ECG device that can record the voltage of the right arm ( $\Phi_R$ ), left arm ( $\Phi_L$ ), and left leg ( $\Phi_F$ ) aside 12-lead ECG. This device allows us to compute the Wilson Central Terminal (WCT) trace for the first time after Bayley and Kinard in 1954.

Since minimisation of the WCT will improve the signal to noise ratio of electrocardiograms with ubiquitous potential clinical applications, we developed a software approach to minimize the amplitude of WCT according to the following main criteria: (1) less variation than WCT during a cardiac cycle; (2) to be possibly zero or near zero; (3) M-WCT amplitude should be less than 0.1 mV to be considered clinically irrelevant. In this approach, we used Genetic Algorithm to find three weights ( $\alpha$ ,  $\beta$ , and  $\delta$ ) with the constraints of ( $0 < \alpha, \beta, \delta < 1$ , and  $\alpha + \beta + \delta = 1$ ) to minimize WCT, to which we referred as "Minimized Wilson Central Terminal" (M-WCT).

$$M\text{-WCT} = \alpha\Phi_L + \beta\Phi_F + \delta\Phi_R$$

Our results, tested on the data recorded from 72 patients confirmed that M-WCT better characterizes the ideal reference potential in terms of amplitude and variation during the cardiac cycle compared to WCT. Specifically, for our population, the WCT presents average peak to peak ampli-

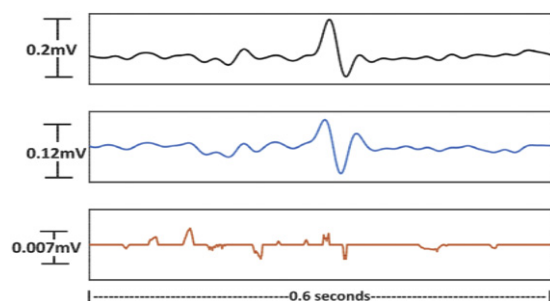


**Figure 1.** Comparison of M-WCT (bottom) with WCT (middle), and Lead II (top).

tude relative to Lead II of 58.85% with an averaged standard deviation of 30.84%, while the M-WCT amplitude is as small as 7.45% of lead II with an averaged standard deviation of 9.04% (Figure 1).

<http://dx.doi.org/10.1016/j.hlc.2018.06.639>

0639

### Mitral Valve Prolapse and Cardiac Arrest: Defining Malignant Mitral Valve Prolapse Syndrome



H. Han<sup>1,2</sup>, F. Ha<sup>1</sup>, A. Teh<sup>1,2</sup>, D. O'Donnell<sup>1,\*</sup>, D. Hare<sup>1,2</sup>, O. Farouque<sup>1,2</sup>, H. Lim<sup>1,2</sup>

<sup>1</sup> *Austin Health, Melbourne, Australia*

<sup>2</sup> *University of Melbourne, Melbourne, Australia*

**Background:** In an attempt to better understand malignant mitral valve prolapse (MVP) syndrome, this study aimed to comprehensively evaluate the scientific literature in relation to case reports and series of MVP and cardiac arrest.

**Method:** A literature search of PubMed and Embase was conducted using Preferred Reporting Items for Systematic Reviews and Meta-Analyses guidelines. Included articles were any cases of MVP with sudden death, or MVP with survived cardiac arrest and documented rhythm reported in English.

**Results:** There were 106 studies describing 149 cases. Median age was 31 years and 68% of cases were female. A total of 53% experienced palpitations and 33% had a history of syncope. Cardiac arrest occurred during routine activities in 45% of cases, and 22% were exertion related. T-wave inversion in the inferior leads were described in 20% of cases. On electrocardiogram, 51% had premature ventricular complexes (PVCs), and 91% had PVCs, couplets or non-sustained ventricular tachycardia (VT) on Holter monitoring. Cardiac rhythms at the time of cardiac arrest were ventricular fibrillation (81%), VT (12%), torsade de-pointes (4%), and asystole (3%). Leaflet involvement was predominantly bileaflet (73%) or posterior leaflet (26%), and 55% had mild mitral regurgitation (MR) or less.

**Conclusion:** This systematic review indicates that malignant MVP syndrome predominantly affected females with a median age of 31 years. The mitral valve was myxomatous with bileaflet prolapse and variable degrees of MR. There was a high incidence of PVCs on Holter monitoring, and cardiac arrest usually occurred as a result of ventricular arrhythmias.

<http://dx.doi.org/10.1016/j.hlc.2018.06.640>

# *Unipolar cardiac leads between history and science*

Hossein Moeinzadeh<sup>1</sup>, Joseph Assad, Paolo Bifulco, Mario Cesarelli, Alistair L. McEwan, Aiden O'Loughlin, Ibrahim M. Shugman, Jonathan C. Tapson, Aravinda Thiagalingam and Gaetano D. Gargiulo

## **Abstract**

The surface electrocardiography (ECG) uses a virtual reference point to measure the potential of chest electrodes. This reference potential is known as *Wilson central terminal (WCT)* and is assumed negligible (near zero) in amplitude. Consequently, the precordial leads have been named as the *unipolar leads*. Although this assumption was found incorrect immediately after this reference potential was introduced, it was difficult to measure its real amplitude. We recently introduced a 15-lead electrocardiography device that can record the traditional ECG leads in combination to the raw potential of limbs and chest electrodes directly referred to the circuit grounding. Consequently, we are able to record the potential of the raw chest electrodes which we named as *true unipolar chest leads*. The aim of this study is to have a clear understanding of the WCT potential and its influence on the chest leads. Our records show that the true unipolar leads may be more sensitive for detecting cardiac diseases in the left anterior descending coronary artery in patients with non-ST elevation reported on chest leads.

**Keywords:** Electrocardiography, Wilson Central Terminal, Unipolar leads, Limb Potential, Left Anterior Descending, Electrocardiography Database

## **Introduction**

The heart impresses an electrical current that flows from the heart through the limbs, which can be used for examining the cardiac function (Webster 1978; Macfarlane et al. 2010). First Waller used two electrodes on the body and found changes in electrometer by heartbeat (Waller 1887; Malmivuo & Plonsey 1995). He applied electrodes on limbs to show the electrical activity of the heart. However, Einthoven made a major breakthrough in Electrocardiography by using the string galvanometer in 1901 (Malmivuo & Plonsey 1995). He used a silver-coated quartz filament (or string) in a strong magnetic field to measure the strength and direction of the *current* of the heart (Fye 1994). The string was moved in the magnetic field when the current of the heart moved through it (Fye 1994). The Einthoven's device was very bulky and far from the hospital, hence, he used the telephone wire to receive the patients' heart impulse from the hospital (Fye 1994; Macfarlane et al. 2010). Later, Einthoven introduced the mathematics relations between three limb leads, which has been known as *Einthoven Triangle* hypothesis

---

<sup>1</sup> MARCS institute for brain, behavior,

Western Sydney University

Sydney, Australia

e-mail: h.moeinzadeh@westernsydney.edu.au

(Einthoven et al. 1913). The vertices of the Einthoven Triangle are electrodes placed on the right hand, left hand, and left leg which are used to measure the limb leads, known as the lead I, lead II and lead III (Einthoven et al. 1913; Malmivuo & Plonsey 1995). In this theory, the human body is characterized as a two dimensional, homogeneous conductor, and part of infinity with the heart located in the centroid of the triangle (Macfarlane et al. 2010; Malmivuo & Plonsey 1995).

$$\begin{aligned}\text{Lead I} &= \Phi_L - \Phi_R \\ \text{Lead II} &= \Phi_F - \Phi_R \\ \text{Lead III} &= \Phi_F - \Phi_L\end{aligned}\tag{1}$$

As the three limb leads construct a closed loop (Figure 1), the Kirchoff's voltage law can show the relation between the limbs (Eq. 2) (Macfarlane et al. 2010).

$$I + III = II\tag{2}$$

Although some researchers suggested a different system to record the heart activity (Anon 1925; Waller 1887; Macfarlane et al. 2010), only the Einthoven limb leads had clinically used for three decades (Kossmann 1985; Fye 1994; Macfarlane et al. 2010). Wilson highlighted the fact that the limb electrodes are far from the heart, and introduced the *unipolar lead* concept (Wilson et al. 1946; Fye 1994; Kossmann 1985; Wilson et al. 1934). In *Wilson hypothesis*, the electrical activity of the heart can be measured by the potential difference between six exploring electrodes on the chest and an *indifferent electrode* of zero potential, which is known as Wilson Central Terminal (WCT) (Wilson et al. 1934). These six leads are designated as unipolar precordial leads (V1:V6) as he assumed the WCT amplitude is equal to zero (Wilson et al. 1934; Macfarlane et al. 2010). The Wilson Central Terminal is measured by the average potential of the right arm ( $\Phi_R$ ), left arm ( $\Phi_L$ ) and left leg ( $\Phi_F$ ) (Wilson et al. 1934; Wilson et al. 1946).

$$\Phi_{WCT} = \frac{1}{3}(\Phi_L + \Phi_R + \Phi_F)\tag{3}$$

$$V_1:V_6 = \Phi_{V1}:\Phi_{V6} - \Phi_{WCT}\tag{4}$$

Wilson also proposed to use three unipolar limb leads (VR, VL, and VF), which were measured by difference potential of limbs' electrode and the WCT reference point (Wilson et al. 1934).

$$\begin{aligned}VL &= \Phi_L - \Phi_{WCT} \\ VR &= \Phi_R - \Phi_{WCT} \\ VF &= \Phi_F - \Phi_{WCT}\end{aligned}\tag{5}$$

Because the three unipolar limb leads had a small amplitude, Goldberger (Goldberger 1942) modified the WCT to increase these leads' amplitude by 50%. The new leads are measured as the potential difference between each limb potential and the average of the other two limb potentials. These leads are known as augmented leads and named as aVR, aVL, and aVF (Goldberger 1942).

$$\begin{aligned}aVL &= \Phi_L - \frac{1}{2}(\Phi_R + \Phi_F) \\ aVR &= \Phi_R - \frac{1}{2}(\Phi_L + \Phi_F)\end{aligned}\tag{6}$$

$$aVF = \Phi_F - \frac{1}{2}(\Phi_R + \Phi_L)$$

The augmented leads were suggested in 1942 finalizing the development of the ECG lead system. The current ECG lead system consists of three Einthoven limb leads, three augmented leads, and six precordial leads (Figure 1) (Malmivuo & Plonsey 1995).

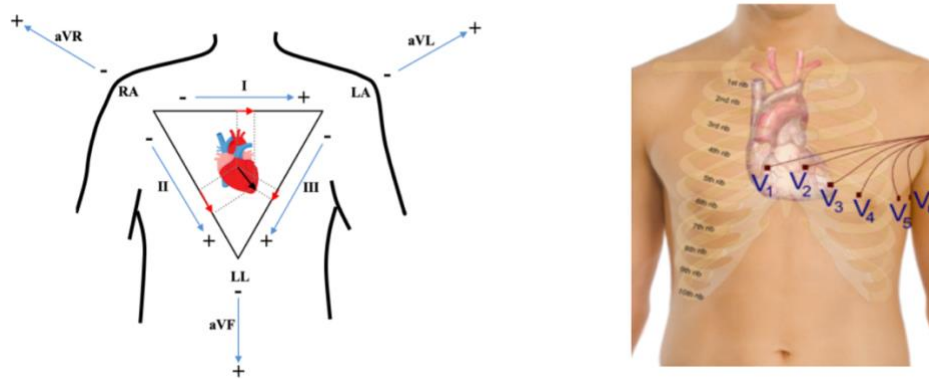


**Figure 1:** Twelve lead electrocardiography

Currently, the Electrocardiography is the most wide-spread non-invasive tool for diagnosis of cardiac diseases, currently in use in every clinical center. However, some of the aforementioned fundamental ECG hypotheses have been challenged either during the development of the Electrocardiography [1901-1942], or afterward. Therefore, we discuss two of these fundamental ECG hypotheses: the Einthoven equilateral Triangle hypothesis, and the Wilson hypothesis in order to make a tangible picture of the Wilson central terminal and its influence on the precordial leads.

### Wilson Central Terminal

Wilson hypothesized that a neutral reference point of the human body could be measured by averaging the limb potentials. This reference point was introduced having null amplitude, being steady, and locating in the center of the Einthoven triangle (Wilson et al. 1934). The potential in the infinite medium has a null amplitude which could be considered as the ideal reference point. In physics, we can only measure the potential difference between two points. However, we can have the potential of one point in case the second point is located in the far distance (infinity) from the first (Burger 1955). Thus, Wilson used three large resistors through which a negligible current would pass (based on Ohm's law) and consequently he was able to measure the limbs' potential (Figure 2, panel a) (Wilson et al. 1934). This assumption was found incorrect and absorbed immediate interests among researchers to measure this systematic error in the Electrocardiography. The proposed methods can be categorized into three different perspectives.

In the first approach, the human body is immersed in a large homogeneous conductor to measure the potential difference between the WCT and the assumed zero potential (the water itself). In 1938, Eckey and Fröhlich immersed a human body into a full bathtub and determined the WCT amplitude to be into a range of 0.2-0.3 [mV] (Eckey, P. & Fröhlich 1938). A year later, Burger conducted the same experiment and immersed five men into a bathtub filled by water and reported the WCT amplitude was 0.26 mV (Burger 1939). In 1946, Wilson submerged a human in the lake Michigan and found that the average absolute amplitude of the WCT could be as large as 0.15 mV (Wilson et al. 1946). Dolgin repeated the same experiment with different adjustment, and confirmed the previous finding (Dolgin et al. 1949). In 1954, Bayley et al. and Bayley and Kinard encased the body of volunteers inside a metal structure and immersed it in water for the duration of the recording (Bayley et al. 1954; Bayley & Kinard 1954). They determined that the WCT is not steady and its amplitude could be as large as 0.4 of Einthoven's leads during the cardiac cycle (Bayley & Kinard 1954; Bayley et al. 1954; Bayley & Schmidt 1955). Thus, they used three rheostats to adjust the weights of the three WCT components in order to minimize the WCT amplitude (Bayley & Kinard 1954). The legitimacy of the first approach was undermined by a variety of factors including the effect of water pressure on ECG recording and degree of the conductivity of surrounding water (Okamoto & Mashima 1998).

Additionally, the zero potential of surrounding water (Wilson et al. 1946; Wolferth & Livezey 1944) and the widespread use of this method (Dower et al. 1959) have been questioned.

In the second approach, the *zero potential* of human body was measured using numerical methods (Fischer et al. 2002; Lynn & Timlake 1968; Wach et al. 1997; Macfarlane et al. 2010) or surface potential mapping (Miyamoto et al. 1996; Miyamoto et al. 1995; Hoekema et al. 1999). In these methods, the zero potential is not exactly aligned with the WCT definition; however, they referred to it as Wilson Center Terminal. The numerical methods are developed based on the theory that summation of the electrical potential at the body surface should be zero (Macfarlane et al. 2010). Miyamoto et al. used 128 electrodes placed on the thorax and averaged their potential to estimate the amplitude of human reference point. They reported the average value of the WCT as  $-0.169$  mV in 10 normal volunteers, and  $-0.051$  mV in all 60 subjects including controls and patients (Miyamoto et al. 1995; Okamoto & Mashima 1998; Miyamoto et al. 1996).

In a third approach, the potential of the right arm, left arm and left leg directly measured using right leg as a reference point (Figure 2, panel b) (Gargiulo et al. 2016). We recently developed a new Electrocardiography device that can measure nine unipolar leads including three limbs' potential and six true unipolar limb leads, in addition to 12 lead ECG (Gargiulo 2015; Gaetano D Gargiulo et al. 2013; Gaetano D. Gargiulo et al. 2013; Gargiulo et al. 2015; Gargiulo et al. 2016). Our results confirm the previous findings that the WCT is not steady and null, and we found out the WCT amplitude could exceed the amplitude of lead II (up to 247% of lead II).

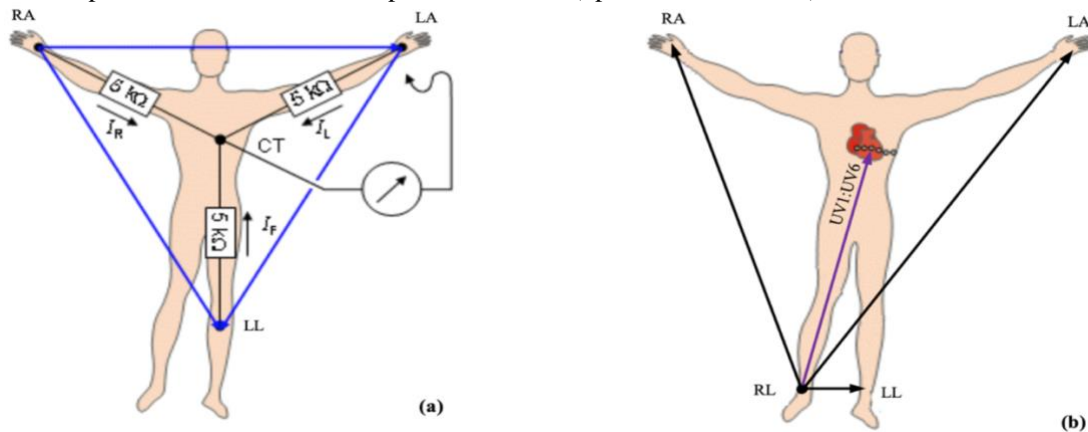


**Figure 2.** Traditional approach (panel a) in comparison with our approach (panel b) to measure the WCT. In our approach, the limb potential and unipolar chest lead are measured in respect to the right leg.

## True Unipolar ECG recording device

Our ECG device is designed to record traditional ECG signals in addition to the nine true unipolar leads including three limb potentials and six unipolar chest leads. The true unipolar leads are the raw biopotential measured from the exploring electrodes directly referred to the *right leg* (RL). Although right leg was not included in the original ECG montage, it was added as necessary return grounding for voltage amplifier as well as a way to reduce the interference from external electric fields (Webster 2009). Reduction of interference from external electrical fields is usually achieved with a technique known as a *driven right leg* or *right leg driver*, which usually implies an injection of a small current into the body (via the right leg electrode) and measuring amplifier circuits (via their reference terminal). In some specific biopotentials applications, the right leg driver is avoided using a technique known as voltage reference bootstrap that might result of advantage to reduce common noise capture. (Macfarlane et al. 2010; Malmivuo & Plonsey 1995; Webster 2009).

Driven right leg circuitries (DRLs) are widely used for the majority of the designs. Using the DRL increases patient safety because the human body is not directly grounded (Webster 2009; Malmivuo & Plonsey 1995; Winter & Webster 1983). Figure 3 shows an example of the DRL application. As can be seen, the human body is driven by a measure of the common mode signal at the measuring electrodes while the amplifier is directly grounded. The technical documentation of the INA118 can be found in (BurrBrown 2000).



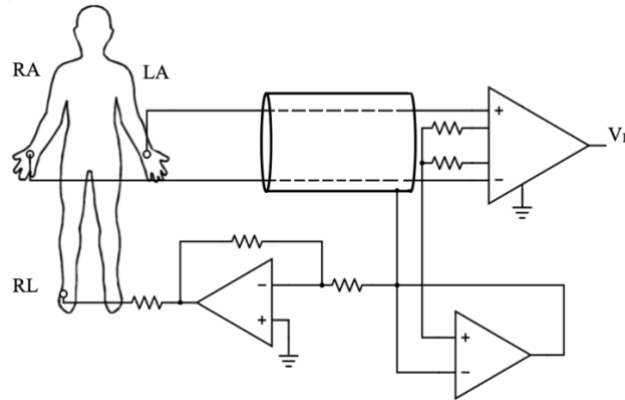


**Figure 3.** ECG amplifier using right leg driver (lead I)

Our hardware system is developed around the INA116 instrumentation amplifier (BurrBrown 2008) from Texas Instruments (Burr-Brown series). This chip has typically a bias current of only handful of femto-Amperes and it incorporates a specialized guard ring amplifier which it is primarily used to preserve the signal to noise ratio (SNR). The guard ring amplifier is used to measure the WCT components, as it generates a replica of the input signal (Gaetano D. Gargiulo et al. 2013; G. Gargiulo et al. 2013; Gargiulo et al. 2015; Gargiulo 2015; Gargiulo et al. 2016). Therefore, the WCT components' voltages are directly measured by using the guard buffer of the limb electrodes. The INA116 chips have a gain set of 1 V/V; two AC coupled active non-inverting low pass filters with gains of 10 V/V and 100 V/V are used to provide the required gain and bandpass filtering.

To ensure that the SNR of the measured signals is sufficient, specialized grounding circuitry is designed utilizing a combination of the right leg circuitry and a modified voltage bootstrap circuitry (Gargiulo 2015; Gargiulo, Paolo Bifulco, et al. 2014; G. D. Gargiulo et al. 2013; G. Gargiulo et al. 2013; Wilson et al. 1946). The non-amplified average of the measurement electrodes is directly inputted to the driven right leg circuitry which is designed to drive 20  $\mu$ A (Fisher et al. 2011; Madias 2008; Undar et al. 1997).

This circuitry is battery powered, and the necessary analogue to digital conversion and data logging is operated by the BIOADC (Gargiulo, P. Bifulco, et al. 2014) which samples data with a 16-bit over a range of  $\pm 5$  V with a sampling rate of 800 Hz. The BIODAC is directly (galvanically insulated USB HUB) connected to a battery-powered laptop, and it comprises an anti-aliasing low-pass filter operating at the Nyquist frequency. Finally, a specialized importing script including a zero-phase lag 50th order bandpass filter (0.05-150 Hz), a zero-phase lag 50th order 50 Hz and harmonics notch IIR filters are used to normalize the frequency components to the diagnostic ECG bandwidth of the acquired signal. Complete details can be found in our recent publication (Gargiulo et al. 2016).

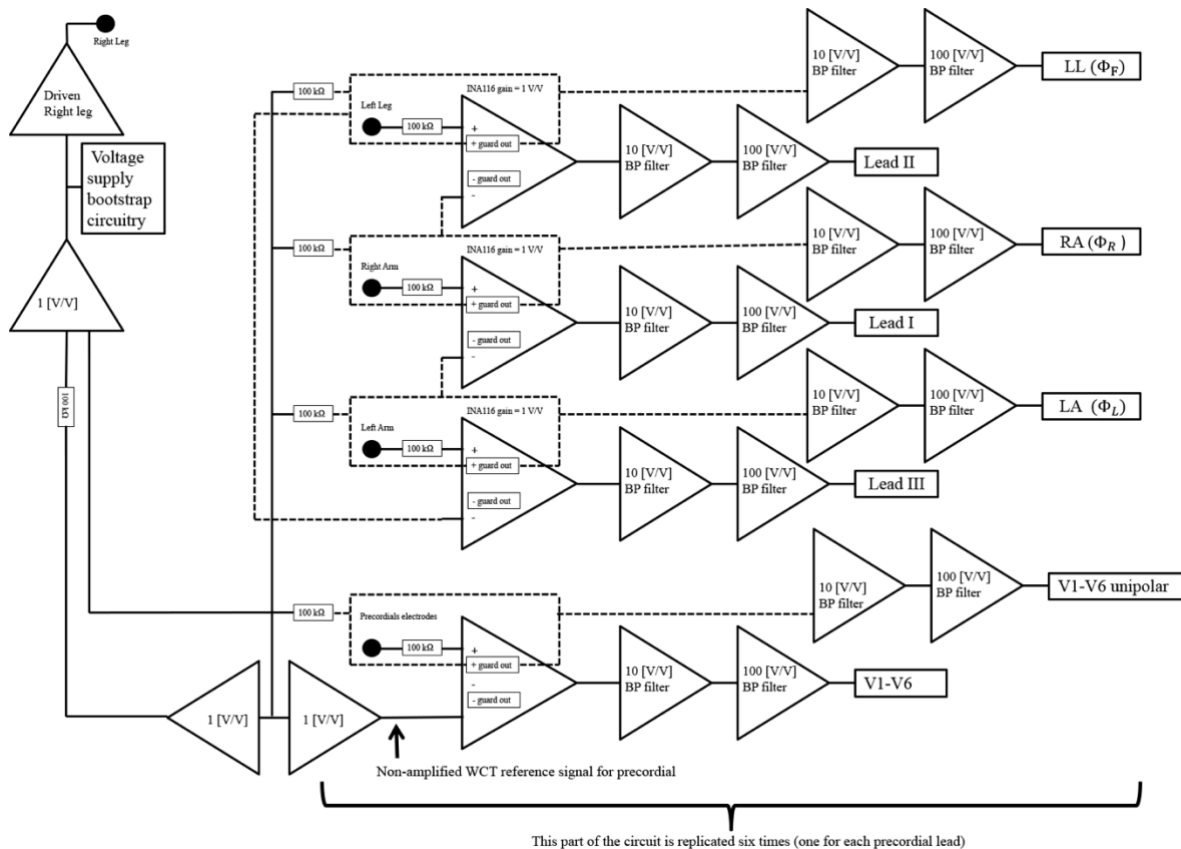


**Figure 4:** Block diagram of the employed hardware (adapted from (Gargiulo et al. 2016)).

## True Unipolar leads

We are able to record the three Einthoven unipolar limb lead (the voltage of right arm, left arm, and left leg) and six true unipolar precordial leads for the first time. We have recorded data from more than 100 patients at the Campbelltown hospital (NSW) over two years (2016-2018). All the patients volunteered for this study and gave written consent (this study was approved by the Ethics Committee of the South West Sydney Health District on 23rd September 2015 with the protocol number HREC/15/LPOOL/302). Some recordings have been removed from the dataset due to poor signal to noise ratio or because of abrupt interruption of the recording (emergency or patient being transferred to another department for an intervention/procedure). The published dataset<sup>2</sup> (Gargiulo & Moeinzadeh 2019) contains 92 patients (27 were female) with an average age of 65.23 years and standard deviation of 12.12 years. The majority of the patients had a history of cardiac disease and were admitted to the hospital from the emergency department because of difficulties in breathing and/or chest pain.

### Einthoven unipolar limb lead

We are able to measure the amplitude of Wilson Central Terminal by averaging the voltage of Einthoven limbs. In this part, we are trying to answer the question *what is the Wilson Central Terminal?* We investigate the legitimacy of two hypotheses:

- 1- *The WCT is null and steady during the cardiac cycle.*
- 2- *The WCT and aVF are inversely proportional.*

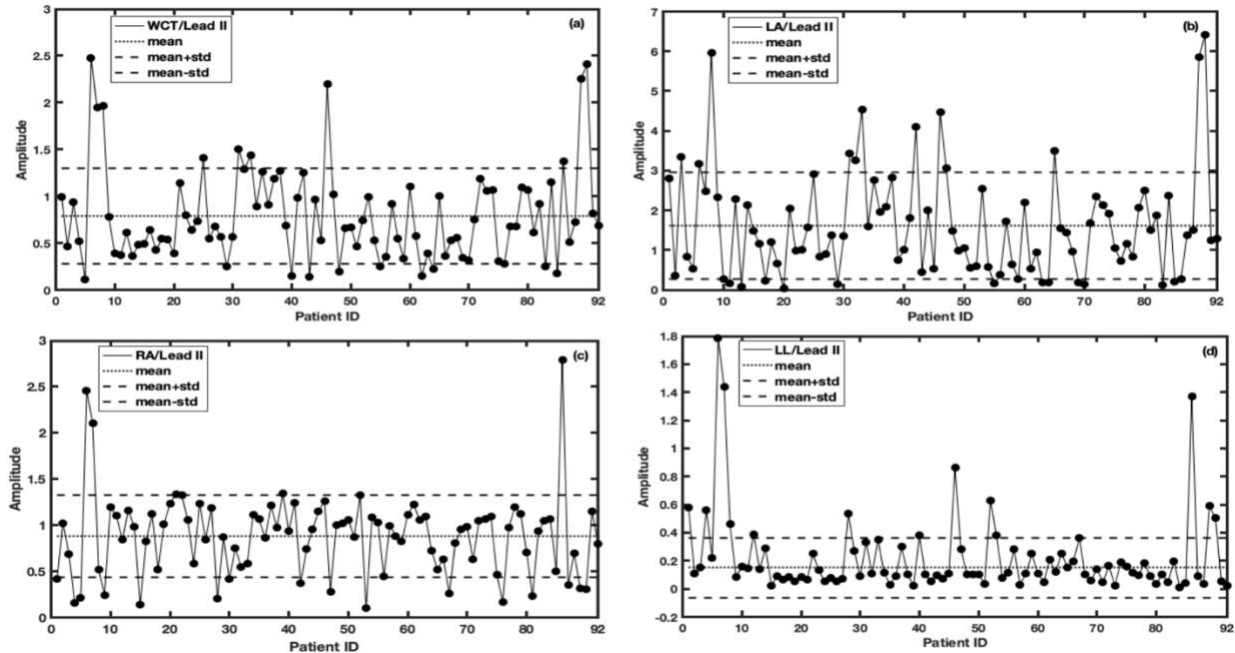
<sup>2</sup> Our dataset name is WCTECGdb, and was published in the Physionet website (<https://alpha.physionet.org/content/wctecgdb/>).



The first hypothesis is the Wilson assumption to measure the precordial leads, which has been proved incorrect by many researchers. However, their approaches were cumbersome, usually having small test case population, and more importantly their validity has been questioned (Wilson et al. 1946; Wolferth & Livezey 1944; Dower et al. 1959). The second hypothesis assumes that the left leg potential has the smallest amplitude among the Einthoven limb potentials, as it has the longest distance from the heart. Hence, considering the assumption that the left leg has near zero amplitude ( $\Phi_F \cong 0$ ), the WCT can obtain using the right arm, and left arm. Consequently, the WCT and aVF are inversely proportional.

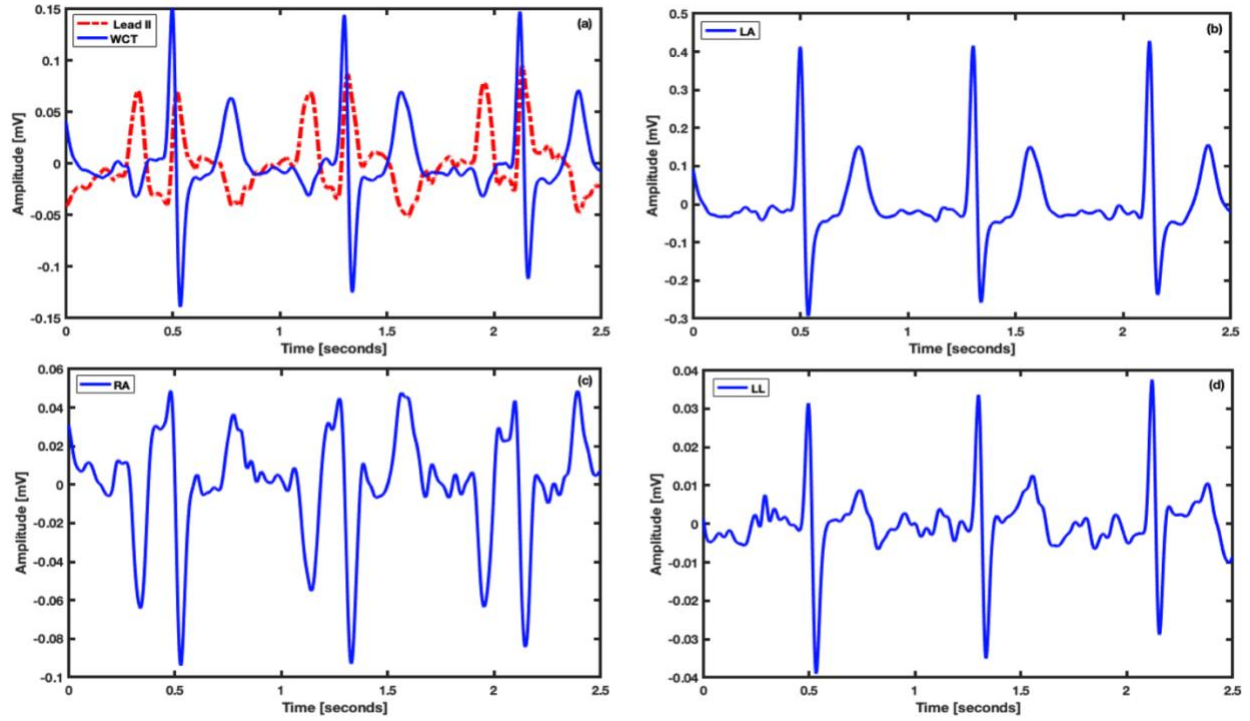
$$\begin{aligned} \Phi_{WCT} &= \frac{1}{3}(\Phi_R + \Phi_L) \xrightarrow{\text{yields}} \Phi_{WCT} = -\frac{2}{3}aVF \\ aVF &= -\frac{1}{2}(\Phi_R + \Phi_L) \end{aligned} \quad (6)$$

To assess the credibility of these two theories, we calculated the average peak to peak amplitude of three beats for all patients. In Figure 5, We report the relative amplitude of the WCT, RA, LA, and LL with respect to lead II. As it is shown in Figure 5 (panel a), the minimum, maximum and average amplitude of the WCT in relation with lead II among all 92 patients are 0.11, 2.47, and 0.78 respectively. The left arm expected to have a higher potential than the right arm, as it is closer to the heart (Figure 4-panel b, c). The left arm in respect with lead II has the average of 1.61 (within range of [0.038 6.41]), while right arm average is 0.88 (within range of [0.01 0.88]) for all 92 patients. Figure 5 (panel d) demonstrates the amplitude of the left leg in respect with lead II. Although the left leg has a small amplitude in comparison with the right and left arms' potentials, it does not have zero amplitude. The left leg potential in relation to lead II is in the range of [0.007 1.78] with an average of 0.22 for all patients.



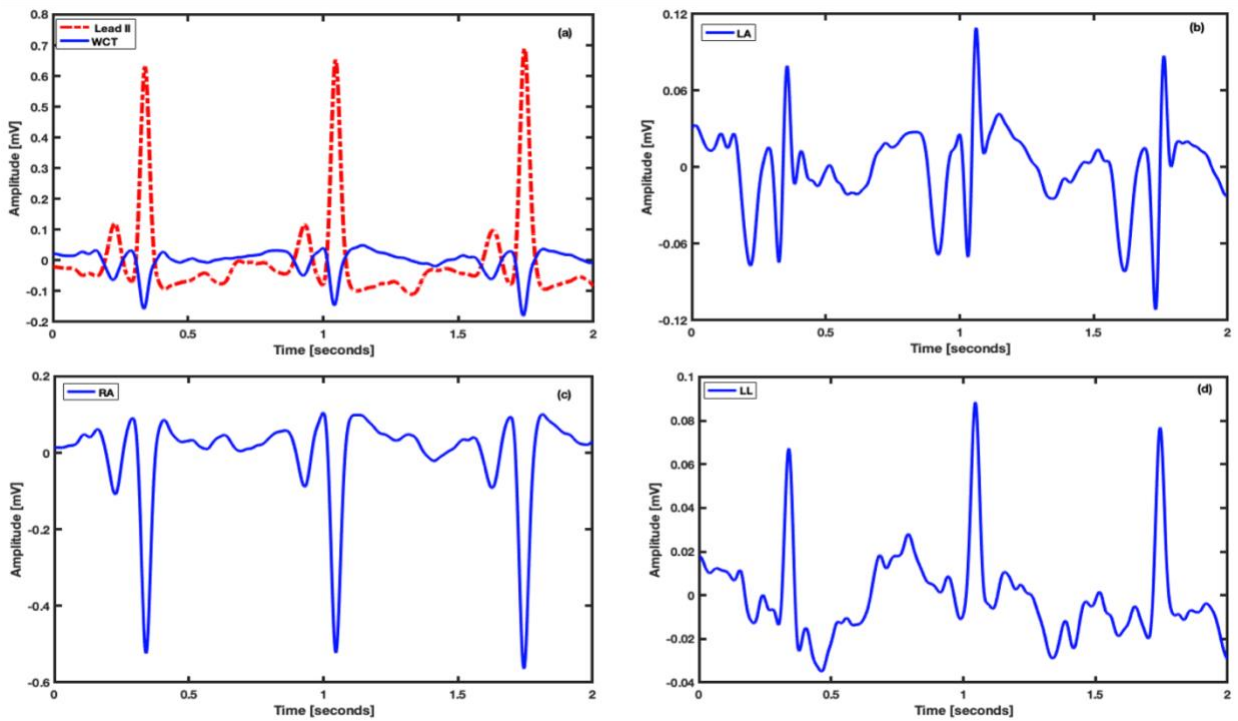
**Figure 5.** The amplitude of the WCT, right arm, left arm and left leg with respect with Lead II.

Our recording shows that the WCT does not have small amplitude and has ECG lead characteristics such as p-wave or QRS complex. The WCT has neutral (Figure 6, 8), negative (Figure 7) or positive (Figure 9) deflection during the cardiac cycle. Figure 6 is an example of the WCT with large amplitude. The WCT signal is as large as 2.41 of lead II and it exhibits all the characteristics of the ECG trace.



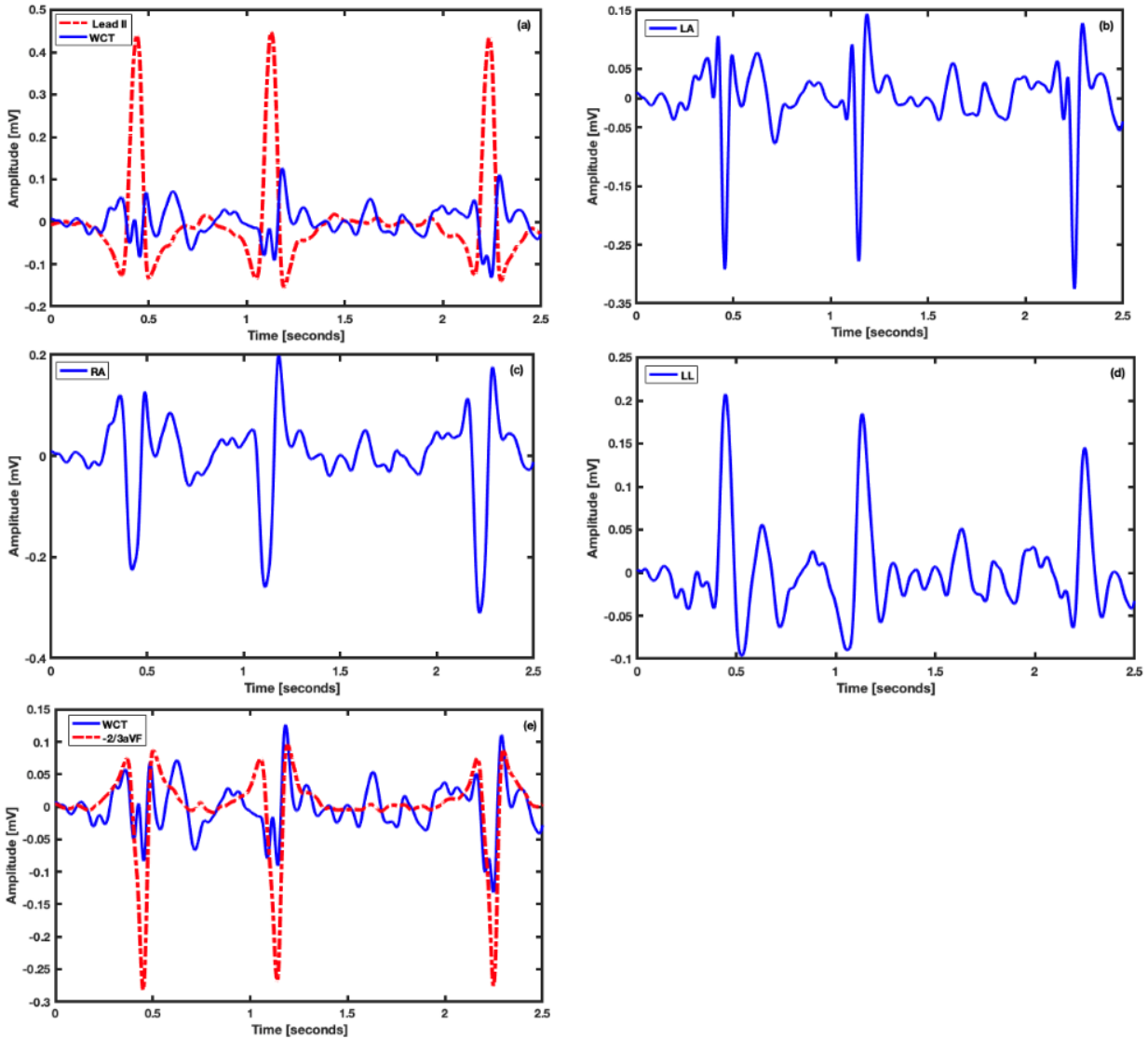
**Figure 6.** Example of neutral WCT. The WCT is 2.41 of lead II amplitude (average); the recording is from a 80-year-old male patient admitted from the emergency department with NSTEMI diagnosis.

Figure 7 is an example of WCT with negative deflection. The left arm, right arm, and left leg show ECG features. Furthermore, the left leg has relatively small potential in comparison with the right arm, and left arm.



**Figure 7:** Example of negative WCT. The WCT is 0.32 of lead II amplitude (average); the recording is from a 54-year-old male patient admitted from the emergency department with ischemic cardiomyopathy diagnosis.

As it can be referred from Eq. 6, the WCT and aVF are highly correlated in case the left leg potential has near zero amplitude. It can be understood from Figure 5 (panel d) that the left leg has small amplitude for most of the patients, however it also has a relatively big amplitude for some patients. Figure 8 and Figure 9 are an example of the WCT and aVF lead having low and high correlation. As can be seen in these figures, the RA, LA, and LL signals have the ECG characteristics. Figure 8, shows a low correlation between the aVF lead and the WCT signal, as the LL amplitude is as large as 0.22 of lead II. In contrast, the LL has a negligible amplitude in Figure 9, consequently the WCT and the aVF lead are highly correlated.



**Figure 8.** Example of neutral WCT that mutates into positive and neutral. There is low a correlation (45%) between the WCT and aVF lead. The LL amplitude is as large as 0.22 of lead II.

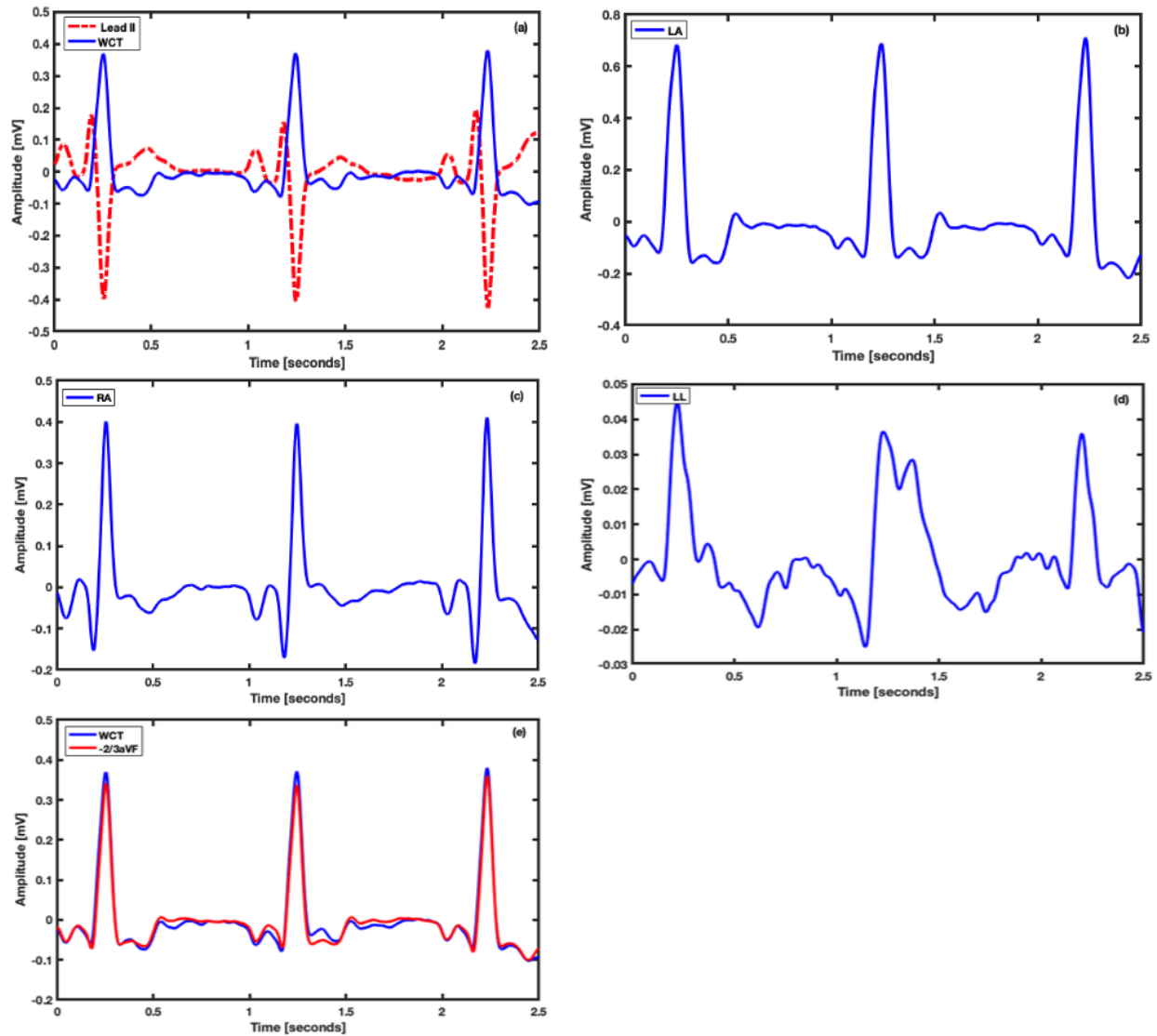


**Figure 9.** Example of positive WCT with small LL amplitude (0.032 of Lead II). The WCT and aVF are highly correlated (98%) as the amplitude of WCT is negligible.

### True unipolar precordial leads

The true unipolar leads and precordial leads are referred as the same concept in the literature. However, it has been known that this terminology is incorrect. The precordial leads initially represent the difference potential between the electrodes placed on the chest and the WCT. Since Wilson assumed the WCT is null, the precordial leads have been referred as unipolar leads. However, our ECG device is able to record the potential of electrodes placed on the chest without using the WCT signal (Gargiulo et al. 2015; Gaetano D. Gargiulo et al. 2013; Gargiulo 2015; Gaetano D Gargiulo et al. 2013). Therefore, we recorded the traditional precordial leads (V1:V6) and what we address as the true unipolar leads (UV1: UV6) at the same time for all patients.

Our recording shows that the WCT is highly individual and has medically relevant amplitude, which impacts the precordial leads' shape and resulting to lose important information in the precordial leads.

We investigated the clinical features of true unipolar leads in comparison with precordial leads for all 92 patients. In this paper, we selected four patients from the WCTECGdb (Gargiulo & Moieznadeh 2019) with Non-ST Elevation Myocardial Infarction (NSTEMI) diagnosis to show the influence of the WCT on precordial leads. Our

records show that the unipolar ECG may be more sensitive for detecting disease in the left anterior descending (LAD) coronary artery in patients presenting with NSTEMI. We are currently recording more data to show the validity of this hypotheses. As the WCT has no effect in the limb leads and augmented leads, we do not include them in the Figure 10, 11, 12 and 13.

- Patient75: He presented with a non-ST segment elevation myocardial infarction. In this type of myocardial infarction, the mechanism of injury is subendocardial myocardial infarction. As it can be referred from Figure 10 (panel a), the t-waves are biphasic in leads V2:V4, while they are inverted in leads UV1:UV6. Consequently, the unipolar ECG may be more sensitive at detecting this type of injury than the standard ECG. As the only difference between unipolar chest lead, and precordial lead is the WCT signal (Eq. 4), the influence of the WCT on UV1 can be clearly seen in Figure 10 (panel b).

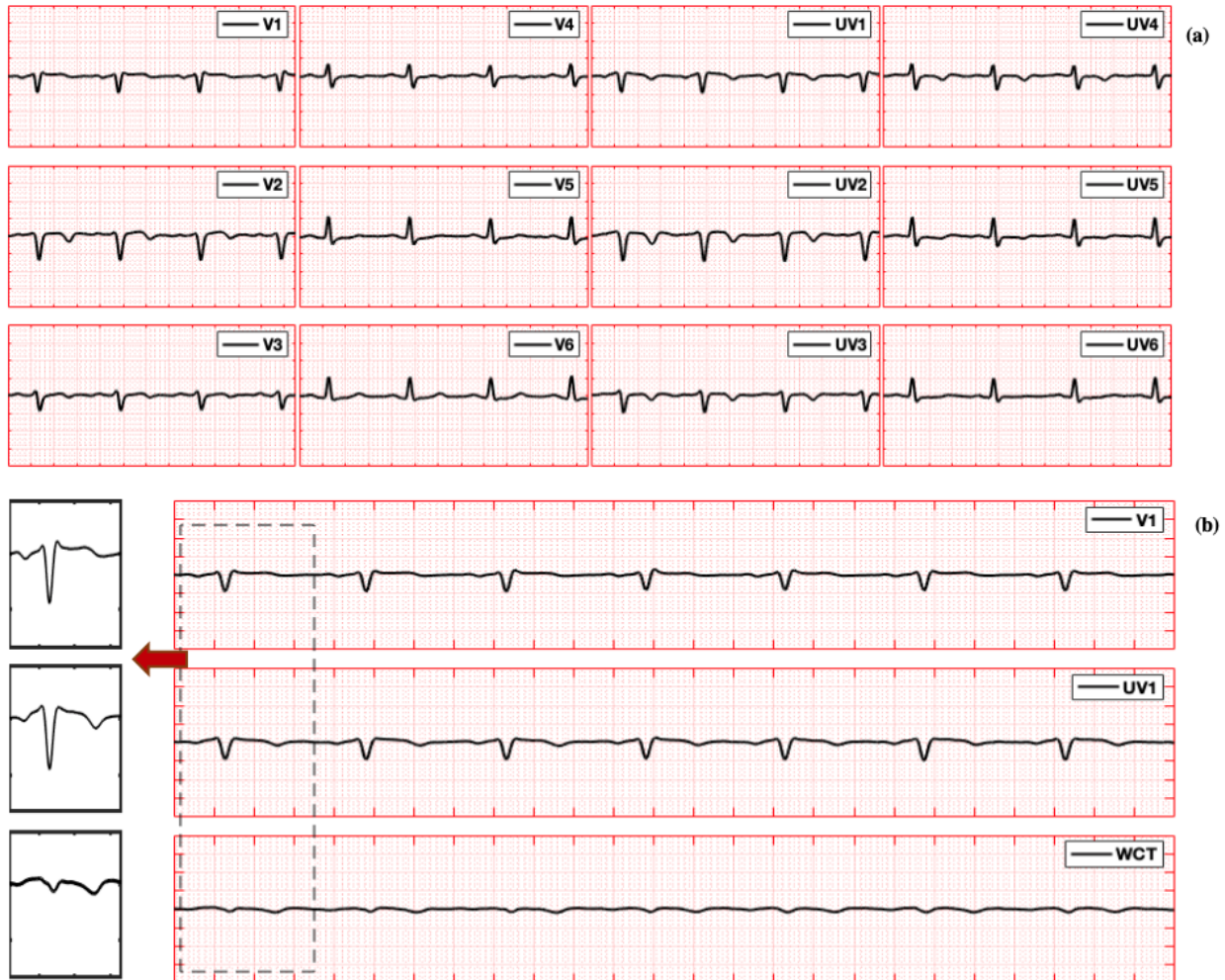


**Figure 10.** Panel (a): comparison of unipolar chest lead (UV1:UV6) with precordial leads (V1:V6). Panel (b): the influence of the WCT on V1; top panel is standard V1 precordial; middle is true unipolar UV1; bottom panel is the WCT signal. The t-wave is inverted in UV1. Recorded from 70 years old male, admitted to a hospital for NSTEMI (patient75).

- Patient46: His angiography showed focal severe mid LAD stenosis which supplied a large collateral to a distal dominant right coronary artery (the native right coronary artery being completely occluded). The patient subsequently underwent coronary artery bypass surgery. As it can be seen in Figure 11, the true unipolar leads show loss of clear T waves which is suggestive of ischemia.



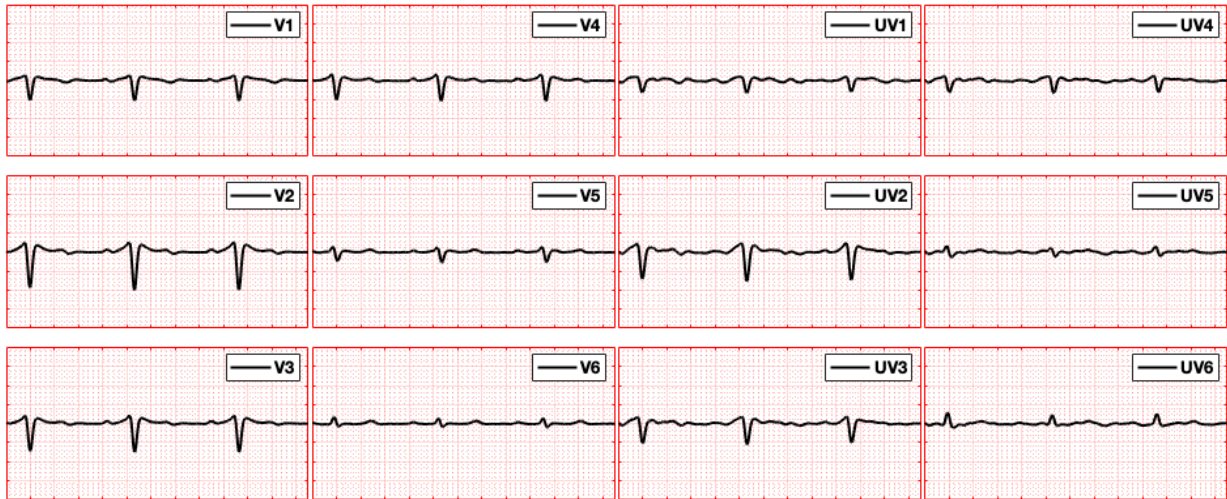


**Figure 11.** Comparison of unipolar chest lead (UV1:UV6) with precordial leads (V1:V6). Recorded from 69 years old male, admitted to a hospital for NSTEMI (patient46).

Patient85: His angiography showed proximal to mid LAD stenosis which was subsequently stented (after optical coherent tomography (OCT) imaging). As seen in Figure 12, the true unipolar leads show more markedly biphasic T waves UV1:UV3. In other words, biphasic T waves in VU1-UV3 typically suggest proximal LAD disease which is known as Wellens Syndrome. This was not apparent on the precordial leads but was predictive of the underlying culprit lesion.

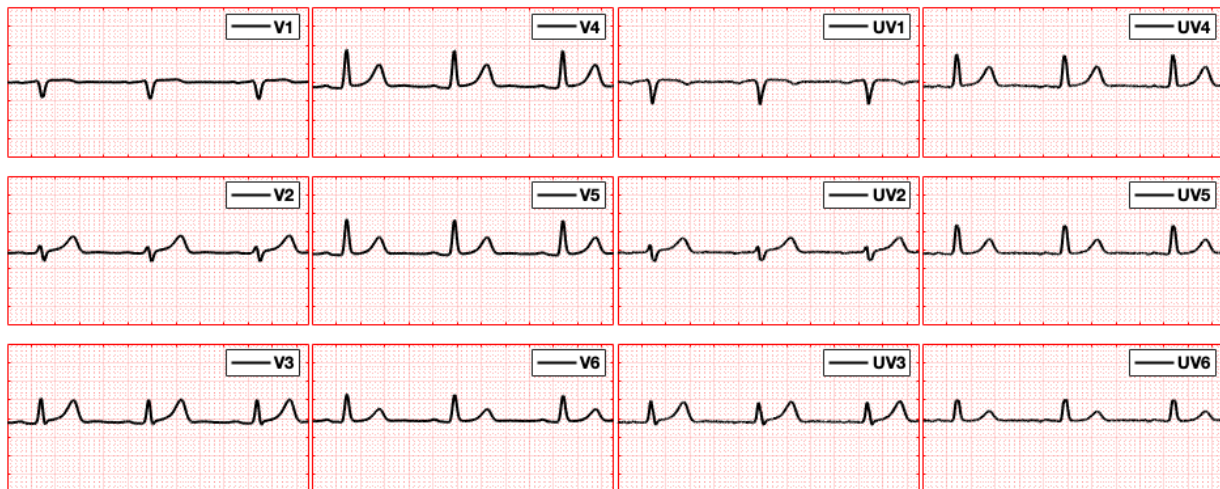


**Figure12.** Comparison of unipolar chest lead (UV1:UV6) with precordial leads (V1:V6). Recorded from 52 years old male, admitted to a hospital for NSTEMI (patient85).

- Patient66: His angiography showed focal severe stenosis in distal RCA and proximal large diagonal branch stenosis of the LAD (both of which were stented). As it can be referred from Figure 13, the true unipolar leads show T wave inversion UV4:UV6 consistent with diagonal branch territory problem/ischemia.

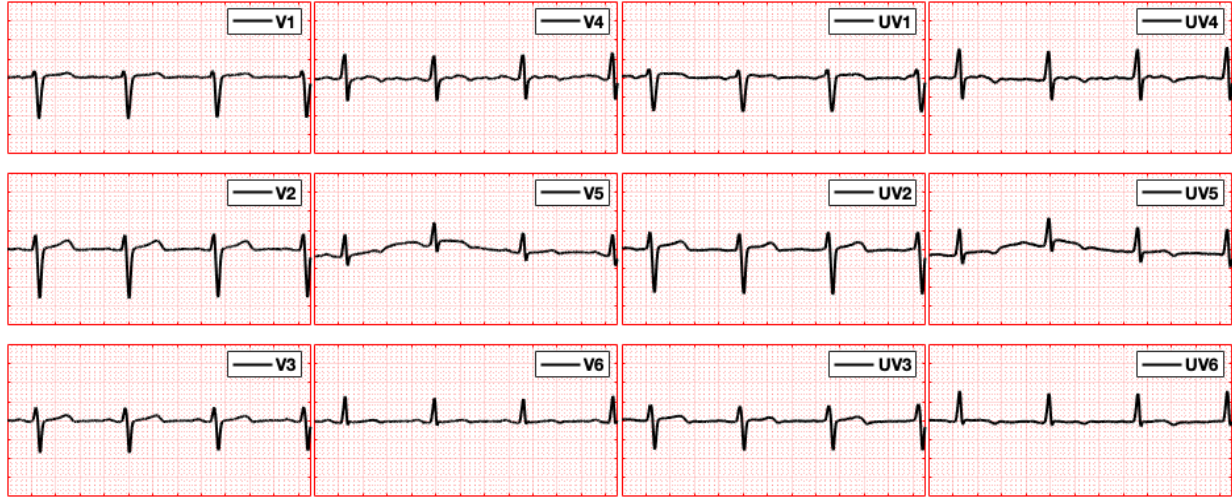


**Figure 13.** Comparison of unipolar chest lead (UV1:UV6) with precordial leads (V1:V6). Recorded from 41 years old male, admitted to a hospital for NSTEMI (patient66).

## The WCT Location

In theory, the WCT is located in the centroid of the Einthoven triangle. However, a research conducted in 2005 shows that many cardiologists do not have a clear understanding of unipolar leads and the WCT concept (Bacharova et al. 2005). As mentioned earlier, although there was an initial wave of interest working on the fault in the WCT assumption after Wilson hypothesized its concept, this error has been widely accepted and the topic received scant research attention. Furthermore, there is no consensus understanding of the Einthoven triangle, as its edges have been considered differently in the literature. Hence, a clear view of the Einthoven triangle hypothesis may lead to a more precise answer to the question, *where is Wilson central terminal?*

Einthoven assumed the human body is two-dimensional conducting homogeneous medium with the shape of a triangle. The heart is regarded as a single dipole in the center of the triangle. The dipole changes its magnitude and direction in every moment which causes to change its electrical field. Considering these assumptions, the potential of every point in the body measured by Eq. 7 (Macfarlane et al. 2010), which  $\Phi$  is the potential of a single current dipole  $\vec{p}$  (with strength  $p$ ) in infinite homogenous medium with a conductivity of ( $\sigma$ ):

$$\Phi = \frac{1}{4\pi\sigma} \frac{p \cos\theta}{R^2} + c \quad (7)$$

$R$  is the length of the vector  $\vec{R}$  directed from dipole source location to the target point, and  $\theta$  is the angle between vectors  $\vec{p}$  and  $\vec{R}$ .

As Goldberger discussed (Goldberger 1945), the distance between the limb electrodes and the dipole are equivalent; therefore the difference between the limb potential amplitudes is only dependent to angles  $\theta_1$ ,  $\theta_2(\theta_1 + 120)$  and  $\theta_3(\theta_1 + 240)$ . It could be easily shown that for every direction of heart vector, the sum of the limb potential is equal to zero (Goldberger 1945).



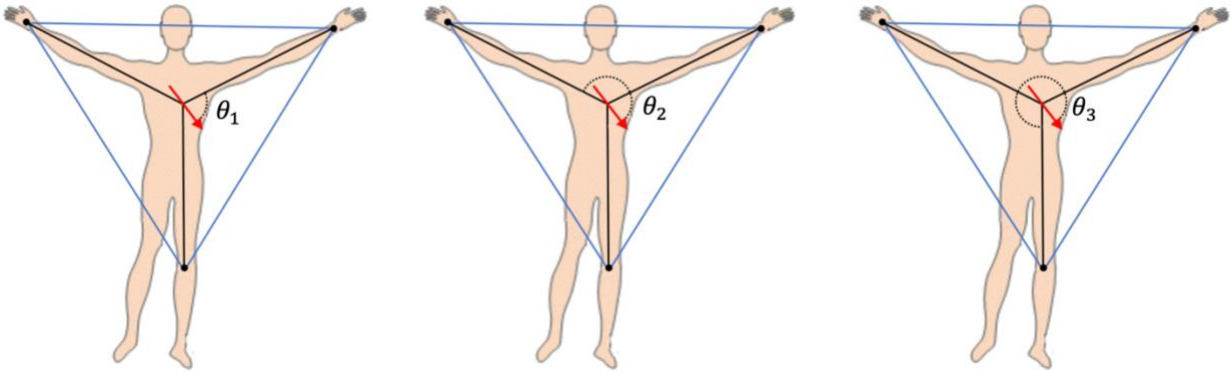


**Figure 14.** Einthoven assumed the potential of each limb only depends on the angle between  $\vec{p}$  and  $\vec{R}$  vectors.

The geometrical position of the limb electrodes shaped the Einthoven triangle (Burger et al. 1961; Einthoven 1903; Goldberger 1945). Wilson assumed symmetrical orientation of the heart vector in respect to the electrodes on the limbs (Bayley & Kinard 1954) and hypothesized that the potential of the dipole (heart) is equal to zero and calculated by the average of the Einthoven limb potentials. Although the Einthoven hypothesis is the major breakthrough in electrocardiography, it has been known his assumptions are oversimplifying the human body, and the heart activity. The same argument can be made for the Wilson hypothesis.

The WCT located in the centroid of Einthoven triangle, represents the potential of the single dipole, and its potential is equal to zero in case three electrodes are placed in the same distance from the heart, and all Einthoven assumptions are correct.

However, as it can be referred from Eq. 7, in case the imaginary line between limb electrodes do not build up the equilateral triangle, the limb potentials depend on the  $R$  amplitude and the angle ( $\theta$ ). Consequently, the centroid of the triangle cannot represent the dipole anymore. Furthermore, the other assumptions (the electrical activity of the heart is a single dipole which located in the center of the body, and the human body is a homogeneous conductor) are ill-posed models of the human body (Goldberger 1945).

In some literatures, there is also a misunderstanding between geometrical space and electrical space. As an example, in the standard surface ECG representation it is possible to see that limb leads are the edges of the Einthoven triangle, this can be easily shown incorrect. The Einthoven law (Eq. 2) contradicts with the fact that equilateral triangle edges are in the same length, and more importantly three limb leads could only construct a triangle (not equilateral) for less than 50% of the cardiac cycle (Gargiulo et al. 2018).

## Discussion

Originally, the heart was theorized to act as a current source and the electrocardiography model measured bio-currents using a very sensitive galvanometer (string galvanometer). As there is no obvious current pathway that includes the heart when the instrument is connected between the two legs and the right leg is the most distant limb from the heart, Einthoven did not include the right leg in the cardiac conduction model. In other words, ECG recordings were intended as a measure of the net current impressed by heart circulating into an external circuit closed by the measurement instrument. Therefore, it was possible for Wilson to complete the transformation from the equilateral triangle (Einthoven's triangle) to the equivalent star circuit (originating the augmented leads), when he faced the problem of finding a reference for precordials. In theory, if each of the Einthoven leads measures the net current impressed by the heart between the two limbs, averaging all the electrodes together should give the best approximation of the point of origin, the neutral point of the cardiac electrical activity.

Impractical use of current measurement devices and the link between current and voltage resulted in replacement of all ECG current measurements with voltage, neglecting that measuring voltage instead of current requires dealing with the different impedances of body sections. In fact, each lead is interpreted as the voltage drop across a composed resistance (impedance, as a matter of fact) due to the net current impressed by the heart to the points of measurement based on Ohm's law (Voltage = Resistance \* Current). For example, lead I (Figure 15) can be

interpreted as the drop of voltage across the sum of the contact impedance at both electrodes that includes the impedance of the two arms and the impedance of the chest across the shoulders that changes with respiration.

Of course, current and voltage measurements are perfectly interchangeable if the body is simply considered as a homogeneous volume conductor (constant resistance) with the limb electrodes placed at equal distance with no or negligible contact impedance. However, in real life recording the contact impedance imbalance between the ECG electrodes is often not verified. Additionally, the limb leads are measured across different sections of the chest, which are different in shape and their resistance changes with respiration and body posture resulting in adding a frequency-dependent delay and a phase difference between voltage and current. The modified phase relationship between voltage and current may also affect the limbs' potential and consequently, the WCT. Moreover, as the voltage potential difference between the reference point (RL) and the other limb electrodes are used to measure the RA, LA and LL potentials, different body and contact impedances may impose different delays upon the limb potentials resulting to an unpredictable alteration of WCT (Gargiulo et al. 2015; Gargiulo 2015).

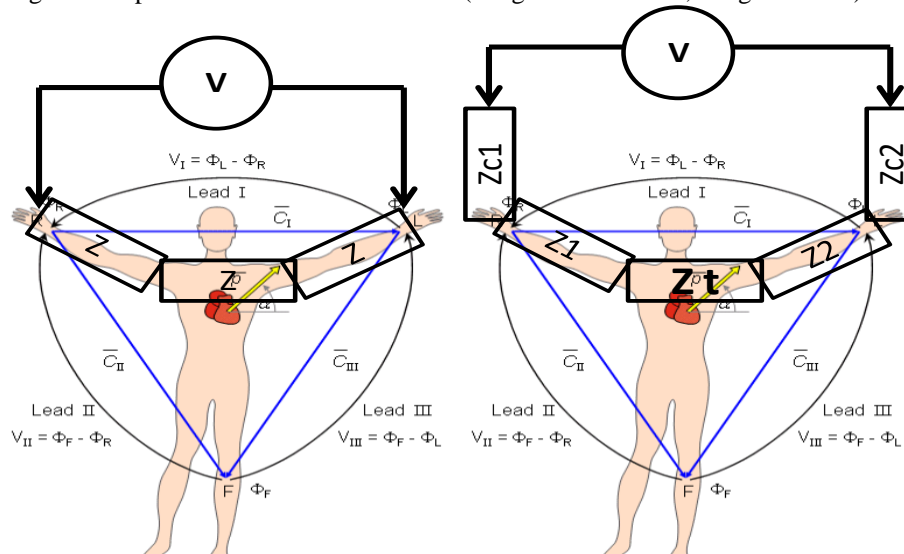


**Figure 15.** Ideal measurement of lead I vs real measurement of lead I. Left panel shows idealized measurement of lead I as voltage; right panel refers to real measurements of lead I in which includes contact impedances ( $Z_{c1}$  and  $Z_{c2}$ ) and variable impedance of torso ( $Z_t$ ).

Based on the Einthoven theory, if the limb electrodes placed on the same distance from the heart, the WCT presents the potential of the dipole. However, it is not the case in practice. The WCT amplitude is highly dependent on where the limb electrodes are placed (Eq. 7). Hence, it is obvious not to have a negligible amplitude in averaging the limbs' potential. On the other hand, the location of the limb electrodes influences the shape and amplitude of precordial leads (Farrell et al. 2008). As our device use right leg as a reference point to measure the potential of the electrodes on the chest, the WCT variation does not affect the true unipolar leads. On the other hand, the true unipolar leads are robust and independent from the limb electrodes' displacement.

## Conclusion

The electrocardiography is the most common tool in the diagnosis of cardiac diseases. In this paper, we discussed two important hypotheses proposed by Einthoven and Wilson which shapes the currently in use electrocardiography tool. It has been known that these two theories simplify the heart activity, and do not provide a precise model for the human body. However, no one can really measure the influence of these false assumptions on the leads. As our ECG device is able to record the potential of the Einthoven limb electrodes and chest electrodes, we were able to show the impact of the WCT on precordial leads. Furthermore, we depicted a clear picture of the WCT concept by answering the questions *what is the Wilson central terminal?* and *where is the Wilson central terminal?* Our records show that the WCT is not null, and it has ECG features such as p-wave and QRS complex with clinically relevant amplitude (as high as 2.47 of lead II). We also compared the limb potential amplitudes. Our records show that the left arm has a high amplitude as it is closer to the heart, and the left leg has a small amplitude for most of the patients. However,

the left leg potential is not negligible for all the patient, and its amplitude with respect to lead II is in a range of [0.007 1.78] and with an average of 0.22 for all patients.

We used two terminologies to address the chest leads, first, precordial leads (V1:V6) referring to the current approach used for recording the chest leads, second, the true unipolar leads (UV1:UV6) addressing our approach used for recording the chest electrodes' potential. We show that the WCT signal is clinically relevant, and has an impact on precordial leads' shape and amplitude. Our preliminary results show that the true unipolar leads may be more sensitive for detecting cardiac diseases in the left anterior descending coronary artery in patients with NSTEMI.

## References






- Anon, 1925. The Mechanism and Graphic Registration of the Heart Beat. *JAMA: The Journal of the American Medical Association*, 85(23), p.1832. Available at: <http://jama.jamanetwork.com/article.aspx?doi=10.1001/jama.1925.02670230064033>.
- Bacharova, L. et al., 2005. Where is the central terminal located? In search of understanding the use of the Wilson central terminal for production of 9 of the standard 12 electrocardiogram leads. *Journal of Electrocardiology*, 38(2), pp.119–127. Available at: <http://www.ncbi.nlm.nih.gov/pubmed/15892021>.
- Bayley, R.H. et al., 1954. The zero of potential of the electric field produced by the heart beat; the problem with reference to homogenous volume conductors. *Circulation research*, 2(1), pp.4–13. Available at: <http://www.ncbi.nlm.nih.gov/pubmed/13116387>.
- Bayley, R.H. & Kinard, C.L., 1954. The zero of potential of the electrical field produced by the heart beat; the problem with reference to the living human subject. *Circulation research*, 2(2), pp.104–111. Available at: <http://www.ncbi.nlm.nih.gov/pubmed/13141373>.
- Bayley, R.H. & Schmidt, A.E., 1955. The Problem of Adjusting the Wilson Central Terminal to a Zero of Potential in the Living Human Subject. *Circulation Research*, 3(1), pp.94–102. Available at: <http://circres.ahajournals.org/cgi/doi/10.1161/01.RES.3.1.94>.
- Burger, H.C., 1955. The zero of potential: A persistent error. *American Heart Journal*, 49(4), pp.581–586. Available at: <http://linkinghub.elsevier.com/retrieve/pii/0002870355900764>.
- Burger, H.C., van Brummelen, A.G.W. & van Herpen, G., 1961. Heart-vector and leads. *American Heart Journal*, 61(3), pp.317–323. Available at: <http://linkinghub.elsevier.com/retrieve/pii/0002870361906019>.
- Burger, R., 1939. Ueber das elektrische Feld des Herzens. *Cardiology*, 3(1–2), pp.56–138. Available at: <https://www.karger.com/Article/FullText/164634>.
- BurrBrown, 2000. INA 118 Precision low power Instrumentation Amplifier. *Technical data*. Available at: <http://www.ti.com/lit/ds/symlink/ina118.pdf>.
- BurrBrown, 2008. INA116. *Technical data*. Available at: <http://www.burbrown.com>.
- Dolgin, M., Grau, S. & Katz, L.N., 1949. Experimental studies on the validity of the central terminal of Wilson as an indifferent reference point. *American heart journal*, 37(6), pp.868–880.
- Dower, G.E., Osborne, J.A. & Moore, A.D., 1959. Measurement of the error in Wilson's central terminal: an accurate definition of unipolar leads. *British heart journal*, 21, pp.352–60. Available at: <http://www.ncbi.nlm.nih.gov/pubmed/13817890>.
- Eckey, P. & Fröhlich, R., 1938. Archiv für Kreislaufforschung. , pp.349–356.
- Einthoven, W., 1903. Die galvanometrische Registrierung des menschlichen Elektrokardiogramms, zugleich eine Beurtheilung der Anwendung des Capillar-Elektrometers in der Physiologie. *Pflüger, Archiv für die Gesamte Physiologie des Menschen und der Thiere*, 99(9–10), pp.472–480. Available at: <http://link.springer.com/10.1007/BF01811855>.
- Einthoven, W., Fahr, G. & de Waart, A., 1913. Über die Richtung und die manifeste Grösse der Potentialschwankungen im menschlichen Herzen und über den Einfluss der Herzlage auf die Form des Elektrokardiogramms. *Pflüger's Archiv für die gesamte Physiologie des Menschen und der Tiere*, 150(6–8), pp.275–315. Available at: <http://link.springer.com/10.1007/BF01697566>.
- Farrell, R.M. et al., 2008. Effects of limb electrode placement on the 12- and 16-lead electrocardiogram. *Journal of Electrocardiology*, 41(6), pp.536–545. Available at: <http://dx.doi.org/10.1016/j.jelectrocard.2008.07.023>.
- Fischer, G. et al., 2002. On modeling the wilson terminal in the boundary and finite element method. *IEEE Transactions on Biomedical Engineering*, 49(3), pp.217–224.
- Fisher, W. et al., 2011. Event-related potentials in impulsively aggressive juveniles: A retrospective chart-review study. *Psychiatry Research*, 187(3), pp.409–413. Available at: <http://linkinghub.elsevier.com/retrieve/pii/S0165178111001661>.

- Fye, W.B., 1994. A History of the origin, evolution, and impact of electrocardiography. *The American Journal of Cardiology*, 73(13), pp.937–949. Available at: <http://linkinghub.elsevier.com/retrieve/pii/000291499490135X>.
- Gargiulo, G., Bifulco, P., et al., 2014. Open platform, 32-channel, portable, data-logger with 32 PGA control lines for wearable medical device development. *Electronics Letters*, 50(16), pp.1127–1129. Available at: <https://digital-library.theiet.org/content/journals/10.1049/el.2014.1791>.
- Gargiulo, G., Bifulco, P., et al., 2014. Problems in Assessment of Novel Biopotential Front-End with Dry Electrode: A Brief Review. *Machines*, 2(1), pp.87–98. Available at: <http://www.mdpi.com/2075-1702/2/1/87/>.
- Gargiulo, G. et al., 2013. True Unipolar ECG Leads Recording (Without the Use of WCT). *Heart, Lung and Circulation*, 22, p.S102.
- Gargiulo, G. & Moeinzadeh, H., 2019. Wilson Central Terminal ECG Database. *PhysioNet*. Available at: <https://alpha.physionet.org/content/wctecgdb/>.
- Gargiulo, G.D. et al., 2015. A 9-independent-leads ECG system from 10 electrodes: A practice preserving WCT-less true unipolar ECG system. In *2015 IEEE Biomedical Circuits and Systems Conference (BioCAS)*. IEEE, pp. 1–4. Available at: <http://ieeexplore.ieee.org/document/7348300/>.
- Gargiulo, G.D. et al., 2013. Towards true unipolar bio-potential recording: a preliminary result for ECG. *Physiological Measurement*, 34(1), pp.N1–N7. Available at: <http://www.ncbi.nlm.nih.gov/pubmed/23248178>.
- Gargiulo, G.D. et al., 2013. Towards true unipolar ECG recording without the Wilson central terminal (preliminary results). *Physiological measurement*, 34(9), pp.991–1012. Available at: <http://stacks.iop.org/0967-3334/34/i=9/a=991?key=crossref.3ee57f77157cc5fa56247c2775f2317d>.
- Gargiulo, G.D., 2015. True Unipolar ECG Machine for Wilson Central Terminal Measurements. *BioMed Research International*, 2015, p.586397. Available at: <http://www.ncbi.nlm.nih.gov/pubmed/26495303>.
- Gargiulo, G.D. et al., 2013. Unipolar ECG circuits: Towards more precise cardiac event identification. In *2013 IEEE International Symposium on Circuits and Systems (ISCAS2013)*. IEEE, pp. 662–665. Available at: <http://ieeexplore.ieee.org/lpdocs/epic03/wrapper.htm?arnumber=6571932>.
- Gargiulo, G.D.G. et al., 2018. On the Einthoven Triangle: A Critical Analysis of the Single Rotating Dipole Hypothesis. *Sensors*, 18(7), p.2353. Available at: <http://www.mdpi.com/1424-8220/18/7/2353>.
- Gargiulo, G.D.G. et al., 2016. On the “Zero of Potential of the Electric Field Produced by the Heart Beat”. A Machine Capable of Estimating this Underlying Persistent Error in Electrocardiography. *Machines*, 4(4), p.18. Available at: <http://www.mdpi.com/2075-1702/4/4/18>.
- Goldberger, E., 1942. A simple, indifferent, electrocardiographic electrode of zero potential and a technique of obtaining augmented, unipolar, extremity leads. *American Heart Journal*, 23(4), pp.483–492. Available at: <http://linkinghub.elsevier.com/retrieve/pii/S000287034290293X>.
- Goldberger, E., 1945. The validity of the Einthoven triangle hypothesis. *American Heart Journal*, 29(3), pp.369–377. Available at: <https://www.sciencedirect.com/science/article/pii/0002870345903383> [Accessed March 4, 2019].
- Hoekema, R., Uijen, G.J., & van Oosterom, A., 1999. On selecting a body surface mapping procedure. *Journal of Electrocardiology*, 32(2), pp.93–101. Available at: <https://linkinghub.elsevier.com/retrieve/pii/S0022073699900882>.
- Kossmann, C.E., 1985. Unipolar electrocardiography of Wilson: A half century later. *American Heart Journal*, 110(4), pp.901–904. Available at: <http://linkinghub.elsevier.com/retrieve/pii/0002870385904843>.
- Lynn, M.S. & Timlake, W.P., 1968. The Use of Multiple Deflations in the Numerical Solution of Singular Systems of Equations, with Applications to Potential Theory. *SIAM Journal on Numerical Analysis*, 5(2), pp.303–322. Available at: <http://epubs.siam.org/doi/10.1137/0705027>.
- Macfarlane, P.W., van Oosterom, A. & Janse, M., 2010. *Comprehensive electrocardiology*, 4.
- Madias, J.E., 2008. On recording the unipolar ECG limb leads via the Wilson’s vs the Goldberger’s terminals: aVR, aVL, and aVF revisited. *Indian pacing and electrophysiology journal*, 8(4), pp.292–7. Available at: <http://www.ncbi.nlm.nih.gov/pmc/articles/PMC2572021/>.
- Malmivuo, J. & Plonsey, R., 1995. *Bioelectromagnetism Principles and Applications of Bioelectric and Biomagnetic Fields*, Oxford University Press. Available at: <http://www.oxfordscholarship.com/view/10.1093/acprof:oso/9780195058239.001.0001/acprof-9780195058239>.
- Miyamoto, N. et al., 1995. On the potential of the Wilson central terminal with respect to an ideal reference for unipolar electrocardiography. *J Electrocardiol*, 28(4), pp.336–337. Available at: <http://linkinghub.elsevier.com/retrieve/pii/S0022073605800548>.
- Miyamoto, N. et al., 1996. The absolute voltage and the lead vector of Wilson’s central terminal. *Japanese heart journal*, 37(2), pp.203–14. Available at: <http://www.ncbi.nlm.nih.gov/pubmed/8676547>.
- Okamoto, Y. & Mashima, S., 1998. The zero potential and Wilson’s central terminal in electrocardiography. *Bioelectrochemistry*

- and Bioenergetics*, 47, pp.291–295.
- Undar, A., Calhoon, J.H. & Rocha, A. da, 1997. Medical instrumentation: Application and design. *Control Engineering Practice*, 5(2), pp.295–296. Available at: <http://linkinghub.elsevier.com/retrieve/pii/S0967066197900307>.
- Wach, P. et al., 1997. Magnetic source imaging in the human heart: estimating cardiac electrical sources from simulated and measured magnetocardiogram data. *Medical & Biological Engineering & Computing*, 35(3), pp.157–166. Available at: <http://link.springer.com/10.1007/BF02530031>.
- Waller, A.D., 1887. A Demonstration on Man of Electromotive Changes accompanying the Heart's Beat. *The Journal of Physiology*, 8(5), pp.229–234.
- Webster, J.G., 1978. Medical Instrumentation-Application and Design. *Journal of Clinical Engineering*, 3(3), p.306.
- Webster, J.G., 2009. *Medical Instrumentation Application and Design*, John Wiley & Sons.
- Wilson, F.N. et al., 1934. Electrocardiograms that represent the potential variations of a single electrode. *American Heart Journal*, 9(4), pp.447–458. Available at: <http://linkinghub.elsevier.com/retrieve/pii/S0002870334900934>.
- Wilson, F.N. et al., 1946. On Einthoven's triangle, the theory of unipolar electrocardiographic leads, and the interpretation of the precordial electrocardiogram. *American Heart Journal*, 32(3), pp.277–310. Available at: <http://doi.wiley.com/10.1111/j.1365-2818.1858.tb04542.x>.
- Winter, B.B. & Webster, J.G., 1983. Reduction of Interference Due to Common Mode Voltage in Biopotential Amplifiers. *Biomedical Engineering, IEEE Transactions on*, 30(1), pp.58–62.
- Wolferth, C.C. & Livezey, M.M., 1944. A study of methods of making so-called unipolar electrocardiograms. *American Heart Journal*, 27(6), pp.764–782. Available at: <https://www.sciencedirect.com/science/article/pii/S000287034490311X> [Accessed February 8, 2019].

Article

# Towards Real-Time Heartbeat Classification: Evaluation of Nonlinear Morphological Features and Voting Method

Rajesh N V P S Kandala <sup>1</sup>, Ravindra Dhuli <sup>2</sup>, Paweł Pławiak <sup>3,4,\*</sup>, Ganesh R. Naik <sup>5</sup>, Hossein Moeinzadeh <sup>5</sup>, Gaetano D. Gargiulo <sup>5,6,7</sup> and Suryanarayana Gunnam <sup>8</sup>

<sup>1</sup> Department of ECE, GVPCE (A), Visakhapatnam 530048, India; kandala.rajesh2014@gmail.com

<sup>2</sup> Department of ECE, VIT University, Andhra Pradesh 522237, India; ravindradhuli@gmail.com

<sup>3</sup> Department of Information and Communications Technology, Faculty of Computer Science and Telecommunications, Cracow University of Technology, Warsaw 24 st., F-3, 31-155 Krakow, Poland

<sup>4</sup> Institute of Theoretical and Applied Informatics, Polish Academy of Sciences, Bałtycka 5, 44-100 Gliwice, Poland

<sup>5</sup> The MARCS Institute, Western Sydney University, Milperra, NSW 2214, Australia; ganesh.naik@westernsydney.edu.au (G.R.N.); h.moeinzadeh@westernsydney.edu.au (H.M.); g.gargiulo@westernsydney.edu.au (G.D.G.)

<sup>6</sup> Department of Electrical Engineering and Information Technology (DIETI), “Federico II” The University of Naples, 80100 Naples, Italy

<sup>7</sup> School of Engineering at Western Sydney University, Penrith, NSW 2747, Australia

<sup>8</sup> Institute of Image Processing and Pattern Recognition, Shanghai Jiao Tong University, Shanghai 200240, China; surya\_gunnam@yahoo.co.in

\* Correspondence: plawiak@pk.edu.pl or plawiak.pawel@gmail.com

Received: 20 September 2019; Accepted: 15 November 2019; Published: 21 November 2019

**Abstract:** Abnormal heart rhythms are one of the significant health concerns worldwide. The current state-of-the-art to recognize and classify abnormal heartbeats is manually performed by visual inspection by an expert practitioner. This is not just a tedious task; it is also error prone and, because it is performed, post-recordings may add unnecessary delay to the care. The real key to the fight to cardiac diseases is real-time detection that triggers prompt action. The biggest hurdle to real-time detection is represented by the rare occurrences of abnormal heartbeats and even more are some rare typologies that are not fully represented in signal datasets; the latter is what makes it difficult for doctors and algorithms to recognize them. This work presents an automated heartbeat classification based on nonlinear morphological features and a voting scheme suitable for rare heartbeat morphologies. Although the algorithm is designed and tested on a computer, it is intended ultimately to run on a portable i.e., field-programmable gate array (FPGA) devices. Our algorithm tested on Massachusetts Institute of Technology- Beth Israel Hospital(MIT-BIH) database as per Association for the Advancement of Medical Instrumentation(AAMI) recommendations. The simulation results show the superiority of the proposed method, especially in predicting minority groups: the fusion and unknown classes with 90.4% and 100%.

**Keywords:** electrocardiogram signal; nonlinear features; improved complete ensemble empirical mode decomposition; inter-patient scheme; voting; classification; FPGA

---

## 1. Introduction

### 1.1. Aim of the Work

Nowadays, mortality rates are increasing due to noncommunicable diseases (NCDs) over infectious diseases. Annually about 70% of deaths are because of the NCDs worldwide. As per

the World Health Organization (WHO) report, cardiovascular diseases (CVDs) are the primary cause of death among other NCDs [1]. The effect of CVDs is more in low and middle-income countries. The report demonstrates that this impact will continue further. This alarming scenario influences not only the health perspective, but also the socio-economic advancement of the country. Therefore, the need for adequate diagnosis and treatment for NCDs, especially for CVDs, is highly essential. This situation demands advancements in healthcare technology.

Cardiac arrhythmias are one of the significant sources of CVDs. All arrhythmias may not be fatal, but some need immediate treatment for the patient to survive. Arrhythmias may occur owing to erratic electrical impulse conduction or formation in the heart. Electrocardiograms (ECGs) are an essential tool to study the electrical activity of the heart. ECG discloses any variations in the heartbeat pattern. Clinicians have to explore the longer duration ECG records in the diagnosis process. However, this manual examination is tiresome because of low amplitude and subtle variations in the ECG [2]. Hence, computer-aided diagnosis (CAD) helps clinicians remarkably. CAD-based heartbeat classification is a significant task before the arrhythmia recognition.

### 1.2. State-of-the-Art

If we look at the literature on heartbeat classification, it can be observed that the Massachusetts Institute of Technology-Beth Israel hospital (MIT-BIH) arrhythmia database [3] is the majority choice. The essential literature of heartbeat classification using this database can be categorized into two types based on the assessment process, viz., class-oriented and subject-oriented. The majority among them are class-oriented based works [4–22].

In the class-oriented approach, from the 16 types of beats including the normal ones in the MIT database, a part or an entire collection of beats are preferred for classification. In [4], 17 types of heartbeats including normal and pacemaker are classified using the features based on various power spectrum density methods. Later, a novel genetic algorithm is used to identify the optimum features to enhance the classification process. Finally, these selected features are fed to the various standard machine learning algorithms. In [19], 13 types of heartbeats are classified using the combination of higher-order statistics (HOS) of the ECG and Hermite basis representation features using a support vector machine (SVM) classifier. In [18], six types of heartbeats are classified by using a local fractal dimension based nearest neighbor classifier. In [21], seven types of heartbeats are classified using gray relational analysis. In [20], Ye et al. designed a heartbeat classification algorithm using dynamic and morphological ECG features. For the morphological feature extraction process, the combination of wavelet transform and the dimensionality reduction technique, namely independent component analysis (ICA), is implemented on the heartbeats. R–R intervals are used as dynamic features. These features are then fed to SVM for classifying 16 types of heartbeats. In [8], a novel genetic ensemble of classifiers machine learning method is proposed. A new genetic training coupled with genetic optimization is used to classify 17 types of heartbeats. In [17], statistical and nonlinear features are derived from the modes obtained from the empirical mode decomposition (EMD) algorithm. Later, these features are provided to one-against-one SVM for classifying five types of heartbeats. In [22], ventricular extra systole or ectopic beats are recognized with the help of morphology matching, R–R intervals, and clustering algorithms. In [6], 17 types of EG beats are classified using hexadecimal local patterns calculated from wavelet sub-bands. In [7], five primary types of heartbeats are classified using ensemble empirical mode decomposition (EEMD) based features subjected to sequential minimal optimization-SVM (SMO-SVM). Besides, Neural networks plays a crucial role in biological signal analysis [23]. Recently, deep learning-based class-oriented schemes come into the picture. Deep learning techniques are a part of machine learning techniques implemented based on more hidden neural networks. In [9,10] these works, 17 types of heartbeats are classified using 1D-CNN and a novel 3-layer deep genetic ensemble of classifiers.

In the subject-oriented approach, the entire MIT-BIH database is subdivided into five groups of heartbeats according to the American National Standards Institute/Advancement of Medical



Instrumentation (ANSI/AAMI) EC57:1998 standard. The list of these groups is non-ectopic (N), supraventricular ectopic (S), ventricular ectopic (V), fusion (F), and unknown (Q). Again, two strategies are observed for classifying these distinct groups: intra-patient and inter-patient schemes. The fundamental disagreement between these two strategies is the separation of training and testing datasets. Intra-patient scheme based methods are widely explored in the literature [24–30]. However, these approaches have less impact in real-time scenarios. Because, in real-time applications, an unknown subject that usually undergoes the testing will be foreign to the constructed model. Thus, the model has to be adequate to capture the inter-individual variations among the ECG. While designing the intra-patient based model, there might be a chance of having common subject information in both training and testing. To mitigate such an issue, De Chazal et al. [31] introduced an inter-patient scheme based heartbeat classification. Here, the overall MIT-BIH database is separated into two groups. One group is assigned to training, and the other one is for testing by ensuring that there is no similar subject data in both groups.

The advantage of the aforementioned computer-aided expert systems can be exploited only after developing real-time systems. In literature, in recent years, some of the field-programmable gate array (FPGA) based ECG signal analysis systems are implemented. In [32], an FPGA based heartbeat classification system is developed using the least-squares linear-phase finite impulse response filter and feed-forward neural network. In [33], three types of common arrhythmia beats, namely, premature ventricular contraction, ventricular fibrillation, and heart block beat along with normal beats, are classified using a real-time FPGA implementation. In [34], an intra-patient scheme based on arrhythmia classification is implemented in the FPGA system. However, most of the successful FPGA implemented systems are followed by an intra-patient scheme. Very few methods are developed in real-time systems based on inter-patient schemes [35]. However, still, these systems failed in detecting rare abnormal beats accurately. Hence, there is a need for developing a new expert system that can succeed in identifying rare heartbeats.

### 1.3. Contribution

In this paper, we presented an efficient inter-patient heartbeat classification algorithm. For any pattern recognition process, identifying an appropriate set of features and classifier is highly significant. From [36], it is noticeable that ECG is a non-stationary, non-Gaussian signal derived from nonlinear systems. Hence, we employed a decomposition method, namely improved complete ensemble empirical mode decomposition (ICEEMD) to obtain features from the ECG beats. This technique is capable of disclosing the implicit information lying in the ECG. Later, different nonlinear measures like entropies and HOS are determined from the modes obtained after ICEEMD. These measures will serve as features for proper discrimination of the heartbeat groups. The fundamental difficulty in processing these groups is the class imbalance. Here, a significant fraction of the heartbeats is non-ectopic. Hence, the results may be biased toward the majority group, which is undesirable. Therefore, to alleviate such an issue, we followed an algorithmic level approach. To achieve this, we employed a majority voting scheme based classification. It is a type of ensemble classification. The advantage of ensemble classification is that it can reduce both variance and bias. In this work, we used different combinations of classifiers, namely, naïve Bayes, linear, and quadratic discriminant functions, J48, and consolidated J48 classifiers for majority voting.

The rest of the paper is ordered as follows: the ECG data set, training, and testing data division of AAMI labeling, experimental details and theoretical background of the methodology are presented in Section 2. Section 3 presents the simulation results of the proposed method. The comparison with existing works, limitations, and future directions are presented in Section 4. The conclusions of the work are presented in Section 5.



## 2. Methods

The block diagram of the proposed method is illustrated in Figure 1. The methodology consists of three stages including pre-processing, feature extraction on training and testing data, and a classification model for evaluation. In this section, the database used and the theoretical background of the used techniques are discussed.

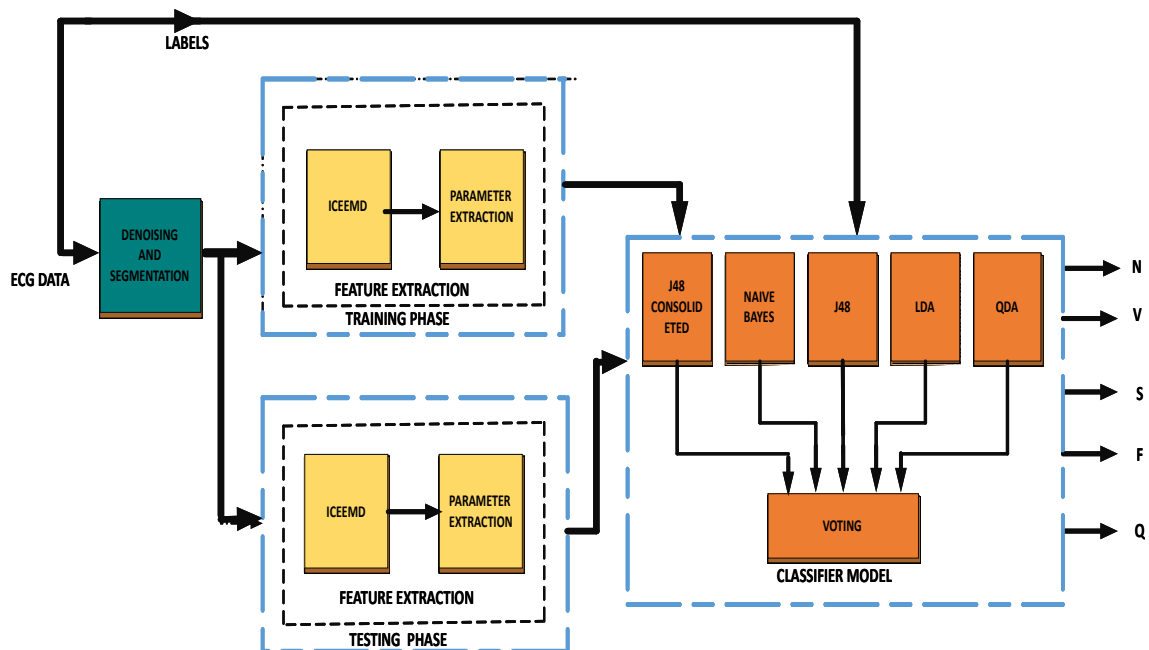


Figure 1. Block diagram of the proposed methodology.

### 2.1. Database

The proposed method is examined using the MIT-BIH arrhythmia database. MIT-BIH is a standard database widely explored for arrhythmia classification. It comprises of Holter monitoring records from several male and female patients. Each record duration is 30 minutes, sampled at 360 Hz. The records consist of both normal and abnormal beats of 15 types.

The annotation files available in the database are obtained from the chart recordings recognized by the experts. This file describes the 'R' peak locations and the labeling of normal and abnormal beats. Based on the recommendations of AAMI, class-labeling was assigned for discriminating various heartbeat groups.

#### AAMI Class Labeling Recommendations

According to the ANSI/AAMI EC57:1998 standard, within the annotation files, beat labels are divided into five groups, namely, N, S, V, F, and Q based on the physiological origin of the beats. Here, the mainly N group consists of normal and bundle branch block beats. S and V groups consist of ectopic beats, originated above and below Atrio Ventricular (A–V) junction of the heart, respectively. The F group consists of the combination of ventricular and normal beats. Unclassifiable beats are placed in the Q group. According to [31], the total number of available heartbeats are divided into training for modeling and testing for evaluation. Details of the number of heartbeats utilized for this work are presented in Table 1.

**Table 1.** Details of the number of beats selected from each group of AAMI classes.

<b>AAMI Classes</b>	<b>MIT-BIH Heartbeats</b>	<b>Total Data</b>	<b>Training (DS1)</b>	<b>Testing (DS2)</b>
N	Normal, left and right bundle branch block atrial and nodal escape beats	83,761	41,746	42,015
S	atrial premature contraction, Aberrated atrial, supra ventricular and junctional premature beats	2614	777	1837
V	premature ventricular contraction, ventricular flutter and escape beats	6893	3787	3106
F	fusion of ventricular and normal beats	526	266	260
Q	paced, unclassifiable, fusion of paced and normal beats	12	6	6

## 2.2. Pre-Processing

Pre-processing is an initial step in any data processing systems. Raw ECG signals will inherently have some artifacts. These may occur due to instrumental noise (power line interference), a physiological signal disturbance (muscular movements), or the environment where the experiment takes place. These artifacts are undesirable and diminish significant features in the ECG. Therefore, to attenuate the effect of this noise, we perform denoising as one of the pre-processing steps. For this, we used a filtering routine proposed by [37] with minimal modification. This operation comprises the following:

1. Mean separation from the noisy ECG,
2. Moving average filter of order five,
3. High-pass filter with cut-off frequency 1 Hz (for baseline wander suppression),
4. Low pass Butter worth filter with cut-off frequency 45 Hz (To suppress any left out high-frequency noise).

We need individual heartbeats from the long-term ECG recording for heartbeat classification. We perform a segmentation process after denoising. In the segmentation process, the annotation chart records with 'R' peak locations are utilized. From the annotation file, it is observed that there are a lot of variations among R-peak positions time-to-time. The difference between the R-peak positions is dynamic. Hence, we applied a window of length 300 samples on ECG signal to obtain an ECG segment that covers the QRS complex which is an important epoch in the ECG. Our segmentation process retains other important epochs like P and T waves, unlike centered R-peak distribution segmentation methods.

## 2.3. Feature Extraction

Feature extraction has a critical role in heartbeat classification. A feature provides crucial information about a signal and facilitates better discrimination of classes. From [36], it is evident that ECG is a non-stationary signal stemming from a nonlinear system. Hence, exploration of ECG with nonlinear methods can improve the performance of a model since they extract subtle information lying in ECG. Therefore, in the feature extraction stage, initially, we perform ICEEMD on ECG segments to get intrinsic mode functions (IMFs). Later, entropy and higher-order cumulants are extracted from the selected modes. In this section, the techniques employed and their support in the methodology development are briefly discussed.

### 2.3.1. ICEEMD

The EMD decomposes a given signal in a full data-dependent approach by exploiting the local characteristics. However, EMD is limited by "mode-mixing" problem while analyzing the real data [38]. Therefore, some noise-assisted data analysis methods can provide a solution. Here, noise is added in a controlled manner for developing new extrema. Thus, the local mean is limited to that of the original version where extrema are generated. A few among these noise assisted methods are EEMD [39] and CEEMD [40]. Among these methods, CEEMD provides a better solution to the mode-mixing problem. However, CEEMD has some limitations:

- (i) Some residual can be present in the modes.
- (ii) During the initial decomposition stages, information may appear "late" with undesired modes, when it is compared to EEMD.

To address these issues, Colominas et al. [41] introduced a new noise aided adaptive data analysis method called ICEEMD. The mathematical details of the ICEEMD are given below [41].

Notation used in algorithm:  $E_l(\cdot)$  =  $l^{\text{th}}$  EMD mode,  $M(\cdot)$  = local mean of the signal,  $\langle \cdot \rangle =$  averaging operator,  $w^{(j)}$  = realization of white Gaussian noise with zero mean and unit variance and  $x$  = input signal.

The algorithm steps:

1. Compute the local means of  $J$  realizations  $x^{(j)} = x + \beta_0 E_1(w^{(j)})$ ,  $j = 1, 2, \dots, J$  using EMD, to obtain first residue  $r_1 = \langle M(x^{(j)}) \rangle$ .
2. At the first stage ( $l = 1$ ), compute the first IMF:

$$C_1 = x - r_1. \quad (1)$$

3. For  $l = 2, \dots, L$ , calculate  $r_l$  as

$$r_l = \langle M(r_{l-1} + \beta_{l-1} E_l(w^{(j)})) \rangle. \quad (2)$$

4. Calculate the  $l^{\text{th}}$  mode as

$$C_l = r_{l-1} - r_l. \quad (3)$$

5. Go to step 3 for next  $l$

Here,  $\beta_l = \epsilon_0 \sigma_{(r_l)}$  is used to obtain the desired SNR at each stage. We choose  $\epsilon_0 = 0.2$ . The resultant IMFs provide significant underlying features of the ECG signal. The ICEEMD is a beneficial tool used for analyzing non-stationary signals originating from nonlinear systems such as bio-signals. The main advantage of ICEEMD is: avoiding the spurious modes and reducing the amount of noise in the mode patterns. Thus, the decomposed IMFs capture the morphology of the signal. Later, entropy and statistical measures are calculated from the first six modes of each ECG segment.

### 2.3.2. Entropy Measures

Entropy measures the uncertainty in a given data. It is often used in signal processing and pattern recognition applications [42]. A high value of entropy maps to higher uncertainty (or) unpredictability. Entropy yields useful information for analyzing non-stationary signals [43]. In this work, we calculated Shannon [44], log energy, and norm entropies [45]. The entropy  $E$  must be an additive cost function such that  $E(0) = 0$  and

$$E(s) = \sum_i E(s_i),$$

where  $s$  is the probability of the given signal and  $i$  represents one of the discrete states. Various entropies are defined below:

- **Shannon Entropy:**

$$E_{\text{Shannon}}(s) = \sum_i s_i^2 \log(s_i^2), \quad (4)$$

- **log Energy Entropy:**

$$E_{\text{log energy}}(s) = \sum_i \log(s_i^2), \quad (5)$$

with the convention  $\log(0) = 0$ .

- **norm Entropy:** The  $l^p$  norm entropy with  $1 \leq p$  is defined as

$$E_{\text{norm}}(s) = \sum_i |(s_i^p)| = \|s\|_p^p. \quad (6)$$

### 2.3.3. HOS

HOS provides a meaningful measure for analyzing non-stationary signals originating from nonlinear systems [46,47]. HOS represents the deviation from Gaussianity and can provide useful information from the non-Gaussian nature of ECG signals. In our work, we utilized second, third, and fourth-order cumulants as HOS. The mathematical details of the HOS can be found in [48].

We construct a feature vector of size  $36 \times 1$  for each heartbeat (6 features  $\times$  6 modes = 36). Later, the training feature set is fed to a classifier for building a model, and that model is evaluated using a testing set.

#### 2.4. Voting Scheme

The final goal of machine learning is to get better-generalized performance. We come across a question “which learning algorithm or classifier is preferred over the other?”. According to a “No free lunch theorem” [49], there is no precise answer to this. One algorithm fits or performs well for a set of training and testing data and may fail for another. The learning algorithm overall performance depends on the prior information, distribution of data, amount of training data, and some cost functions. The performance generalization depends on the bias and variance errors. Always, there will be a trade-off between bias and variance. Ensemble classifiers form a better choice, to improve the performance generalization by reducing bias and variance. Combining several classifiers for the final decision is called an ensemble classification or mixture-of-experts model or modular classification.

The primary motivation behind the classifier ensemble is improving the classification performance using the complementary information offered by various classifiers. Kittler et al. [50] developed a scheme for combining classifiers using voting based on a set of rules: min-rule, max-rule, product-rule, sum-rule, and median-rule. From our experiments, we preferred product rule which outperforms others.

**Mathematical Framework:** Consider a pattern recognition model where a pattern  $y$  is to be assigned with one of the  $m$  possible classes ( $\omega_1, \omega_2, \dots, \omega_m$ ). Say there are  $R$  number of classifiers used for combining. Let us assume that each classifier possesses a different representation of measurement vector  $\mathbf{x}_i, i = 1, 2, \dots, R$ .

The density function for each class  $\omega_k$  in the measurement space is  $p(\mathbf{x}_i|\omega_k)$  and the prior probability is  $P(\omega_k)$ . We assume that the models are mutually exclusive.

From the Bayesian framework,  $y$  is assigned to the class  $\omega_j$  having a maximum posterior probability out of  $\omega_k$  classes:

$$\text{assign } y \rightarrow \omega_j \text{ if } P(\omega_j|\mathbf{x}_1, \mathbf{x}_2, \dots, \mathbf{x}_R) = \max_k P(\omega_k|\mathbf{x}_1, \mathbf{x}_2, \dots, \mathbf{x}_R). \quad (7)$$

Rewriting the posterior probability  $P(\omega_k|\mathbf{x}_1, \mathbf{x}_2, \dots, \mathbf{x}_R)$  using the Bayes theorem:

$$P(\omega_k|\mathbf{x}_1, \mathbf{x}_2, \dots, \mathbf{x}_R) = \frac{p(\mathbf{x}_1, \mathbf{x}_2, \dots, \mathbf{x}_R|\omega_k)P(\omega_k)}{P(\mathbf{x}_1, \mathbf{x}_2, \dots, \mathbf{x}_R)}. \quad (8)$$

Here,  $P(\mathbf{x}_1, \mathbf{x}_2, \dots, \mathbf{x}_R)$  can be expressed in terms of conditional measurement distribution as

$$p(\mathbf{x}_1, \mathbf{x}_2, \dots, \mathbf{x}_R) = \sum_{j=1}^m p(\mathbf{x}_1, \mathbf{x}_2, \dots, \mathbf{x}_R|\omega_j)P(\omega_j). \quad (9)$$

**Product Rule:**  $p(\mathbf{x}_1, \mathbf{x}_2, \dots, \mathbf{x}_R|\omega_j)$  represents the joint probability distribution of the measurements computed by the classifiers. Assuming that these representations are statistically independent, we can rewrite the joint probability distribution as

$$p(\mathbf{x}_1, \mathbf{x}_2, \dots, \mathbf{x}_R|\omega_k) = \prod_{i=1}^R p(\mathbf{x}_i|\omega_k). \quad (10)$$

Based on  $p(\mathbf{x}_i|\omega_k)$ , the measurement process model for  $i^{\text{th}}$  representation is developed. Substituting Equation (10) and Equation (9) into Equation (8)

$$P(\omega_k|\mathbf{x}_1, \mathbf{x}_2, \dots, \mathbf{x}_R) = \frac{P(\omega_k) \prod_{i=1}^R p(\mathbf{x}_i|\omega_k)}{\sum_{j=1}^m p(\omega_j) \prod_{i=1}^R p(\mathbf{x}_i|\omega_j)} \quad (11)$$

and using Equation (11) in Equation (7), we obtain the decision rule

$$\text{assign } \mathbf{y} \rightarrow \omega_j \text{ if } P(\omega_j) \prod_{i=1}^R p(\mathbf{x}_i | \omega_j) = \max_{k=1}^n P(\omega_k) \prod_{i=1}^R p(\mathbf{x}_i | \omega_k). \quad (12)$$

Rewriting in terms of the posterior probabilities obtained from the respective learning algorithms,

$$\text{assign } \mathbf{y} \rightarrow \omega_j \text{ if } \frac{1}{P^{(R-1)}(\omega_j)} \prod_{i=1}^R p(\omega_j | \mathbf{x}_i) = \max_{k=1}^n \frac{1}{P^{(R-1)}(\omega_k)} \prod_{i=1}^R p(\omega_k | \mathbf{x}_i). \quad (13)$$

Equation (13) represents the likelihood decision rule obtained after combining the posterior probabilities generated by different classifiers using the product rule.

In this work, we used five different classifiers for ensembling using a voting scheme to enhance the performance of the system: naïve Bayes [51], linear and quadratic discriminant functions [52], J48 [53], and J48 consolidated classifiers [54]. A brief description of these classifiers is given below.

**Naïve Bayes Classifier:** It is a probability-based learning algorithm developed on the Bayesian framework. According to Bayes theorem, an unknown  $\mathbf{y}$  is categorized into the one among the  $R$  classes, with high posteriori probability:

$$\mathbf{y} \rightarrow \omega_k \text{ if } \arg \max_{\omega_k \in \omega} P(\omega | \mathbf{y}) P(\mathbf{y}), \quad (14)$$

where  $\omega = \{\omega_1, \omega_2, \dots, \omega_R\}$  is a vector of  $R$  classes.

Naïve Bayes is a modified version of Bayes classifier, based on the assumption that the features in an unknown example vector are independent. Therefore, posteriori probability can be written as

$$P(\omega | \mathbf{y}) = P(\mathbf{y} | \omega) P(\omega) = P(y_1, y_2, \dots, y_m | \omega) = P(y_1 | \omega) P(y_2 | \omega) \dots P(y_m | \omega) P(\omega). \quad (15)$$

Hence, Equation (14) can be modified as

$$\mathbf{y} \leftarrow \arg \max_{\omega_k} P(\omega = \omega_k) \prod_i P(y_i | \omega = \omega_k). \quad (16)$$

With this final rule, the naïve Bayes classifier operates. The parameters used for the Naïve Bayes Classifier is given in Table 2.

**Table 2.** Naïve Bayes Classifier parameters used in this work.

Parameters	Naïve Bayes
Use Kernel Estimator	False
Use supervise Discretization	True

In general, the naïve Bayes classifier assumes that the given features follow the normal distribution. In Table 2, use the Kernel Estimator parameter set to false to follow this assumption. Supervised discretization converts a specific range of attribute values to binary values. Here, the term supervised is coined because the class information of the training instances is used for discretization. However, this process is possible only when the class labels are nominal. The advantage of supervised discretization in naïve Bayes classifier is present in [55].

**Linear and Quadratic Discriminant Analysis Based Classifiers:** The approach of discriminant analysis is to derive a decision boundary or a discriminant function based on the linear combinations of features that best separate the given classes. The assumption made is: examples from different

categories follow Gaussian distribution. For instance, the discrimination function for two-class problems based on Bayes theory can be written as

$$(\mathbf{y} - \boldsymbol{\mu}_1)^T \boldsymbol{\Sigma}_1^{-1} (\mathbf{y} - \boldsymbol{\mu}_1) + \ln |\boldsymbol{\Sigma}_1| - (\mathbf{y} - \boldsymbol{\mu}_2)^T \boldsymbol{\Sigma}_2^{-1} (\mathbf{y} - \boldsymbol{\mu}_2) > T, \quad (17)$$

where  $\boldsymbol{\mu}_1, \boldsymbol{\mu}_2$  are the mean vectors of class 1 and class 2,  $\boldsymbol{\Sigma}_1, \boldsymbol{\Sigma}_2$  are the covariance matrices of class 1 and class 2 and  $T$  is the threshold value.

The above function without further assumptions represents the quadratic discriminate function. If the covariance matrices  $\boldsymbol{\Sigma}_1 = \boldsymbol{\Sigma}_2 = \boldsymbol{\Sigma}$ , then the discriminant function simplifies to a dot product.

$$\mathbf{x} \cdot \mathbf{y} > \text{constant}, \quad (18)$$

where  $\mathbf{x} = \boldsymbol{\Sigma}^{-1}(\boldsymbol{\mu}_1 - \boldsymbol{\mu}_2)$ ,  $\text{constant} = \frac{1}{2}(T - \boldsymbol{\mu}_1^T \boldsymbol{\Sigma} \boldsymbol{\mu}_1 - \boldsymbol{\mu}_2^T \boldsymbol{\Sigma} \boldsymbol{\mu}_2)$ . This decision rule represents the classification based on linear discriminant.

The parameters used for linear discriminant analysis (LDA) and quadrature discriminant analysis (QDA) classifiers are given below in Table 3.

**Table 3.** LDA and QDA classifier parameters used in this work.

Parameters	LDA	QDA
Ridge	$1.0 \times 10^{-6}$	$1.0 \times 10^{-6}$

Ridge parameters in the discriminant analysis classifiers reduce the overfitting problem by penalizing the large quantity coefficients. In our work, we use the default values as given in Table 3.

**J48 Classifier:** Recently, decision tree-based algorithms have become popular in machine learning strategies. In practice, J48 is an execution of popular C 4.5 algorithms proposed by Quinlan [53]. According to this algorithm, the decision process involves the construction of a tree based on the feature splitting. The superiority of matching  $\mathbf{y}$  to a class label  $\omega_k \in \boldsymbol{\omega}$  depends on the choice of feature splitting based on the value of information gain.

Information gain is measured with the help of difference entropy as the difference between the entropy of the central node to the sum of entropies of the leaf nodes. It measures how well a given feature splits the training data under its class label. A feature node having high information gain is preferred.

**J48 Consolidated (J48-C) Classifier:** It is a consolidated version of C 4.5 classifier. ‘‘J48 consolidated’’ is an implementation of a consolidated tree’s construction algorithm, proposed by Arbelaz et al. [54] in WEKA. The basic idea is building a single tree using several subsamples. In each iteration, we will find a better feature using information gain content similar to J48. After finding the best feature split, all the subsamples are divided using the same features. More details can be found in [54]. The parameters used for J48 and J48-C classifiers are given in below Table 4.

**Table 4.** J48 and J48-C classifier parameters used in this work.

Parameters	J48	J48-C
Minimum Objects	1000	1000
Use MDL correction	True	True
Number of folds	3	3
Sub-tree raising	True	True

Details of the parameters can be find in WEKA 3.9 version [56].

J48 and J48-C classifiers are decision tree classifiers in which tree splitting criteria play a significant role. The above-mentioned parameters determine the growth and direction of the tree structures that influence the final model accuracy. Sub-tree raising considers raising of a sub-tree when pruning is

enabled. The minimum number of objects determines the number of instances per leaf. Minimum description length (MDL) correction is a statistical measure like information gain to identify the best split tree. The number of folds determines the data used for error reduce pruning; here, one fold is for pruning and the other folds for building the tree.

All the parameters are fixed based on the final results. All the details of the parameters can be found in WEKA 3.9 version [56].

### 3. Results

In this work, we are classifying the five classes: N, V, S, F, Q. The training set is constructed with the array of records as DS1 = [101, 106, 108, 109, 112, 114, 115, 116, 118, 119, 122, 124, 201, 203, 205, 207, 208, 209, 215, 220, 223, 230], and DS2 = [100, 103, 105, 111, 113, 117, 121, 123, 200, 202, 210, 212, 213, 214, 219, 221, 222, 228, 231, 232, 233, 234]. Here, the numerical values represent the patient record number. Four records (102, 104, 107 and 217) having paced beats are exempted from both DS1 and DS2 data sets.

We start with scatter plots for justifying the choice of features in discriminating against the heartbeats. Individual performance of five classifiers naïve Bayes, LDA, QDA, J48, and J48 consolidated is presented, and analysis using a voting scheme with various combinations of these classifiers is considered. The performance is illustrated for each combination. We used the WEKA 3.9 version (University of Waikato, New Zealand) [56] for implementing the classification algorithms and scatter plots. Data pre-processing and feature extraction is implemented using MATLAB 2018a (Mathworks, MA, USA). All the experiments are carried out in Windows 8, 8 GB RAM, and 64-bit operating system.

#### The Performance Measures

An algorithm's efficiency can be validated with appropriate performance measures. In this work, Sensitivity (SEN), False Positive Rate (FPR), Positive Predictive Value (PPV), and Overall Accuracy (OA) are used as performance measures to compare with the state-of-the-art methods, following the AAMI recommendations. The confusion matrix required for calculating these measures is given in Table 5. For V and S classes, the measures are calculated as per [31]. For remaining classes, we followed [57].

**Table 5.** Confusion matrix.

Actua Labels	Predicted Labels					Sum
	N	V	S	F	Q	
N	$N_n$	$N_v$	$N_s$	$N_f$	$N_q$	$R_N$
V	$V_n$	$V_v$	$V_s$	$V_f$	$V_q$	$R_V$
S	$S_n$	$S_v$	$S_s$	$S_f$	$S_q$	$R_S$
F	$F_n$	$F_v$	$F_s$	$F_f$	$F_q$	$R_F$
Q	$Q_n$	$Q_v$	$Q_s$	$Q_f$	$Q_q$	$R_Q$
Sum	$C_N$	$C_V$	$C_S$	$C_F$	$C_Q$	$R/C$

Performance measure from Table 5 can be calculated as follows:

The sum measures of row-wise and column-wise calculations are:

$$\begin{aligned}
 R_N &= N_n + N_v + N_s + N_f + N_q; & C_N &= N_n + V_n + S_n + F_n + Q_n; \\
 R_V &= V_n + V_v + V_s + V_f + V_q; & C_V &= N_v + V_v + S_v + F_v + Q_v; \\
 R_S &= S_n + S_v + S_s + S_f + S_q; & C_S &= N_s + V_s + S_s + F_s + Q_s; \\
 R_F &= F_n + F_v + F_s + F_f + F_q; & C_F &= N_f + V_f + S_f + F_f + Q_f; \\
 R_Q &= Q_n + Q_v + Q_s + Q_f + Q_q; & C_Q &= N_q + V_q + S_q + F_q + Q_q; \\
 R &= R_N + R_V + R_S + R_F + R_Q; & C &= C_N + C_V + C_S + C_F + C_Q; \\
 R &= C.
 \end{aligned} \tag{19}$$



The false-positive and false negative values for each class are defined as below:

$$\begin{aligned}
 FN_N &= R_N - N_n; & FP_N &= C_N - N_n; \\
 FN_V &= R_V - V_v; & FP_V &= C_V - (V_v + F_v + Q_v); \\
 FN_S &= R_S - S_s; & FP_S &= C_S - (S_s + Q_s); \\
 FN_F &= R_F - F_f; & FP_F &= C_N - F_f; \\
 FN_Q &= R_Q - Q_q; & FP_Q &= C_N - Q_q.
 \end{aligned} \tag{20}$$

The other useful measures, true positives, and negatives can be calculated for Classes N,V,S,F,Q:

$$\begin{aligned}
 TP_N &= N_n; & TN_N &= R - (R_N + C_N - N_n); \\
 TP_V &= V_v; & TN_V &= R - (R_V + C_V - V_v); \\
 TP_S &= S_s; & TN_S &= R - (R_S + C_S - S_s); \\
 TP_F &= F_f; & TN_F &= R - (R_F + C_F - F_f); \\
 TP_Q &= Q_q; & TN_Q &= R - (R_Q + C_Q - Q_q).
 \end{aligned} \tag{21}$$

The performance measures are given by

$$SEN = \frac{TP}{TP + FN}; FPR = \frac{FP}{TN + FP}; PPV = \frac{TP}{TP + FP}; OA = \frac{TP_N + TP_V + TP_S + TP_F + TP_Q}{R},$$

where  $TP$  = True Positive,  $TN$  = True Negative,  $FP$  = False Positive, and  $FN$  = False Negative.

We present the scatter plots with marginal histograms on the testing data set DS2, for features in the two-dimensional feature space. These scatter plots reveal how different features spread in feature space, thereby revealing the relationship between different heartbeat classes. Figure 2 shows the two-dimensional scatter plot between cumulant 2 of IMF1 to norm entropy value of IMF2. In this plot, we can observe that N and V beats are dominantly spread across space. In addition, the histogram plots also reveal the good discrimination between N, V, and Q classes out of the five classes. The next plot from Figure 3 gives the relation between the log energy entropy of IMF1 to cumulant 2 of IMF1. In this figure, we can see the spreading of N, V, S, and F classes in the space. In particular, this space provides good discrimination between N, V, and S classes. From Figures 4–6, we can observe that log energy entropy values extracted from different IMFs provide a good perception of N, V, and S classes.

In the same way, Figures 7–8 give better discrimination of Q beats, which are very rare indeed. In these figures, the characteristic feature is the norm entropy. In addition, different combinations of features with norm entropy reveal different class spreads and discrimination capabilities. As a whole, we can say that the combinations of selected features from different IMFs can predict the required hypothesis.

After dividing the training and testing feature sets, we need to learn a model for classification. In this work, we used an ensemble learner for classification. Ensemble classifiers use multiple learning algorithms and combine all the decisions. It can be more accurate than the individual classifiers. The main advantage of the ensemble classifiers is that we can achieve low bias error and low variance error. Ensembles using multiple trained (high variance/ low bias) models can average out of the variance, leaving just the bias. In addition, ensemble classifiers are preferred for imbalanced datasets. Our DS1 and DS2 datasets are highly imbalanced with majority N group class and minor F and Q classes. Therefore, in this work, we used a voting scheme based on product rule to ensemble the classifiers. The individual classifier performance on DS2 (testing data) is presented in Tables 6 and 7. Confusion matrices calculated for LDA, QDA, naïve Bayes, J48 and J48-C classifiers are shown in Table 6. The performance measures for the corresponding matrices based on Table 5 are presented in Table 7.

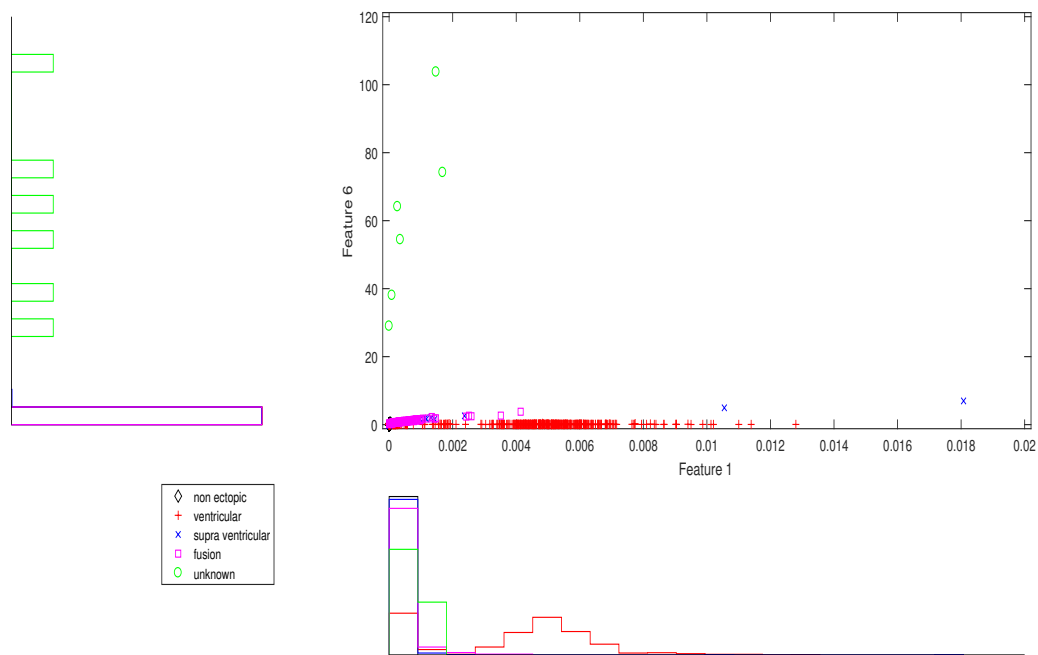


Figure 2. Scatter plot with marginal histogram for CUM2 (IMF1) vs. norm entropy (IMF1).

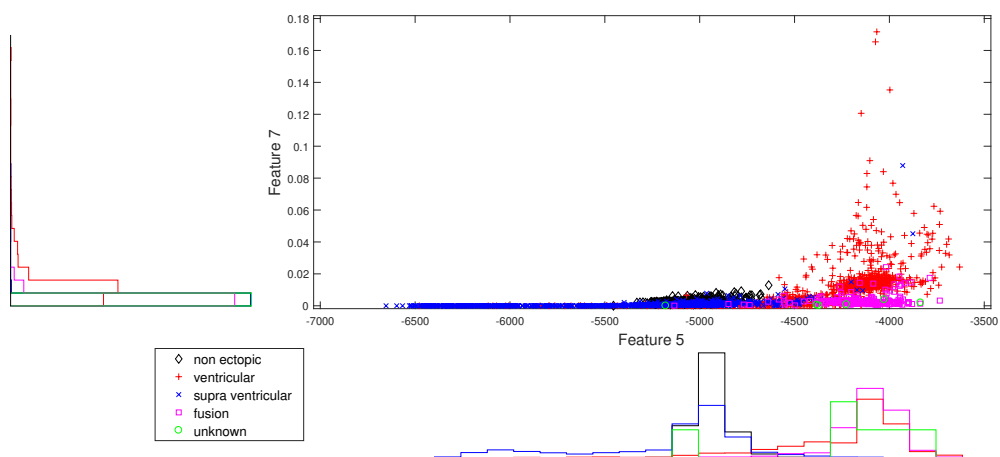


Figure 3. Scatter plot with marginal histogram for log entropy (IMF1) vs. CUM2 (IMF1).

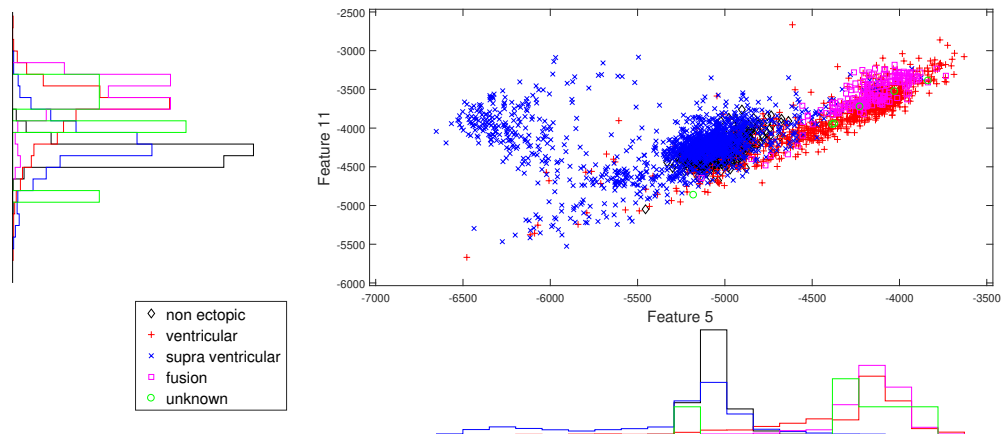


Figure 4. Scatter plot with marginal histogram for log entropy (IMF1) vs. log entropy (IMF2).

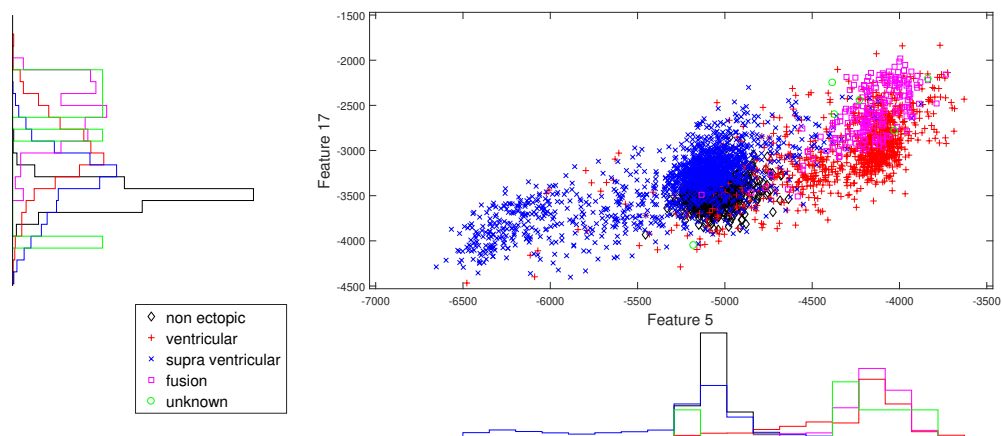


Figure 5. Scatter plot with marginal histogram for log entropy (IMF1) vs. log entropy (IMF3).

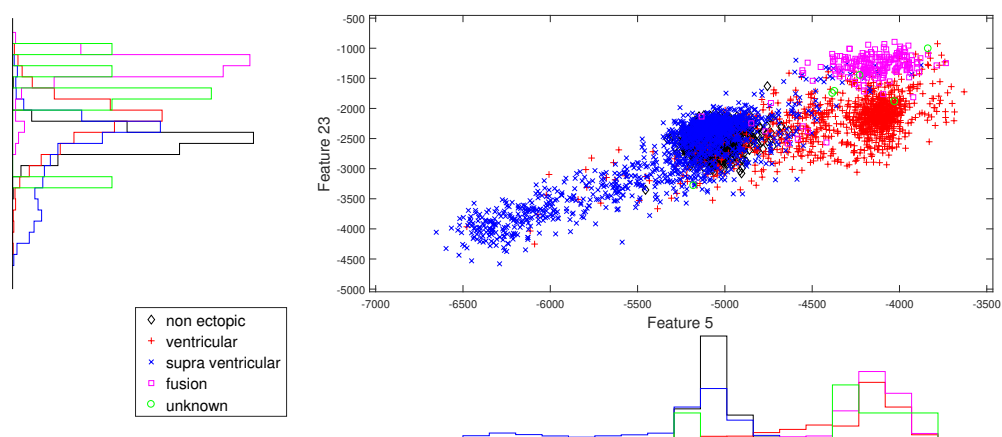
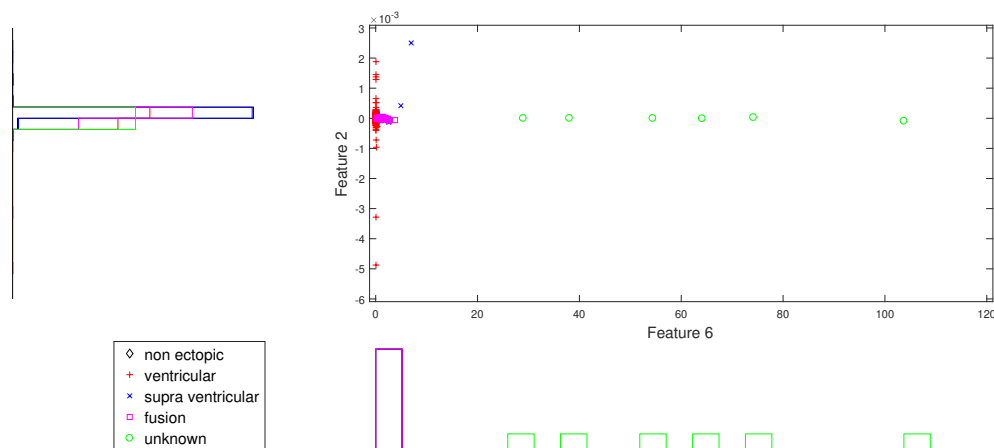
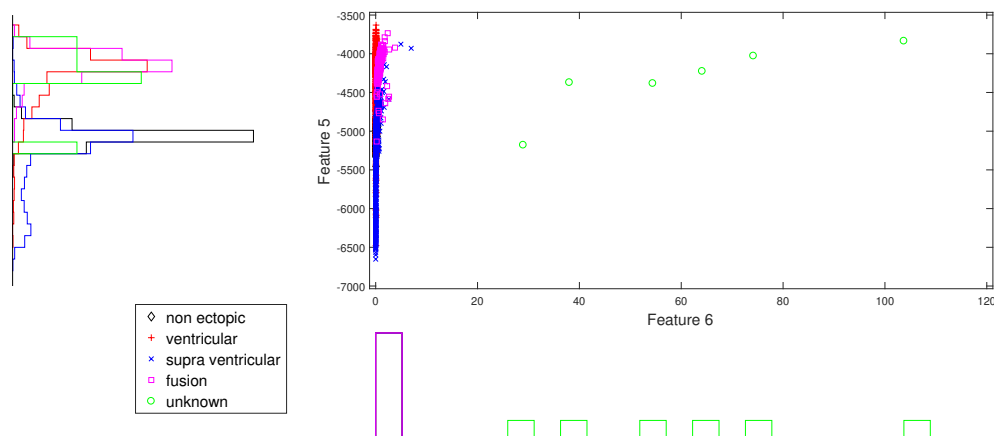


Figure 6. Scatter plot with marginal histogram for log entropy (IMF1) vs. log entropy (IMF4).



**Figure 7.** Scatter plot with marginal histogram for norm entropy (IMF1) vs. CUM2 (IMF1).



**Figure 8.** Scatter plot with marginal histogram for norm entropy (IMF1) vs. log entropy (IMF1).

From this table, we can see that each classifier yields different prediction. LDA and J48 give better classification for the N and V classes. It is an understandable phenomenon because of the dominating number of examples in N and V. LDA and J48-C provides better discrimination to Q group. The other classifiers J48-C and naïve Bayes are providing better SEN results for F group. Finally, S class is predicted accurately by J48-C and QDA classifiers. The other important point is, although all classifiers yield better results for the specific group of categories, the OA is dominated by the N class discrimination. Therefore, it is noticeable that OA is no longer a useful performance measure for imbalanced data classification.

In Table 8, the confusion matrix after combining J48, LDA, and naïve Bayes classifiers using the voting scheme is presented. The corresponding performance measures are demonstrated in Table 9. From the results, it is evident that this combination yields better results for N, V, F, and Q classes and average result for S class. The critical point is N, and S classes have more morphological similarities. Therefore, individual classifiers are giving complementary results for N and S. However, this ensemble selection enhances the prediction generalization for both classes.

**Table 6.** Confusion matrices for LDA, QDA, naïve Bayes, J48, and J48-C classifiers.

		LDA					QDA				
		N	V	S	F	Q	N	V	S	F	Q
N	40,842	33	47	1093	0	2777	266	36,394	2578	0	0
V	319	2787	0	0	0	5	3101	0	0	0	0
S	1831	1	2	3	0	95	56	1675	11	0	0
F	171	0	0	89	0	91	64	20	85	0	0
Q	0	0	0	0	6	0	6	0	0	0	0
		naïve Bayes					J48				
		N	V	S	F	Q	N	V	S	F	Q
N	36,222	745	997	3289	762	41,801	214	0	0	0	0
V	930	1874	52	231	19	363	2743	0	0	0	0
S	1321	3	133	27	353	1819	18	0	0	0	0
F	8	0	2	245	5	259	1	0	0	0	0
Q	1	0	0	4	1	5	1	0	0	0	0
		J48-C									
		N	V	S	F	Q					
		N	0	6941	28,966	5290	818				
		V	0	2205	894	6	1				
		S	0	24	1785	19	9				
		F	0	30	23	191	16				
		Q	0	0	0	0	6				

**Table 7.** Performance measures for LDA, QDA, naïve Bayes, J48 and J48-C classifiers.

		LDA				QDA			
		OA = 92.60	SEN%	FPR%	PPV%	OA = 16.20	SEN%	FPR%	PPV%
N		97.2	44.6	94.6		6.6	3.7	93.6	
V		89.7	0.1	98.8		99.8	0.9	88.8	
S		0.1	0.1	4.1		91.2	80.2	4.4	
F		34.2	2.3	7.5		32.7	5.5	3.2	
Q		100	0	100		0	0	0	
		naïve Bayes				J48			
		OA = 81.47	SEN%	FPR%	PPV%	OA = 94.32	SEN%	FPR%	PPV%
N		86.2	43.4	94.1		99.5	47	94.5	
V		60.3	1.7	71.5		88.3	0.5	92.1	
S		7.2	2.3	11.2		0	0	0	
F		94.2	7.6	6.5		0	0	0	
Q		16.7	2.4	0.1		0	0	0	
		J48-C							
		OA = 8.86	SEN%	FPR%	PPV%				
		N	0	0	0				
		V	71.0	15.9	24.0				
		S	97.2	65.8	5.6				
		F	73.5	11.3	3.5				
		Q	100	1.8	0.7				

**Table 8.** Confusion matrix for combining J48, LDA, and naïve Bayes classifiers using a Voting scheme.

		Voting (J48, LDA, naïve Bayes)				
		N	V	S	F	Q
N	39,542	53	489	1931	0	0
V	395	2708	3	0	0	0
S	1473	1	353	10	0	0
F	22	5	1	232	0	0
Q	0	0	0	0	0	6

**Table 9.** Performance measures for combining J48, LDA, and naïve Bayes classifiers using a Voting scheme.

<b>Voting (J48, LDA, naïve Bayes)</b>			
OA = 90.71	SEN%	FPR%	PPV%
N	94.1	36.3	95.4
V	87.2	0.1	97.9
S	19.2	1.1	41.7
F	89.2	4.1	10.7
Q	100	0	100

Similarly, we performed ensemble voting for different combinations and the results are presented in Tables 10–15. Each combination provides various enhanced results in some aspects.

**Table 10.** Confusion matrix for combining J48, naïve Bayes, and QDA classifiers using a voting scheme.

<b>Voting (J48, naïve Bayes, QDA)</b>					
	N	V	S	F	Q
N	35,629	253	3836	2297	0
V	11	3095	0	0	0
S	1188	11	624	14	0
F	28	61	11	160	0
Q	0	6	0	0	0

**Table 11.** Performance measures for combining J48, naïve Bayes, and QDA classifiers using a Voting scheme.

<b>Voting (J48, naïve Bayes, QDA)</b>			
OA = 83.6	SEN%	FPR%	PPV%
N	84.8	23.6	96.7
V	99.6	0.8	90.3
S	34	8.5	14
F	61.5	4.9	6.5
Q	0	0	0

**Table 12.** Confusion matrix for combining J48-C, naïve Bayes, and QDA classifiers using a Voting scheme.

<b>Voting (J48-C, naïve Bayes, QDA)</b>					
	N	V	S	F	Q
N	29,730	255	9089	2491	0
V	8	3098	0	0	0
S	1031	8	779	19	0
F	21	61	12	166	0
Q	0	6	0	0	0

As mentioned earlier, the dataset is dominated by N, V, and S classes, respectively. The F and Q classes are sporadic. Therefore, in some works, only N, V, and S classes are considered for classification. We provide the results for such schemes in Tables 16–25. Here, first results are also presented for individual classifiers; later, the ensemble voting scheme is performed on different combinations of classifiers. Each one gives better classifications than individual classifiers.

**Table 13.** Performance measures for combining J48-C, naïve Bayes, and QDA classifiers using a Voting scheme.

<b>Voting (J48-C, naïve Bayes, QDA)</b>			
OA = 71.51	SEN%	FPR%	PPV%
N	70.8	20.3	96.6
V	99.7	0.7	90.4
S	42.4	20.1	7.9
F	63.8	6.3	5.3
Q	0	0	0

**Table 14.** Confusion matrix for combining J48-C, naïve Bayes, and LDA classifiers using a Voting scheme.

<b>Voting (J48-C, naïve Bayes, LDA)</b>					
	N	V	S	F	Q
N	38,329	66	942	2678	0
V	553	2532	20	1	0
S	1405	2	416	14	0
F	20	4	1	235	0
Q	0	0	0	0	6

**Table 15.** Performance measures for combining J48-C, naïve Bayes, and LDA classifiers using a Voting scheme.

<b>Voting (J48-C, naïve Bayes, LDA)</b>			
OA = 87.91	SEN%	FPR%	PPV%
N	91.2	38	95.1
V	81.5	0.2	97.2
S	22.6	2.1	30.2
F	90.4	5.7	8
Q	100	0	100

**Table 16.** Confusion matrices for various classifiers (N, V, and S classes).

	<b>LDA</b>			<b>QDA</b>		
	N	V	S	N	V	S
N	41,875	27	113	4569	480	36,966
V	280	2826	0	5	3101	0
S	1835	0	2	105	56	1676
	<b>naïve Bayes</b>			<b>J48</b>		
	N	V	S	N	V	S
N	37,385	2968	1662	41,998	17	0
V	922	2120	64	1095	2011	0
S	1336	18	483	1837	0	0
	<b>J48-C</b>					
		N	V	S		
	N	34,999	7016	0		
	V	651	2455	0		
S	1585	252	0			

**Table 17.** Performance measures for various classifiers (N,V, S classes).

<b>LDA</b>				<b>QDA</b>			
OA = 95.19	SEN%	FPR%	PPV%	OA = 19.90	SEN%	FPR%	PPV%
N	99.7	42.8	95.2		10.9	2.2	97.6
V	91.0	0.1	99.1		99.8	1.2	85.3
S	0.1	0.3	1.7		91.2	81.9	4.3
<b>naïve Bayes</b>				<b>J48</b>			
OA = 85.15	SEN%	FPR%	PPV%	OA = 93.71	SEN%	FPR%	PPV%
N	89	45.7	94.3		100	59.3	93.5
V	68.3	6.8	41.5		64.7	0	99.2
S	26.3	3.8	21.9		0	0	0
<b>J48-C</b>							
				OA = 79.76	SEN%	FPR%	PPV%
				N	83.3	45.2	94
				V	79	16.6	25.2
				S	0	0	0

**Table 18.** Confusion matrix for combining J48, LDA, and naïve Bayes classifiers using a Voting scheme (N,S,V).

<b>Voting ( J48, LDA, naïve Bayes)</b>			
	N	V	S
N	40,918	361	736
V	205	2897	4
S	1469	3	365

**Table 19.** Performance measures for combining J48, LDA, and naïve Bayes classifiers using Voting scheme (N,S,V).

<b>Voting ( J48, LDA, naïve Bayes)</b>			
OA = 94.08	SEN%	FPR%	PPV%
N	97.4	33.9	96.1
V	93.3	0.8	88.8
S	19.9	1.6	33

**Table 20.** Confusion matrix for combining J48, naïve Bayes, and QDA classifiers using Voting scheme (N,S,V).

<b>Voting ( J48, naïve Bayes, QDA)</b>			
	N	V	S
N	37,421	574	4020
V	12	3094	0
S	1203	8	626



**Table 21.** Performance measures for combining J48, naïve Bayes, and QDA classifiers using Voting scheme (N,S,V).

<b>Voting ( J48, naïve Bayes, QDA)</b>			
OA = 87.61	SEN%	FPR%	PPV%
N	89.1	24.6	96.9
V	99.6	1.3	84.2
S	34.1	8.9	13.5

**Table 22.** Confusion matrix for combining J48-C, naïve Bayes, and QDA classifiers using Voting scheme (N,S,V).

<b>Voting ( J48-C, naïve Bayes, QDA)</b>			
	N	V	S
N	32011	598	9406
V	7	3099	0
S	1062	8	767

**Table 23.** Performance measures for combining J48-C, naïve Bayes, and QDA classifiers using Voting scheme (N,S,V).

<b>Voting ( J48-C, naïve Bayes, QDA)</b>			
OA = 76.40	SEN%	FPR%	PPV%
N	76.2	21.6	96.8
V	99.8	1.4	83.6
S	41.8	20.8	7.5

**Table 24.** Confusion matrix for combining J48-C, naïve Bayes, and LDA classifiers using Voting scheme (N,S,V).

<b>Voting ( J48-C, naïve Bayes, LDA)</b>			
	N	V	S
N	40,248	688	1079
V	359	2735	12
S	1407	2	428

**Table 25.** Performance measures for combining J48-C, naïve Bayes, LDA classifiers using Voting scheme (N,S,V).

<b>Voting ( J48-C, naïve Bayes, LDA)</b>			
OA = 92.44	SEN%	FPR%	PPV%
N	95.8	35.7	95.8
V	88.1	1.6	79.9
S	23.3	2.4	28.2

#### 4. Discussion

This section contains a discussion on simulating the proposed methodology illustrated in Figure 1. In this work, we employ an adaptive non-stationary and nonlinear decomposition method, namely ICEEMD, to analyze the ECG heartbeats. ICEEMD produces a local and entirely data-driven separation of a signal in the form of fast and slow oscillations called IMFs. The main advantage of ICEEMD is that it successfully avoids the spurious nodes and reduces the amount of noise in the modes.

Later, six nonlinear morphological features: higher-order cumulants, log, Shannon energy, and norm entropies are extracted from the first six IMFs of each heartbeat, to generate a  $36 \times 1$  feature vector. Then, these feature vectors are divided based on training and testing sets DS1 and DS2 as specified above. Statistics (median and interquartile range) of these features for each class are presented in Table 26. Variation of attributes corresponding to different heartbeats can be observed from this table.

In Table 6, we presented the individual performance of various classifiers on the given problem. Here, all classifier models offer separate results for all the classes. Each model performs well for a specific class or classes. However, it fails in providing the overall better performance. For example, the S class contains 1837 beats, the J48, LDA, and naïve Bayes are predicting 51, 2, 1516 beats, respectively. Whenever we combine these three models using the voting scheme as shown in Table 12, this combined model identified 779 beats correctly. The voting scheme uses the product of probabilities rule. In this scheme, it is assumed that each model representation for a given class is statistically independent. It is because of the different representation capabilities of each model. From this, a final decision rule is formed as described in Section 2.4. This decision rule quantifies the probability of class choice from combined hypothesis models and the same type of results we can observe for other classes. In this work, we implemented four voting schemes with different classifier combinations. Each combination again provides different but better results than individual classifier models. The proposed combinations of classifier details are given in Table 27.

Table 26. Median  $\pm$  interquartile range of features extracted on DS1.

Feature Number	Features	N	S	V	F	Q
1	CUM2(IMF1)	$1.0 \times 10^{-6} \pm 4.0 \times 10^{-6}$	$8.0 \times 10^{-6} \pm 4.03 \times 10^{-5}$	$7.50 \times 10^{-5} \pm 0.00045775$	$0.000162 \pm 0.000326$	$0.0001405 \pm 0.009121$
2	CUM3(IMF1)	$0 \pm 0$	$0 \pm 0$	$0 \pm 2.0 \times 10^{-6}$	$0 \pm 5.0 \times 10^{-6}$	$0 \pm 0.000313$
3	CUM4(IMF1)	$0 \pm 0$	$0 \pm 0$	$1.0 \times 10^{-6} \pm 2.58 \times 10^{-5}$	$2.50 \times 10^{-6} \pm 1.1 \times 10^{-5}$	$4.5 \times 10^{-6} \pm 0.006113$
4	Shan(IMF1)	$0.004769 \pm 0.009686$	$0.017643 \pm 0.06530625$	$0.112159 \pm 0.4199265$	$0.216149 \pm 0.330006$	$0.153638 \pm 1.47632$
5	log(IMF1)	$-4792.4962 \pm 379.828$	$-4735.1172 \pm 286.978$	$-4532.44 \pm 467.507$	$-4358.371 \pm 271.824$	$-4604.445 \pm 1783.20$
6	norm(IMF1)	$0.1004 \pm 0.0726$	$0.1538 \pm 0.1719$	$0.0815 \pm 0.05794$	$0.5541 \pm 0.5434$	$18.1790 \pm 20.55612$
7	CUM2(IMF2)	$0.001 \pm 0.00347$	$0.00109 \pm 0.0035$	$0.00028 \pm 0.00137$	$0.00107 \pm 0.00143$	$0.00411 \pm 0.0134$
8	CUM3(IMF2)	$8.0 \times 10^{-6} \pm 5.20 \times 10^{-5}$	$4.0 \times 10^{-6} \pm 5.10 \times 10^{-5}$	$0 \pm 6.0 \times 10^{-6}$	$5.0 \times 10^{-6} \pm 2.10 \times 10^{-5}$	$0 \pm 0.000387$
9	CUM4(IMF2)	$1.50 \times 10^{-5} \pm 0.000185$	$2.10 \times 10^{-5} \pm 0.000128$	$2.0 \times 10^{-6} \pm 4.20 \times 10^{-5}$	$1.60 \times 10^{-5} \pm 5.20 \times 10^{-5}$	$0.00046 \pm 0.002581$
10	Shan(IMF2)	$1.3074 \pm 2.9180$	$1.3675 \pm 3.4250$	$0.431 \pm 1.429$	$1.4044 \pm 1.44285$	$2.90440 \pm 6.76104$
11	log(IMF2)	$-4055.72 \pm 403.632$	$-4045.57 \pm 565.833$	$-4064.90 \pm 479.11$	$-3788.21 \pm 266.57$	$-4023.39 \pm 1366.58$
12	norm(IMF2)	$2.41 \pm 3.81$	$2.57 \pm 4.95$	$2.744 \pm 1.768$	$2.69 \pm 2.04$	$18.17 \pm 20.556$
13	CUM2(IMF3)	$0.0069 \pm 0.0097$	$0.00534 \pm 0.009013$	$0.00443 \pm 0.00936$	$0.011997 \pm 0.00909$	$0.004148 \pm 0.008015$
14	CUM3(IMF3)	$-7.80 \times 10^{-5} \pm 0.000322$	$-8.60 \times 10^{-5} \pm 0.0003605$	$-3.10 \times 10^{-5} \pm 0.000246$	$-0.00019 \pm 0.00062$	$8.95 \times 10^{-5} \pm 0.000266$
15	CUM4(IMF3)	$0.000235 \pm 0.000863$	$0.000104 \pm 0.0006515$	$0.000117 \pm 0.000747$	$0.0005255 \pm 0.000767$	$0.0001945 \pm 0.000396$
16	Shan(IMF3)	$6.3075515 \pm 6.075866$	$5.532014 \pm 6.254886$	$4.570122 \pm 5.93904725$	$10.002892 \pm 5.49255$	$3.8205085 \pm 6.888019$
17	log(IMF3)	$-3114.4106 \pm 443.70730$	$-3071.71175 \pm 705.504$	$-3178.659 \pm 531.3571$	$-2731.2660 \pm 467.4692$	$-3341.5431 \pm 891.0573$
18	norm(IMF3)	$9.3564 \pm 7.6444$	$8.69133 \pm 8.37546$	$7.585 \pm 4.1465$	$14.85 \pm 7.440$	$18.179 \pm 20.55$
19	CUM2(IMF4)	$0.013817 \pm 0.0210$	$0.01233 \pm 0.01653$	$0.0215 \pm 0.03611$	$0.0370 \pm 0.0297$	$0.0069 \pm 0.0102$
20	CUM3(IMF4)	$-0.00012 \pm 0.00081$	$-6.80 \times 10^{-5} \pm 0.000469$	$-0.00014 \pm 0.001305$	$-0.001542 \pm 0.00207$	$0 \pm 0.00039$
21	CUM4(IMF4)	$0.000147 \pm 0.000734$	$4.60 \times 10^{-5} \pm 0.0003225$	$0.000404 \pm 0.00189$	$0.00027 \pm 0.00124$	$0.000138 \pm 0.00018$
22	Shan(IMF4)	$13.05585 \pm 12.76457$	$12.2365 \pm 11.295$	$16.104 \pm 15.135$	$25.934 \pm 15.110$	$7.113 \pm 10.471$
23	log(IMF4)	$-2150.494 \pm 533.542$	$-2143.567 \pm 611.308$	$-2206.943 \pm 794.75$	$-1614.17 \pm 480.99$	$-2593.22 \pm 1271.81$
24	norm(IMF4)	$19.367 \pm 15.509$	$18.686 \pm 14.240$	$16.26 \pm 9.166$	$35.59 \pm 20.941$	$18.179 \pm 20.556$
25	CUM2(IMF5)	$0.0084 \pm 0.018$	$0.0066 \pm 0.0156$	$0.033 \pm 0.0648$	$0.056 \pm 0.058$	$0.0075 \pm 0.0149$
26	CUM3(IMF5)	$1.0 \times 10^{-6} \pm 0.00017$	$0 \pm 0.000103$	$-1.0 \times 10^{-6} \pm 0.00146$	$1.40 \times 10^{-5} \pm 0.0022$	$0 \pm 0.000405$
27	CUM4(IMF5)	$-7.00 \times 10^{-6} \pm 0.00012$	$-6.0 \times 10^{-6} \pm 0.000127$	$-3.0 \times 10^{-5} \pm 0.00193$	$-0.00236 \pm 0.00621$	$-5.50 \times 10^{-6} \pm 0.000287$
28	Shan(IMF5)	$10.358 \pm 15.6374$	$8.68112 \pm 14.823$	$25.882 \pm 29.195$	$39.2240 \pm 25.737$	$8.992 \pm 16.965$
29	log(IMF5)	$-1917.009 \pm 593.83$	$-1992.177 \pm 872.920$	$-1567.422 \pm 918.993$	$-1216.140 \pm 489.3834$	$-2179.500 \pm 1495.143$
30	norm(IMF5)	$17.118 \pm 19.0735$	$14.983 \pm 19.2726$	$19.495 \pm 14.659$	$52.96 \pm 32.190$	$18.179 \pm 20.556$
31	CUM2(IMF6)	$0.0040 \pm 0.0092$	$0.0028 \pm 0.00723$	$0.0184 \pm 0.04606$	$0.0571 \pm 0.0827$	$0.0073 \pm 0.01072$
32	CUM3(IMF6)	$1.0 \times 10^{-6} \pm 0.00010$	$0 \pm 6.80 \times 10^{-5}$	$2.0 \times 10^{-6} \pm 0.0011117$	$8.0 \times 10^{-6} \pm 0.00527$	$0 \pm 0.0002$
33	CUM4(IMF6)	$-1.50 \times 10^{-5} \pm 0.00011$	$-8.0 \times 10^{-5} \pm 6.25 \times 10^{-5}$	$-0.00024 \pm 0.00205$	$-0.00389 \pm 0.01428$	$-4.40 \times 10^{-5} \pm 0.00017$
34	Shan(IMF6)	$6.50405 \pm 11.11697$	$5.26119 \pm 9.9055$	$20.0112 \pm 31.26347$	$44.49 \pm 39.5131$	$10.284 \pm 13.481$
35	log(IMF6)	$-1903.169 \pm 637.510$	$-1983.32 \pm 713.457$	$-1470.196 \pm 744.176$	$-1062.5 \pm 546.13$	$-1682.363 \pm 1296.591$
36	norm(IMF6)	$13.0914 \pm 15.1495$	$11.4410 \pm 14.268$	$10.566 \pm 12.262$	$57.357 \pm 46.317$	$18.179 \pm 20.556$

Note: CUM2-second order cumulat, CUM3-third order cumulant, CUM4-Fourth order cumulant, Shan-Shannon entropy, log-Log entropy, norm- norm entropy.

#### 4.1. Comparative Analysis

To assess the performance of our proposed methodology, we compared our results with the existing methods in the literature. Comparisons are presented in Tables 28 and 29. The features and classification schemes employed by various researchers listed in Tables 28 and 29 are given in Table 27. In Table 28, we compare our four sets of voting schemes with the works which followed AAMI recommendations based on [31] division scheme. In addition, Table 29 shows the performance measure comparison with the literature on only N, V, and S classification. In Table 28, our proposed methods yield almost similar performance compared to the state-of-the-art for N, S, and V classes; however, in case of F and Q classes, our proposed work one and four outperforms the other compared methods. From Table 29, it is evident that our proposed methods one and three are efficiently distinguished the classes N, S, and V. The best results of our method are highlighted in bold. Overall, the measures of our work are appreciable compared with other approaches.

**Table 27.** Methodology description of recent state-of-the-art compared in our work.

Literature	Feature Extraction	Classification
[58]		
method-1	R-R intervals	Optimum Path Forest (OPF)
method-2	Wavelet based features	OPF
method-3	Mean, standard deviation and average power of wavelet sub-band	OPF
method-4	Auto correlation and energy ratio of wavelet bands	OPF
method-5	Fast-ICA	OPF
method-6	(Wavelet+ICA+RR interval)	OPF
[59]	(ECG+VCG) complex network based features	SVM
[42]	Wavelet packet decomposition based entropy features	Random Forest
[60]		
method-1	Wavelet based features	Hierarchical Classification (tree approach)
method-2	Mean, standard deviation and average power of wavelet sub-band	Hierarchical Classification (tree approach)
method-3	Auto correlation and energy ratio of wavelet bands	Hierarchical Classification (tree approach)
method-4	Fast-ICA	Hierarchical Classification (tree approach)
method-5	(Wavelet+ICA+RR interval)	Hierarchical Classification (tree approach)
[61]	Temporal Vectrcardiogram(TCG) based features	SVM
[62]	A combination of projected features (features derived from the projected matrix and DCT) and RR intervals	SVM
[63]	TCG feature selection by PSO	SVM
<b>proposed work</b>		
method-1	Entropy and statistical features calculated on ICEEMD modes	Voting ( J48, LDA, naïve Bayes)
method-2	Entropy and statistical features calculated on ICEEMD modes	Voting ( J48, QDA, naïve Bayes)
method-3	Entropy and statistical features calculated on ICEEMD modes	Voting ( J48-C, QDA, naïve Bayes)
method-4	Entropy and statistical features calculated on ICEEMD modes	Voting ( J48-C, LDA, naïve Bayes)

**Table 28.** Performance comparison with recent literature (N, S, V, F, and Q classes).

Literature	N	S	V	F	Q
	SEN/FPR/PPV	SEN/FPR/PPV	SEN/FPR/PPV	SEN/FPR/PPV	SEN/FPR/PPV
[58]					
method-1	84.5/-/-	1.0/-/-	77.7/-/-	38.4/-/-	0/-/-
method-2	86.4/-/-	2.3/-/-	40.8/-/-	0.5/-/-	0/-/-
method-3	84.8/-/-	18.3/-/-	77.8/-/-	7.5/-/-	0/-/-
method-4	92.5/-/-	3.0/-/-	61.8/-/-	16.8/-/-	0/-/-
method-5	95.7/-/-	17.7/-/-	74.7/-/-	3.9/-/-	0/-/-
method-6	93.2/-/-	12.1/-/-	85.5/-/-	18.3/-/-	0/-/-
[59]	89.3/25.2/96.6	38.6/6.7/18	81.2/4.9/53.6	0/0/0	0/0/0
[42]	94.67/3.92/99.73	20/3.69/0.16	94.20/0.71/89.78	50/0.78/0.52	0/0/0
[60]					
method-1	92.3/22.2/97.1	28.5/2.6/29.6	83.5/5.51/51.2	19.1/1.07/12.3	0/0/-
method-2	93.6/57.1/93.0	0.49/0.47/3.81	67.9/3.99/54.2	0/1.63/0	0/0/0
method-3	98.2/41.2/95.1	4.72/0.71/20.3	81.7/1.25/82.0	2.58/0.40/4.88	0/0/0
method-4	98.6/39.8/95.3	9.15/0.56/38.6	83.2/1.21/82.7	0.26/0.38/0.53	0/0/-
method-5	94.7/31.2/96.1	37.4/6.19/18.8	43.9/1.48/67.4	0.52/0.72/0.56	0/0/-
<b>proposed work</b>					
method-1	<b>94.1/36.3/95.4</b>	19.2/1.1/41.7	87.2/0.1/97.9	<b>89.2/4.1/10.7</b>	<b>100/0/100</b>
method-2	84.8/23.6/96.7	34/8.5/14	<b>99.6/0.8/90.3</b>	<b>61.5/4.9/6.5</b>	0/0/0
method-3	70.8/20.3/96.6	<b>42.4/20.1/7.9</b>	<b>99.7/0.7/90.4</b>	<b>63.8/6.3/5.3</b>	0/0/0
method-4	91.2/38/95.1	22.6/2.1/30.2	81.5/0.2/97.2	<b>90.4/5.7/8</b>	<b>100/0/100</b>

**Table 29.** Performance comparison with recent literature (N, S, and V classes).

Literature	N	S	V
	SEN/FPR/PPV	SEN/FPR/PPV	SEN/FPR/PPV
[61]	95/27.9/96.5	29.6/3.1/26.4	85.1/3.01/66.3
[62]	98.4/-/95.4	29.5/-/38.4	70.8/-/85.1
[63] method on VCG	79.1/27.0/96.3	31.2/8.4/13.0	89.5/7.2/46.1
<b>proposed work</b>			
method-1	<b>97.4/33.9/96.1</b>	19.9/1.6/33	<b>93.3/0.8/88.8</b>
method-2	89.1/24.6/96.9	34.1/8.9/13.5	<b>99.6/1.3/84.2</b>
method-3	76.2/21.6/96.8	<b>41.8/20.8/7.5</b>	<b>99.8/1.4/83.6</b>
method-4	95.8/35.7/95.8	23.3/2.4/28.2	88.1/1.6/79.9

#### 4.2. Limitation and Future Scope

Despite the proposed method giving significant results, the performance of the S class is still limited when compared to other classes. Similar behavior is observed in other state-of-the-art methods. Hence, there is a need to explore a new set of attributes and learning algorithms to improve this. In addition, incorporating other physiological signals such as blood pressure, plethysmographic signals along with ECG may improve the description of “heart functioning.”

#### 5. Conclusions

In this work, we implemented a computer-aided inter-patient heartbeat classification algorithm. We employed a nonlinear decomposition method called ICEEMED, to extract some important information lying in ECG. Later, HOS and entropy measures are calculated on the modes obtained after ICEEMD and used as features. Class imbalance is one of the critical challenges in medical diagnosis. We addressed this issue by utilizing the voting scheme as the learning model. The extracted features are then fed to this model for classification. To design this model, naïve Bayes, linear and quadratic discriminating functions, J48 and J48 consolidated classifiers are explored. The proposed method showed promising results compared to state-of-the-art techniques. Our method opens new frontiers to the successful identification of rare heartbeat groups enabling a real-time heart monitoring system.

**Author Contributions:** Conceptualization, R.N.V.P.S.K.; methodology, K.N.V.P.S.R.; software, R.N.V.P.S.K.; validation, K.N.V.P.S.R.; formal analysis, R.N.V.P.S.K.; investigation, R.N.V.P.S.K.; resources, R.N.V.P.S.K.; data curation, R.N.V.P.S.K.; writing—original draft preparation, R.N.V.P.S.K. and R.D.; writing—review and editing, R.N.V.P.S.K., R.D., P.P., G.R.N., H.M., G.D.G. and S.G.; visualization, R.N.V.P.S.K.; supervision, R.N.V.P.S.K., R.D. and P.P.

**Funding:** This research received no external funding.

**Conflicts of Interest:** The authors declare no conflict of interest.

#### References

- Alwan, A. *Global Status Report on Noncommunicable Diseases 2010*; World Health Organization: Geneva, Switzerland, 2011.
- Augustyniak, P.; Tadeusiewicz, R. Assessment of electrocardiogram visual interpretation strategy based on scanpath analysis. *Physiol. Meas.* **2006**, *27*, 597. [[CrossRef](#)] [[PubMed](#)]
- Moody, G.B.; Mark, R.G. The impact of the MIT-BIH arrhythmia database. *IEEE Eng. Med. Biol. Mag.* **2001**, *20*, 45–50. [[CrossRef](#)] [[PubMed](#)]
- Pławiak, P. Novel methodology of cardiac health recognition based on ECG signals and evolutionary-neural system. *Expert Syst. Appl.* **2018**, *92*, 334–349. [[CrossRef](#)]
- Yang, J.; Bai, Y.; Lin, F.; Liu, M.; Hou, Z.; Liu, X. A novel electrocardiogram arrhythmia classification method based on stacked sparse auto-encoders and softmax regression. *Int. J. Mach. Learn. Cybern.* **2018**, *9*, 1733–1740. [[CrossRef](#)]

6. Tuncer, T.; Dogan, S.; Pławiak, P.; Acharya, U.R. Automated arrhythmia detection using novel hexadecimal local pattern and multilevel wavelet transform with ECG signals. *Knowl. Based Syst.* **2019**, 104923. [[CrossRef](#)]
7. Rajesh, K.N.; Dhuli, R. Classification of ECG heartbeats using nonlinear decomposition methods and support vector machine. *Comput. Biol. Med.* **2017**, *87*, 271–284. [[CrossRef](#)]
8. Pławiak, P. Novel genetic ensembles of classifiers applied to myocardium dysfunction recognition based on ECG signals. *Swarm Evol. Comput.* **2018**, *39*, 192–208. [[CrossRef](#)]
9. Yıldırım, Ö.; Pławiak, P.; Tan, R.S.; Acharya, U.R. Arrhythmia detection using deep convolutional neural network with long duration ECG signals. *Comput. Biol. Med.* **2018**, *102*, 411–420. [[CrossRef](#)]
10. Pławiak, P.; Acharya, U.R. Novel deep genetic ensemble of classifiers for arrhythmia detection using ECG signals. *Neural Comput. Appl.* **2019**, pp. 1–25.
11. Pławiak, P.; Abdar, M. Novel Methodology for Cardiac Arrhythmias Classification Based on Long-Duration ECG Signal Fragments Analysis. In *Biomedical Signal Processing*; Springer: Singapore, 2020; pp. 225–272.
12. Khalaf, A.F.; Owis, M.I.; Yassine, I.A. A novel technique for cardiac arrhythmia classification using spectral correlation and support vector machines. *Expert Syst. Appl.* **2015**, *42*, 8361–8368. [[CrossRef](#)]
13. Mert, A. ECG feature extraction based on the bandwidth properties of variational mode decomposition. *Physiol. Meas.* **2016**, *37*, 530. [[CrossRef](#)] [[PubMed](#)]
14. Li, H.; Liang, H.; Miao, C.; Cao, L.; Feng, X.; Tang, C.; Li, E. Novel ECG signal classification based on KICA nonlinear feature extraction. *Circ. Syst. Signal Process.* **2016**, *35*, 1187–1197. [[CrossRef](#)]
15. Alickovic, E.; Subasi, A. Medical decision support system for diagnosis of heart arrhythmia using DWT and random forests classifier. *J. Med. Syst.* **2016**, *40*, 108. [[CrossRef](#)] [[PubMed](#)]
16. Martis, R.J.; Acharya, U.R.; Lim, C.M.; Mandana, K.; Ray, A.K.; Chakraborty, C. Application of higher order cumulant features for cardiac health diagnosis using ECG signals. *Int. J. Neural Syst.* **2013**, *23*, 1350014. [[CrossRef](#)] [[PubMed](#)]
17. Sharma, P.; Ray, K.C. Efficient methodology for electrocardiogram beat classification. *IET Signal Process.* **2016**, *10*, 825–832. [[CrossRef](#)]
18. Mishra, A.K.; Raghav, S. Local fractal dimension based ECG arrhythmia classification. *Biomed. Signal Process. Control* **2010**, *5*, 114–123. [[CrossRef](#)]
19. Osowski, S.; Hoai, L.T.; Markiewicz, T. Support vector machine-based expert system for reliable heartbeat recognition. *IEEE Trans. Biomed. Eng.* **2004**, *51*, 582–589. [[CrossRef](#)]
20. Ye, C.; Kumar, B.V.; Coimbra, M.T. Heartbeat classification using morphological and dynamic features of ECG signals. *IEEE Trans. Biomed. Eng.* **2012**, *59*, 2930–2941.
21. Lin, C.H. Classification enhancible grey relational analysis for cardiac arrhythmias discrimination. *Med. Biol. Eng. Comput.* **2006**, *44*, 311–320. [[CrossRef](#)]
22. Cuesta-Frau, D.; Biagetti, M.O.; Quinteiro, R.A.; Mico-Tormos, P.; Aboy, M. Unsupervised classification of ventricular extrasystoles using bounded clustering algorithms and morphology matching. *Med. Biol. Eng. Comput.* **2007**, *45*, 229–239. [[CrossRef](#)]
23. Tadeusiewicz, R. Neural networks as a tool for modeling of biological systems. *Bio-Algorithms Med.-Syst.* **2015**, *11*, 135–144. [[CrossRef](#)]
24. Kutlu, Y.; Kuntalp, D. A multi-stage automatic arrhythmia recognition and classification system. *Comput. Biol. Med.* **2011**, *41*, 37–45. [[CrossRef](#)] [[PubMed](#)]
25. Martis, R.J.; Acharya, U.R.; Min, L.C. ECG beat classification using PCA, LDA, ICA and discrete wavelet transform. *Biomed. Signal Process. Control* **2013**, *8*, 437–448. [[CrossRef](#)]
26. Martis, R.J.; Acharya, U.R.; Lim, C.M.; Suri, J.S. Characterization of ECG beats from cardiac arrhythmia using discrete cosine transform in PCA framework. *Knowl.-Based Syst.* **2013**, *45*, 76–82. [[CrossRef](#)]
27. Elhaj, F.A.; Salim, N.; Harris, A.R.; Swee, T.T.; Ahmed, T. Arrhythmia recognition and classification using combined linear and nonlinear features of ECG signals. *Comput. Methods Prog. Biomed.* **2016**, *127*, 52–63. [[CrossRef](#)]
28. Li, P.; Wang, Y.; He, J.; Wang, L.; Tian, Y.; Zhou, T.s.; Li, T.; Li, J.s. High-Performance Personalized Heartbeat Classification Model for Long-Term ECG Signal. *IEEE Trans. Biomed. Eng.* **2017**, *64*, 78–86.
29. Desai, U.; Martis, R.J.; Nayak, C.G.; Sarika, K.; Seshikala, G. Machine intelligent diagnosis of ECG for arrhythmia classification using DWT, ICA and SVM techniques. In Proceedings of the India Conference (INDICON), New Delhi, India, 17–20 December 2015; pp. 1–4.

30. Desai, U.; Martis, R.J.; GURUDAS NAYAK, C.; Seshikala, G.; Sarika, K.; SHETTY K, R. Decision support system for arrhythmia beats using ECG signals with DCT, DWT and EMD methods: A comparative study. *J. Mech. Med. Biol.* **2016**, *16*, 1640012. [[CrossRef](#)]
31. De Chazal, P.; O'Dwyer, M.; Reilly, R.B. Automatic classification of heartbeats using ECG morphology and heartbeat interval features. *IEEE Trans. Biomed. Eng.* **2004**, *51*, 1196–1206. [[CrossRef](#)]
32. Egila, M.G.; El-Moursy, M.A.; El-Hennawy, A.E.; El-Simary, H.A.; Zaki, A. FPGA-based electrocardiography (ECG) signal analysis system using least-square linear phase finite impulse response (FIR) filter. *J. Elec. Syst. Inf. Technol.* **2016**, *3*, 513–526. [[CrossRef](#)]
33. Raj, S.; Maurya, K.; Ray, K.C. A knowledge-based real time embedded platform for arrhythmia beat classification. *Biomed. Eng. Lett.* **2015**, *5*, 271–280. [[CrossRef](#)]
34. Zairi, H.; Talha, M.K.; Meddah, K.; Slimane, S.O. FPGA-based system for artificial neural network arrhythmia classification. *Neural Comput. Appl.* **2019**, 1–16. [[CrossRef](#)]
35. Jewajinda, Y.; Chongstitvatana, P. FPGA-based online-learning using parallel genetic algorithm and neural network for ECG signal classification. In Proceedings of the ECTI-CON2010: The 2010 ECTI International Conference on Electrical Engineering/Electronics, Computer, Telecommunications and Information Technology, Chiang Mai, Thailand, 19–21 May 2010; pp. 1050–1054.
36. Rajesh, K.N.; Dhuli, R. Classification of imbalanced ECG beats using re-sampling techniques and AdaBoost ensemble classifier. *Biomed. Signal Process. Control* **2018**, *41*, 242–254. [[CrossRef](#)]
37. Amann, A.; Tratnig, R.; Unterkofler, K. Reliability of old and new ventricular fibrillation detection algorithms for automated external defibrillators. *Biomed. Eng. Online* **2005**, *4*, 60. [[CrossRef](#)] [[PubMed](#)]
38. Huang, N.E.; Shen, Z.; Long, S.R.; Wu, M.C.; Shih, H.H.; Zheng, Q.; Yen, N.C.; Tung, C.C.; Liu, H.H. The empirical mode decomposition and the Hilbert spectrum for nonlinear and non-stationary time series analysis. *Proc. R. Soc. Lond. A Math. Phys. Eng. Sci.* **1998**, *454*, 903–995. [[CrossRef](#)]
39. Wu, Z.; Huang, N.E. Ensemble empirical mode decomposition: A noise-assisted data analysis method. *Adv. Adapt. Data Anal.* **2009**, *1*, 1–41. [[CrossRef](#)]
40. Torres, M.E.; Colominas, M.A.; Schlotthauer, G.; Flandrin, P. A complete ensemble empirical mode decomposition with adaptive noise. In Proceedings of the Acoustics, speech and signal processing (ICASSP), Prague, Czech Republic, 22–27 May 2011; pp. 4144–4147.
41. Colominas, M.A.; Schlotthauer, G.; Torres, M.E. Improved complete ensemble EMD: A suitable tool for biomedical signal processing. *Biomed. Signal Process. Control* **2014**, *14*, 19–29. [[CrossRef](#)]
42. Li, T.; Zhou, M. ECG classification using wavelet packet entropy and random forests. *Entropy* **2016**, *18*, 285. [[CrossRef](#)]
43. Rosso, O.A.; Blanco, S.; Yordanova, J.; Kolev, V.; Figliola, A.; Schürmann, M.; Başar, E. Wavelet entropy: A new tool for analysis of short duration brain electrical signals. *J. Neurosci. Method.* **2001**, *105*, 65–75. [[CrossRef](#)]
44. Shannon, C.E. A mathematical theory of communication, Part I, Part II. *Bell Syst. Tech. J.* **1948**, *27*, 623–656. [[CrossRef](#)]
45. Coifman, R.R.; Wickerhauser, M.V. Entropy-based algorithms for best basis selection. *IEEE Trans. Inf. Theory* **1992**, *38*, 713–718. [[CrossRef](#)]
46. Martis, R.J.; Acharya, U.R.; Ray, A.K.; Chakraborty, C. Application of higher order cumulants to ECG signals for the cardiac health diagnosis. In Proceedings of the 2011 Annual International Conference on Engineering in Medicine and Biology Society (EMBC), Boston, MA, USA, 30 August–3 September 2011; pp. 1697–1700.
47. Nikias, C.L.; Mendel, J.M. Signal processing with higher-order spectra. *IEEE Signal Process. Mag.* **1993**, *10*, 10–37. [[CrossRef](#)]
48. Swami, A.; Mendel, J.M.; Nikias, C.L.M. Higher-order spectral analysis toolbox. *Tech. Support Product Enhanc. Suggest.* **1984**.
49. Wolpert, D.H.; Macready, W.G. No free lunch theorems for optimization. *IEEE Trans. Evolut. Comput.* **1997**, *1*, 67–82. [[CrossRef](#)]
50. Kittler, J.; Hatef, M.; Duin, R.P.; Matas, J. On combining classifiers. *IEEE Trans. Pattern Anal. Mach. Intell.* **1998**, *20*, 226–239. [[CrossRef](#)]
51. John, G.H.; Langley, P. Estimating continuous distributions in Bayesian classifiers. In Proceedings of the Eleventh conference on Uncertainty in Artificial Intelligence, Montréal, QC, Canada, 18–20 August 1995; pp. 338–345.



52. Duda, R.O.; Hart, P.E.; Stork, D.G. *Pattern Classification*; John Wiley & Sons: Hoboken, NJ, USA, 2012.
53. Quinlan, J.R. *C4. 5: Programs for Machine Learning*; Elsevier: Amsterdam, The Netherlands, 2014.
54. Arbelaz Gallego, O.; Gurrutxaga, I.; Lozano, F.; Muguerza, J.; Pérez, J.M. J48Consolidated: An Implementation of CTC Algorithm for WEKA. 2016. Available online: <https://addi.ehu.es/handle/10810/17314> (accessed on 17 November 2019).
55. Yang, Y.; Webb, G.I. Discretization for naive-Bayes learning: managing discretization bias and variance. *Mach. Learn.* **2009**, *74*, 39–74. [[CrossRef](#)]
56. Witten, I.H.; Frank, E.; Hall, M.A.; Pal, C.J. *Data Mining: Practical Machine Learning Tools and Techniques*; Morgan Kaufmann: Burlington, MA, USA, 2016.
57. Powers, D.M. Evaluation: From Precision, Recall and F-Measure to ROC, Informedness, Markedness and Correlation. Available online: [https://bioinfpublication.org/files/articles/2\\_1\\_1\\_JMLT.pdf](https://bioinfpublication.org/files/articles/2_1_1_JMLT.pdf) (accessed on 19 November 2019).
58. Luz, E.J.D.S.; Nunes, T.M.; De Albuquerque, V.H.C.; Papa, J.P.; Menotti, D. ECG arrhythmia classification based on optimum-path forest. *Expert Syst. Appl.* **2013**, *40*, 3561–3573. [[CrossRef](#)]
59. Queiroz, V.; Luz, E.; Moreira, G.; Guarda, Á.; Menotti, D. Automatic cardiac arrhythmia detection and classification using vectorcardiograms and complex networks. In Proceedings of the 2015 37th Annual International Conference on Engineering in Medicine and Biology Society (EMBC), Ilan, Italy, 25–29 August 2015; pp. 5203–5206.
60. Luz, E.J.D.S.; Merschmann, L.H.; Menotti, D.; Moreira, G.J. Evaluating a hierarchical approach for heartbeat classification from ECG. *Int. J. Bioinf. Res. Appl.* **2017**, *13*, 146–160. [[CrossRef](#)]
61. Garcia, G.; Moreira, G.; Luz, E.; Menotti, D. Improving automatic cardiac arrhythmia classification: Joining temporal-VCG, complex networks and SVM classifier. In Proceedings of the 2016 International Joint Conference on Neural Networks (IJCNN), Vancouver, BC, Canada, 24–29 July 2016; pp. 3896–3900.
62. Chen, S.; Hua, W.; Li, Z.; Li, J.; Gao, X. Heartbeat classification using projected and dynamic features of ECG signal. *Biomed. Signal Process. Control* **2017**, *31*, 165–173. [[CrossRef](#)]
63. Garcia, G.; Moreira, G.; Menotti, D.; Luz, E. Inter-Patient ECG Heartbeat Classification with Temporal VCG Optimized by PSO. *Sci. Rep.* **2017**, *7*, 10543. [[CrossRef](#)]



© 2019 by the authors. Licensee MDPI, Basel, Switzerland. This article is an open access article distributed under the terms and conditions of the Creative Commons Attribution (CC BY) license (<http://creativecommons.org/licenses/by/4.0/>).



# Einthoven Unipolar Leads: Towards a better understanding of Wilson Central Terminal

Hossein Moeinzadeh  
MARCS Institute for Brain,  
Behavior and Development,  
Western Sydney University  
Sydney, Australia  
h.moeinzadeh@westernsydney.  
edu.au

Joseph Assad  
Department of Cardiology,  
Liverpool Hospital  
Sydney, Australia  
jg.assad@gmail.com

Paolo Bifulco  
Department of Biomedical  
Engineering  
The University of Naples  
"Federico II"  
Naples, Italy  
pabifulc@unina.it

Mario Cesarelli  
Department of Biomedical  
Engineering  
The University of Naples  
"Federico II"  
Naples, Italy  
cesarelli@unina.it

Aiden O'Loughlin  
School of Medicine,  
Western Sydney University  
Sydney, Australia  
aiden.oloughlin@gmail.com

Ibrahim M. Shugman  
Cardiology Department,  
Campbelltown Hospital,  
Sydney, Australia  
shugmano@hotmail.com

Gaetano D. Gargiulo  
School of Computing, Engineering  
and Mathematics,  
Western Sydney University  
Sydney, Australia  
g.gargiulo@westernsydney.edu.au

**Abstract**—Einthoven unipolar leads include the potential of the right arm, left arm, and left leg which, by definition, are used to form the Wilson central terminal (WCT) as the average of these three limbs leads. In a traditional 12-lead ECG system, it is not possible to measure WCT directly. It is assumed to both be steady during the cardiac cycle with the assumed value most commonly being  $-2/3$  of the augmented vector foot (aVF) lead. Using our novel ECG device that records Einthoven unipolar leads in addition to traditional 12-lead ECG signals, we investigate whether the WCT and aVF are proportional and the WCT can accurately be replaced by  $-2/3$  of the aVF lead. We use the Einthoven unipolar leads features to evaluate both of the assumptions in regards to the WCT amplitude and value.

**Keywords**—*Electrocardiography, Wilson Central Terminal, Einthoven Unipolar Leads, Augmented leads.*

## I. INTRODUCTION

Electrocardiography (ECG) is probably one of the most common non-invasive diagnostic tool for cardiac diseases [1]. It shows the electrical activity of the heart as voltage variation over time using a total of ten electrodes, six are placed on the chest and three placed on the right arm (RA), left arm (LA), and left leg (LL), as well as one reference electrode placed on the right leg (RL) [1]. The six signals obtained from the chest electrodes have been named precordial leads (V1 to V6 or C1 to C6) and are measured as the potential difference between a human body virtual reference potential and the chest electrodes [1]. The reference potential is named Wilson Central Terminal (WCT) after Wilson who discovered it and defined it as average potential of the three limbs mentioned above [1], [2]. Three limb leads (I, II, and III) measure the potential between the different pairs of limb electrodes, additional limb leads are the three augmented limb leads (aVR, aVL, and aVF), which measure each of the limb electrodes against a combination of

the other two. The full set of twelve leads constitute the so called 12-lead ECG [1].

Although the WCT had been initially assumed to have null amplitude, many researchers dispute this assumption [3]–[6] and have found that the WCT amplitude could be as large as 0.4 of lead II. Consequently, the WCT amplitude could be medically relevant [4]–[6] since the precordial leads of the traditional ECG may miss some information. However, this systematic error has been widely accepted in clinical practice as the WCT measurement historically required a complicated apparatus [5], [7]. Although there have been some attempts to minimize the WCT amplitude [5], [8], [9], these attempts have been either unsuccessful [5] or the medical impact of its minimization remained unknown [8], [9].

On the contrary, our ECG device could record the potential of limb electrodes simultaneously with the 12-lead ECG signals [10], [11]. In this ECG device, we used the already used right leg (ground return) as the global reference point to measure the potential of the limbs hence of the WCT [10], [11]. We recorded data from 92 participants recruited from the Campbelltown hospital (NSW) patients' cohort. Our dataset (WCTECGdb) is publicly available from the Physionet website<sup>1</sup> [12]–[15]. Our records show that the WCT is highly variant with a large amplitude, which is also align with the findings in the literature. We measured the peak to peak amplitudes of the WCT potential in relation to lead II and found out that the WCT/II amplitude is in range of 0.11 to 2.7 with an average of 0.78 among all patients in the dataset. Furthermore, the WCT clearly shows all the ECG

---

<sup>1</sup> <https://physionet.org/content/wctecgdb/>

characteristics such as QRS complex and p-wave for most of the patients.

In this paper, we aim to present a clear perspective of the Einthoven unipolar leads characteristics. We discuss the feasibility of the WCT signal replacing the current most common practice of using the aVF lead.

## II. PROBLEM FORMULATION

Einthoven hypothesized the human body inscribed into an equilateral triangle in which the vertices are the electrodes placed on the left arm, right arm, and left leg. It could be easily shown that the sum of the Einthoven unipolar leads (RA, LA, and LL) is always equal to zero [16], which presents the potential of the heart (dipole). Later, Wilson suggested using the average of the Einthoven unipolar leads as the reference point (the WCT) for precordial lead recordings.

$$\text{WCT} = \frac{1}{3}(\text{RA} + \text{LA} + \text{LL}) \quad (1)$$

The voltage amplitude of each limb is highly dependent on its distance to the heart. Therefore, the right arm has a lower amplitude than the left arm as the heart is located on the left side of the chest, and left foot should have a very small amplitude as it is far from the heart. In this paper, we refer to this assumption as *Einthoven unipolar leads hypothesis*. Provided that the left leg amplitude is approximately zero, the WCT and aVF are claimed to be proportional.

$$\text{aVF} = -\frac{1}{2}(\text{LA} + \text{RA}) \stackrel{\text{LL} \approx 0}{\implies} \text{WCT} = -\frac{2}{3} \text{aVF} \quad (2)$$

Although these hypotheses could easily solve the problem of measuring the WCT signal, they could not be verified as there was no practical approach to record the WCT signal or the Einthoven unipolar leads. We developed a 15-Lead ECG device which is able to record the potential of Einthoven limb leads and the standard 12 lead ECG signals. Consequently, we are able to find the legitimacy of these hypotheses using the recorded WCT and aVF signals.

## III. METHOD

The new developed ECG device uses the right leg as the ground reference terminal for measuring all signals. It is designed with the use of a special chip: INA116 instrumentation amplifier [17], commercially available from Texas Instruments (Burr-Brown series) [10], [11], [18], [19] which has a bias current of typically few fA and integrates a specialized guard ring amplifier which preserves the signal to noise ratio (SNR). This ECG system uses a specialized grounding circuitry incorporating the right leg signal and a modified version of voltage bootstrap circuitry to preserve the measured signals [10], [11], [20], [21].

As the guard ring amplifier generates a replica of the input signal, it was used to measure the WCT components. Hence, the guard buffer of the limb electrodes was used for the direct measurement of the voltage of WCT components. To provide the required gain and bandpass filtering, three gain cells were employed for a total gain of 1000 V/V, the two last cells also perform active low-pass filtering. To obtain an ECG signal

with a diagnostic quality, capacitors' values that used to set the high-pass and low-pass frequencies of the gain cells are selected so that the required bandwidth is obtained even in the worst-case scenario (i.e. when the tolerance of the capacitor causes a -10% change in the initial value). Further software filtering (50th order IIR band pass filter into the range 0.05-149 Hz and harmonics IIR notch filters at powerline frequency) are used to normalize the frequency content of all the signals.

Using a combination of the right leg circuitry and a modified bootstrap circuitry, a specialized grounding circuitry was implemented to ensure providing sufficient SNR for the measured signals. The bootstrap circuitry directly offers the instrumentation amplifiers' reference voltage using a damped version of the mean value of the potential of all electrodes [10], [19], [21]–[23]. The non-amplified average of the measurement electrodes is directly inputted to the driven right leg circuitry which is designed to contain current drive to 20  $\mu\text{A}$  [24], [25].

A dual 9 V power supply (disposable batteries) was used to power the circuitry. Digital conversion and data logging is performed the BIOADC [20] sampling at 800 Hz over a resolution of  $\pm 5$  V. The BIOADC has an anti-aliasing low-pass filter with cut-off frequency of Nyquist rate and it was directly connected to a battery-powered laptop via a galvanically insulated USB. The detailed description of the hardware can be found in [11].

## IV. RESULTS AND DISCUSSION

Our dataset (WCGECGdb) was recently published in the Physionet website and it contains 540 ten seconds segments recording from 92 patients [12].

For *most* of the patients, the Einthoven unipolar leads have ECG features such as QRS complexes and P waves. As can be seen in Fig.1, the right arm has a smaller amplitude than the left arm, and the left leg has the smallest amplitude, consistent with the Einthoven unipolar leads hypothesis.

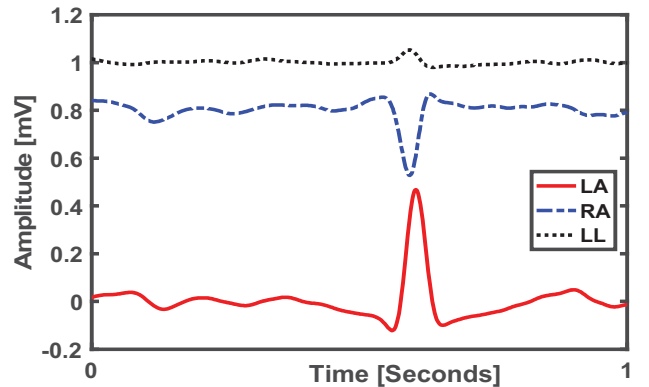


Fig. 1. Comparison of the Einthoven unipolar leads. The RA is shifted 0.8 mV and the left arm is shifted 1.0 mV from the original place for better visualization. Recorded from 68 years old female (Patient ID: 15).

However, this is not seen in all patients. We calculated the average of three peak to peak amplitudes of the right arm, left arm, and left leg in relation to lead II for all patients (Table 1 and Fig.2). The need to use multiple peaks to measure the ECG

peaks is because it is known that the width of the ECG peaks as well as its baseline wandering are influenced by the respiration. Taking into account multiple peaks minimizes this influence [1].

As it is shown in Fig.2, the left arm has a higher amplitude than the right arm for only 58 patients showing that Einthoven unipolar leads hypothesis is not valid for all patients.

TABLE I. THE MINIMUM, MAXIMUM AND AVERAGE AMPLITUDE OF THE EINTHOVEN UNIPOLAR LEADS IN RELATION WITH LEAD II AMONG ALL 92 PATIENTS

	LA/II	RA/II	LL/II
<b>Average</b>	1.6	0.88	0.22
<b>Maximum</b>	6.41	2.79	1.78
<b>Minimum</b>	0.038	0.01	0.007

As it is referred from Table 1 and Fig.2, the left leg has the smallest amplitude among the Einthoven limbs' potential. However, it has no negligible amplitude for all patients demonstrating that the aVF and the WCT are not proportional. Fig.3 and Fig.4 illustrate the relation between the WCT and the aVF lead when the left leg has small and large amplitude, respectively.

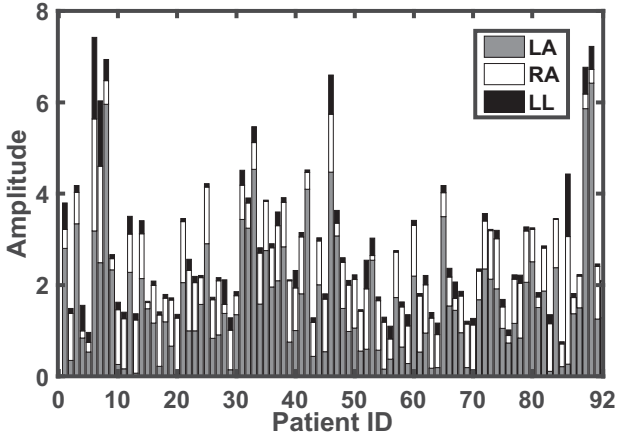


Fig. 2. The amplitudes of the Einthoven unipolar leads in relation with lead II. The limb potential is not consistent with the initial assumption (LA>RA>LL) for all patients; the left leg does not have small amplitude for all patients; the RA has a larger amplitude than the LA for 29 patients.

We measured the *correlation* and *Sprague-Geer* [26], [27] metric between -2/3aVF and the WCT for three consecutive beats. The Sprague-Geer metric shows the agreement between these two signals by measuring three errors:  $M_{S\&G}$  (magnitude error),  $P_{S\&G}$  (phase error), and  $C_{S\&G}$  (overall error).

$$M_{S\&G} = \sqrt{\frac{\sum_{i=1}^N p_i^2}{\sum_{i=1}^N m_i^2} - 1} \quad (3)$$

$$P_{S\&G} = \frac{1}{\pi} \cos^{-1} \frac{\sum_{i=1}^N p_i m_i}{\sqrt{\sum_{i=1}^N m_i^2 \sum_{i=1}^N p_i^2}} \quad (4)$$

$$C_{S\&G} = \sqrt{M_{S\&G}^2 + P_{S\&G}^2} \quad (5)$$

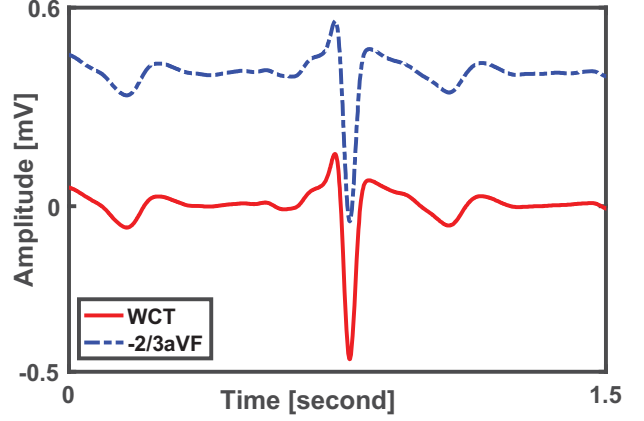


Fig. 3. Comparison of the WCT and -2/3aVF lead. The LA, RA and LL amplitudes in relation with lead II are 0.9, 1.19 and 0.07 respectively. The aVF is shifted 0.4 mV from the original place for better visualization. Recorded from 59 years old male (Patient ID: 27).

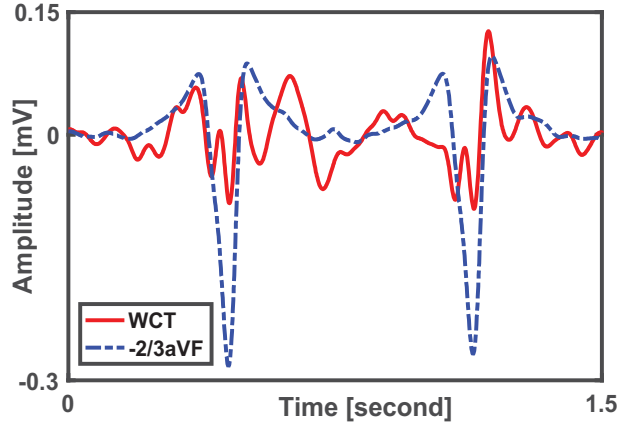


Fig. 4. Comparison of the WCT and -2/3aVF lead. The LA, RA and LL amplitudes in relation with lead II are 0.53, 0.21 and 0.22 respectively. Recorded from 87 years old male (Patient ID: 5).

Table 2 shows the average and standard deviation of correlation and Sprague-Geer metric for all 92 patients. These results confirm that the WCT and -2/3aVF do not have an agreement for many patients as they are not highly correlated, and the Sprague-Geer errors are considerably large.

TABLE II. THE CORRELATION AND SPRAGUE-GEER METRIC BETWEEN  $-2/3aVF$  AND THE WCT. AVERAGE AND STANDARD DEVIATION ARE MEASURED FOR THREE CONSECUTIVE BEATS AMONG 92 PATIENTS.

	Correlation	M <sub>s&amp;g</sub>	P <sub>s&amp;g</sub>	C <sub>s&amp;g</sub>
Average	0.73	-0.19	0.21	0.35
Standard deviation	0.26	0.32	0.13	0.26

Nevertheless, it is too early to conclude that the WCT cannot be replaced by  $-2/3aVF$ . We only provided a statistical comparison of these two signals, and it still required to assess the medical impact of using  $-2/3aVF$  instead of the WCT on measuring the precordial leads. In other words, if the differences between these two signals are not medically significant, the WCT can be replaced by  $-2/3aVF$ , even though these two signals do not have a statistical agreement.

## V. CONCLUSION

In this paper, we used our recent published dataset named WCTECGdb, which included the WCT components (Einthoven unipolar leads) to investigate whether the WCT and aVF are proportional. We used statistical metrics to develop a better understanding of Einthoven unipolar leads. Our results show that unlike the initial assumption, the left leg potential is not negligible for all patients, and it can influence the shape and amplitude of the WCT signal. Consequently, the WCT and aVF are not proportional. However, a larger clinical investigation is required to measure the medical impact of this finding.

## ACKNOWLEDGMENT

We gratefully thank all the nurses and patients at Campbelltown hospital who voluntarily enrolled in this study. We also thank Mr. Colin Symons who helped to build the ECG device prototype.

The office for Research Engagement and Development with Industry (REDI) at the Western Sydney University has funded this research.

## REFERENCES

[1] J. Malmivuo and R. Plonsey, *Bioelectromagnetism Principles and Applications of Bioelectric and Biomagnetic Fields*. Oxford University Press, 1995.

[2] F. N. Wilson, F. D. Johnston, A. G. Macleod, and P. S. Barker, "Electrocardiograms that represent the potential variations of a single electrode," *Am. Heart J.*, vol. 9, no. 4, pp. 447–458, Apr. 1934.

[3] H. C. Burger, "The zero of potential: A persistent error," *Am. Heart J.*, vol. 49, no. 4, pp. 581–586, Apr. 1955.

[4] R. H. Bayley and C. L. Kinard, "The zero of potential of the electrical field produced by the heart beat; the problem with reference to the living human subject," *Circ. Res.*, vol. 2, no. 2, pp. 104–111, Mar. 1954.

[5] R. H. Bayley and A. E. Schmidt, "The Problem of Adjusting the Wilson Central Terminal to a Zero of Potential in the Living Human Subject," *Circ. Res.*, vol. 3, no. 1, pp. 94–102, Jan. 1955.

[6] R. H. Bayley, E. W. Reynolds, C. L. Kinard, and J. F. Head, "The zero of potential of the electric field produced by the heart beat; the problem with reference to homogenous volume conductors," *Circ. Res.*, vol. 2, no. 1, pp. 4–13, Jan. 1954.

[7] G. E. Dower, J. A. Osborne, and A. D. Moore, "Measurement of the error in Wilson's central terminal: an accurate definition of unipolar leads," *Br. Heart J.*, vol. 21, pp. 352–60, Jul. 1959.

[8] H. Moeinzadeh *et al.*, "Computing a new central terminal for ECG recording using combined genetic algorithm and linear regression from real patient data," in *Proceedings of the Genetic and Evolutionary Computation Conference Companion*, 2017, pp. 293–294.

[9] H. Moeinzadeh *et al.*, "Minimization of the Wilson's Central Terminal voltage potential via a genetic algorithm," *BMC Res. Notes*, vol. 11, no. 1, p. 915, Dec. 2018.

[10] G. D. Gargiulo *et al.*, "On the 'Zero of Potential of the Electric Field Produced by the Heart Beat'. A Machine Capable of Estimating this Underlying Persistent Error in Electrocardiography," *Machines*, vol. 4, no. 4, p. 18, Oct. 2016.

[11] G. D. Gargiulo, "True Unipolar ECG Machine for Wilson Central Terminal Measurements," *Biomed Res. Int.*, vol. 2015, p. 586397, 2015.

[12] G. Gargiulo and H. Moeinzadeh, "Wilson Central Terminal ECG Database," *PhysioNet*, 2019.

[13] A. L. Goldberger *et al.*, "PhysioBank, PhysioToolkit, and PhysioNet: Components of a New Research Resource for Complex Physiologic Signals," *Circulation*, vol. 101, no. 23, pp. e215–e220, 2000.

[14] H. Moeinzadeh *et al.*, "A Modern Wilson's Central Terminal Electrocardiography Database," *Hear. Lung Circ.*, vol. 27, pp. S293–S294, 2018.

[15] H. Moeinzadeh *et al.*, "Unipolar Cardiac Leads Between History and Science," 2020, pp. 203–224.

[16] E. Goldberger, "The validity of the Einthoven triangle hypothesis," *Am. Heart J.*, vol. 29, no. 3, pp. 369–377, Mar. 1945.

[17] BurrBrown, "INA116," *Tech. data*, 2008.

[18] G. D. Gargiulo, J. Tapson, A. van Schaik, A. McEwan, and A. Thiagalingam, "Unipolar ECG circuits: Towards more precise cardiac event identification," in *2013 IEEE International Symposium on Circuits and Systems (ISCAS2013)*, 2013, pp. 662–665.

[19] G. Gargiulo *et al.*, "True Unipolar ECG Leads Recording (Without the Use of WCT)," *Hear. Lung Circ.*, vol. 22, p. S102, 2013.

[20] G. Gargiulo, P. Bifulco, M. Cesarelli, A. Fratini, and M. Romano, "Problems in Assessment of Novel Biopotential Front-End with Dry Electrode: A Brief Review," *Machines*, vol. 2, no. 1, pp. 87–98, 2014.

[21] B. B. Winter and J. G. Webster, "Reduction of Interference Due to Common Mode Voltage in Biopotential Amplifiers," *Biomed. Eng. IEEE Trans.*, vol. 30, no. 1, pp. 58–62, 1983.

[22] G. D. Gargiulo *et al.*, "Towards true unipolar ECG recording without the Wilson central terminal (preliminary results)," *Physiol. Meas.*, vol. 34, no. 9, pp. 991–1012, Sep. 2013.

[23] G. Gargiulo, P. Bifulco, M. Cesarelli, A. McEwan, and A. Wabnitz, "Open platform, 32-channel, portable, data-logger with 32 PGA control lines for wearable medical device development," *Electron. Lett.*, vol. 50, no. 16, pp. 1127–1129, Jul. 2014.

[24] In-Duk Hwang and J. G. Webster, "Direct Interference Canceling for Two-Electrode Biopotential Amplifier," *IEEE Trans. Biomed. Eng.*, vol. 55, no. 11, pp. 2620–2627, Nov. 2008.

[25] J. G. Webster, *Medical Instrumentation Application and Design*. John Wiley & Sons, 2009.

[26] M. A. Sprague and T. L. Geers, "A spectral-element/finite-element analysis of a ship-like structure subjected to an underwater explosion," *Comput. Methods Appl. Mech. Eng.*, vol. 195, no. 17–18, pp. 2149–2167, Mar. 2006.

[27] T. L. Geers, "An objective error measure for the comparison of calculated and measured transient response histories," *Shock Vib. Bull.*, vol. 54, no. 2, pp. 99–107, 1984.



Communication

# WCTECGdb: A 12-Lead Electrocardiography Dataset Recorded Simultaneously with Raw Exploring Electrodes' Potential Directly Referred to the Right Leg

Hossein Moeinzadeh <sup>1,\*</sup>, Joseph Assad <sup>2</sup>, Paolo Bifulco <sup>3</sup>, Mario Cesarelli <sup>3</sup>, Aiden O'Loughlin <sup>4</sup>, Jonathan C. Tapson <sup>1</sup>, Ibrahim M. Shugman <sup>5</sup>, Aravinda Thiagalingam <sup>6</sup> and Gaetano D. Gargiulo <sup>7</sup>

<sup>1</sup> The MARCS Institute, Western Sydney University, Milperra 2214, Australia; j.tapson@westernsydney.edu.au

<sup>2</sup> Department of Cardiology, Liverpool Hospital, Liverpool 2170, Australia; jg.assad@gmail.com

<sup>3</sup> Department of Electrical Engineering and Information Technology (DIETI), "Federico II" The University of Naples, 80100 Naples, Italy; pabifulc@unina.it (P.B.); cesarell@unina.it (M.C.)

<sup>4</sup> School of Medicine, Western Sydney University, Campbelltown 2006, Australia; aiden.oloughlin@gmail.com

<sup>5</sup> Cardiology Department, Campbelltown Hospital, Campbelltown 2006, Australia; shugmano@hotmail.com

<sup>6</sup> School of Medicine, The University of Sydney, Sydney 2006, Australia; aravinda.thiagalingam@sydney.edu.au

<sup>7</sup> School of Engineering, Western Sydney University, Kingswood 2747, Australia; g.gargiulo@westernsydney.edu.au

\* Correspondence: h.moeinzadeh@westernsydney.edu.au

Received: 11 April 2020; Accepted: 28 May 2020; Published: 8 June 2020



**Abstract:** With this paper we communicated the existence of a surface electrocardiography (ECG) recordings dataset, named WCTECGdb, that aside from the standard 12-lead signals includes the raw electrode biopotential for each of the nine exploring electrodes referred directly to the right leg. This dataset, comprises of 540 ten second segments recorded from 92 patients at Campbelltown Hospital, NSW Australia, and is now available for download from the Physionet platform. The data included in the dataset confirm that the Wilson's Central Terminal (WCT) has a relatively large amplitude (up to 247% of lead II) with standard ECG characteristics such as a *p*-wave and a *t*-wave, and is highly variable during the cardiac cycle. As further examples of application for our data, we assess: (1) the presence of a conductive pathway between the legs and the heart concluding that in some cases is electrically significant and (2) the initial assumption about the limbs potential stating the dominance of the left arm concluding that this is not always the case and that might requires case to case assessment.

**Keywords:** electrocardiography; Wilson's Central Terminal; unipolar leads

## 1. Introduction

The surface electrocardiography (ECG) demonstrates the electrical activity of the heart as it spreads towards the surface of the human body. Its most common incarnation is referred as 12-lead ECG, and it is known as one of the most valuable non-invasive diagnostic tools for cardiac assessment [1,2]. The 12-lead ECG is composed of three limb leads; three augmented leads and six precordial leads. The three limb leads (also known as bipolar leads) are referred as Lead I, Lead II, and Lead III, and

calculated by the potential difference of electrodes placed on right arm (RA), left arm (LA), and left leg (LL) [2]:

$$\begin{aligned} I &= LA - RA \\ II &= LL - RA \\ III &= LL - LA \end{aligned} \quad (1)$$

Leads augmented Vector Left (aVL), augmented Vector Right (aVR) and augmented Vector Foot (aVF) are referred to as augmented leads (also known as Goldberger leads) and are measured as the potential difference between each limb electrodes and the average of the other two limb potentials [3]:

$$\begin{aligned} aVL &= LA - \frac{1}{2}(RA + LL) \\ aVR &= RA - \frac{1}{2}(LA + LL) \\ aVF &= LL - \frac{1}{2}(RA + LA) \end{aligned} \quad (2)$$

The six precordial leads (V1 to V6) are synthesized by calculating the difference potential between each of the six chest electrodes potential (UV1:UV6) and the virtual reference point, known as Wilson Central Terminal (WCT) [4]. This reference point is measured as the average potentials of the right arm, left arm, and left leg electrodes' potential [4]:

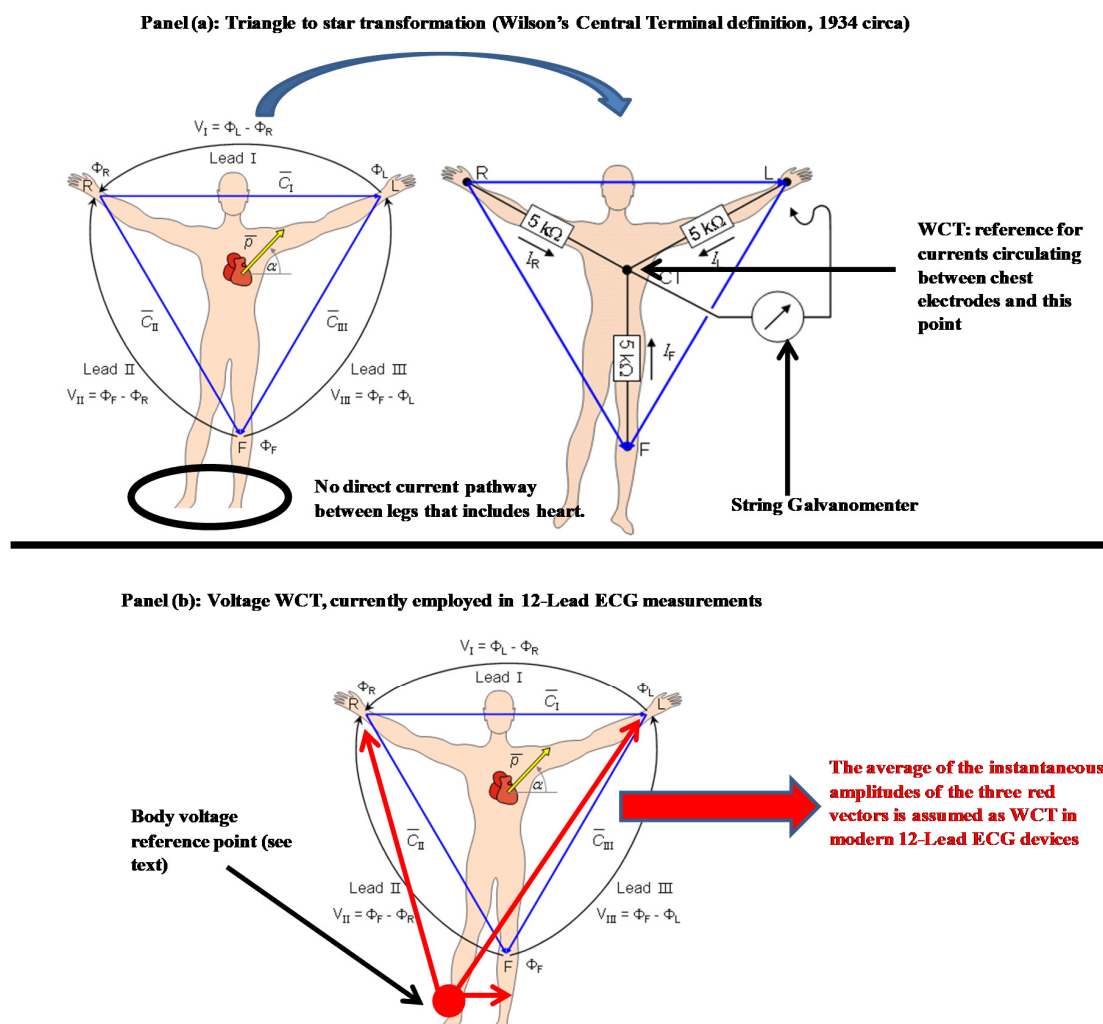
$$WCT = \frac{(LA + RA + LL)}{3} \quad (3)$$

$$V_1 : V_6 = UV1 : UV6 - WCT \quad (4)$$

While current measurements are considered absolute, voltage measurements are relative to a reference point. It is important to note that the original electrocardiography model was originally conceived using current measurements (string galvanometer). The original cardiac conduction model was rendered into a voltage model invoking the simplified homogeneous volume conductor hypothesis and the Ohm's law, when the solid-state electronic amplifier made its debut in this field. For this reason, when considering the unipolar electrodes potentials in Equations (3) and (4) as they are supposedly measured to a common voltage reference this seems to cancel out. Unfortunately, in the case of the human body, where this reference point is directly or indirectly referred to the right leg, and the conductive pathways between exploring electrodes and this connection are not homogenous the cancellation of the reference point may not be perfect. This is particularly true for the WCT where potentials of chest electrodes, already referenced to right leg, are furtherly referenced to an average of electrodes (themselves referenced to the right leg) placed at a different distance from reference. As it is beyond the purpose of this paper to digress into the details of the model and the hardware utilized, we refer the reader to our previously published papers and in particular to [5] of which we adopted the conduction model depicted in Figure 1. In this paper, to simplify the notation we use the term unipolar lead to refer to the potential of Einthoven limbs' electrodes (LA, RA, and LL) and the potential of the six electrodes on the chest (UV1:UV6).

Despite the 12-lead ECG has been used clinically for decades, there is still no mutual understanding of the WCT among researchers or cardiologists [6]. It is true that other more realistic cardiac conduction models have been proposed during the years, i.e., the Frank model [7] but these have not gained the traction required to enter clinical practice; exploring the reasons why these methods have not received the same research attention of the 12-lead ECG systems is beyond the scope of this brief communication. With this paper we would like to officially announce the availability of an ECG dataset available for download via the Physionet platform, under the name of WCTECGdb [8–11]. Although many ECG datasets with different features have been published [12–14], the WCTECGdb is a unique dataset as it contains the WCT signal and the unipolar leads. The dataset contains 540 ten seconds segments recorded from 92 volunteer patients. Each record comprises of signals for three limb leads, six precordials, three WCT components, six unipolar leads, and the WCT signal. In this paper,

we demonstrate the characteristics of limb potentials, which lead to having a better understanding of the WCT signal. We also show that unipolar leads can be used to synthesize the traditional ECG leads. Together with the dataset we briefly discuss the potential clinical advantages of these new recordings together with some exemplificative applications of the data like the investigation over the relative amplitudes of unipolar limb leads to assess the presence of a conductive pathway between the legs and the heart as well as a comparison between the WCT potential and other leads.



## 2. Dataset Characterization

As mentioned, we have recorded data from patients at the Campbelltown hospital (New South Wales, Australia) over two years (2016–2018). All the patients volunteered for this study and gave written consent. This study was approved by the Ethics Committee of the South West Sydney Health District on 23 September 2015 with the protocol number HREC/15/LPOOL/302. The granted ethics clearance has been extended (it is still current, although all the non-necessary clinical trials have been suspended due to the COVID-19 outbreak) to increase the number of recordings.

We segmented each recording to ten second sections. Consequently, as the duration of the recording is different, each patient has a different number of segments, ranging between one to thirty-one. We recorded data from 92 patients (27 were female), and the total number of ten seconds segments is 540 for all patients. The average age of the patient population is 65.23 years (with a

standard deviation of 12.12 years); patients had a history of cardiac disease and had been admitted to the hospital from the emergency department because of difficulties in breathing and/or chest pain.

This dataset comprises of raw and noise removed (cleaned) signals for the three limb leads, six precordial leads, nine unipolar leads including three WCT components, and six unipolar precordial leads. As the WCT is the average of the limb potential, we only added the cleaned WCT signal into the dataset. To pre-process our signals, we used the same filters employed for our other published studies. We employed a bandpass filter (0.05–149 Hz) and a powerline with harmonics up to the Nyquist frequency notch filter bank. All filters were implemented in MATLAB as 50th order IIR and applied with a zero-phase lag (bidirectional) [1].

In the uploaded dataset, we included supplementary information for each recorded segment such as the patient's 'age', 'gender', 'patient diagnosis', and the 'reconstructed precordials' (if there is any). Each file in our dataset contained the signals and supplementary information listed in Table 1. Cleaned and raw signals were included in the dataset. The raw signals are specified by '-raw' in the dataset (e.g., V2-raw) and refer to originally recorded signals prior to the noise filtering process. The WCT signal is only presented in a clean format.

**Table 1.** The signal names and the detail of the recording presented for each segment.

<b>Signals</b>	I-raw	I	limb lead I
	II-raw	II	limb lead II
	III-raw	III	limb lead III
	V1-raw:V6-raw	V1:V6	precordial leads
	LA-raw, RA-raw, LL-raw	LA, RA, LL	three WCT components
	UV1-raw:UV6-raw	UV1:UV6	unipolar chest leads
		WCT	the WCT signal
<b>Detail</b>		Age Gender Patient diagnosis Reconstructed precordials *	

\* Only included for 8 segments that needed to be synthesized for some of the precordial leads.

The patient diagnosis as supplied in the dataset is presented in Table 2; unfortunately, the hospital could not provide us the diagnosis for ten patients. This is reflected in Table 2 under the patient diagnosis column as "not reported".

**Table 2.** Patient diagnosis list.

Patient Diagnosis	Count	Patient Diagnosis	Count
Angina	1	Non-ST segment elevation myocardial infarction (NSTEMI)	23
Atrial fibrillation	9	Pulmonary embolism-Atrial fibrillation	1
Atrial flutter	1	Pulmonary embolism	1
Atypical chest pain	5	Rapid atrial fibrillation with new cardiomyopathy	1
Cardiomyopathy	1	Rapid atrial fibrillation-pericarditis	1
Chest pain	1	Severe Mitral Stenosis	1
Complete Heart block	1	Sinus bradycardia	2
Congestive cardiac failure (CHF) exacerbation	1	Slow atrial fibrillation	1



Table 2. Cont.

Patient Diagnosis	Count	Patient Diagnosis	Count
Congestive cardiac failure (CCF)	1	ST segment elevation myocardial infarction (STEMI)	4
Coronary artery disease	3	Stable angina	7
Epigastric pain	1	Supraventricular tachycardia (SVT)	2
Fall secondary to alcohol intoxication	1	Syncope	3
Gastritis (non-cardiac chest pain)	1	Unstable angina	1
Hypertrophic obstructive cardiomyopathy	1	Urosepsis	1
Inferior ST segment elevation myocardial infarction (STEMI)	1	Ventricular tachycardia (VT)	3
Myocardial infarction-Type 2	1	Not reported	10

We included synthesized precordial leads instead of directly measured signals for a total of 8 segments (from 5 patients), due to a poor signal to noise ratio and/or the final stage amplifier saturation. The signal saturation usually is seen when large contact impedances and electrode polarization generate large DC drifts at the unipolar potential that once amplified by the gain stages result in saturation of the output amplifier. As we recorded the potential of chest electrodes (UV1:UV6) and the WCT signal, we are able to reconstruct the missing precordial leads using Equation (4). It should be noted that both cleaned and raw data are reconstructed for these signals. We flagged these signals in the header file as “reconstructed precordials” and present the list of patients and signals in Table 3.

Table 3. List of patients with reconstructed precordial leads.

Patient ID	Segment ID	Reconstructed Precordial Leads
Patient7	Seg1	V2, V2-raw
	Seg2	V2, V2-raw
	Seg3	V1, V1-raw
Patient8	Seg1	V1, V2, V1-raw, V2-raw
	Seg2	V1, V2, V1-raw, V2-raw
Patient10	Seg1	V2, V2-raw
Patient14	Seg1	V2, V2-raw
Patient31	Seg1	V2, V2-raw

### 3. Lead's Reconstruction

Each file contains two sets of recordings: (1) standard ECG leads including three limb leads (I, II, and III) and six precordial leads (V1:V6); (2) unipolar ECG leads comprising of three limb potential (LA, RA, and LL), six unipolar chest leads (UV1:UV6), and the WCT signal. It could be possible to reconstruct the standard ECG leads using unipolar leads by utilizing the Equations (1) and (4). Figure 2 illustrates the recorded leads in comparison with reconstructed (represented by subscribed ‘R’) ECG signals. The reconstructed leads are shifted by 0.2 mV from the original place to better presentation. Figure 2 shows that the synthesized and recorded leads are highly correlated and seem exactly the same.

We used the Sprague and Geers’ metric [15,16] to show the agreement between recorded and reconstructed signals.  $M_{S\&G}$  provides the magnitude error,  $P_{S\&G}$  gives the phase error, and  $C_{S\&G}$  presents the overall error between recorded signals ( $m$ ) and reconstructed signals ( $p$ ) which both have a length of  $N$ . There is a more than 99% correlation between the reconstructed and recorded

leads, which clarifies that the recorded and reconstructed signals are identical. The small differences (indistinguishable since that correlation for every lead exceeds 0.99) are due to components' tolerances and mismatches. Table 4 presents the summary of the Sprague and Geers' error and correlation between recorded and reconstructed leads for the 92 patients.

$$M_{S\&G} = \sqrt{\sum_{i=1}^N p_i^2 / \sum_{i=1}^N m_i^2} - 1 \quad (5)$$

$$P_{S\&G} = \frac{1}{\pi} \cos^{-1} \sum_{i=1}^N p_i m_i / \sqrt{\sum_{i=1}^N m_i^2 \sum_{i=1}^N p_i^2} \quad (6)$$

$$C_{S\&G} = \sqrt{M_{S\&G}^2 + P_{S\&G}^2} \quad (7)$$

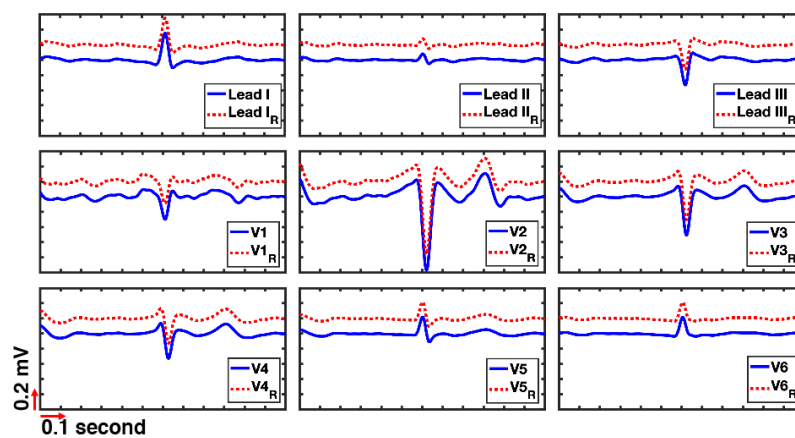


**Figure 2.** Comparison between recorded and reconstructed leads, shown with subscripted 'R'. The reconstructed leads are shifted by 0.2 mV from the original place for better visualization (patient ID 6).

**Table 4.** The average Sprague and Geers' error and correlation between recorded and reconstructed leads for 92 patients.

	Lead I	Lead II	Lead III	V1	V2	V3	V4	V5	V6
$M_{S\&G}$	0.012	0.013	0.023	0.017	0.026	0.020	0.019	0.018	0.023
$P_{S\&G}$	0	0	0	0	0	0	0	0	0
$C_{S\&G}$	0.012	0.013	0.023	0.017	0.026	0.020	0.019	0.018	0.023
Correlation	0.998	0.997	0.995	0.992	0.995	0.998	0.998	0.997	0.996

#### 4. Results and Discussion

We measured and reported the amplitude of the WCT as the percentage of lead II [5,17,18]. Our results support previous findings [19–21] to measure the WCT signal and showed that the WCT amplitude could be as high as 247% of lead II. Figure 3 is an example of a large WCT amplitude in relation to lead II. Furthermore, the WCT is highly individual, and it presents the standard ECG characteristics such as the *p*-wave and the *t*-wave. The distribution of the WCT polarity mostly has positive deflection, with some negative deflections and a handful of neutral polarities. We define as 'neutral polarities' those signals whose QRS as a bipolar mode of approximately equal positive and negative deflection [22]. Figure 4 demonstrates an example of positive, negatives, and neutral deflection of the WCT.

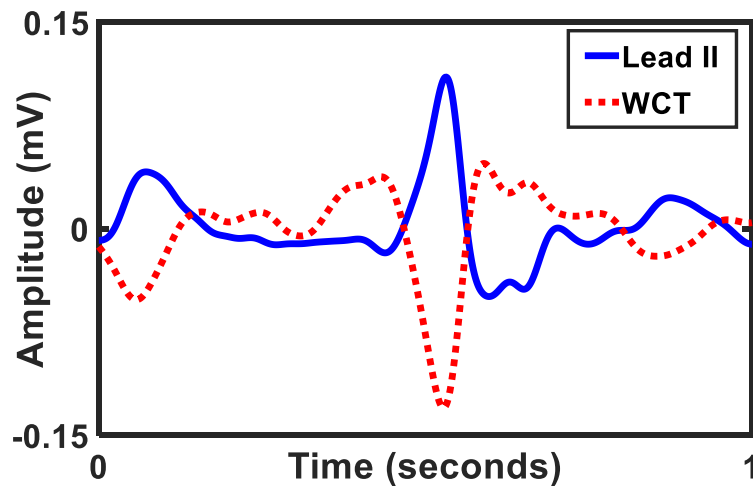


Figure 3. Example of the WCT and lead II amplitude (patient ID 32).

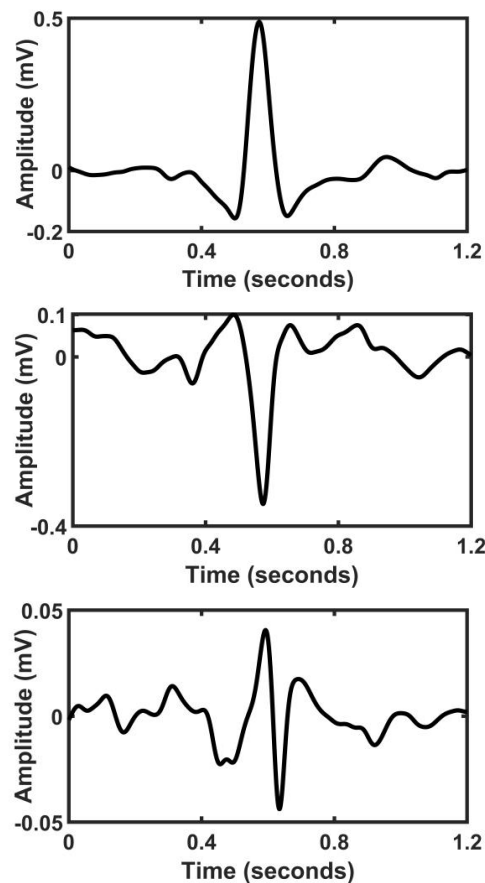
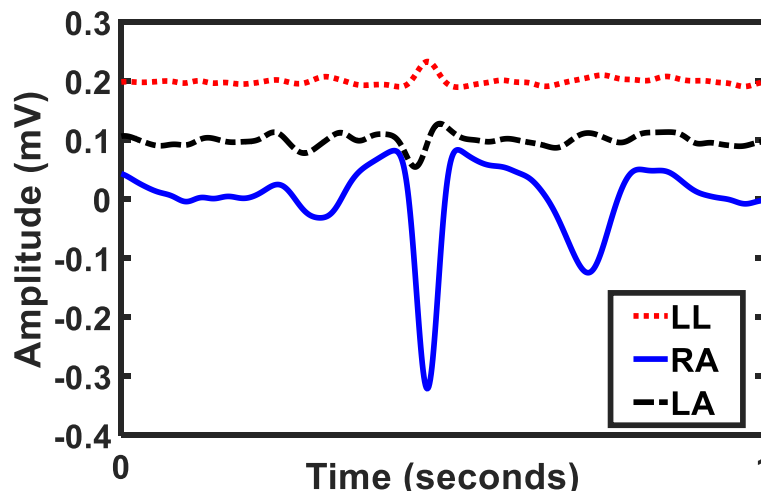


Figure 4. **Top** panel: the WCT with positive deflection (patient ID 44); **middle** panel: the WCT with negative deflection (patient ID 50); and **bottom** panel: the WCT with neutral deflection (patient ID 67).

This dataset provides the opportunity to have a better understanding of the limb potentials, as it contains the right arm, left arm, and left leg potential. The potential of limb electrodes depends on their location in relation to the heart. Since the left arm electrode is closer to the heart, it is assumed to have a larger amplitude while the left leg electrode has the largest distance from the heart and thus its potential amplitude assumed to be small or even negligible. However, our recordings show that this assumption was not correct for all patients. Figure 5 is an example of the patient with the right arm potential higher than the left arm and the left leg potentials. In this patient, the peak to peak amplitude

of the left leg and the left arm were very close to each other, and in comparison, with the right arm potential, their amplitude was negligible.



**Figure 5.** Comparison of the left arm (LA), right arm (RA), and left leg (LL) potentials. The RA has the peak to peak amplitude of 0.4 mV, while the LA has 0.07 mV, and the LL has 0.04 mV (patient ID 13).

We measured the peak to peak amplitudes of limbs' potential for three beats and reported the results in respect to lead II (Figures 6 and 7). Our recordings show that the RA had a higher potential than the LA for 29 patients (Figure 6).

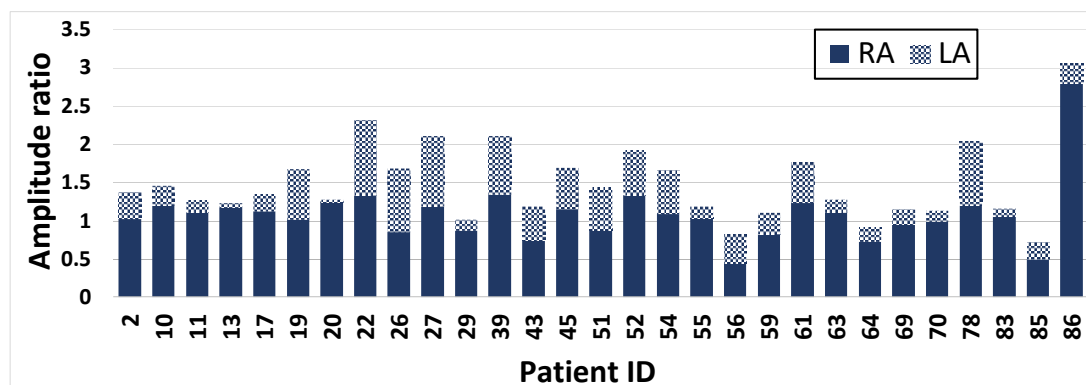


**Figure 6.** Patients with the RA potential higher than the LA potential. The average of three peak to peak amplitudes of the RA and the LA are measured respect with lead II.

Furthermore, the left leg did not have a small amplitude for all patients (the LL/lead II was in the range of [0.007 mV, 1.78 mV] with an average of 0.22 mV); therefore, it could have a clinical influence on the WCT amplitude and the precordial leads for some patients. However, the average potential of the RA, LA, and LL with respect to lead II among all patients were 0.88, 1.61, and 0.22, respectively, which were aligned with the initial assumption. Figure 7 demonstrates the WCT and the Einthoven limbs' potential amplitude with respect to lead II for all the 92 patients.

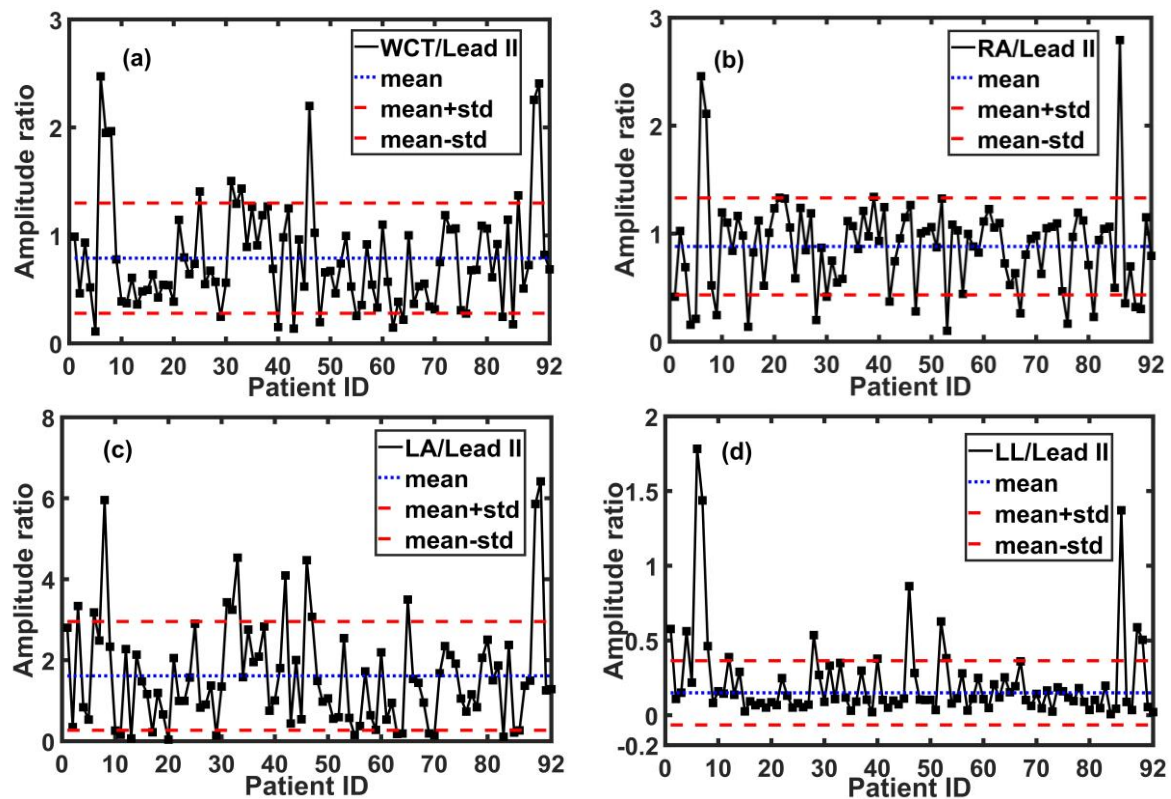


**Figure 7.** The amplitude of the WCT, LA, RA, and LL with respect to lead II for all 92 patients. Panel (a): the WCT/lead II is in the range of [0.11, 2.47] with an average of 0.78; Panel (b): the RA/lead II is in the range of [0.01, 2.7] with an average of 0.88; Panel (c): the LA/lead II is in the range of [0.038, 6.41] with an average of 1.61; and Panel (d): the LL/lead II is in the range of [0.007, 1.78] with an average of 0.22.

## 5. Conclusions

In this paper, we presented a unique dataset, which contained the WCT signal, six unipolar chest leads associated with three Einthoven limb leads, and six precordial leads. We recorded from 92 patients at Campbelltown Hospital (Campbelltown, Australia). We split each recording into ten second sections. Consequently, there were 540 segments in this dataset. Our recordings demonstrated that the WCT had ECG characteristics such as *p*-wave and *t*-wave. Additionally, our results confirmed the previous finding that the WCT is not a steady voltage reference during the cardiac cycle, thus, the WCT may be a new clinically relevant signal due to its high amplitude. We also presented the Einthoven limbs potential features for the first time. Our data undermined the initial assumption that the LL had a negligible amplitude and the LA had the highest potential among three Einthoven limbs. Furthermore, we showed that the 12-lead ECG signals could be synthesized using our unipolar leads (referred directly to the right leg) with a high correlation ( $>0.99$ ).

## 6. Appendix Further Notes on the WCT and Hardware

As mentioned in the paper the WCT has been the object of debate since its inception and to date there is not a common understanding of what is WCT and where it is located.

What is the Wilson Central Terminal? The ideal reference point characterized by having (a) zero amplitude and (b) constant and steady in all places/times [23]. Only the infinity has these features, however, to find the feasible reference point respect to the volume conductor in the size of the human body, Wilson suggested using the central terminal [4,23]. As the electrical activity of the heart was assumed to be a single dipole in the centroid of the Einthoven triangle, he suggested averaging the potential of the limbs electrodes in order to estimate the potential of the dipole. Wilson assumed

by using three large resistors connected to the limb electrodes, only a negligible current could pass. Therefore, each limb potential could be obtained. Nevertheless, Wilson's theory initially absorbed researchers' attention to work on measuring the real amplitude of the WCT [19–21,24–28]. The initial findings showed that the WCT amplitude could be as large as 40% of Einthoven's ECG signals [19,21]. However, due to the difficulty of the WCT measurement, the method of measuring ECG using the WCT has been widely accepted and received scant research attention since the 1960s.

Where is the Wilson Central Terminal? In theory, the WCT is formulated based on the simplified assumption that the electrical activity of the heart can be reduced to a single electrical dipole rotating around a fixed point in the chest [2,7] and located in the centre of the Einthoven's triangle. This hypothesis is built upon the assumption that the geometrical positions of the limbs' electrode construct the equilateral triangle, which is very unlikely in the routine ECG recording. In other words, the Einthoven triangle is not really an equilateral triangle, and the average potential of the limbs' electrode cannot represent the assumed zero potential of the dipole (Figure 8).

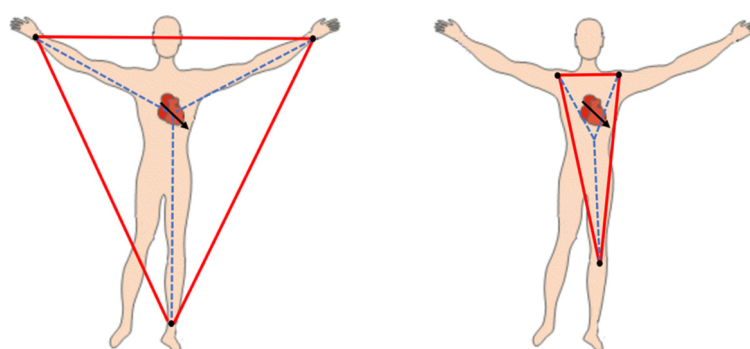


**Figure 8.** The measured WCT depends on the limb electrodes' position. The WCT amplitude and location vary by changing the electrodes placed on the limbs.

What is the true unipolar chest leads? The precordial leads (V1:V6) have been referred to as unipolar leads in the literature, as the WCT is assumed having a "null" amplitude in the cardiac cycle. Contrary to the initial assumption, the WCT has a large amplitude and variability during the cardiac cycle, and the precordial leads are actually bipolar and should not be considered as "true unipolar". Therefore, the WCT might remove important information from the potentials of chest electrodes. Furthermore, changing the position of electrodes on the limb causes the WCT amplitude to change and result in changing the precordial leads [29] (Figure 8).

In the past four years, we have developed and perfected (currently under trial) a new device, which enables recording of unipolar ECGs without using the WCT [22]. Our device indeed is a voltage recording device, as such it requires a reference point and a differential approach. Overall, our device uses a combined supply voltage bootstrap technique (to minimize the common mode noise) and a body reference placed to the right leg. According to the original inception of the surface electrocardiography postulated by Einthoven, as there is not a direct circuit that would make a current to flow between the legs that includes the heart directly in its pathway, we assumed that the right leg is the ideal reference point as it has the largest distance from the dipole (heart). One can note that although there is no zero-potential in the human body, it is widely accepted that the right leg's potential is near zero [30]. Therefore, we used this approximation to develop a new method to measure and store the WCT by recording directly from limb electrodes [1]. Our ECG device is able to record (1) the traditional ECG leads using the WCT as the reference point; and (2) the potential of electrodes on the limbs (RA, LA, and LL) and chest (UV1:UV6) using the right leg (RL) as the reference point. Therefore, we can measure the WCT amplitude, and the approximate unipolar leads, which are the raw biopotential measured from the exploring electrodes directly referred to the right leg (RL). The full hardware is fully described in [17].



**Author Contributions:** Author H.M. conceptualized this study and wrote the necessary code. G.D.G., H.M., I.M.S., and A.O. performed data recording in hospital. All the authors contributed to the data analysis and to the writing of the text. Authors J.A., I.M.S., A.O., and A.T. gave also clinical advice. All authors have read and agreed to the published version of the manuscript.

**Funding:** This study is supported by the office for Research Engagement and Development with Industry (REDI) at the Western Sydney University and by the MARCS Institute (Biomedical Engineering and Neuro-Science BENS group).

**Acknowledgments:** The authors wish to thank the patients at Campbelltown Hospital (NSW) who volunteered for this study, the nurses and the ECG technicians who helped with the data collection, Colin Symons (Technical Officer at MARCS institute) that helped with construction of the prototype, developed the custom ECG cable required as well as the device enclosure. The authors also gratefully acknowledge Texas Instruments who supplied chip samples for the construction of the prototype.

**Conflicts of Interest:** The authors declare no conflict of interest.

## Glossary

- Electrocardiography: bioelectrical recording from the heart. Abbreviated ECG and EKG. It contains three limb leads, three augmented leads, and six precordial leads.
- Reconstructed precordials: the difference between the potential of chest electrodes (UV1:UV6) and measured WCT potential using our new ECG device  $V_1^R : V_6^R = UV1 : UV6 - WCT$ . In this manuscript is referred to the chest leads, which are synthesized due to having difficulty in recording.
- Unipolar lead: voltage or potential of an electrode referred to the zero-reference point.
- Wilson's Central Terminal: the imaginary reference point of the human body used to measure the precordial leads. Abbreviated as WCT. It is calculated by averaging the potential of right arm, left arm, and left leg, and has been assumed to have a zero amplitude.

## References

1. Gargiulo, G.D. True Unipolar ECG Machine for Wilson Central Terminal Measurements. *Biomed Res. Int.* **2015**, *2015*, 586397. [[CrossRef](#)]
2. Malmivuo, J.; Plonsey, R. *Bioelectromagnetism Principles and Applications of Bioelectric and Biomagnetic Fields*; Oxford University Press: Oxford, UK, 1995; ISBN 9780195058239.
3. Goldberger, E. A simple, indifferent, electrocardiographic electrode of zero potential and a technique of obtaining augmented, unipolar, extremity leads. *Am. Heart J.* **1942**, *23*, 483–492. [[CrossRef](#)]
4. Wilson, F.N.; Johnston, F.D.; Macleod, A.G.; Barker, P.S. Electrocardiograms that represent the potential variations of a single electrode. *Am. Heart J.* **1934**, *9*, 447–458. [[CrossRef](#)]
5. Gargiulo, G.D.G.; Bifulco, P.; Cesarelli, M.; McEwan, A.L.A.; Moeinzadeh, H.; O'Loughlin, A.; Shugman, I.I.M.; Tapson, J.C.J.; Thiagalingam, A. On the Einthoven Triangle: A Critical Analysis of the Single Rotating Dipole Hypothesis. *Sensors* **2018**, *18*, 2353. [[CrossRef](#)]
6. Bacharova, L.; Selvester, R.H.; Engblom, H.; Wagner, G.S. Where is the central terminal located? In search of understanding the use of the Wilson central terminal for production of 9 of the standard 12 electrocardiogram leads. *J. Electrocardiol.* **2005**, *38*, 119–127. [[CrossRef](#)] [[PubMed](#)]
7. Frank, E. General Theory of Heart-Vector Projection. *Circ. Res.* **1954**, *2*, 258–270. [[CrossRef](#)] [[PubMed](#)]
8. Moeinzadeh, H.; Gargiulo, G. Wilson Central Terminal ECG Database (version 1.0.1). *PhysioNet* **2019**. [[CrossRef](#)]
9. Moeinzadeh, H.; Assad, J.; Bifulco, P.; Cesarelli, M.; McEwan, A.L.; O'Loughlin, A.; Shugman, I.M.; Tapson, J.C.; Thiagalingam, A.; Gargiulo, G.D. Unipolar Cardiac Leads between History and Science. In *Biomedical Signal Processing*; Springer: Singapore, Singapore, 2020; pp. 203–224.
10. Goldberger, A.L.; Amaral, L.A.N.; Glass, L.; Hausdorff, J.M.; Ivanov, P.C.; Mark, R.G.; Mietus, J.E.; Moody, G.B.; Peng, C.-K.K.; Stanley, H.E. PhysioBank, PhysioToolkit, and PhysioNet: Components of a new research resource for complex physiologic signals. *Circulation* **2000**, *101*, e215–e220. [[CrossRef](#)]
11. Moeinzadeh, H.; Gargiulo, G.; Bifulco, P.; Cesarelli, M.; O'Loughlin, A.; Shugman, M.I.; Thiagalingam, A. A Modern Wilson's Central Terminal Electrocardiography Database. *Hear. Lung Circ.* **2018**, *27*, S293–S294. [[CrossRef](#)]

12. Liu, F.; Liu, C.; Zhao, L.; Zhang, X.; Wu, X.; Xu, X.; Liu, Y.; Ma, C.; Wei, S.; He, Z.; et al. An Open Access Database for Evaluating the Algorithms of Electrocardiogram Rhythm and Morphology Abnormality Detection. *J. Med. Imaging Heal. Informatics* **2018**, *8*, 1368–1373. [[CrossRef](#)]
13. Moody, G.B.; Mark, R.G. The impact of the MIT-BIH Arrhythmia Database. *IEEE Eng. Med. Biol. Mag.* **2001**, *20*, 45–50. [[CrossRef](#)]
14. Boussejot, R.; Kreiseler, D.; Schnabel, A. Nutzung der EKG-Signaldatenbank CARDIODAT der PTB über das Internet. *Biomed. Tech. Eng.* **2009**, 317–318. [[CrossRef](#)]
15. Sprague, M.A.; Geers, T.L. A spectral-element/finite-element analysis of a ship-like structure subjected to an underwater explosion. *Comput. Methods Appl. Mech. Eng.* **2006**, *195*, 2149–2167. [[CrossRef](#)]
16. Geers, T.L. An objective error measure for the comparison of calculated and measured transient response histories. *Shock Vib. Bull.* **1984**, *54*, 99–107.
17. Gargiulo, G.D.G.; Bifulco, P.; Cesarelli, M.; McEwan, A.L.A.; Moeinzadeh, H.; O’Loughlin, A.; Shugman, I.M.I.M.; Tapson, J.C.J.; Thiagalingam, A. On the “Zero of Potential of the Electric Field Produced by the Heart Beat”. A Machine Capable of Estimating this Underlying Persistent Error in Electrocardiography. *Machines* **2016**, *4*, 18. [[CrossRef](#)]
18. Moeinzadeh, H.; Gargiulo, G.D.; Bifulco, P.; Cesarelli, M.; McEwan, A.L.; O’Loughlin, A.; Shugman, I.M.; Tapson, J.C.; Thiagalingam, A. Computing a new central terminal for ECG recording using combined genetic algorithm and linear regression from real patient data. In Proceedings of the Genetic and Evolutionary Computation Conference Companion, Berlin, Germany, 15–19 July 2017; ACM: New York, NY, USA, 2017; pp. 293–294.
19. Bayley, R.H.; Reynolds, E.W.; Kinard, C.L.; Head, J.F. The zero of potential of the electric field produced by the heart beat; the problem with reference to homogenous volume conductors. *Circ. Res.* **1954**, *2*, 4–13. [[CrossRef](#)]
20. Bayley, R.H.; Schmidt, A.E. The Problem of Adjusting the Wilson Central Terminal to a Zero of Potential in the Living Human Subject. *Circ. Res.* **1955**, *3*, 94–102. [[CrossRef](#)]
21. Bayley, R.H.; Kinard, C.L. The zero of potential of the electrical field produced by the heart beat; the problem with reference to the living human subject. *Circ. Res.* **1954**, *2*, 104–111. [[CrossRef](#)]
22. Gargiulo, G.D.; McEwan, A.L.; Bifulco, P.; Cesarelli, M.; Jin, C.; Tapson, J.; Thiagalingam, A.; van Schaik, A. Towards true unipolar ECG recording without the Wilson central terminal (preliminary results). *Physiol. Meas.* **2013**, *34*, 991–1012. [[CrossRef](#)]
23. Burger, H.C. The zero of potential: A persistent error. *Am. Heart J.* **1955**, *49*, 581–586. [[CrossRef](#)]
24. Wolfers, C.C.; Livezey, M.M. A study of methods of making so-called unipolar electrocardiograms. *Am. Heart J.* **1944**, *27*, 764–782. [[CrossRef](#)]
25. Burger, R.; Wuhrmann, F. Ueber das elektrische Feld des Herzens. *Cardiology* **1939**, *3*, 56–138. [[CrossRef](#)]
26. Wilson, F.N.; Johnston, F.D.; Rosenbaum, F.F.; Barker, P.S. On Einthoven’s triangle, the theory of unipolar electrocardiographic leads, and the interpretation of the precordial electrocardiogram. *Am. Heart J.* **1946**, *32*, 277–310. [[CrossRef](#)]
27. Dolgin, M.; Grau, S.; Katz, L.N. Experimental studies on the validity of the central terminal of Wilson as an indifferent reference point. *Am. Heart J.* **1949**, *37*, 868–880. [[CrossRef](#)]
28. Okamoto, Y.; Mashima, S. The zero potential and Wilson’s central terminal in electrocardiography. *Bioelectrochemistry Bioenerg.* **1998**, *47*, 291–295. [[CrossRef](#)]
29. Farrell, R.M.; Syed, A.; Syed, A.; Gutterman, D.D. Effects of limb electrode placement on the 12- and 16-lead electrocardiogram. *J. Electrocardiol.* **2008**, *41*, 536–545. [[CrossRef](#)]
30. Krasteva, V.; Jekova, I.; Schmid, R. Simulating arbitrary electrode reversals in standard 12-lead ECG. *Sensors* **2019**, *19*, 2920. [[CrossRef](#)]

